Innovations in Musculoskeletal Tumor Surgery

From Margin Optimization to Stable Fixation

Zeger Rijs

Innovations in Musculoskeletal Tumor Surgery
From Margin Optimization to Stable Fixation

Zeger Rijs

Innovations in Musculoskeletal Tumor Surgery

From Margin Optimization to Stable Fixation

Proefschrift

ter verkrijging van
de graad van doctor aan de universiteit Leiden,
op gezag van de rector magnificus prof.dr.ir. H. Bijl,
volgens besluit van het college voor promoties
te verdedigen op dinsdag 11 februari 2025
klokke 16:00 uur

door

Zeger Rijs

geboren te Amsterdam
in 1993

Table of Contents

1

GENERAL INTRODUCTION AND THESIS OUTLINE

Musculoskeletal tumors are classified as sarcomas in case of malignancy. Sarcomas encompass a rare and complex group of mesenchymal tumors that may show a broad range of differentiation. They can originate in bone or soft tissues, representing less than 1% of all adult malignancies and approximately 10% of all pediatric cancers [1-3]. Bone sarcomas, of which some can expand from bone into soft tissue, make up 20%, whereas soft tissue sarcomas (STS) comprise 80% of all sarcomas [2].

The clinical presentation of sarcomas is highly variable and depends upon tumor localization and aggressiveness. Generally, bone sarcomas are painful and most frequently arise in the long bones, particularly in areas with rapid bone growth during childhood and adolescence [4]. Contrarily, STS often manifest as a slowly enlarging, painless mass, primarily in the soft tissue of the extremities (59%), followed by the torso (18%), retroperitoneum (13%), and head and neck (10%) [5]. Due to the lack of symptoms in many STS cases, delayed presentation and diagnosis are common [6]. Moreover, the tumor's rarity often leads to misdiagnoses [7]. Consequently, patients frequently undergo inadequate diagnostic procedures or lack preoperative imaging before resection. Subsequently, up to 50% of patients with STS undergo an unplanned, non-oncologic excision for an inadvertently misdiagnosed mass, which is known as a "whoops" resection [8]. Such a whoops resection has multiple implications, including an increased risk of local recurrence and morbidity [7]. In order to minimize those whoops resections, guidelines state that the following features warrant further evaluation at an experienced sarcoma center: size of the mass is greater than 5 cm, the mass is deeply situated (into or below the muscle fascia) and/or (a history of) rapid growth of the mass [9].

Histopathology plays a crucial role in accurately diagnosing and classifying sarcomas, as different types of sarcomas have distinct histological features. The "World Health Organization Classification of Soft Tissue Tumours" was updated in 2020 for the purpose of uniformity in the classification because over 70 STS subtypes have been described, each with distinct behavioral, clinical, and prognostic features [2,5]. Immunohistochemistry (IHC) and molecular testing can aid in identifying the specific sarcoma subtype, which is crucial because the diagnosis guides treatment decisions and prognostic assessments. To this end, an experienced and specialized treatment team is essential. In the Netherlands, the Bone Tumor Committee embodies such a team. This multidisciplinary group consists of pathologists, radiologists, pediatric and medical oncologists, and orthopedic-, head and neck- and neurosurgeons. The committee reassesses edge cases on a monthly basis, and the combined experience of this group results in alteration of a diagnosis and subsequent treatment strategy in approximately 20% of the discussed cases, which emphasizes the complexity of a radiological and histological diagnosis [10,11]. Centralization increases the caseload for the individual centers, which is critical for the multidisciplinary team to build and maintain sufficient experience and knowledge. For adult sarcoma patients in the Netherlands, bone sarcoma care is centralized in the academic hospitals of Amsterdam (AMC), Groningen (UMCG), Nijmegen (Radboudumc), and Leiden (LUMC). In 2018 the Princess Máxima Center (PMC) for pediatric oncology was opened to centralize and optimize care for pediatric patients with a bone sarcoma. With regards to STS,

centers of expertise include AMC, UMCG, Radboudumc, LUMC, PMC (for pediatric patients), Antoni van Leeuwenhoek (AvL/NKI), Maastricht UMC+, and Erasmus MC.

Historically, amputation was the mainstay of treatment for extremity sarcoma. Wardrop was the first to publish an illustration of such an amputation for "soft cancer" in 1809 (figure 1) [12]. Although amputation yields a maximal oncological result, functional impairment and phantom pain are significant downsides [13]. Alternative treatment options arose in the 1970s, supported by the possibility of early detection by radiological imaging and treatment options such as radio- and chemotherapy. Between 1975 and 1981, an innovative randomized controlled trial was performed in which one group received amputation at or above the joint proximal to the tumor, and the other group limb-sparing resection plus postoperative radiotherapy. No significant differences were reported in disease-free survival rates or overall survival rates after 5 years [14]. With regards to the limb-sparing group, multivariate analyses indicated that the only correlate of local recurrence was the resection margin, as positive margins had a higher likelihood of local recurrence compared with those with negative margins, even when postoperative radiotherapy was used [14]. As a result, treatment shifted from amputation to limb-sparing surgery with the goal of achieving negative margins for improved clinical outcomes.

Figure 1. The first illustration of an amputated arm with "soft cancer" by Wardrop in 1809 [12].

Although the importance of negative margins is well established, achieving them remains challenging, particularly when tumor tissue is surrounded by vital neurovascular, visceral or bony structures, located in deeper or complex anatomical regions, or growing in an highly infiltrative pattern [15]. A growing sarcoma compresses surrounding normal tissue, leading to the formation of suppressed normal tissue with poorly defined margins and fingerlike tumor projections which can infiltrate adjacent tissues [16]. Current preoperative imaging modalities, such as magnetic resonance imaging (MRI) and computed tomography (CT), are used to identify the tumor location. However, these preoperative images fail to precisely correlate with the intraoperative situation due to various reasons. First, these images are limited to a two-dimensional space, while surgery is performed in a three-dimensional environment. Secondly, they do not precisely overlap with the intraoperative situation due to tissue manipulation and positioning. Thirdly, infiltrative growing sarcoma subtypes, such as Myxofibrosarcoma, have long slender tails, which are difficult to detect with preoperative imaging but can be seen by

histology after surgical resection [17]. Due to these drawbacks, surgeons currently mostly rely on tactile and visual feedback during surgery, hampering accurate tumor border identification.

Intraoperative tumor margins are not regularly checked by consulting a pathologist during the operation, examining the provided tissue for irradical resection margins by performing frozen section histochemistry [18]. Importantly, this technique suffers from sampling errors as surgeons often struggle to identify which suspicious regions should be sent for histopathologic assessment [19]. Besides, frozen section analysis is time-consuming and expensive because the frozen tissue has to be sliced and stained before microscopical examination by a pathologist can be performed, which takes approximately 15-30 minutes per section [20,21]. As a consequence, this technique is of limited utility, and incomplete resections with inherent undesirable outcomes, such as an increased risk of local recurrence and decreased survival, remain relatively common in sarcoma patients [15,22-24]. As such, innovative techniques facilitating real-time intraoperative tumor delineation are of utmost importance to optimize patient outcomes after sarcoma surgery, which is the focus of part I of this thesis.

Once adequate resection of the tumor has been established, the next phase involves reconstruction and fixation. Tumor resections can cause large residual osseous defects and loss of soft tissue stabilizers, with potentially deleterious effects on both function and viability of the limb [25]. Therefore, reconstructions with biological constructs, such as autografts and allografts, and/or orthopedic implants are often required to maintain limb function and bone strength [26]. Reconstructive implants encompass a range of options including megaprosthesis, plates, nails, and spine implants [27]. Ideally, these implants allow complete bone healing by providing stability with a material specific stiffness that is close to the stiffness of bone, minimize the risk of infection and implant failure, and address specific requirements for oncological patients. These specific requirements include facilitating adequate surveillance imaging for residual tumor or local tumor recurrence during follow-up, as well as enabling precise planning and delivery of postoperative radiotherapy.

Metal, like stainless steel or titanium, has been the foundation for many orthopedic implants due to multiple advantages such as strength, ease of machining and low cost [28]. However, a major disadvantage is the radiodensity of metal which causes artifacts on radiographic imaging, complicating recognition of residual tumor or local tumor recurrence [29]. This precludes accurate radiographic visualization for oncological follow-up and bone union and impedes precise postoperative radiation planning and delivery. Moreover, the stiffness of metal (200 gigapascal [GPa] for stainless steel and 110 GPa for titanium) is much higher than the human cortical bone (12 GPa), which may shield the underlying bone from stress and could lead to reduced bone quality [30]. Other disadvantages of metal implants include limited fatigue life, potential for generation of wear debris, and cold welding. Consequently, there is a demand for improved orthopedic implants, which is discussed in detail in Part II of this thesis.

Part I: Fluorescence-guided surgery

An upcoming tool enhancing adequate resection margins in surgical oncology is fluorescence-guided surgery (FGS), which exploits the advantages of near-infrared (NIR) light. Light in the NIR spectrum (650-900nm) has a tissue penetration depth of several millimeters to a centimeter and almost no autofluorescence is exhibited by biological tissue [31]. Besides, the surgical field is not altered by NIR light because light in this spectrum is invisible to the human eye [32]. Requirements for FGS include a fluorescent tracer and a dedicated camera system of which several are clinically available [33,34]. FGS can be subdivided into non-targeted and targeted (tumor-specific), depending on the tracer. Non-targeted FGS mostly uses the clinically available fluorescent dye indocyanine green (ICG). Once administered intravenously, ICG accumulates in tumors due to their leaky vascular capillaries and decreased lymphatic drainage, which is referred to as the enhanced permeability and retention (EPR) effect (figure 2) [35].
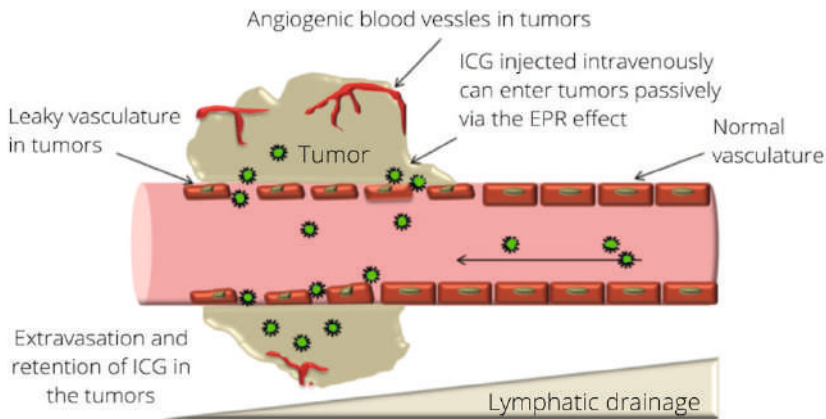
Figure 2. *Graphical overview of the enhanced permeability and retention (EPR) effect after intravenous injection of indocyanine green (ICG) for non-targeted fluorescence-guided surgery. Adapted and modified from Jhaveri and Torchilin [36].*

However, use of the EPR effect for imaging is unpredictable because it is influenced by factors such as tumor type, size, presence of necrosis, location, inflammation, and vascular mediators. This can result in inconsistent ICG signal intensity across heterogeneous sarcomas [37]. Consequently, it can lead to false negative as well as false positive fluorescence signal. This can potentially lead to under- or over-resection, resulting in incomplete tumor resections, increased functional impairments, and wound complications [38]. Targeted FGS, which can be achieved by utilizing a tumor-specific tracer (i.e., fluorophores conjugated to sarcoma-specific targeting moieties such as antibodies or peptides), could theoretically overcome the drawbacks of ICG (Figure 3). Targeted FGS has already been explored for various tumor types with encouraging results, indicating its potential in future sarcoma surgery [39].
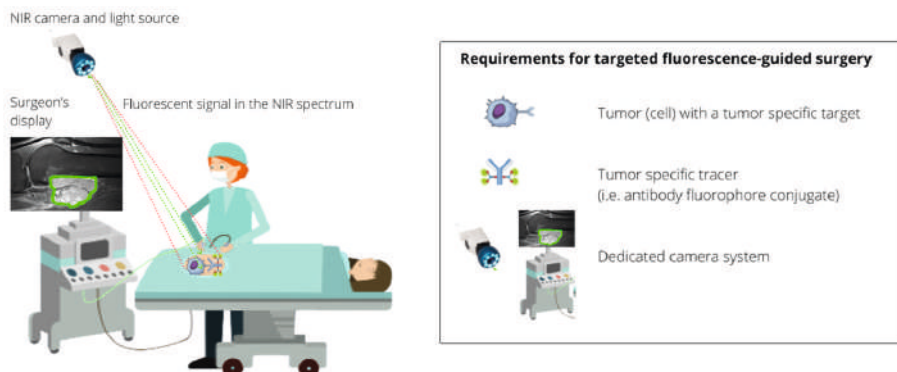
Figure 3. *Targeted fluorescence-guided surgery. A tumor-specific NIR fluorescent tracer, such as an anti- body conjugated with a fluorophore, is administered intravenously or topically to a sarcoma patient. The tracer binds specifically to the tumor (cells), and the surgeon is able to delineate tumor tissue from adjacent healthy tissue with the help of a dedicated camera system. The surgical field is not altered because NIR light is invisible to the human eye. The surgeon may see the camera records on a computer monitor, goggles, or wall projector (monitor form is shown in this figure).*

To date, clinically available tracers that specifically target sarcomas do not exist. Therefore, **Part I** of this thesis focusses on the preclinical identification of biomarkers suitable for targeted FGS in sarcomas. In this regard, **Chapter 2** aims to systematically select candidate biomarkers for specific intraoperative NIR fluorescence imaging, based on previously published IHC studies. There is a particular focus on three relatively common and aggressive STS subtypes with relatively high percentages of incomplete resections and local recurrences; Myxofibrosarcoma, Undifferentiated Soft Tissue Tumors (formerly known as Undifferentiated Pleomorphic Sarcoma), and Synovial Sarcoma. For cost- and time efficient clinical translation purposes, the search has been restricted to clinically available monoclonal antibodies of which safety profiles have already been demonstrated. Candidate biomarkers are ranked according to a modified selection scoring system. Based on the results of this study, **Chapter 3** comprehensively evaluates the most promising biomarkers in an IHC evaluation study with Myxofibrosarcoma tissue samples containing adjacent healthy tissue. A pathologist specializing in sarcomas has annotated the margin between the tumor and adjacent healthy tissue in each Myxofibrosarcoma tissue sample. Subsequently, an objective scoring method is developed and consequently evaluates the difference in staining intensity between the tumor and adjacent healthy tissue, which is crucial for the application of FGS. Next, **Chapter 4** introduces the concept of FGS for the most prevalent pediatric bone and soft tissue sarcomas, specifically Osteosarcoma, Ewing Sarcoma, and Rhabdomyosarcoma. This chapter delves into the prospects for clinical translation, assessing current literature as well as the advantages and limitations associated with non-targeted and targeted FGS. Furthermore, a comprehensive array of potential targets is presented. Subsequently, we explore the utility of antibody-based tracers, due to their time- and cost-efficient translational perspective. Lastly, **Chapter**

5 advances with IHC-, flow cytometry- and fluorescence microscopy- experiments to evaluate potential targets for FGS in pediatric Ewing Sarcoma. Next, in order to demonstrate feasibility, we present the topical application of three antibody-based NIR tracers on freshly resected human tissue.

Part II: Carbon-Fiber Implants

Once adequate resection of the tumor has been established, the next phase involves reconstruction and fixation. A promising alternative to current metal implants is carbon-fiber (CF), reinforced with polyetheretherketone. CF has several material specific advantages over current metal implants. First, its radiolucency allows for precise radiation planning and delivery. In addition, CF's radiolucency allows for better radiologic visualization of local tumor recurrences and bone healing, thereby facilitating improved postoperative follow-up for oncological patients [40]. Second, the modulus of elasticity of CF (13 GPa) is close to cortical bone, which theoretically leads to less stress shielding and improved bone quality compared to patients treated with metal implants [41]. Subsequently, good bone quality enhances functionality and reduces the risk of fractures. Third, CF has the capability to withstand prolonged fatigue strength compared with current metal plates during in vitro tests [42]. Although CF implants are increasingly used within the field of orthopedic surgery, including spine, trauma, and oncology, their reported experience remains limited and is often based on a single center's experience. Multicenter collaboration is essential to acquire sufficient data from these CF implants, especially for sarcoma patients. Therefore, we created an international collaboration, the "Carbon-Fiber International Collaboration Initiative" research group, and set up an online registry. Prominent academic and non-academic hospitals from Europe, the Middle East, the United Kingdom, and the United States of America joined the initiative and entered their data concerning oncological patients treated with CF implants in the registry. In this thesis we report on the first results, including data from patients treated with CF plates, nails, and spine implants. The registry is designed to continuously include new cases and will provide an ongoing database to assess safety and effectiveness of CF implants.

The primary objective of **Chapter 6** is to identify complications of the treatment of patients with bone tumors. Between February 2015 and May 2021, 13 centers have retrospectively registered 96 patients with bone tumors that are reconstructed using CF plates. Complications have been identified, and timing and etiology of complications were noted. Complications were tabulated and classified based on mechanical, non-mechanical and pediatric complications. Subsequently, the systematic review in **Chapter 7** summarizes all available evidence up until June 2023 on the use of CF plates for traumatic and (impending) pathological fracture fixation. With regards to CF nails, **Chapter 8** describes clinical outcomes of 239 patients treated with CF nails for oncologic indications in the long bones. Next, **Chapter 9** evaluates the radiolucent properties of CF spine implants. Artefacts on computed tomography images in patients with spinal oligometastatic disease are compared between CF and titanium in 22 patients undergoing stereotactic ablative radiotherapy. **Chapter 10** discusses the outcomes of all chapters, places them into a clinical context and concludes with future perspectives.

References

1. Siegel, R.L.; Miller, K.D.; Wagle, N.S.; Jemal, A. Cancer statistics, 2023. *CA Cancer J Clin* **2023**, *73*, 17-48, doi:10.3322/caac.21763.

2. Moch, H. Soft Tissue and Bone Tumours WHO Classification of Tumours/Volume 3. *WHO Classification of Tumours* **2020**, *3*.

3. Miller, K.D.; Fidler-Benaoudia, M.; Keegan, T.H.; Hipp, H.S.; Jemal, A.; Siegel, R.L. Cancer statistics for adolescents and young adults, 2020. *CA Cancer J Clin* **2020**, *70*, 443-459, doi:10.3322/caac.21637.

4. Ferguson, J.L.; Turner, S.P. Bone Cancer: Diagnosis and Treatment Principles. *Am Fam Physician* **2018**, *98*, 205-213.

5. Lawrence, W., Jr.; Donegan, W.L.; Natarajan, N.; Mettlin, C.; Beart, R.; Winchester, D. Adult soft tissue sarcomas. A pattern of care survey of the American College of Surgeons. *Ann Surg* **1987**, *205*, 349-359, doi:10.1097/00000658-198704000-00003.

6. Ilaslan, H.; Schils, J.; Nageotte, W.; Lietman, S.A.; Sundaram, M. Clinical presentation and imaging of bone and soft-tissue sarcomas. *Cleve Clin J Med* **2010**, *77 Suppl 1*, S2-7, doi:10.3949/ccjm.77.s1.01.

7. Grignol, V.P.; Lopez-Aguiar, A.G. The Implications of an Unplanned Sarcoma Excision (the "Whoops" Operation). *Surg Clin North Am* **2022**, *102*, 529-538, doi:10.1016/j.suc.2022.04.002.

8. Zaidi, M.Y.; Ethun, C.G.; Liu, Y.; Poultsides, G.; Howard, J.H.; Mogal, H.; Tseng, J.; Votanopoulos, K.; Fields, R.C.; Cardona, K. The impact of unplanned excisions of truncal/extremity soft tissue sarcomas: A multi-institutional propensity score analysis from the US Sarcoma Collaborative. *J Surg Oncol* **2019**, *120*, 332-339, doi:10.1002/jso.25521.

9. Styring, E.; Billing, V.; Hartman, L.; Nilbert, M.; Seinen, J.M.; Veurink, N.; Vult von Steyern, F.; Rydholm, A. Simple guidelines for efficient referral of soft-tissue sarcomas: a population-based evaluation of adherence to guidelines and referral patterns. *J Bone Joint Surg Am* **2012**, *94*, 1291-1296, doi:10.2106/jbjs.K.01271.

10. Mankin, H.J.; Mankin, C.J.; Simon, M.A. The hazards of the biopsy, revisited. Members of the Musculoskeletal Tumor Society. *J Bone Joint Surg Am* **1996**, *78*, 656-663, doi:10.2106/00004623-199605000-00004.

11. Blay, J.Y.; Honoré, C.; Stoeckle, E.; Meeus, P.; Jafari, M.; Gouin, F.; Anract, P.; Ferron, G.; Rochwerger, A.; Ropars, M., et al. Surgery in reference centers improves survival of sarcoma patients: a nationwide study. *Ann Oncol* **2019**, *30*, 1143-1153, doi:10.1093/annonc/mdz124.

12. Wardrop, J. *Observations on Fungus Hæmatodes Or Soft Cancer: In Several of the Most Important Organs of the Human Body: Containing Also a Comparative View of the Structure of Fungus Hæmatodes and Cancer. With Cases and Dissections*; G. Ramsay: 1809.

13. Davis, A.M.; Devlin, M.; Griffin, A.M.; Wunder, J.S.; Bell, R.S. Functional outcome in amputation versus limb sparing of patients with lower extremity sarcoma: a matched case-control study. *Arch Phys Med Rehabil* **1999**, *80*, 615-618, doi:10.1016/s0003-9993(99)90161-2.

14. Rosenberg, S.A.; Tepper, J.; Glatstein, E.; Costa, J.; Baker, A.; Brennan, M.; DeMoss, E.V.; Seipp, C.; Sindelar, W.F.; Sugarbaker, P., et al. The treatment of soft-tissue sarcomas of the extremities: prospective randomized evaluations of (1) limb-sparing surgery plus radiation therapy compared with amputation and (2) the role of adjuvant chemotherapy. *Ann Surg* **1982**, *196*, 305-315, doi:10.1097/00000658-198209000-00009.

15. Jang, W.Y.; Kim, H.S.; Han, I. Impact of surgical margin on survival in extremity soft tissue sarcoma: A systematic review and meta-analysis. *Medicine (Baltimore)* **2021**, *100*, e24124, doi:10.1097/md.0000000000024124.

16. Abdelhafeez, A.; Talbot, L.; Murphy, A.J.; Davidoff, A.M. Indocyanine Green-Guided Pediatric Tumor Resection: Approach, Utility, and Challenges. *Front Pediatr* **2021**, *9*, 689612, doi:10.3389/fped.2021.689612.

17. Yoo, H.J.; Hong, S.H.; Kang, Y.; Choi, J.Y.; Moon, K.C.; Kim, H.S.; Han, I.; Yi, M.; Kang, H.S. MR imaging of myxofibrosarcoma and undifferentiated sarcoma with emphasis on tail sign; diagnostic and prognostic value. *Eur Radiol* **2014**, *24*, 1749-1757, doi:10.1007/s00330-014-3181-2.

18. Radhamony, N.G.; Sugath, S.; Dhanan, B.; Kattoor, J.; Kachare, N. Limited utility of intraoperative frozen sections in primary malignant tumours involving long bones - A multicenter analysis of 475 cases. *Ann Med Surg (Lond)* **2021**, *72*, 103108, doi:10.1016/j.amsu.2021.103108.

19. Shah, M.S.; Garg, V.; Kapoor, S.K.; Dhaon, B.K.; Gondal, R. Fine-needle aspiration cytology, frozen section, and open biopsy: relative significance in diagnosis of musculoskeletal tumors. *J Surg Orthop Adv* **2003**, *12*, 203-207.

20. Black, C.; Marotti, J.; Zarovnaya, E.; Paydarfar, J. Critical evaluation of frozen section margins in head and neck cancer resections. *Cancer* **2006**, *107*, 2792-2800, doi:10.1002/cncr.22347.

21. Bui, M.M.; Smith, P.; Agresta, S.V.; Cheong, D.; Letson, G.D. Practical issues of intraoperative frozen section diagnosis of bone and soft tissue lesions. *Cancer Control* **2008**, *15*, 7-12, doi:10.1177/107327480801500102.

22. Novais, E.N.; Demiralp, B.; Alderete, J.; Larson, M.C.; Rose, P.S.; Sim, F.H. Do surgical margin and local recurrence influence survival in soft tissue sarcomas? *Clin Orthop Relat Res* **2010**, *468*, 3003-3011, doi:10.1007/s11999-010-1471-9.

23. Sambri, A.; Caldari, E.; Fiore, M.; Zucchini, R.; Giannini, C.; Pirini, M.G.; Spinnato, P.; Cappelli, A.; Donati, D.M.; De Paolis, M. Margin Assessment in Soft Tissue Sarcomas: Review of the Literature. *Cancers (Basel)* **2021**, *13*, doi:10.3390/cancers13071687.

24. Stojadinovic, A.; Leung, D.H.; Hoos, A.; Jaques, D.P.; Lewis, J.J.; Brennan, M.F. Analysis of the prognostic significance of microscopic margins in 2,084 localized primary adult soft tissue sarcomas. *Ann Surg* **2002**, *235*, 424-434, doi:10.1097/00000658-200203000-00015.

25. Salzer, M.; Knahr, K. Resection of malignant bone tumors. *Recent Results Cancer Res* **1976**, 10.1007/978-3-642-80997-2_21, 239-256, doi:10.1007/978-3-642-80997-2_21.

26. Zhao, Z.; Yan, T.; Guo, W.; Yang, R.; Tang, X.; Wang, W. Surgical options and reconstruction strategies for primary bone tumors of distal tibia: A systematic review of complications and functional outcome. *J Bone Oncol* **2019**, *14*, 100209, doi:10.1016/j.jbo.2018.100209.

27. Tapscott DC, W.C. Orthopedic Implant Materials. Availabe online: https://www.ncbi.nlm.nih.gov/books/NBK560505/ (accessed on

28. Hak, D.J.; Banegas, R.; Ipaktchi, K.; Mauffrey, C. Evolution of plate design and material composition. *Injury* **2018**, *49 Suppl 1*, S8-s11, doi:10.1016/s0020-1383(18)30295-x.

29. Laux, C.J.; Villefort, C.; Ehrbar, S.; Wilke, L.; Guckenberger, M.; Müller, D.A. Carbon Fiber/Polyether Ether Ketone (CF/PEEK) Implants Allow for More Effective Radiation in Long Bones. *Materials (Basel)* **2020**, *13*, doi:10.3390/ma13071754.

30. Jockisch, K.A.; Brown, S.A.; Bauer, T.W.; Merritt, K. Biological response to chopped-carbon-fiber-reinforced peek. *J Biomed Mater Res* **1992**, *26*, 133-146, doi:10.1002/jbm.820260202.

31. Vahrmeijer, A.L.; Hutteman, M.; van der Vorst, J.R.; van de Velde, C.J.; Frangioni, J.V. Image-guided cancer surgery using near-infrared fluorescence. *Nat Rev Clin Oncol* **2013**, *10*, 507-518, doi:10.1038/nrclinonc.2013.123.

32. Schaafsma, B.E.; Mieog, J.S.; Hutteman, M.; van der Vorst, J.R.; Kuppen, P.J.; Löwik, C.W.; Frangioni, J.V.; van de Velde, C.J.; Vahrmeijer, A.L. The clinical use of indocyanine green as a near-infrared fluorescent contrast agent for image-guided oncologic surgery. *J Surg Oncol* **2011**, *104*, 323-332, doi:10.1002/jso.21943.

33. D'Souza, A.V.; Lin, H.; Henderson, E.R.; Samkoe, K.S.; Pogue, B.W. Review of fluorescence guided surgery systems: identification of key performance capabilities beyond indocyanine green imaging. *J Biomed Opt* **2016**, *21*, 80901, doi:10.1117/1.Jbo.21.8.080901.

34. Lauwerends, L.J.; van Driel, P.; Baatenburg de Jong, R.J.; Hardillo, J.A.U.; Koljenovic, S.; Puppels, G.; Mezzanotte, L.; Löwik, C.; Rosenthal, E.L.; Vahrmeijer, A.L., et al. Real-time fluorescence imaging in intraoperative decision making for cancer surgery. *Lancet Oncol* **2021**, *22*, e186-e195, doi:10.1016/s1470-2045(20)30600-8.

35. Matsumura, Y.; Maeda, H. A new concept for macromolecular therapeutics in cancer chemotherapy: mechanism of tumoritropic accumulation of proteins and the antitumor agent smancs. *Cancer Res* **1986**, *46*, 6387-6392.

36. Jhaveri, A.M.; Torchilin, V.P. Multifunctional polymeric micelles for delivery of drugs and siRNA. *Front Pharmacol* **2014**, *5*, 77, doi:10.3389/fphar.2014.00077.

37. Nicoli, F.; Saleh, D.B.; Baljer, B.; Chan, C.D.; Beckingsale, T.; Ghosh, K.M.; Ragbir, M.; Rankin, K.S. Intraoperative Near-infrared Fluorescence (NIR) Imaging With Indocyanine Green (ICG) Can Identify Bone and Soft Tissue Sarcomas Which May Provide Guidance for Oncological Resection. *Ann Surg* **2021**, *273*, e63-e68, doi:10.1097/sla.0000000000003857.

38. Tummers, Q.R.; Hoogstins, C.E.; Peters, A.A.; de Kroon, C.D.; Trimbos, J.B.; van de Velde, C.J.; Frangioni, J.V.; Vahrmeijer, A.L.; Gaarenstroom, K.N. The Value of Intraoperative Near-Infrared Fluorescence Imaging Based on Enhanced Permeability and Retention of Indocyanine Green: Feasibility and False-Positives in Ovarian Cancer. *PLoS One* **2015**, *10*, e0129766, doi:10.1371/journal.pone.0129766.

39. Hernot, S.; van Manen, L.; Debie, P.; Mieog, J.S.D.; Vahrmeijer, A.L. Latest developments in molecular tracers for fluorescence image-guided cancer surgery. *Lancet Oncol* **2019**, *20*, e354-e367, doi:10.1016/s1470-2045(19)30317-1.

40. Yeung, C.M.; Bhashyam, A.R.; Patel, S.S.; Ortiz-Cruz, E.; Lozano-Calderón, S.A. Carbon Fiber Implants in Orthopaedic Oncology. *J Clin Med* **2022**, *11*, doi:10.3390/jcm11174959.

41. Bagheri, Z.S.; Tavakkoli Avval, P.; Bougherara, H.; Aziz, M.S.; Schemitsch, E.H.; Zdero, R. Biomechanical analysis of a new carbon fiber/flax/epoxy bone fracture plate shows less stress shielding compared to a standard clinical metal plate. *J Biomech Eng* **2014**, *136*, 091002, doi:10.1115/1.4027669.

42. Mugnai, R.; Tarallo, L.; Capra, F.; Catani, F. Biomechanical comparison between stainless steel, titanium and carbon-fiber reinforced polyetheretherketone volar locking plates for distal radius fractures. *Orthop Traumatol Surg Res* **2018**, *104*, 877-882, doi:10.1016/j.otsr.2018.05.002.

PART I.

FLUORESCENCE-GUIDED SURGERY

2

CANDIDATE BIOMARKERS FOR SPECIFIC INTRAOPERATIVE NEAR-INFRARED IMAGING OF SOFT TISSUE SARCOMAS: A SYSTEMATIC REVIEW

Z. Rijs[1], A.N. Shifai[1], S.E. Bosma[1], P.J.K. Kuppen[2], A.L. Vahrmeijer[2], S. Keereweer[3], J.V.M.G. Bovée[4], M.A.J. van de Sande[1], C.F.M. Sier[2], P.B.A.A. van Driel[5]

[1] Department of Orthopedic Surgery, Leiden University Medical Center, Leiden, The Netherlands
[2] Department of Surgery, Leiden University Medical Center, Leiden, The Netherlands
[3] Department of Otorhinolaryngology Head and Neck Surgery, Erasmus Medical Center Cancer institute, Rotterdam, The Netherlands
[4] Department of Pathology, Leiden University Medical Center, Leiden, The Netherlands
[5] Department of Orthopedic Surgery, Isala Hospital, Zwolle, The Netherlands

Simple Summary

Near-infrared imaging of tumors during surgery facilitates the oncologic surgeon to distinguish malignant from healthy tissue. The technique is based on fluorescent tracers binding to tumor biomarkers on malignant cells. Currently, there are no clinically available fluorescent tracers that specifically target soft tissue sarcomas. This review searched the literature to find candidate biomarkers for soft tissue sarcomas, based on clinically used therapeutic antibodies. The search revealed 7 biomarkers: TEM1, VEGFR-1, EGFR, VEGFR-2, IGF-1R, PDGFRα, and CD40. These biomarkers are abundantly present on soft tissue sarcoma tumor cells and are already being targeted with humanized monoclonal antibodies. The conjugation of these antibodies with a fluorescent dye will yield in specific tracers for image-guided surgery of soft tissue sarcomas to improve the success rates of tumor resections.

Abstract

Surgery is the mainstay of treatment for localized soft tissue sarcomas (STS). The curative treatment highly depends on complete tumor resection, as positive margins are associated with local recurrence (LR) and prognosis. However, determining the tumor margin during surgery is challenging. Real-time tumor-specific imaging can facilitate complete resection by visualizing tumor tissue during surgery. Unfortunately, STS specific tracers are presently not clinically available. In this review, STS-associated cell surface-expressed biomarkers, which are currently already clinically targeted with monoclonal antibodies for therapeutic purposes, are evaluated for their use in near-infrared fluorescence (NIRF) imaging of STS. Clinically targeted biomarkers in STS were extracted from clinical trial registers and a PubMed search was performed. Data on biomarker characteristics, sample size, percentage of biomarker-positive STS samples, pattern of biomarker expression, biomarker internalization features, and previous applications of the biomarker in imaging were extracted. The biomarkers were ranked utilizing a previously described scoring system. Eleven cell surface-expressed biomarkers were identified from which 7 were selected as potential biomarkers for NIRF imaging: TEM1, VEGFR-1, EGFR, VEGFR-2, IGF-1R, PDGFRα, and CD40. Promising biomarkers in common and aggressive STS subtypes are TEM1 for Myxofibrosarcoma, TEM1, and PDGFRα for Undifferentiated Soft Tissue Sarcoma and EGFR for Synovial Sarcoma.

2

Introduction

Soft tissue sarcomas (STS) are a heterogeneous group of mesenchymal tumors that represent 1% of all malignancies [1]. The incidence in Europe is estimated at 4–5/100.000 per year, accumulating to approximately 18,000 new patients in Europe per year [2]. While most STS are diagnosed in the extremities (60%), they can arise anywhere in the body [3]. There are over 50 histological subtypes of STS, each with distinct behavioral, clinical, and prognostic features [1]. Surgery of STS is the mainstay of treatment for localized disease. For the aim of curative surgery, a tumor needs to be removed with a margin of normal tissue as the tumor pseudocapsule and reactive zone are expected to contain tumor cells [4]. Clinical outcome after surgical treatment is highly dependent on surgical resection margins, as tumor-positive margins are clearly associated with local recurrence (LR), and indirectly associated with overall survival [5-7]. Further, close or positive margins often necessitate the need for adjuvant radiotherapy to reduce the risk for LR with about 50%, but this increases the risk for local complications [8]. However, determining the surgical margin is challenging, particularly when tumor tissue is surrounded by vital structures or in STS subtypes with a highly infiltrative growth pattern, such as Myxofibrosarcoma (MFS), Undifferentiated Soft Tissue Sarcoma (USTS, previously called undifferentiated pleomorphic sarcoma), and Synovial Sarcoma (SS). In these specific tumors, preoperative surgical planning is complicated by current limitations in preoperative radiological imaging. The infiltrative growth of sarcoma with long slender tails, clearly diagnosed by histology after surgical resection, is sometimes difficult to detect with preoperative imaging [9]. Consequently, despite centralizing STS treatment and (neo)adjuvant treatment modalities, positive margins and LR are still common. Positive margins are 13%, 20% and 28%, with LR rates of 12% (5-year follow up), 40% (10-year follow up), and 45% (5-year follow up) in SS, MFS, and USTS respectively [10-13]. The real-time intraoperative tumor-specific imaging of STS could help the surgeon to discriminate tumor from normal tissue, improving complete tumor resections and reducing LR rates. Near-infrared fluorescence (NIRF) imaging is one of the most upcoming technologies in real-time targeted imaging as it facilitates surgeons to visualize tumor tissue during surgery. It has been explored for various tumor types with promising results and is expected to play an important role in future surgery of STS [14].

Three important parameters define successful NIRF tumor-specific imaging: a tumor-specific biomarker, a targeting moiety conjugated to a fluorescent dye/fluorophore (tracer), and a NIRF camera system. In NIRF imaging, light in the near-infrared (NIR) wavelength is used (650–900 nm). In this region, tissue penetration of light is relatively high, due to low tissue absorption, and the autofluorescence of normal tissue is limited [15]. Light in the NIR region is invisible to the human eye and therefore a dedicated NIRF camera system is needed, which has the advantage that the surgical field is not altered by the fluorescence from the tracer. Clinical NIRF cameras of various companies are available [16].

The search for a tumor-specific biomarker for NIRF imaging of STS is complex, because of the rarity and heterogeneity of the disease. The ideal biomarker should be highly and

homogenously expressed on tumor cells of most subtypes of STS, while being absent on adjacent healthy tissue. Like for other cancers, the biomarker should preferably be located on the cell surface of malignant cells to permit direct targeting and have the possibility of internalization (endocytosis of an extracellular molecule upon binding to a specific protein on the cell surface) to facilitate a long-lasting fluorescence signal. Ideally, this biomarker is still present on residual cells after neoadjuvant therapy.

Fluorescent tracers for tumor biomarkers are generated by the conjugation of a fluorescent dye/fluorophore to a targeting moiety. Various fluorophores are available and some are clinically approved [14]. Targeting moieties consist of proteins, like monoclonal antibodies or fragments thereof, peptides, RNA aptamers, or other small synthetic molecules. Monoclonal antibodies are the most widely used targeting moieties in biotherapy and imaging. The advantages of antibodies are their specificity, affinity, flexibility, and relatively long plasma half-life. To minimize immune reactions, human(ized) versions are mostly used. A disadvantage of antibodies for the use of imaging is the relatively high costs of development, which is particularly relevant for rare diseases like STS. In the past decade, therapeutic antibodies have been equipped with NIRF dyes and evaluated for imaging of common cancer types, like breast and colorectal cancer [14].

Elaborating on this approach, the aim of this systematic review is to select candidate biomarkers for specific intraoperative NIRF imaging of soft tissue sarcomas. STS are a rare and heterogeneous group of tumors. The development of a specific tracer for NIRF imaging that is not already clinically used in therapy would be very challenging as it would be costly and time consuming. Therefore, the search is restricted to clinically available monoclonal antibodies of which the safety profiles are already demonstrated and a translation towards a tracer for NIRF imaging can be expected. The overall purpose of this evaluation is to find optimal biomarkers for the three most common and aggressive STS subtypes MFS, USTS, and SS, which account for challenging resections and currently result in high rates of local recurrences.

Materials and Methods

Search strategy
An initial search was performed to find clinically available monoclonal antibodies targeting STS. The EU Clinical Trials Register (www.clinicaltrialsregister.eu/) and clinical trials.gov (clinicaltrials.gov/) databases were searched with the keyword "Soft tissue sarcoma", and all clinically available monoclonal antibodies targeting STS were listed. Next, a PubMed search with the respective biomarkers targeted by those monoclonal antibodies was created with the assistance of a medical librarian (Appendix A). The search was done in August 2019 and updated in September 2020 due to the publication of multiple relevant articles between August 2019 and September 2020. This systematic review was performed following the Preferred

Reporting Items for Systematic Reviews and Meta-Analysis (PRISMA) guidelines of 2009 (registration ID: CRD42020206473) [17].

Eligibility Criteria
Studies were eligible for inclusion if they met the following criteria: (1) report of expression of cell surface-expressed biomarkers in STS for which a clinically available antibody was present, (2) at least 95% of the included tumor samples were primary STS, (3) sample size of at least 4, (4) published in the English language, and (5) full text was available. The eligibility of the studies was assessed by two authors (Z.R. and A.N.S.). Disagreements were discussed with a third reviewer (P.B.A.A.D.). Animal studies, xenograft studies, cell line studies, articles without positive and negative control samples, case reports, reviews, viewpoints, conference reports, meeting abstracts, letters to journals, or editors were excluded.

Data Extraction
The following data were extracted from eligible studies: target characteristics, sample size, type of sample, percentage of positive STS samples, localization of expression, pattern of expression, positive and negative controls, internalization, and previously imaged. A second tumor type independent search was performed for data on internalization and previous imaging of targets where no information was found after the first search (Appendix B). Data on safety profiles of monoclonal antibodies was acquired through the search of Appendix A.

Biomarker Selection Scoring System
In order to select the optimal biomarkers for tumor specific NIRF imaging in STS, we developed a target selection scoring system. The scoring system is based on the modified version of the Target Selection Criteria (TASC), developed by Bosma et al. [18]. The scoring system is based on five domains (Table 1).

1. Sample size. The number of samples indicate how much evidence is acquired.
2. Percentage of biomarker-positive STS samples. This is calculated based on the amount of STS samples that positively showed presence of the biomarker in each included article, independent of the percentage of positive tumor cells within each sample. Immunohistochemistry was used to assess the percentage of positive STS in tissue samples.
3. Pattern of expression. Ideally, the target is expressed diffusely by all tumor cells (particularly at the tumor border) to guide surgical resection. The pattern of expression is defined as diffuse when expression is randomly spread throughout the tumor sample and focal when expression is located in a specific region of the tumor sample. When different samples show variable expression patterns (diffuse and focal), the expression pattern for the whole cohort is defined as heterogeneous. No distinction was made based on exact location of expression within tumor samples. While this review included studies evaluating tissue samples and tissue microarrays, data regarding the pattern of expression was extracted from studies including tissue samples.

4. Internalization. This is important because internalization after binding of the tracer creates a long-lasting signal for tumor-specific imaging.
5. Previously imaged. If there is prove that imaging is possible, it has more potential to be translated to the clinics. The distinction between imaging with or without NIRF is important for its applicability in NIRF imaging. This criterium was tumor type independent.

The maximum score for a target is 9 points, 7 was chosen as the cut-off value for promising targets for tumor specific NIRF imaging in STS.

Table 1. Target selection scoring system.

Score	0	1	2
Sample size	0-100	101-500	>500
Percentage of positive STS samples	0-33%	33-67%	>67%
Pattern of expression*	Focal	Heterogeneous	Diffuse
Internalization	not described	Yes	
Previously imaged	not described	Yes, but not with NIRF imaging	Yes, with NIRF imaging

*Note. * Pattern of expression is focal when expression is located in a specific region of the tumor sample and diffuse when expression is randomly spread throughout the tumor sample. When different samples show variable expression patterns (diffuse and focal), the expression pattern is defined as heterogeneous.*

Results

Study selection
Our analysis of the EU Clinical Trials Register (https://www.clinicaltrialsregister.eu/) and clinical trials.gov (https://clinicaltrials.gov/) revealed the following clinically available monoclonal antibodies targeting STS-associated cell surface-expressed biomarkers (Table 2): Ontuxizumab (MORAb-004) [trial number: NCT01574716] targeting tumor endothelial marker 1 (TEM1), recombinant monoclonal antibody Aflibercept [NCT00390234] and humanized monoclonal antibody Bevacizumab [NCT03913806] targeting vascular endothelial growth factor A (VEGF-A), thereby indirectly targeting vascular endothelial growth factor receptor-1 (VEGFR-1) and vascular endothelial growth factor receptor-2 (VEGFR-2), Ramucirumab [NCT04145700] targeting VEGFR-2, Cetuximab [NCT00148109] targeting epidermal growth factor receptor (EGFR), Ganitumab (AMG 479) [NCT03041701], Teprotumumab [NCT00642941], Cixutumumab [NCT01016015] and Figitumumab [NCT00927966] targeting insulin-like growth factor 1 receptor (IGF-1R), Olaratumab [NCT03126591] targeting plateled derived growth factor α (PDGFRα), APX005M [NCT03719430] targeting cluster of differentiation 40 (CD40), Atezolizumab [NCT03474094], Avelumab [NCT04242238], Durvalumab [NCT03317457], and Envafolimab [NCT04480502] targeting programmed death-ligand 1 (PD-L1), ABBV-085 [NCT02565758] targeting leucine-rich repeat containing 15 (LRRC15), CAB-ROR2-ADC [NCT03504488] targeting receptor tyrosine kinase-like

orphan receptor 2 (ROR2) and Ipilimumab [NCT04118166] and Tremelimumab [NCT03317457] targeting cytotoxic T-Lymphocyte-associated protein 4 (CTLA-4).

The PubMed search based on the cell surface-expressed biomarkers targeted by clinically available monoclonal antibodies identified 1856 articles (Figure 1). After screening of the titles and abstracts, 1604 articles were excluded. Subsequently, 252 full-text articles were assessed for eligibility. 171 articles did not meet eligibility criteria: 107 articles did not study expression of the included biomarkers on human STS cells, for 19 articles data was not suitable for extraction, 16 articles had a sample size of less than 4 samples, 11 articles did not have full-text available, 10 articles had more than 5% of samples which were not primary STS and therefore their results were no longer a valid representation of STS samples, and 8 articles were reviews or letters to journals without an accompanying methods section. Data regarding internalization and previously imaged was not always described in STS. Therefore, a separate search was performed to obtain these data from other tissue types (Appendix B). This resulted in an additional 16 included articles. Ultimately, 97 articles were included for this review.

Table 2. Summarized data regarding eleven reviewed biomarkers (in descending order of the modified target selection criteria score).

Biomarker	Therapeutic antibody	N	% positive STS (mean% + range)	Pattern of Expression	Internalization	Previously imaged	Score	Literature
Tumor endothelial marker 1 (TEM1/ endosialin/ CD248)	Ontuxizumab (MORAb-004)	768	77% (55 - 100)	Diffuse	Yes, [19]	NIRF imaging [20]	9	[20-23]
Vascular endothelial growth factor receptor-1 (VEGFR-1)	Aflibercept Bevacizumab	477	76% (22 - 100)	Diffuse	Yes, [24]	NIRF imaging [24,25]	8	[26-33]
Epidermal growth factor receptor (EGFR)	Cetuximab	1918	53% (0 - 100)	Diffuse	Yes, [34]	NIRF imaging [35]	8	[21,36-70]
Vascular endothelial growth factor receptor-2 (VEGFR-2)	Aflibercept Bevacizumab Ramucirumab	449	71% (11 - 100)	Diffuse	Yes, [71]	NIRF imaging [72]	7	[27-30,32,33,73-75]
Insulin-like growth factor 1 receptor (IGF-1R)	Ganitumab (AMG 479) Teprotumumab Cixutumumab Figitumumab	507	63% (25 - 100)	Diffuse	Yes, [76]	NIRF imaging [77]	7	[57,58,78-84]
Platelet derived growth factor receptor α (PDGFRα)	Olaratumab	1536	64% (0 - 100)	Diffuse	Yes, [85]	NIRF imaging [86]	7	[21,28,30,32,36-43,45,76,82,87-92]
Cluster of differentiation 40 (CD40)	APX005M	153	62% (17 - 86)	Diffuse	Yes, [93]	NIRF imaging [94]	7	[95-98]
Programmed death-ligand 1 (PD-L1/ CD 274/ B7-H1)	Atezolizumab Avelumab Durvalumab Envafolimab	1492	31% (0 - 76)	Heterogeneous (focal and diffuse)	Yes, [99]	NIRF imaging [100]	6	[101-118]

2

Table 2. Summarized data regarding eleven reviewed biomarkers (in descending order of the modified target selection criteria score). *(continued)*

Biomarker	Therapeutic antibody	N	% positive STS (mean% + range)	Pattern of Expression	Internalization	Previously imaged	Score	Literature
Leucine-rich repeat containing 15 (LRRC15)	ABBV-085	635	40%	Diffuse	Not described	Not described	4	[102]
Receptor tyrosine kinase-like orphan receptor 2 (ROR2)	CAB-ROR2-ADC	237	72%	Not described	Not described	Not described	3	[119]
Cytotoxic T-Lymphocyte-associated protein 4 (CTLA-4 / CD152)	Ipilimumab Tremelimumab	10	30%	Not described	Yes, [120]	Not with NIRF imaging [120]	2	[53]

Abbreviations: N, total number of samples; STS, soft tissue sarcoma; NIRF, near-infrared fluorescence.
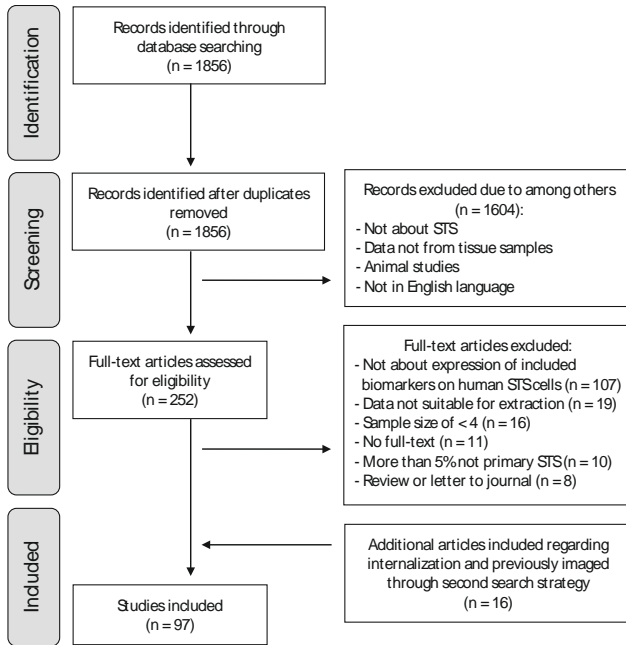
Figure 1. *Flowchart study selection process.*

Candidate biomarkers

A modified Target Selection Criteria TASC)-scoring system was applied to eleven cell surface-expressed biomarkers (Table 1). Seven promising candidate targets for NIRF imaging emerged with a minimum score of 7 out of 9. The biomarkers arranged in descending order based on their scores were: TEM1 (9), VEGFR-1 (8), EGFR (8), VEGFR-2 (7), IGF-1R (7), PDGFRα (7) and CD40 (7). Further details of these biomarkers are described below and in Table 2, focusing on their physiological role, expression in STS, the availability of clinically used monoclonal antibodies targeting these biomarkers, and latest developments.

TEM1

Tumor Endothelial Marker 1, also referred to as Endosialin or CD248, is a highly glycosylated type I transmembrane protein classified among the C-type lectin-like domain superfamily 14. It has been suggested that TEM1 plays a critical role in wound healing and angiogenesis [121,122]. Moreover, while it is expressed minimally in normal conditions, it is markedly upregulated in the setting of injury and malignant tumor growth. In (soft tissue) sarcomas TEM1 was observed to be present on malignant cells [22]. Stromal TEM1 promotes spontaneous metastasis and TEM1-expressing pericytes were shown to facilitate distant site metastasis by stimulating tumor cell intravasation [123]. Furthermore, TEM1 expression is associated with enhanced tumor growth, presumably due to tumor-specific angiogenesis [124].

The presence of the biomarker in STS samples, regardless of the percentage of positive tumor cells, was determined on both tumor and stromal cells for TEM1. In STS, 77% (range 55 – 100%, n=768) of the samples showed presence of TEM1 on average, reported in 4 different articles [20-23]. Staining was performed in 17 subtypes of STS (Appendix C). The expression pattern for TEM1 was diffuse. Corresponding to the expression in other cancer types, TEM1 expression is correlated with advanced tumor grade in STS [121,125].

In MFS it was demonstrated that TEM1 was present in all 34 investigated samples, with a diffuse pattern of expression [21]. Staining was negative or very limited in normal adjacent tissue such as muscular fascia and peripheral nerve bundles. For USTS an average of 81% (range 73 – 89%, n=128) of the samples expressed TEM1, with a diffuse pattern of expression [22,23]. In SS, 71% (range 62 – 80%, n=70) of the tissue samples stained positive for TEM1. The pattern of expression was heterogeneous with samples expressing TEM1 either focally or diffusely. Besides, Thway et al. [23] demonstrated in representative images that the spindle cell component of biphasic SS samples are positive, while the glandular epithelial areas are negative. Regarding monophasic SS, both positive and negative samples were reported [22,23]. Data are summarized in Table 3.

Exclusively Ontuxizumab has been clinically investigated as a therapeutic drug in STS [126]. However, it still has to be modified into a NIRF imaging tracer. A high-affinity human single-chain variable fragment (scFv)-Fc fusion protein (78Fc) targeting TEM1 has been engineered and conjugated with the near-infrared fluorochrome VivoTag-S750, which proved to be an efficient tracer in preclinical osteosarcoma and lung cancer models [20,22,125,127].

In conclusion, TEM1 can be targeted in NIRF imaging by Ontuxizumab upon conjugation to a NIRF dye and small proteins have been produced pre-clinically for similar purposes. A major advantage of TEM1 is that it has minimal to no expression on adjacent normal tissue and therefore it is characterized by a high tumor-to-background ratio. Additional benefits are its diffuse pattern of expression, the high frequency of positivity (STS 77%, MFS 100%, USTS 81% and SS 71%), and its correlation with advanced tumor grades. A disadvantage is its heterogeneous pattern of expression in the SS subtype with samples illustrating focal expression of TEM1.

VEGFR
The VEGFR family consists of the 3 members VEGFR-1, -2 and -3 which are receptors for ligands VEGF-A, -B, -C, -D, and Placenta Growth Factor [128]. The receptors contain a split tyrosine kinase domain and a ligand-binding part. The individual VEGFR members have separate roles in various signaling pathways, but as a family they collectively function as the principal driver of angiogenesis and lymph angiogenesis. Hence, VEGFRs are mainly expressed on vascular and lymphatic endothelial cells in healthy tissue [128-130]. In various tumor types, including STS, they are expressed by both endothelial cells and tumor cells [131]. Here they stimulate

tumor growth [132]. VEGFR-1 and VEGFR-2 have been clinically targeted by antibodies in STS, in contrast to VEGFR-3. Therefore, only VEGFR-1 and VEGFR-2 will be evaluated.

VEGFR-1 presence was found in an average of 76% (range 22 – 100%, n=477) of the STS patients in 8 different studies [26-33]. Staining was performed in 15 STS subtypes (Appendix C). The VEGFR-1 expression pattern was demonstrated to be diffuse. Expression was found in the cytoplasm, and on the nuclear and cell membrane [26,29]. VEGFR-2 expression was present in 71% (range 11 – 100%, n=449) on average in 9 different studies, and 16 STS subtypes were evaluated [27-30,32,33,73-75]. The pattern of expression was heterogeneous, and expression was found in the cytoplasm, and on the nuclear and cell membrane [29,75]. Interestingly, Kilvaer et al. [131] states that VEGFR overexpression is correlated with increased tumor grade.

No data were found for VEGFR immunohistochemical staining in MFS. One paper reported on the presence of VEGFR-1 and VEGFR-2 in USTS and SS [30]. VEGFR-1 and VEGFR-2 expression was found in 68% and 6% of 81 USTS samples respectively. In SS, this was 70% and 4% for respectively VEGFR-1 and VEGFR-2 in 27 samples (Table 3). Moreover, the pattern of expression was described for neither USTS nor SS [30]. Additionally, no distinction was made between monophasic and biphasic SS in the published data.

Ramucirumab binds to VEGFR-2 and is currently in its recruitment phase for clinical testing in SS [133]. Besides, VEGFR-1 and VEGFR-2 may be targeted indirectly using Bevacizumab-IRDye800CW or Aflibercept upon conjugation to a NIRF dye [24,25,134,135]. Recently published study results showed visualization of all 15 included STS patients with Bevacizumab-IRDye800CW targeting VEGF-A. In this paper, *in vivo* tumor-to-background ratios of 2.0-2.5 were found with doses of 10-25mg tracer and no tracer-related adverse events occurred within 2 weeks after surgery [134]. Additionally, targeting tumors with Bevacizumab-IRDye800CW has been investigated extensively in clinical trials for several tumor types [134,136-138]. Here, its tolerable safety profile was confirmed in primary breast cancer patients [139].

In conclusion, VEGFR-1 and VEGFR-2 are receptors that may be targeted indirectly with a tracer, Bevacizumab-IRDye800CW, that has already widely proven its benefit in multiple cancer types. Direct targeting of VEGFR-2 however may additionally be performed with Ramucirumab. Major advantages of VEGFR-1 are the high frequency of positivity in STS (76%), the diffuse pattern of expression in tumors and increasing expression associated with enhanced tumor grade. However, while VEGFR-1 is commonly present in USTS and SS, there is no data concerning its pattern of expression in these STS subtypes. Furthermore, advantages of VEGFR-2 are its high presence of 71% in STS samples and increasing expression associated with enhanced tumor grade. Disadvantages are a heterogeneous, and therefore unpredictable, pattern of expression in the evaluated tissue samples and the fact that only 6% of USTS and 4% of SS are positive. Additionally, both VEGFRs are commonly expressed in healthy tissue, potentially resulting in a low tumor-to-background ratio.

EGFR

Epidermal Growth Factor Receptor is a transmembrane glycoprotein belonging to the ErbB/HER family together with 3 additional distinct receptor tyrosine kinases: ErbB2/HER2, ErbB3/HER3, and ErbB4/HER4 [140]. Seven different ligands trigger intracellular signals for fundamental cellular functions including proliferation, differentiation, migration and survival of tumor cells [141,142]. EGFR is mainly expressed in proliferating keratinocytes [143,144]. In tumors, EGFR overexpression can trigger tumor invasion and metastasis. Furthermore, it is a central regulator of autophagy, which is strongly involved in resistance to cancer therapies [145,146].

EGFR expression in STS was described in 36 scientific papers [21,36-70]. The presence of EGFR on STS tissue was observed in an average of 53% of the samples (range 0 – 100%, n=1918). Expression was evaluated in 29 different subtypes of STS (Appendix C). The pattern of expression was diffuse. Importantly, EGFR expression in STS was strongly correlated to higher histological grade [41,43,65].

In MFS, EGFR presence was observed in an average of 38% (range 0 – 89%, n=97) of the samples in 3 articles (Table 3) [21,48,60]. This wide range might be explained by the fact that 1 article included 10 low-grade MFS samples of which none expressed EGFR. The remaining 2 articles had a higher percentage of positive samples with a diffuse pattern of expression. This confirms the positive correlation of EGFR expression with increased histological grade STS [21,48,60]. For USTS, EGFR expression was detected in an average of 62% (range 5 – 95%, n=287) of the samples with a heterogeneous pattern of expression. Similar to MFS, a wide range was observed with 1 article reporting 5% of 200 samples to be positive for EGFR staining, 1 article reporting 58% in 24 samples and 2 articles reporting 91% and 95% positive samples in 44 and 19 samples, respectively. Here, the correlation to increased histological grade could not explain the variable expression [45,52,60,65]. Lastly, EGFR presence was seen in an average of 86% (range 71 – 100%, n=160) of the SS samples. The pattern of expression was noticeably heterogeneous, extending from focal to diffuse expression [46,52,60,63-65]. Furthermore, Gusterson et al. [52] and Sato et al. [60] compared the spindle cell and epithelial components of biphasic SS samples. They described that the former is strongly positive, whereas the latter is mainly negative for EGFR expression. Regarding monophasic SS, both positive and negative samples were reported.

Currently, Cetuximab is the only clinically investigated EGFR-targeting monoclonal antibody for STS [147]. It has been conjugated to IRDye800 and examined in several clinical trials in other tumor types. To appraise its utility in the detection of metastatic lymph nodes in pancreatic cancer, a total of 144 human lymph nodes were evaluated *ex-vivo*. The Cetuximab-IRDye800 conjugate demonstrated a sensitivity and specificity of 100% and 78% [148]. Additionally, no grade 2 or higher adverse events were observed with Cetuximab-IRDye800 in glioblastoma and head and neck squamous cell carcinoma [149,150].

A clinical trial investigating the use of ABY-029, an affibody conjugated to IRDye800CW targeting EGFR, is in the recruitment phase for targeting STS [151]. Based on pre-clinical research it is a promising tracer for STS and safe for human use [35,152]. Other clinical trials in their recruitment phase explore the use of Panitumumab-IRDye800 in imaging of head and neck cancer, lung cancer, and metastatic lymph nodes [153-155].

In summary, there are multiple promising tracers available which can be applied for NIR fluorescence-guided surgery in STS. Main advantages of EGFR, apart from the readily available tracers, are its diffuse pattern of expression in STS in general, the increased expression in STS of higher histological grade, and the high frequency of expression (88%) among SS samples. Yet, drawbacks are the mediocre percentage (54%) of positive tumor samples in STS in general and the highly heterogeneous expression pattern in SS.

IGF-1R

Insulin-like Growth Factor 1 Receptor is a receptor tyrosine kinase that is activated upon binding with IGF-1 or IGF-2. Under normal physiological circumstances this provokes a chain of signaling events that induce cellular transformations such as hypertrophy in skeletal muscle. IGF-1R is upregulated in multiple malignancies, including prostate, breast and lung cancer, where it is involved in tumor growth. Besides, it enables cancer cells to resist the cytotoxic properties of radiotherapy and chemotherapeutic drugs by inducing an anti-apoptotic effect [18].

IGF-1R presence was detected in 63% (range 25 – 100%, n=507) of STS samples on average in 9 different studies [57,58,78-84]. Staining was performed in 15 subtypes of STS (Appendix C). The receptor was dispersed diffusely in the cytoplasm, and on the nuclear and cell membrane [57,79,81]. No correlation between histological grade and IGF-1R expression was observed [58,78].

No data are available on IGF-1R presence in MFS. Presence of IGF-1R in USTS and SS was evaluated in 1 and 4 articles respectively [76,79,81,82,84]. IGF-1R presence was found in 25% of the USTS samples (n=120), while in SS an average of 57% (range 35 – 100%, n=195) of the samples stained positive. The pattern of expression was described for neither (Table 3). However, Friedrichs et al. [79] reported that vast areas of tumorous tissue showed membranous staining in monophasic (comprising spindle cells) SS. In contrast, biphasic SS samples displayed predominantly positive staining in the epithelial component. Regarding monophasic SS, both positive and negative samples were reported [76,79,82,84].

Clinical trials targeting IGF-1R in STS have been conducted with Teprotumumab, Cixutumumab, Figitumumab and Ganitumab [156-160]. Nevertheless, these monoclonal antibodies have not been evaluated for their potential in NIRF imaging.

AVE-1642, a humanized anti-IGF-1R antibody, labelled with Alexa 680 has been pre-clinically investigated in *in vivo* breast cancer models and adequately identified receptor expression [161].

Overall, IGF-1R may be targeted in NIRF imaging by several potential antibodies after conjugation to a NIRF dye. In addition, pre-clinical advances have resulted in promising tracers that may find future clinical use. An advantage of IGF-1R is its relatively common (63%) presence in all STS samples. However, its expression has no correlation with tumor grade, and data on pattern of expression in MFS, USTS and SS is limited.

PDGFR

Platelet-Derived Growth Factor is a receptor tyrosine kinase characterized by two isoforms, PDGFRα and PDGFRβ [162]. The receptors can be activated after binding by ligands from the PDGF-family. Upon activation, PDGFR is known to control angiogenesis in endothelial cells, and cell migration and growth in mesenchymal cells. Moreover, in healthy tissue both PDGFRs are mainly expressed in mesenchymal cells during inflammation, whereas during non-inflammatory conditions the expression is minimal [163,164]. In tumor biology, PDGFR activation stimulates cell growth and enhances metastatic behavior by attracting fibroblasts, which secrete factors that promote proliferation and migration of tumor cells. Both PDGFRα and -β are expressed by tumor cells of STS, yet expression of specifically PDGFRα is evaluated in this review as a monoclonal antibody against this receptor has been clinically tested in STS, while not against PDGFRβ [37,41,165,166].

Based on the literature search, PDGFRα was present in 64% of STS samples on average (range 0 – 100%, n=1536) in 21 different articles [21,28,30,32,36-43,45,76,82,87-92]. Expression was evaluated in 22 different subtypes of STS (Appendix C). The pattern of expression was diffuse, and expression was identified in the cytoplasm, and on the nuclear and cell membrane of the tumor cells [40,88,167].

PDGFRα expression in the specific STS subtypes of interest, MFS, USTS and SS, have been evaluated separately in respectively 1, 4 and 5 articles. In MFS PDGFRα was present in 77% of 34 tissue samples [21]. In USTS, 78% of the tumors (range 63 – 99%, n=475) were positive for PDGFRα, while for SS 69% (range 44 – 84%, n=136) stained positive. Moreover, expression was reported to be diffuse in USTS. No data regarding the pattern of expression of MFS and SS were reported [30,45,80,82,90,92]. However, opposing data was published regarding differences in expression of either spindle cell or epithelial components in biphasic SS. While Fleuren et al. [90] displayed images where exclusively the spindle cell component expressed PDGFRα, Lopez-Guerrero et al. [92] reported that membranous staining was more prominent in the epithelial component. Regarding monophasic SS, both positive and negative samples were reported. Data are summarized in Table 3.

Multiple drugs targeting PDGFRα are currently FDA approved or subject to clinical trials. However, Olaratumab is the only monoclonal antibody that has been clinically investigated for STS. It binds specifically PDGFRα [168]. No clinical NIRF imaging studies have been performed using Olaratumab conjugated with a fluorophore in any cancer type.

In summary, PDGFRα may be targeted in NIRF imaging by Olaratumab after conjugation to a NIRF dye. Advantages of PDGFRα are its relatively regular (65%) presence in STS samples and its diffuse pattern of expression in specifically USTS with 78% of samples expressing PDGFRα. Disadvantages are the non-reported patterns of expression for MFS and SS, and no article addressed a correlation between enhanced PDGFRα expression and histological grade.

CD40

Cluster of Differentiation 40 is a member of the tumor necrosis factor family and can be ligated by CD40 Ligand (CD40L). CD40 is detected on dendritic cells, B-cells and myeloid cells that can mediate cytotoxic T-cell priming upon CD40L ligation [169]. Moreover, it is constitutively expressed on platelets, smooth muscle cells and endothelial cells [170]. In cancer, CD40 has been found in nearly all B-cell malignancies and many solid tumors, where it induces a direct cytotoxic effect in the absence of immune accessory cells [171]. It is hypothesized that it confers a growth and survival stimulus via signaling pathways such as PI3Kinase/Akt and NFκB and/ or that it modulates anti-tumor immune responses [172].

CD40 was present in 62% of STS samples (range 17 – 86%, n=153) on average in 4 different scientific papers [95-98]. The pattern of expression was diffuse, when assessed in 7 subtypes (Appendix C). Expression was observed on the membrane and in the cytoplasm of tumor cells [95-98]. No association between enhanced CD40 expression and histological grade was found after comparing low-grade to high-grade STS samples [97]. Furthermore, no articles published data regarding CD40 expression on MFS, USTS and SS separately.

A phase II clinical trial applying APX005M, a second-generation agonistic CD40 monoclonal antibody, combined with Doxorubicin in STS is currently recruiting participants [173]. Nonetheless, the antibody has not yet been evaluated for NIRF imaging and no other CD40-targeting drug has thus far been clinically examined for CD40.

Apart from 2 articles focusing on respectively B-cell activation by targeting CD40 with nanoparticles and cerebral ischemia by targeting CD40 with an anti-CD40 antibody conjugated to Cy5.5, no pre-clinical advances in the field of NIRF imaging can be addressed using CD40 as a target [94,174].

In conclusion, APX005M may be utilized as tracer after conjugation to a NIRF dye for imaging in STS. Pre-clinical studies have developed tracers targeting CD40, yet these have not been tested in STS models thus far. Advantages of CD40 are a diffuse pattern of expression and the fact that expression is relatively common (62%) in STS samples in general. Disadvantages are the small number of evaluated STS samples and the lack of data regarding CD40 expression in MFS, USTS and SS.

Table 3. Summarized data regarding biomarkers in Myxofibrosarcoma, Undifferentiated Soft Tissue Sarcoma, and Synovial Sarcoma.

Biomarker	N	Positive tumors mean% (range)	Expression pattern	Present after RTx	Literature
Myxofibrosarcoma					
TEM1	34	100 (100)	Diffuse	Yes, [21]	[21]
EGFR	97	38 (0 – 89)	Heterogeneous	Yes, [21]	[21,48,60]
PDGFRα	34	77 (77)	Not described	Yes, [21]	[21]
Undifferentiated Soft Tissue Sarcoma					
TEM1	128	81 (73 – 89)	Diffuse	N.D.	[22,23]
VEGFR-1	81	68 (68)	Not described	N.D.	[30]
EGFR	287	62 (5 – 95)	Heterogeneous	N.D.	[45,52,60,65]
VEGFR-2	81	6 (6)	Not described	N.D.	[30]
IGF-1R	120	25 (25)	Not described	N.D.	[82]
PDGFRα	432	79 (63 – 99)	Diffuse	N.D.	[30,45,82]
Synovial Sarcoma					
TEM1	70	71 (62 – 80)	Heterogeneous	N.D.	[22,23]
VEGFR-1	27	70 (70)	Not described	N.D.	[21]
EGFR	160	86 (71 – 100)	Heterogeneous	Yes, [175]	[46,52,60,63-65]
VEGFR-2	27	4 (4)	Not described	N.D.	[21]
IGF-1R	195	57 (35 – 80)	Not described	N.D.	[76,79,81,84]
PDGFRα	136	69 (44 – 84)	Not described	N.D.	[30,76,90,92]

Abbreviations: N, total number of samples and/or cell lines; STS, soft tissue sarcoma; RTx, radiotherapy; N.D. not described. No distinction was made between monophasic and biphasic Synovial Sarcoma.

Potential NIRF imaging tracers safety profile

In this review, 7 potential targets for fluorescence-guided surgery of STS (TEM1, VEGFR-1, EGFR, VEGFR-2, IGF-1R, PDGFRα, and CD40) were selected based on antibodies that are clinically available and mostly used in the antibody-based therapy of STS. Several tracers have already proven to be well suitable for NIRF imaging. Among these tracers, Bevacizumab-IRDye800CW targeting VEGF-A (indirectly VEGFR-1 and VEGFR-2) has already shown promising results in STS [134]. Besides, Cetuximab-IRDye800 targeting EGFR is an adequate tracer in several tumor types [148-150]. This section elaborates on clinically available monoclonal antibodies which can be modified into tracers: Ontuxizumab targeting TEM1, Teprotumumab, Cixutumumab and Figitumumab targeting IGF-1R, and Olaratumab targeting PDGFRα [126,158-160,176-179]. APX005M targeting CD40 is currently under investigation and therefore its efficacy and safety profile in STS are yet to be determined. In contrast to therapy, a single dose of tracer is injected for imaging and an increase in adverse effects compared to therapy is not expected. Further, no increase in adverse effects is expected after conjugation of a fluorophore and antibody [134,180-182]. This paragraph summarizes the safety profiles of each clinically available monoclonal antibody extracted from advanced clinical trials conducted with STS-patients

to evaluate their potential for translation towards NIRF imaging. Only high grade (grade ≥3) Adverse Events (AE) are displayed.

Ontuxizumab was compared to a placebo when both were combined with Gemcitabine and Docetaxel. While the total of grade ≥3 AEs was not reported, the incidence of Serious Adverse Events (SAE) was comparable between Ontuxizumab and placebo (50% vs 48%). The most frequent treatment related SAEs were pyrexia (4% vs 0%) and anemia (1% vs 3%) (Appendix D). No substantial differences were observed in laboratory values or electrocardiogram parameters [126].

Targeting IGF-1R, Teprotumumab, Cixutumab, and Figitumumab were investigated as a monotherapy. These trials have reported a minor incidence of high-grade AEs. AEs such as hyperglycemia, pain, thrombocytopenia, and vomiting were the most common high-grade AEs with incidences ranging from 3–5%. Of all included study subjects, 10% and 17% of patients acquired grade ≥3 AEs for Teprotumumab and Figitumumab, respectively. Among these 3 antibodies, Teprotumumab was demonstrated to have the most tolerable and Cixutumumab the most toxic safety profile in STS [158-160].

Two studies on Olaratumab reported grade ≥3 Adverse Events (AE) in 58–67% of the patients when combined with Doxorubicin alone [177,183]. In addition, 2 studies observed contrasting AEs when Olaratumab plus Doxorubicin was compared to Doxorubicin. A phase 2 trial observed an increased incidence of high-grade AEs for the combination therapy while a phase 3 trial found no significant differences and therefore concluded no additional adverse events to be attributed to Olaratumab [176,177]. Hematologic grade ≥3 AEs were most common in these trials with incidences reaching 40–50% (Appendix D).

Discussion

Research aim

The success of surgical treatment for localized STS highly depends on complete tumor resection as positive margins are associated with LR and decreased overall survival. Determining the surgical margin is a major challenge for STS surgeons as they generally try to balance the aim of a functional limb against the risk of LR. Real-time tumor-specific imaging can improve surgical margins by visualizing tumor tissue during resection. This review selected TEM1 (score 9), VEGFR-1 (score 8), EGFR (score 8), VEGFR-2 (score 7), IGF-1R (score 7), PDGFRα (score 7) and CD40 (score 7) as most promising cell surface-expressed biomarkers for tumor-specific NIRF imaging in STS, for which clinically available monoclonal antibodies are already present. Additionally, these potential future NIRF tracers, which are antibodies that have already been clinically tested in STS but not yet conjugated to a NIRF-dye for imaging practices, are expected to be safe for their use in NIRF guided surgery.

Comparing the selected biomarkers
All of the suitable biomarkers have already been evaluated for NIRF imaging pre-clinically, demonstrating their potential [19,23,24,71,80,85,93]. Furthermore, all of the selected cell surface-expressed biomarkers internalize after binding with an antibody (derivative) [18,23,33,70,75,84,92]. This causes a better tumor-to-background ratio and a long-lasting signal important for fluorescence-guided surgery [14]. However, indirect targeting of VEGFR-1 and VEGFR-2 by targeting VEGF-A with for instance Bevacizumab-IRDye800CW has not been proven to result in internalization of tracers.

TEM1 and VEGFR-1 were most frequently present in STS samples, 77% and 76% respectively. VEGFR-2 was third most frequently expressed (71%), followed by PDGFRα (64%), IGF-1R (63%), CD40 (62%), and EGFR (53%). Furthermore, apart from CD40 (n=153), presence of every biomarker of the top 7 has been studied in a large number of STS samples. Therefore, the summarized data in this review are a good representation of biomarker presence in STS patients: EGFR (n=1918), PDGFRα (n=1536), TEM1 (n=768), IGF-1R (n=507), VEGFR-1 (n=477), and VEGFR-2 (n=449).

A particularly important parameter for successful NIRF imaging, which is not included in the TASC score, is the tumor-to-background ratio of a biomarker. With the currently available literature it is impossible to address the expression of each biomarker in healthy tissue, and thus the tumor-to-background ratio, because data on expression of the biomarkers in normal tissue is very limited. Nevertheless, VEGFR-1 and VEGFR-2 are highly expressed in healthy tissue, while TEM1 and PDGFRα are biomarkers with low expression in healthy tissue. TEM1 has already shown high tumor-to-background ratios with immunohistochemistry [21]. However, both biomarkers are expressed in inflammatory tissue as well as in tumors [22,184]. As STS can be surrounded by inflammation during their growth, it is possible that no clear distinction can be made between tumor and surrounding inflammatory tissue [185]. Unfortunately, none of the selected studies reported on inflammation status of surrounding tissue. In addition, neoadjuvant therapy is frequently used in STS treatment. Successful fluorescence-guided surgery is only possible if overexpression of cell surface-expressed biomarkers is preserved after neoadjuvant therapy. It was demonstrated that EGFR, TEM1 and PDGFRα expression is preserved after neoadjuvant radiotherapy of MFS [21]. This has also been confirmed for EGFR in SS [175]. No other data is available on expression of these or the remaining evaluated biomarkers after neoadjuvant therapy in STS. Therefore, further research is needed to assess if surrounding inflammatory tissue or neoadjuvant therapy interferes with tumor border identification in STS.

MFS, USTS and SS
We chose to focus on MFS, USTS and SS because of their aggressive and infiltrative growth pattern. TEM1 was present in 100% of the MFS samples (Table 3). Besides, its pattern of expression was diffuse in all tested MFS samples [21]. This indicates that TEM1 is likely to be extensively expressed in tumors of every individual MFS patient. Besides, a sharp contrast

between tumor and adjacent normal tissue, such as fascia, muscle, and fat, was seen on microscopic pictures of stained MFS samples. This clearly identifies the tumor border and therefore TEM1 seems the most promising biomarker to facilitate complete MFS resections using NIRF imaging [21].

For USTS the average presence of TEM1 and PDGFRα was 81 and 79% of the tumor samples. Apart from being expressed in a substantial percentage of USTS samples, TEM1 and PDGFRα were primarily expressed diffusely [21,22,29,44,81]. However, there is no data published regarding contrast between expression on tumor and normal tissue in USTS. According to the human protein atlas TEM1 and PDGFRα expression is not detected in skeletal muscle tissue and adipose tissue. For smooth muscle tissue, TEM1 displays low expression, while PDGFRα is not detected [186]. These characteristics suggest that TEM1 and PDGFRα are promising biomarkers for NIRF imaging in USTS patients.

In SS, presence of TEM1 and EGFR was demonstrated in 71 and 86% of the assessed samples. EGFR and TEM1 are both characterized by a variable expression pattern in SS [22,23,46,52,60,63-65]. Moreover, both targets are reported to be not or minimally expressed in the epithelial components of biphasic SS tumors, while it was expressed in the spindle cell components. This might complicate NIRF imaging of biphasic SS tumors when solely targeting either of these biomarkers. Interestingly, EGFR remains present on SS after neoadjuvant radiotherapy. This has not been researched for TEM1, therefore providing EGFR a further advantage over TEM1 [175].

Lastly, most biomarkers are not present in 100% of the evaluated STS (subtype) tumor samples. The disadvantage of not knowing expression in advance to surgery can be overcome by evaluating the expression of each biomarker in preoperative biopsies to assess which biomarker would be most appropriate to target for NIRF imaging during surgery.

Comparison of potential NIRF imaging tracers
Several monoclonal antibodies targeting STS have already been adjusted to tracers suitable for NIRF imaging and additional monoclonal antibodies used in therapy may be applicable for future NIRF imaging in STS after conjugation to a fluorescent dye/fluorophore. Five distinct antibodies have been assessed for their toxicity profile in STS (Appendix D). Nevertheless, comparing the results of these drugs is complicated as Olaratumab and Ontuxizumab have solely been investigated combined with chemo-therapeutic agents. Still, no evident increase in high-grade toxicity was detected for both antibodies when compared to placebo suggesting a tolerable safety profile. These results are confirmed in trials investigating Olaratumab in metastatic gastrointestinal stromal tumor (GIST) and Ontuxizumab in metastatic colorectal cancer where respectively 10 and 11% grade of ≥3 treatment-related adverse events were reported [178,187]. These data are similar to the percentages of patients acquiring grade ≥3 AE after treatment with IGF-1R targeting antibodies (Teprotomumab, Figitumumab and Cixutumumab) and therefore all antibodies studied here can be safely modified into NIRF imaging tracers.

It should, however, be emphasized that data on toxicity in antibody-based therapy are presumably an overestimation for imaging, because doses of antibodies injected for NIRF imaging are substantially lower compared to therapeutic doses. For instance, a single dose of 10mg Bevacizumab-IRDye800CW was found to be optimal for NIRF imaging in STS, whereas therapeutic doses comprise of 5-15mg/kg Bevacizumab every 2-3 weeks [149]. Consequently, the serum concentration of the antibody (conjugated to a fluorophore) is lower when used for NIRF imaging and less toxicity of these monoclonal antibodies is expected [188]. Preferably, dose-finding studies, where single and low doses of the five evaluated compounds have been given to STS patients, should be reviewed to predict toxicity when used for NIRF imaging, yet such articles have not been published.

Strengths and limitations
A first limitation is that the heterogeneity of the included studies complicates ranking of the biomarkers. Studies have used various antibodies for immunohistochemistry. The percentage of positive tumors may be variable depending on type of antibodies, dilutions, epitope, and clone used [189]. Also, immunohistochemistry protocols differ between labs which may cause variable results while the same type of antibodies is used. This creates discrepancy in immunohistochemical results published by different researchers. Secondly, the heterogeneity of STS complicates selecting the optimal biomarkers. There are over 50 subtypes of STS, and different subtypes have different biomarker expression patterns [65]. Therefore, finding one optimal biomarker for each subtype is challenging.

A strength is our focus on MFS, USTS and SS as they are STS subtypes which show an infiltrative growth pattern, and as a consequence have high percentages of positive margins and high percentages of LR. Patients with these subtypes might benefit the most from implementation of NIRF imaging. Nevertheless, published data regarding some biomarkers in MFS is scarce. Another strength is that clinically available monoclonal antibodies were the starting point of this systematic review. This was because primary development of a NIRF tumor-specific tracer for a rare disease such as STS is time consuming and costly which hampers rapid clinical implementation. However, alternative antigens that might be interesting for tumor-specific imaging in STS can be missed be-cause no clinically available antibodies (or antibody derivatives) are available. Nevertheless, clinical implementation is of utmost importance to prove feasibility of NIRF imaging for STS surgery and subsequently stimulate primary development of STS specific tracers. This progression is enabled by this review as each evaluated biomarker is accompanied by a clinically available antibody (derivative) that can be transformed into a NIRF tracer.

Conclusions

In STS, TEM1, VEGFR-1, EGFR, VEGFR-2, IGF-1R, PDGFRα and CD40 were identified in descending order as the most suitable biomarkers for NIRF imaging according to the modified TASC-scoring system. However, as the category of STS comprises an extensive and heterogenous group of tumors, it was chosen to specify the most optimal target for three common subtypes with infiltrative growth that are characterized by high rates of local recurrence: MFS, USTS and SS. While TEM1 was the optimal target for MFS, both TEM1 and PDGFRα were concluded to be most promising for USTS. In SS EGFR was considered most promising, yet closely followed by TEM1, VEGFR-1 and PDGFRα. However, as expression of biomarkers and its extent is often not certain, evaluation of the expression of biomarkers in preoperative biopsies could assist in designating the appropriate tracer for every patient. More importantly, for their potential use in NIRF imaging, data on contrast of expression on malignant and adjacent normal tissue is needed. Altogether, this systematic review paves the way for implementing fluorescence-guided surgery to optimize STS treatment.

2

References

1. Board, W.C.o.T.E. *Tissue and Bone Tumours: WHO Classification of Tumours*, 5th edition, volume 3 (5th ed.) ed.; IARC Publications: 2020.

2. Stiller, C.A.; Trama, A.; Serraino, D.; Rossi, S.; Navarro, C.; Chirlaque, M.D.; Casali, P.G. Descriptive epidemiology of sarcomas in Europe: report from the RARECARE project. *Eur J Cancer* **2013**, *49*, 684-695, doi:10.1016/j.ejca.2012.09.011.

3. Group., E.E.S.N.W. Soft tissue and visceral sarcomas: ESMO Clinical Practice Guidelines for diagnosis, treatment and follow-up. *Ann Oncol* **2014**, *25 Suppl 3*, iii102-112, doi:10.1093/annonc/mdu254.

4. Enneking, W.F.; Spanier, S.S.; Goodman, M.A. A system for the surgical staging of musculoskeletal sarcoma. 1980. *Clin Orthop Relat Res* **2003**, 10.1097/01.blo.0000093891.12372.0f, 4-18, doi:10.1097/01.blo.0000093891.12372.0f.

5. Smolle, M.A.; Sande, M.V.; Callegaro, D.; Wunder, J.; Hayes, A.; Leitner, L.; Bergovec, M.; Tunn, P.U.; van Praag, V.; Fiocco, M., et al. Individualizing Follow-Up Strategies in High-Grade Soft Tissue Sarcoma with Flexible Parametric Competing Risk Regression Models. *Cancers* **2019**, *12*, doi:10.3390/cancers12010047.

6. Willeumier, J.; Fiocco, M.; Nout, R.; Dijkstra, S.; Aston, W.; Pollock, R.; Hartgrink, H.; Bovee, J.; van de Sande, M. High-grade soft tissue sarcomas of the extremities: surgical margins influence only local recurrence not overall survival. *Int Orthop* **2015**, *39*, 935-941, doi:10.1007/s00264-015-2694-x.

7. Zagars, G.K.; Ballo, M.T.; Pisters, P.W.; Pollock, R.E.; Patel, S.R.; Benjamin, R.S.; Evans, H.L. Prognostic factors for patients with localized soft-tissue sarcoma treated with conservation surgery and radiation therapy: an analysis of 1225 patients. *Cancer* **2003**, *97*, 2530-2543, doi:10.1002/cncr.11365.

8. O'Sullivan, B.; Davis, A.M.; Turcotte, R.; Bell, R.; Catton, C.; Chabot, P.; Wunder, J.; Kandel, R.; Goddard, K.; Sadura, A., et al. Preoperative versus postoperative radiotherapy in soft-tissue sarcoma of the limbs: a randomised trial. *Lancet* **2002**, *359*, 2235-2241, doi:10.1016/s0140-6736(02)09292-9.

9. Yoo, H.J.; Hong, S.H.; Kang, Y.; Choi, J.Y.; Moon, K.C.; Kim, H.S.; Han, I.; Yi, M.; Kang, H.S. MR imaging of myxofibrosarcoma and undifferentiated sarcoma with emphasis on tail sign; diagnostic and prognostic value. *Eur Radiol* **2014**, *24*, 1749-1757, doi:10.1007/s00330-014-3181-2.

10. Chen, S.; Huang, W.; Luo, P.; Cai, W.; Yang, L.; Sun, Z.; Zheng, B.; Yan, W.; Wang, C. Undifferentiated Pleomorphic Sarcoma: Long-Term Follow-Up from a Large Institution. *Cancer Manag Res* **2019**, *11*, 10001-10009, doi:10.2147/CMAR.S226896.

11. Lewis, J.J.; Antonescu, C.R.; Leung, D.H.; Blumberg, D.; Healey, J.H.; Woodruff, J.M.; Brennan, M.F. Synovial sarcoma: a multivariate analysis of prognostic factors in 112 patients with primary localized tumors of the extremity. *J Clin Oncol* **2000**, *18*, 2087-2094, doi:10.1200/jco.2000.18.10.2087.

12. Look Hong, N.J.; Hornicek, F.J.; Raskin, K.A.; Yoon, S.S.; Szymonifka, J.; Yeap, B.; Chen, Y.L.; DeLaney, T.F.; Nielsen, G.P.; Mullen, J.T. Prognostic factors and outcomes of patients with myxofibrosarcoma. *Ann Surg Oncol* **2013**, *20*, 80-86, doi:10.1245/s10434-012-2572-3.

13. Odei, B.; Rwigema, J.C.; Eilber, F.R.; Eilber, F.C.; Selch, M.; Singh, A.; Chmielowski, B.; Nelson, S.D.; Wang, P.C.; Steinberg, M., et al. Predictors of Local Recurrence in Patients With Myxofibrosarcoma. *Am J Clin Oncol* **2018**, *41*, 827-831, doi:10.1097/coc.0000000000000382.

14. Hernot, S.; van Manen, L.; Debie, P.; Mieog, J.S.D.; Vahrmeijer, A.L. Latest developments in molecular tracers for fluorescence image-guided cancer surgery. *Lancet Oncol* **2019**, *20*, e354-e367, doi:10.1016/s1470-2045(19)30317-1.

15. Keereweer, S.; Van Driel, P.B.; Snoeks, T.J.; Kerrebijn, J.D.; Baatenburg de Jong, R.J.; Vahrmeijer, A.L.; Sterenborg, H.J.; Lowik, C.W. Optical image-guided cancer surgery: challenges and limitations. *Clin Cancer Res* **2013**, *19*, 3745-3754, doi:10.1158/1078-0432.Ccr-12-3598.

16. Barth, C.W.; Gibbs, S.L. Fluorescence Image-Guided Surgery - a Perspective on Contrast Agent Development. *Proc SPIE Int Soc Opt Eng* **2020**, *11222*, doi:10.1117/12.2545292.

17. Moher, D.; Liberati, A.; Tetzlaff, J.; Altman, D.G. Preferred reporting items for systematic reviews and meta-analyses: the PRISMA statement. *PLoS Med* **2009**, *6*, e1000097, doi:10.1371/journal.pmed.1000097.

18. Bosma, S.E.; van Driel, P.B.; Hogendoorn, P.C.; Dijkstra, P.S.; Sier, C.F. Introducing fluorescence guided surgery into orthopedic oncology: A systematic review of candidate protein targets for Ewing sarcoma. *Journal of surgical oncology* **2018**, *118*, 906-914, doi:10.1002/jso.25224.

19. Lange, S.E.; Zheleznyak, A.; Studer, M.; O'Shannessy, D.J.; Lapi, S.E.; Van Tine, B.A. Development of 89Zr-Ontuxizumab for in vivo TEM-1/endosialin PET applications. *Oncotarget* **2016**, *7*, 13082-13092, doi:10.18632/oncotarget.7552.

20. Guo, Y.; Hu, J.; Wang, Y.; Peng, X.; Min, J.; Wang, J.; Matthaiou, E.; Cheng, Y.; Sun, K.; Tong, X., et al. Tumour endothelial marker 1/endosialin-mediated targeting of human sarcoma. *Eur J Cancer* **2018**, *90*, 111-121, doi:10.1016/j.ejca.2017.10.035.

21. de Gooyer, J.M.; Versleijen-Jonkers, Y.M.H.; Hillebrandt-Roeffen, M.H.S.; Frielink, C.; Desar, I.M.E.; de Wilt, J.H.W.; Flucke, U.; Rijpkema, M. Immunohistochemical selection of biomarkers for tumor-targeted image-guided surgery of myxofibrosarcoma. *Sci Rep* **2020**, *10*, 2915, doi:10.1038/s41598-020-59735-4.

22. Rouleau, C.; Curiel, M.; Weber, W.; Smale, R.; Kurtzberg, L.; Mascarello, J.; Berger, C.; Wallar, G.; Bagley, R.; Honma, N., et al. Endosialin protein expression and therapeutic target potential in human solid tumors: sarcoma versus carcinoma. *Clin Cancer Res* **2008**, *14*, 7223-7236, doi:10.1158/1078-0432.ccr-08-0499.

23. Thway, K.; Robertson, D.; Jones, R.L.; Selfe, J.; Shipley, J.; Fisher, C.; Isacke, C.M. Endosialin expression in soft tissue sarcoma as a potential marker of undifferentiated mesenchymal cells. *British journal of cancer* **2016**, *115*, 473-479, doi:10.1038/bjc.2016.214.

24. Zhang, J.; Razavian, M.; Tavakoli, S.; Nie, L.; Tellides, G.; Backer, J.M.; Backer, M.V.; Bender, J.R.; Sadeghi, M.M. Molecular imaging of vascular endothelial growth factor receptors in graft arteriosclerosis. *Arterioscler Thromb Vasc Biol* **2012**, *32*, 1849-1855, doi:10.1161/atvbaha.112.252510.

25. Saban, M.R.; Backer, J.M.; Backer, M.V.; Maier, J.; Fowler, B.; Davis, C.A.; Simpson, C.; Wu, X.R.; Birder, L.; Freeman, M.R., et al. VEGF receptors and neuropilins are expressed in the urothelial and neuronal cells in normal mouse urinary bladder and are upregulated in inflammation. *American journal of physiology. Renal physiology* **2008**, *295*, F60-72, doi:10.1152/ajprenal.00618.2007.

26. Andersson, M.K.; Goransson, M.; Olofsson, A.; Andersson, C.; Aman, P. Nuclear expression of FLT1 and its ligand PGF in FUS-DDIT3 carrying myxoid liposarcomas suggests the existence of an intracrine signaling loop. *BMC Cancer* **2010**, *10*, 249, doi:10.1186/1471-2407-10-249.

27. Arita, S.; Kikkawa, F.; Kajiyama, H.; Shibata, K.; Kawai, M.; Mizuno, K.; Nagasaka, T.; Ino, K.; Nomura, S. Prognostic importance of vascular endothelial growth factor and its receptors in the uterine sarcoma. *International journal of gynecological cancer : official journal of the International Gynecological Cancer Society* **2005**, *15*, 329-336, doi:10.1111/j.1525-1438.2005.15225.x.

28. Gaumann, A.; Strubel, G.; Bode-Lesniewska, B.; Schmidtmann, I.; Kriegsmann, J.; Kirkpatrick, C.J. The role of tumor vascularisation in benign and malignant cardiovascular neoplasms: a comparison of cardiac myxoma and sarcomas of the pulmonary artery. *Oncology reports* **2008**, *20*, 309-318.

29. Itakura, E.; Yamamoto, H.; Oda, Y.; Tsuneyoshi, M. Detection and characterization of vascular endothelial growth factors and their receptors in a series of angiosarcomas. *J Surg Oncol* **2008**, *97*, 74-81, doi:10.1002/jso.20766.

30. Kampmann, E.; Altendorf-Hofmann, A.; Gibis, S.; Lindner, L.H.; Issels, R.; Kirchner, T.; Knosel, T. VEGFR2 predicts decreased patients survival in soft tissue sarcomas. *Pathology, research and practice* **2015**, *211*, 726-730, doi:10.1016/j.prp.2015.04.015.

2

31. Lee, Y.J.; Chung, J.G.; Chien, Y.T.; Lin, S.S.; Hsu, F.T. Suppression of ERK/NF-κB Activation Is Associated With Amentoflavone-Inhibited Osteosarcoma Progression In Vivo. *Anticancer Res* **2019**, *39*, 3669-3675, doi:10.21873/anticanres.13515.

32. Yonemori, K.; Tsuta, K.; Ando, M.; Hirakawa, A.; Hatanaka, Y.; Matsuno, Y.; Chuman, H.; Yamazaki, N.; Fujiwara, Y.; Hasegawa, T. Contrasting prognostic implications of platelet-derived growth factor receptor-beta and vascular endothelial growth factor receptor-2 in patients with angiosarcoma. *Ann Surg Oncol* **2011**, *18*, 2841-2850, doi:10.1245/s10434-011-1640-4.

33. Young, R.J.; Woll, P.J.; Staton, C.A.; Reed, M.W.; Brown, N.J. Vascular-targeted agents for the treatment of angiosarcoma. *Cancer chemotherapy and pharmacology* **2014**, *73*, 259-270, doi:10.1007/s00280-013-2345-0.

34. Harding, J.; Burtness, B. Cetuximab: an epidermal growth factor receptor chemeric human-murine monoclonal antibody. *Drugs Today (Barc)* **2005**, *41*, 107-127, doi:10.1358/dot.2005.41.2.882662.

35. Samkoe, K.S.; Sardar, H.S.; Bates, B.D.; Tselepidakis, N.N.; Gunn, J.R.; Hoffer-Hawlik, K.A.; Feldwisch, J.; Pogue, B.W.; Paulsen, K.D.; Henderson, E.R. Preclinical imaging of epidermal growth factor receptor with ABY-029 in soft-tissue sarcoma for fluorescence-guided surgery and tumor detection. *J Surg Oncol* **2019**, *119*, 1077-1086, doi:10.1002/jso.25468.

36. Anderson, S.E.; Nonaka, D.; Chuai, S.; Olshen, A.B.; Chi, D.; Sabbatini, P.; Soslow, R.A. p53, epidermal growth factor, and platelet-derived growth factor in uterine leiomyosarcoma and leiomyomas. *International journal of gynecological cancer : official journal of the International Gynecological Cancer Society* **2006**, *16*, 849-853, doi:10.1111/j.1525-1438.2006.00542.x.

37. Armistead, P.M.; Salganick, J.; Roh, J.S.; Steinert, D.M.; Patel, S.; Munsell, M.; El-Naggar, A.K.; Benjamin, R.S.; Zhang, W.; Trent, J.C. Expression of receptor tyrosine kinases and apoptotic molecules in rhabdomyosarcoma: correlation with overall survival in 105 patients. *Cancer* **2007**, *110*, 2293-2303, doi:10.1002/cncr.23038.

38. Baek, M.H.; Park, J.Y.; Rhim, C.C.; Kim, J.H.; Park, Y.; Kim, K.R.; Nam, J.H. Investigation of New Therapeutic Targets in Undifferentiated Endometrial Sarcoma. *Gynecologic and obstetric investigation* **2017**, *82*, 329-339, doi:10.1159/000454769.

39. Cheng, X.; Yang, G.; Schmeler, K.M.; Coleman, R.L.; Tu, X.; Liu, J.; Kavanagh, J.J. Recurrence patterns and prognosis of endometrial stromal sarcoma and the potential of tyrosine kinase-inhibiting therapy. *Gynecol Oncol* **2011**, *121*, 323-327, doi:10.1016/j.ygyno.2010.12.360.

40. Cossu-Rocca, P.; Contini, M.; Uras, M.G.; Muroni, M.R.; Pili, F.; Carru, C.; Bosincu, L.; Massarelli, G.; Nogales, F.F.; De Miglio, M.R. Tyrosine kinase receptor status in endometrial stromal sarcoma: an immunohistochemical and genetic-molecular analysis. *International journal of gynecological pathology : official journal of the International Society of Gynecological Pathologists* **2012**, *31*, 570-579, doi:10.1097/PGP.0b013e31824fe289.

41. Cuppens, T.; Annibali, D.; Coosemans, A.; Trovik, J.; Ter Haar, N.; Colas, E.; Garcia-Jimenez, A.; Van de Vijver, K.; Kruitwagen, R.P.; Brinkhuis, M., et al. Potential Targets' Analysis Reveals Dual PI3K/mTOR Pathway Inhibition as a Promising Therapeutic Strategy for Uterine Leiomyosarcomas-an ENITEC Group Initiative. *Clin Cancer Res* **2017**, *23*, 1274-1285, doi:10.1158/1078-0432.Ccr-16-2149.

42. Hoffman, A.; Ghadimi, M.P.; Demicco, E.G.; Creighton, C.J.; Torres, K.; Colombo, C.; Peng, T.; Lusby, K.; Ingram, D.; Hornick, J.L., et al. Localized and metastatic myxoid/round cell liposarcoma: clinical and molecular observations. *Cancer* **2013**, *119*, 1868-1877, doi:10.1002/cncr.27847.

43. Iwasaki, S.; Sudo, T.; Miwa, M.; Ukita, M.; Morimoto, A.; Tamada, M.; Ueno, S.; Wakahashi, S.; Yamaguchi, S.; Fujiwara, K., et al. Endometrial stromal sarcoma: clinicopathological and immunophenotypic study of 16 cases. *Arch Gynecol Obstet* **2013**, *288*, 385-391, doi:10.1007/s00404-013-2766-3.

44. Park, J.Y.; Kim, K.R.; Nam, J.H. Immunohistochemical analysis for therapeutic targets and prognostic markers in low-grade endometrial stromal sarcoma. *International journal of gynecological cancer : official journal of the International Gynecological Cancer Society* **2013**, *23*, 81-89, doi:10.1097/IGC.0b013e3182738361.

45. Ruping, K.; Altendorf-Hofmann, A.; Chen, Y.; Kampmann, E.; Gibis, S.; Lindner, L.; Katenkamp, D.; Petersen, I.; Knosel, T. High IGF2 and FGFR3 are associated with tumour progression in undifferentiated pleomorphic sarcomas, but EGFR and FGFR3 mutations are a rare event. *J Cancer Res Clin Oncol* **2014**, *140*, 1315-1322, doi:10.1007/s00432-014-1700-9.

46. Barbashina, V.; Benevenia, J.; Aviv, H.; Tsai, J.; Patterson, F.; Aisner, S.; Cohen, S.; Fernandes, H.; Skurnick, J.; Hameed, M. Oncoproteins and proliferation markers in synovial sarcomas: a clinicopathologic study of 19 cases. *Journal of cancer research and clinical oncology* **2002**, *128*, 610-616, doi:10.1007/s00432-002-0389-3.

47. Cascio, M.J.; O'Donnell, R.J.; Horvai, A.E. Epithelioid sarcoma expresses epidermal growth factor receptor but gene amplification and kinase domain mutations are rare. *Mod Pathol* **2010**, *23*, 574-580, doi:10.1038/modpathol.2010.2.

48. Cates, J.M.; Memoli, V.A.; Gonzalez, R.S. Cell cycle and apoptosis regulatory proteins, proliferative markers, cell signaling molecules, CD209, and decorin immunoreactivity in low-grade myxofibrosarcoma and myxoma. *Virchows Arch* **2015**, *467*, 211-216, doi:10.1007/s00428-015-1778-8.

49. Dewaele, B.; Floris, G.; Finalet-Ferreiro, J.; Fletcher, C.D.; Coindre, J.M.; Guillou, L.; Hogendoorn, P.C.; Wozniak, A.; Vanspauwen, V.; Schoffski, P., et al. Coactivated platelet-derived growth factor receptor {alpha} and epidermal growth factor receptor are potential therapeutic targets in intimal sarcoma. *Cancer research* **2010**, *70*, 7304-7314, doi:10.1158/0008-5472.can-10-1543.

50. Ganti, R.; Skapek, S.X.; Zhang, J.; Fuller, C.E.; Wu, J.; Billups, C.A.; Breitfeld, P.P.; Dalton, J.D.; Meyer, W.H.; Khoury, J.D. Expression and genomic status of EGFR and ErbB-2 in alveolar and embryonal rhabdomyosarcoma. *Modern pathology : an official journal of the United States and Canadian Academy of Pathology, Inc* **2006**, *19*, 1213-1220, doi:10.1038/modpathol.3800636.

51. Garcia, C.; Kubat, J.S.; Fulton, R.S.; Anthony, A.T.; Combs, M.; Powell, C.B.; Littell, R.D. Clinical outcomes and prognostic markers in uterine leiomyosarcoma: a population-based cohort. *International journal of gynecological cancer : official journal of the International Gynecological Cancer Society* **2015**, *25*, 622-628, doi:10.1097/igc.0000000000000370.

52. Gusterson, B.; Cowley, G.; McIlhinney, J.; Ozanne, B.; Fisher, C.; Reeves, B. Evidence for increased epidermal growth factor receptors in human sarcomas. *Int J Cancer* **1985**, *36*, 689-693, doi:10.1002/ijc.2910360612.

53. Helbig, D.; Ihle, M.A.; Putz, K.; Tantcheva-Poor, I.; Mauch, C.; Buttner, R.; Quaas, A. Oncogene and therapeutic target analyses in atypical fibroxanthomas and pleomorphic dermal sarcomas. *Oncotarget* **2016**, *7*, 21763-21774, doi:10.18632/oncotarget.7845.

54. Kovarik, C.L.; Barrett, T.; Auerbach, A.; Cassarino, D.S. Acral myxoinflammatory fibroblastic sarcoma: case series and immunohistochemical analysis. *Journal of cutaneous pathology* **2008**, *35*, 192-196, doi:10.1111/j.1600-0560.2007.00791.x.

55. Leibl, S.; Moinfar, F. Mammary NOS-type sarcoma with CD10 expression: a rare entity with features of myoepithelial differentiation. *The American journal of surgical pathology* **2006**, *30*, 450-456, doi:10.1097/00000478-200604000-00004.

56. Moinfar, F.; Gogg-Kamerer, M.; Sommersacher, A.; Regitnig, P.; Man, Y.G.; Zatloukal, K.; Denk, H.; Tavassoli, F.A. Endometrial stromal sarcomas frequently express epidermal growth factor receptor (EGFR, HER-1): potential basis for a new therapeutic approach. *The American journal of surgical pathology* **2005**, *29*, 485-489, doi:10.1097/01.pas.0000155149.83541.24.

2

57. Asmane, I.; Watkin, E.; Alberti, L.; Duc, A.; Marec-Berard, P.; Ray-Coquard, I.; Cassier, P.; Decouvelaere, A.V.; Ranchere, D.; Kurtz, J.E., et al. Insulin-like growth factor type 1 receptor (IGF-1R) exclusive nuclear staining: a predictive biomarker for IGF-1R monoclonal antibody (Ab) therapy in sarcomas. *Eur J Cancer* **2012**, *48*, 3027-3035, doi:10.1016/j.ejca.2012.05.009.

58. Conti, A.; Espina, V.; Chiechi, A.; Magagnoli, G.; Novello, C.; Pazzaglia, L.; Quattrini, I.; Picci, P.; Liotta, L.A.; Benassi, M.S. Mapping protein signal pathway interaction in sarcoma bone metastasis: linkage between rank, metalloproteinases turnover and growth factor signaling pathways. *Clin Exp Metastasis* **2014**, *31*, 15-24, doi:10.1007/s10585-013-9605-6.

59. Lazar, A.J.; Lahat, G.; Myers, S.E.; Smith, K.D.; Zou, C.; Wang, W.L.; Lopez-Terrada, D.; Lev, D. Validation of potential therapeutic targets in alveolar soft part sarcoma: an immunohistochemical study utilizing tissue microarray. *Histopathology* **2009**, *55*, 750-755, doi:10.1111/j.1365-2559.2009.03436.x.

60. Sato, O.; Wada, T.; Kawai, A.; Yamaguchi, U.; Makimoto, A.; Kokai, Y.; Yamashita, T.; Chuman, H.; Beppu, Y.; Tani, Y., et al. Expression of epidermal growth factor receptor, ERBB2 and KIT in adult soft tissue sarcomas: a clinicopathologic study of 281 cases. *Cancer* **2005**, *103*, 1881-1890, doi:10.1002/cncr.20986.

61. Sun, X.; Chang, K.C.; Abruzzo, L.V.; Lai, R.; Younes, A.; Jones, D. Epidermal growth factor receptor expression in follicular dendritic cells: a shared feature of follicular dendritic cell sarcoma and Castleman's disease. *Human pathology* **2003**, *34*, 835-840, doi:10.1016/s0046-8177(03)00356-3.

62. Tamborini, E.; Casieri, P.; Miselli, F.; Orsenigo, M.; Negri, T.; Piacenza, C.; Stacchiotti, S.; Gronchi, A.; Pastorino, U.; Pierotti, M.A., et al. Analysis of potential receptor tyrosine kinase targets in intimal and mural sarcomas. *The Journal of pathology* **2007**, *212*, 227-235, doi:10.1002/path.2177.

63. Tawbi, H.; Thomas, D.; Lucas, D.R.; Biermann, J.S.; Schuetze, S.M.; Hart, A.L.; Chugh, R.; Baker, L.H. Epidermal growth factor receptor expression and mutational analysis in synovial sarcomas and malignant peripheral nerve sheath tumors. *Oncologist* **2008**, *13*, 459-466, doi:10.1634/theoncologist.2007-0166.

64. Teng, H.W.; Wang, H.W.; Chen, W.M.; Chao, T.C.; Hsieh, Y.Y.; Hsih, C.H.; Tzeng, C.H.; Chen, P.C.; Yen, C.C. Prevalence and prognostic influence of genomic changes of EGFR pathway markers in synovial sarcoma. *J Surg Oncol* **2011**, *103*, 773-781, doi:10.1002/jso.21852.

65. Vesely, K.; Jurajda, M.; Nenutil, R.; Vesela, M. Expression of p53, cyclin D1 and EGFR correlates with histological grade of adult soft tissue sarcomas: a study on tissue microarrays. *Neoplasma* **2009**, *56*, 239-244.

66. Xie, X.; Ghadimi, M.P.; Young, E.D.; Belousov, R.; Zhu, Q.S.; Liu, J.; Lopez, G.; Colombo, C.; Peng, T.; Reynoso, D., et al. Combining EGFR and mTOR blockade for the treatment of epithelioid sarcoma. *Clin Cancer Res* **2011**, *17*, 5901-5912, doi:10.1158/1078-0432.ccr-11-0660.

67. Yang, J.L.; Gupta, R.D.; Goldstein, D.; Crowe, P.J. Significance of Phosphorylated Epidermal Growth Factor Receptor and Its Signal Transducers in Human Soft Tissue Sarcoma. *International journal of molecular sciences* **2017**, *18*, doi:10.3390/ijms18061159.

68. Yang, J.L.; Hannan, M.T.; Russell, P.J.; Crowe, P.J. Expression of HER1/EGFR protein in human soft tissue sarcomas. *European journal of surgical oncology : the journal of the European Society of Surgical Oncology and the British Association of Surgical Oncology* **2006**, *32*, 466-468, doi:10.1016/j.ejso.2006.01.012.

69. Alves, P.M.; de Arruda, J.A.A.; Arantes, D.A.C.; Costa, S.F.S.; Souza, L.L.; Pontes, H.A.R.; Fonseca, F.P.; Mesquita, R.A.; Nonaka, C.F.W.; Mendonça, E.F., et al. Evaluation of tumor-infiltrating lymphocytes in osteosarcomas of the jaws: a multicenter study. *Virchows Arch* **2019**, *474*, 201-207, doi:10.1007/s00428-018-2499-6.

70. Capobianco, G.; Pili, F.; Contini, M.; De Miglio, M.R.; Marras, V.; Santeufemia, D.A.; Cherchi, C.; Dessole, M.; Cherchi, P.L.; Cossu-Rocca, P. Analysis of epidermal growth factor receptor (EGFR) status in endometrial stromal sarcoma. *Eur J Gynaecol Oncol* **2012**, *33*, 629-632.

71. Backer, M.V.; Levashova, Z.; Patel, V.; Jehning, B.T.; Claffey, K.; Blankenberg, F.G.; Backer, J.M. Molecular imaging of VEGF receptors in angiogenic vasculature with single-chain VEGF-based probes. *Nature medicine* **2007**, *13*, 504-509, doi:10.1038/nm1522.

72. Winkler, A.M.; Rice, P.F.; Weichsel, J.; Watson, J.M.; Backer, M.V.; Backer, J.M.; Barton, J.K. In vivo, dual-modality OCT/LIF imaging using a novel VEGF receptor-targeted NIR fluorescent probe in the AOM-treated mouse model. *Molecular imaging and biology* **2011**, *13*, 1173-1182, doi:10.1007/s11307-010-0450-6.

73. Liu, L.; Kakiuchi-Kiyota, S.; Arnold, L.L.; Johansson, S.L.; Wert, D.; Cohen, S.M. Pathogenesis of human hemangiosarcomas and hemangiomas. *Human pathology* **2013**, *44*, 2302-2311, doi:10.1016/j.humpath.2013.05.012.

74. Pakos, E.E.; Goussia, A.C.; Tsekeris, P.G.; Papachristou, D.J.; Stefanou, D.; Agnantis, N.J. Expression of vascular endothelial growth factor and its receptor, KDR/Flk-1, in soft tissue sarcomas. *Anticancer research* **2005**, *25*, 3591-3596.

75. Stacher, E.; Gruber-Mosenbacher, U.; Halbwedl, I.; Dei Tos, A.P.; Cavazza, A.; Papotti, M.; Carvalho, L.; Huber, M.; Ermert, L.; Popper, H.H. The VEGF-system in primary pulmonary angiosarcomas and haemangioendotheliomas: new potential therapeutic targets? *Lung Cancer* **2009**, *65*, 49-55, doi:10.1016/j.lungcan.2008.10.031.

76. Ho, A.L.; Vasudeva, S.D.; Lae, M.; Saito, T.; Barbashina, V.; Antonescu, C.R.; Ladanyi, M.; Schwartz, G.K. PDGF receptor alpha is an alternative mediator of rapamycin-induced Akt activation: implications for combination targeted therapy of synovial sarcoma. *Cancer Res* **2012**, *72*, 4515-4525, doi:10.1158/0008-5472.can-12-1319.

77. Zhou, H.; Qian, W.; Uckun, F.M.; Zhou, Z.; Wang, L.; Wang, A.; Mao, H.; Yang, L. IGF-1 receptor targeted nanoparticles for image-guided therapy of stroma-rich and drug resistant human cancer. *Proc SPIE Int Soc Opt Eng* **2016**, *9836*, doi:10.1117/12.2224914.

78. Ahlen, J.; Wejde, J.; Brosjo, O.; von Rosen, A.; Weng, W.H.; Girnita, L.; Larsson, O.; Larsson, C. Insulin-like growth factor type 1 receptor expression correlates to good prognosis in highly malignant soft tissue sarcoma. *Clin Cancer Res* **2005**, *11*, 206-216.

79. Friedrichs, N.; Kuchler, J.; Endl, E.; Koch, A.; Czerwitzki, J.; Wurst, P.; Metzger, D.; Schulte, J.H.; Holst, M.I.; Heukamp, L.C., et al. Insulin-like growth factor-1 receptor acts as a growth regulator in synovial sarcoma. *J Pathol* **2008**, *216*, 428-439, doi:10.1002/path.2438.

80. Ho, A.L.; Vasudeva, S.D.; Laé, M.; Saito, T.; Barbashina, V.; Antonescu, C.R.; Ladanyi, M.; Schwartz, G.K. PDGF receptor alpha is an alternative mediator of rapamycin-induced Akt activation: implications for combination targeted therapy of synovial sarcoma. *Cancer Res* **2012**, *72*, 4515-4525, doi:10.1158/0008-5472.Can-12-1319.

81. Palmerini, E.; Benassi, M.S.; Quattrini, I.; Pazzaglia, L.; Donati, D.; Benini, S.; Gamberi, G.; Gambarotti, M.; Picci, P.; Ferrari, S. Prognostic and predictive role of CXCR4, IGF-1R and Ezrin expression in localized synovial sarcoma: is chemotaxis important to tumor response? *Orphanet J Rare Dis* **2015**, *10*, 6, doi:10.1186/s13023-014-0222-5.

82. Roland, C.L.; May, C.D.; Watson, K.L.; Al Sannaa, G.A.; Dineen, S.P.; Feig, R.; Landers, S.; Ingram, D.R.; Wang, W.L.; Guadagnolo, B.A., et al. Analysis of Clinical and Molecular Factors Impacting Oncologic Outcomes in Undifferentiated Pleomorphic Sarcoma. *Ann Surg Oncol* **2016**, *23*, 2220-2228, doi:10.1245/s10434-016-5115-5.

83. Van der Ven, L.T.; Roholl, P.J.; Gloudemans, T.; Van Buul-Offers, S.C.; Welters, M.J.; Bladergroen, B.A.; Faber, J.A.; Sussenbach, J.S.; Den Otter, W. Expression of insulin-like growth factors (IGFs), their receptors and IGF binding protein-3 in normal, benign and malignant smooth muscle tissues. *British journal of cancer* **1997**, *75*, 1631-1640, doi:10.1038/bjc.1997.278.

84. Xie, Y.; Skytting, B.; Nilsson, G.; Brodin, B.; Larsson, O. Expression of insulin-like growth factor-1 receptor in synovial sarcoma: association with an aggressive phenotype. *Cancer Res* **1999**, *59*, 3588-3591.

85. Moroncini, G.; Maccaroni, E.; Fiordoliva, I.; Pellei, C.; Gabrielli, A.; Berardi, R. Developments in the management of advanced soft-tissue sarcoma - olaratumab in context. *Onco Targets Ther* **2018**, *11*, 833-842, doi:10.2147/ott.S127609.

86. Camorani, S.; Hill, B.S.; Collina, F.; Gargiulo, S.; Napolitano, M.; Cantile, M.; Di Bonito, M.; Botti, G.; Fedele, M.; Zannetti, A., et al. Targeted imaging and inhibition of triple-negative breast cancer metastases by a PDGFRbeta aptamer. *Theranostics* **2018**, *8*, 5178-5199, doi:10.7150/thno.27798.

87. Adams, S.F.; Hickson, J.A.; Hutto, J.Y.; Montag, A.G.; Lengyel, E.; Yamada, S.D. PDGFR-alpha as a potential therapeutic target in uterine sarcomas. *Gynecologic oncology* **2007**, *104*, 524-528, doi:10.1016/j.ygyno.2006.09.013.

88. Liegl, B.; Gully, C.; Reich, O.; Nogales, F.F.; Beham, A.; Regauer, S. Expression of platelet-derived growth factor receptor in low-grade endometrial stromal sarcomas in the absence of activating mutations. *Histopathology* **2007**, *50*, 448-452, doi:10.1111/j.1365-2559.2007.02634.x.

89. Rossi, G.; Valli, R.; Bertolini, F.; Marchioni, A.; Cavazza, A.; Mucciarini, C.; Migaldi, M.; Federico, M.; Trentini, G.P.; Sgambato, A. PDGFR expression in differential diagnosis between KIT-negative gastrointestinal stromal tumours and other primary soft-tissue tumours of the gastrointestinal tract. *Histopathology* **2005**, *46*, 522-531, doi:10.1111/j.1365-2559.2005.02128.x.

90. Fleuren, E.D.G.; Vlenterie, M.; van der Graaf, W.T.A.; Hillebrandt-Roeffen, M.H.S.; Blackburn, J.; Ma, X.; Chan, H.; Magias, M.C.; van Erp, A.; van Houdt, L., et al. Phosphoproteomic Profiling Reveals ALK and MET as Novel Actionable Targets across Synovial Sarcoma Subtypes. *Cancer Res* **2017**, *77*, 4279-4292, doi:10.1158/0008-5472.Can-16-2550.

91. Hiraki-Hotokebuchi, Y.; Yamada, Y.; Kohashi, K.; Yamamoto, H.; Endo, M.; Setsu, N.; Yuki, K.; Ito, T.; Iwamoto, Y.; Furue, M., et al. Alteration of PDGFRbeta-Akt-mTOR pathway signaling in fibrosarcomatous transformation of dermatofibrosarcoma protuberans. *Human pathology* **2017**, *67*, 60-68, doi:10.1016/j.humpath.2017.07.001.

92. Lopez-Guerrero, J.A.; Navarro, S.; Noguera, R.; Carda, C.; Farinas, S.C.; Pellin, A.; Llombart-Bosch, A. Mutational analysis of the c-KIT AND PDGFRalpha in a series of molecularly well-characterized synovial sarcomas. *Diagnostic molecular pathology : the American journal of surgical pathology, part B* **2005**, *14*, 134-139.

93. Sieber, T.; Schoeler, D.; Ringel, F.; Pascu, M.; Schriever, F. Selective internalization of monoclonal antibodies by B-cell chronic lymphocytic leukaemia cells. *Br J Haematol* **2003**, *121*, 458-461, doi:10.1046/j.1365-2141.2003.04305.x.

94. Klohs, J.; Grafe, M.; Graf, K.; Steinbrink, J.; Dietrich, T.; Stibenz, D.; Bahmani, P.; Kronenberg, G.; Harms, C.; Endres, M., et al. In vivo imaging of the inflammatory receptor CD40 after cerebral ischemia using a fluorescent antibody. *Stroke* **2008**, *39*, 2845-2852, doi:10.1161/strokeaha.107.509844.

95. Kennedy, M.M.; Biddolph, S.; Lucas, S.B.; Howells, D.D.; Picton, S.; McGee, J.O.; O'Leary, J.J. CD40 upregulation is independent of HHV-8 in the pathogenesis of Kaposi's sarcoma. *Molecular pathology : MP* **1999**, *52*, 32-36, doi:10.1136/mp.52.1.32.

96. Mechtersheimer, G.; Barth, T.; Ludwig, R.; Staudter, M.; Moller, P. Differential expression of leukocyte differentiation antigens in small round blue cell sarcomas. *Cancer* **1993**, *71*, 237-248, doi:10.1002/1097-0142(19930101)71:1<237::aid-cncr2820710137>3.0.co;2-j.

97. Ottaiano, A.; De Chiara, A.; Perrone, F.; Botti, G.; Fazioli, F.; De Rosa, V.; Mozzillo, N.; Ravo, V.; Morrica, B.; Gallo, C., et al. Prognostic value of CD40 in adult soft tissue sarcomas. *Clin Cancer Res* **2004**, *10*, 2824-2831, doi:10.1158/1078-0432.ccr-0139-03.

98. Pammer, J.; Plettenberg, A.; Weninger, W.; Diller, B.; Mildner, M.; Uthman, A.; Issing, W.; Sturzl, M.; Tschachler, E. CD40 antigen is expressed by endothelial cells and tumor cells in Kaposi's sarcoma. *The American journal of pathology* **1996**, *148*, 1387-1396.

99. Kalim, M.; Wang, S.; Liang, K.; Khan, M.S.I.; Zhan, J. Engineered scPDL1-DM1 drug conjugate with improved in vitro analysis to target PD-L1 positive cancer cells and intracellular trafficking studies in cancer therapy. *Genet Mol Biol* **2020**, *42*, e20180391, doi:10.1590/1678-4685-gmb-2018-0391.

100. Zhang, M.; Jiang, H.; Zhang, R.; Jiang, H.; Xu, H.; Pan, W.; Gao, X.; Sun, Z. Near-infrared fluorescence-labeled anti-PD-L1-mAb for tumor imaging in human colorectal cancer xenografted mice. *Journal of cellular biochemistry* **2019**, *120*, 10239-10247, doi:10.1002/jcb.28308.

101. Asanuma, K.; Nakamura, T.; Hayashi, A.; Okamoto, T.; Iino, T.; Asanuma, Y.; Hagi, T.; Kita, K.; Nakamura, K.; Sudo, A. Soluble programmed death-ligand 1 rather than PD-L1 on tumor cells effectively predicts metastasis and prognosis in soft tissue sarcomas. *Sci Rep* **2020**, *10*, 9077, doi:10.1038/s41598-020-65895-0.

102. Ben-Ami, E.; Barysauskas, C.M.; Solomon, S.; Tahlil, K.; Malley, R.; Hohos, M.; Polson, K.; Loucks, M.; Severgnini, M.; Patel, T., et al. Immunotherapy with single agent nivolumab for advanced leiomyosarcoma of the uterus: Results of a phase 2 study. *Cancer* **2017**, *123*, 3285-3290, doi:10.1002/cncr.30738.

103. D'Angelo, S.P.; Shoushtari, A.N.; Agaram, N.P.; Kuk, D.; Qin, L.X.; Carvajal, R.D.; Dickson, M.A.; Gounder, M.; Keohan, M.L.; Schwartz, G.K., et al. Prevalence of tumor-infiltrating lymphocytes and PD-L1 expression in the soft tissue sarcoma microenvironment. *Human pathology* **2015**, *46*, 357-365, doi:10.1016/j.humpath.2014.11.001.

104. Gabrych, A.; Pęksa, R.; Kunc, M.; Krawczyk, M.; Izycka-Swieszewska, E.; Biernat, W.; Bień, E. The PD-L1/PD-1 axis expression on tumor-infiltrating immune cells and tumor cells in pediatric rhabdomyosarcoma. *Pathology, research and practice* **2019**, *215*, 152700, doi:10.1016/j.prp.2019.152700.

105. Kawamura, A.; Kawamura, T.; Riddell, M.; Hikita, T.; Yanagi, T.; Umemura, H.; Nakayama, M. Regulation of programmed cell death ligand 1 expression by atypical protein kinase C lambda/iota in cutaneous angiosarcoma. *Cancer science* **2019**, *110*, 1780-1789, doi:10.1111/cas.13981.

106. Kim, C.; Kim, E.K.; Jung, H.; Chon, H.J.; Han, J.W.; Shin, K.H.; Hu, H.; Kim, K.S.; Choi, Y.D.; Kim, S., et al. Prognostic implications of PD-L1 expression in patients with soft tissue sarcoma. *BMC Cancer* **2016**, *16*, 434, doi:10.1186/s12885-016-2451-6.

107. Kim, J.S.; Kim, M.W.; Park, D.Y. Indirect ultrasound guidance increased accuracy of the glenohumeral injection using the superior approach: a cadaveric study of injection accuracy. *Ann Rehabil Med* **2013**, *37*, 202-207, doi:10.5535/arm.2013.37.2.202.

108. Klein, S.; Mauch, C.; Wagener-Ryczek, S.; Schoemmel, M.; Buettner, R.; Quaas, A.; Helbig, D. Immune-phenotyping of pleomorphic dermal sarcomas suggests this entity as a potential candidate for immunotherapy. *Cancer immunology, immunotherapy : CII* **2019**, *68*, 973-982, doi:10.1007/s00262-019-02339-3.

109. Kosemehmetoglu, K.; Ozogul, E.; Babaoglu, B.; Tezel, G.G.; Gedikoglu, G. Programmed Death Ligand 1 (PD-L1) Expression in Malignant Mesenchymal Tumors. *Turk patoloji dergisi* **2017**, *1*, 192-197, doi:10.5146/tjpath.2017.01395.

110. Orth, M.F.; Buecklein, V.L.; Kampmann, E.; Subklewe, M.; Noessner, E.; Cidre-Aranaz, F.; Romero-Pérez, L.; Wehweck, F.S.; Lindner, L.; Issels, R., et al. A comparative view on the expression patterns of PD-L1 and PD-1 in soft tissue sarcomas. *Cancer immunology, immunotherapy : CII* **2020**, *69*, 1353-1362, doi:10.1007/s00262-020-02552-5.

111. Park, H.K.; Kim, M.; Sung, M.; Lee, S.E.; Kim, Y.J.; Choi, Y.L. Status of programmed death-ligand 1 expression in sarcomas. *Journal of translational medicine* **2018**, *16*, 303, doi:10.1186/s12967-018-1658-5.

112. Paydas, S.; Bagir, E.K.; Deveci, M.A.; Gonlusen, G. Clinical and prognostic significance of PD-1 and PD-L1 expression in sarcomas. *Medical oncology (Northwood, London, England)* **2016**, *33*, 93, doi:10.1007/s12032-016-0807-z.

113. Pollack, S.M.; He, Q.; Yearley, J.H.; Emerson, R.; Vignali, M.; Zhang, Y.; Redman, M.W.; Baker, K.K.; Cooper, S.; Donahue, B., et al. T-cell infiltration and clonality correlate with programmed cell death protein 1 and programmed death-ligand 1 expression in patients with soft tissue sarcomas. *Cancer* **2017**, *123*, 3291-3304, doi:10.1002/cncr.30726.

114. Shanes, E.D.; Friedman, L.A.; Mills, A.M. PD-L1 Expression and Tumor-infiltrating Lymphocytes in Uterine Smooth Muscle Tumors: Implications for Immunotherapy. *The American journal of surgical pathology* **2019**, *43*, 792-801, doi:10.1097/pas.0000000000001254.

115. Torabi, A.; Amaya, C.N.; Wians, F.H., Jr.; Bryan, B.A. PD-1 and PD-L1 expression in bone and soft tissue sarcomas. *Pathology* **2017**, *49*, 506-513, doi:10.1016/j.pathol.2017.05.003.

116. Vargas, A.C.; Maclean, F.M.; Sioson, L.; Tran, D.; Bonar, F.; Mahar, A.; Cheah, A.L.; Russell, P.; Grimison, P.; Richardson, L., et al. Prevalence of PD-L1 expression in matched recurrent and/or metastatic sarcoma samples and in a range of selected sarcomas subtypes. *PLoS One* **2020**, *15*, e0222551, doi:10.1371/journal.pone.0222551.

117. Yan, L.; Wang, Z.; Cui, C.; Guan, X.; Dong, B.; Zhao, M.; Wu, J.; Tian, X.; Hao, C. Comprehensive immune characterization and T-cell receptor repertoire heterogeneity of retroperitoneal liposarcoma. *Cancer science* **2019**, *110*, 3038-3048, doi:10.1111/cas.14161.

118. Zheng, B.; Wang, J.; Cai, W.; Lao, I.; Shi, Y.; Luo, X.; Yan, W. Changes in the tumor immune microenvironment in resected recurrent soft tissue sarcomas. *Ann Transl Med* **2019**, *7*, 387, doi:10.21037/atm.2019.07.43.

119. Edris, B.; Espinosa, I.; Muhlenberg, T.; Mikels, A.; Lee, C.H.; Steigen, S.E.; Zhu, S.; Montgomery, K.D.; Lazar, A.J.; Lev, D., et al. ROR2 is a novel prognostic biomarker and a potential therapeutic target in leiomyosarcoma and gastrointestinal stromal tumour. *The Journal of pathology* **2012**, *227*, 223-233, doi:10.1002/path.3986.

120. Ehlerding, E.B.; England, C.G.; Majewski, R.L.; Valdovinos, H.F.; Jiang, D.; Liu, G.; McNeel, D.G.; Nickles, R.J.; Cai, W. ImmunoPET Imaging of CTLA-4 Expression in Mouse Models of Non-small Cell Lung Cancer. *Mol Pharm* **2017**, *14*, 1782-1789, doi:10.1021/acs.molpharmaceut.7b00056.

121. Hong, Y.K.; Lee, Y.C.; Cheng, T.L.; Lai, C.H.; Hsu, C.K.; Kuo, C.H.; Hsu, Y.Y.; Li, J.T.; Chang, B.I.; Ma, C.Y., et al. Tumor Endothelial Marker 1 (TEM1/Endosialin/CD248) Enhances Wound Healing by Interacting with Platelet-Derived Growth Factor Receptors. *J Invest Dermatol* **2019**, *139*, 2204-2214.e2207, doi:10.1016/j.jid.2019.03.1149.

122. Naylor, A.J.; McGettrick, H.M.; Maynard, W.D.; May, P.; Barone, F.; Croft, A.P.; Egginton, S.; Buckley, C.D. A differential role for CD248 (Endosialin) in PDGF-mediated skeletal muscle angiogenesis. *PLoS One* **2014**, *9*, e107146, doi:10.1371/journal.pone.0107146.

123. Teicher, B.A. CD248: A therapeutic target in cancer and fibrotic diseases. *Oncotarget* **2019**, *10*, 993-1009, doi:10.18632/oncotarget.26590.

124. Pietrzyk, Ł. Biomarkers Discovery for Colorectal Cancer: A Review on Tumor Endothelial Markers as Perspective Candidates. *Dis Markers* **2016**, *2016*, 4912405, doi:10.1155/2016/4912405.

125. Rouleau, C.; Smale, R.; Fu, Y.S.; Hui, G.; Wang, F.; Hutto, E.; Fogle, R.; Jones, C.M.; Krumbholz, R.; Roth, S., et al. Endosialin is expressed in high grade and advanced sarcomas: evidence from clinical specimens and preclinical modeling. *Int J Oncol* **2011**, *39*, 73-89, doi:10.3892/ijo.2011.1020.

126. Jones, R.L.; Chawla, S.P.; Attia, S.; Schöffski, P.; Gelderblom, H.; Chmielowski, B.; Le Cesne, A.; Van Tine, B.A.; Trent, J.C.; Patel, S., et al. A phase 1 and randomized controlled phase 2 trial of the safety and efficacy of the combination of gemcitabine and docetaxel with ontuxizumab (MORAb-004) in metastatic soft-tissue sarcomas. *Cancer* **2019**, *125*, 2445-2454, doi:10.1002/cncr.32084.

127. Li, C.; Wang, J.; Hu, J.; Feng, Y.; Hasegawa, K.; Peng, X.; Duan, X.; Zhao, A.; Mikitsh, J.L.; Muzykantov, V.R., et al. Development, optimization, and validation of novel anti-TEM1/CD248 affinity agent for optical imaging in cancer. *Oncotarget* **2014**, *5*, 6994-7012, doi:10.18632/oncotarget.2188.

128. Karaman, S.; Leppanen, V.M.; Alitalo, K. Vascular endothelial growth factor signaling in development and disease. *Development* **2018**, *145*, doi:10.1242/dev.151019.

129. Chiumia, D.; Hankele, A.K.; Groebner, A.E.; Schulke, K.; Reichenbach, H.D.; Giller, K.; Zakhartchenko, V.; Bauersachs, S.; Ulbrich, S.E. Vascular Endothelial Growth Factor A and VEGFR-1 Change during Preimplantation in Heifers. *International journal of molecular sciences* **2020**, *21*, doi:10.3390/ijms21020544.

130.   Shibuya, M. Vascular Endothelial Growth Factor (VEGF) and Its Receptor (VEGFR) Signaling in Angiogenesis: A Crucial Target for Anti- and Pro-Angiogenic Therapies. *Genes Cancer* **2011**, *2*, 1097-1105, doi:10.1177/1947601911423031.

131.   Kilvaer, T.K.; Valkov, A.; Sorbye, S.; Smeland, E.; Bremnes, R.M.; Busund, L.T.; Donnem, T. Profiling of VEGFs and VEGFRs as prognostic factors in soft tissue sarcoma: VEGFR-3 is an independent predictor of poor prognosis. *PloS one* **2010**, *5*, e15368, doi:10.1371/journal.pone.0015368.

132.   Patwardhan, P.P.; Musi, E.; Schwartz, G.K. Preclinical Evaluation of Nintedanib, a Triple Angiokinase Inhibitor, in Soft-tissue Sarcoma: Potential Therapeutic Implication for Synovial Sarcoma. *Mol Cancer Ther* **2018**, *17*, 2329-2340, doi:10.1158/1535-7163.Mct-18-0319.

133.   Clinicaltrials.gov Ramucirumab. Availabe online: https://clinicaltrials.gov/ct2/show/NCT04145700?term=ramucirumab&cond=Soft+Tissue+Sarcoma&draw=2&rank=1 (accessed on 22 June 2020).

134.   Steinkamp, P.J.; Pranger, B.K.; Li, M.; Linssen, M.D.; Voskuil, F.J.; Been, L.B.; van Leeuwen, B.L.; Suurmeijer, A.J.H.; Nagengast, W.B.; Kruijff, S.K., et al. Fluorescence-guided visualization of soft tissue sarcomas by targeting vascular endothelial growth factor-A: a phase 1 single-center clinical trial. *J Nucl Med* **2020**, 10.2967/jnumed.120.245696, doi:10.2967/jnumed.120.245696.

135.   Mackay, H.J.; Buckanovich, R.J.; Hirte, H.; Correa, R.; Hoskins, P.; Biagi, J.; Martin, L.P.; Fleming, G.F.; Morgan, R.; Wang, L., et al. A phase II study single agent of aflibercept (VEGF Trap) in patients with recurrent or metastatic gynecologic carcinosarcomas and uterine leiomyosarcoma. A trial of the Princess Margaret Hospital, Chicago and California Cancer Phase II Consortia. *Gynecologic oncology* **2012**, *125*, 136-140, doi:10.1016/j.ygyno.2011.11.042.

136.   Harlaar, N.J.; Koller, M.; de Jongh, S.J.; van Leeuwen, B.L.; Hemmer, P.H.; Kruijff, S.; van Ginkel, R.J.; Been, L.B.; de Jong, J.S.; Kats-Ugurlu, G., et al. Molecular fluorescence-guided surgery of peritoneal carcinomatosis of colorectal origin: a single-centre feasibility study. *Lancet Gastroenterol Hepatol* **2016**, *1*, 283-290, doi:10.1016/s2468-1253(16)30082-6.

137.   Mitsiades, N.; Yu, W.H.; Poulaki, V.; Tsokos, M.; Stamenkovic, I. Matrix metalloproteinase-7-mediated cleavage of Fas ligand protects tumor cells from chemotherapeutic drug cytotoxicity. *Cancer research* **2001**, *61*, 577-581.

138.   de Jongh, S.J.; Tjalma, J.J.J.; Koller, M.; Linssen, M.D.; Vonk, J.; Dobosz, M.; Jorritsma-Smit, A.; Kleibeuker, J.H.; Hospers, G.A.P.; Havenga, K., et al. Back-Table Fluorescence-Guided Imaging for Circumferential Resection Margin Evaluation Using Bevacizumab-800CW in Patients with Locally Advanced Rectal Cancer. *J Nucl Med* **2020**, *61*, 655-661, doi:10.2967/jnumed.119.232355.

139.   Lamberts, L.E.; Koch, M.; de Jong, J.S.; Adams, A.L.L.; Glatz, J.; Kranendonk, M.E.G.; Terwisscha van Scheltinga, A.G.T.; Jansen, L.; de Vries, J.; Lub-de Hooge, M.N., et al. Tumor-Specific Uptake of Fluorescent Bevacizumab-IRDye800CW Microdosing in Patients with Primary Breast Cancer: A Phase I Feasibility Study. *Clin Cancer Res* **2017**, *23*, 2730-2741, doi:10.1158/1078-0432.Ccr-16-0437.

140.   Wang, Z. ErbB Receptors and Cancer. *Methods Mol Biol* **2017**, *1652*, 3-35, doi:10.1007/978-1-4939-7219-7_1.

141.   Pellat, A.; Vaquero, J.; Fouassier, L. Role of ErbB/HER family of receptor tyrosine kinases in cholangiocyte biology. *Hepatology* **2018**, *67*, 762-773, doi:10.1002/hep.29350.

142.   Singh, B.; Carpenter, G.; Coffey, R.J. EGF receptor ligands: recent advances. *F1000Res* **2016**, *5*, F1000 Faculty Rev-2270, doi:10.12688/f1000research.9025.1.

143.   Duan, C.; Li, C.W.; Zhao, L.; Subramaniam, S.; Yu, X.M.; Li, Y.Y.; Chen de, H.; Li, T.Y.; Shen, L.; Shi, L., et al. Differential Expression Patterns of EGF, EGFR, and ERBB4 in Nasal Polyp Epithelium. *PLoS One* **2016**, *11*, e0156949, doi:10.1371/journal.pone.0156949.

144.   Huisman, B.W.; Burggraaf, J.; Vahrmeijer, A.L.; Schoones, J.W.; Rissmann, R.A.; Sier, C.F.M.; van Poelgeest, M.I.E. Potential targets for tumor-specific imaging of vulvar squamous cell carcinoma: A systematic review of candidate biomarkers. *Gynecologic oncology* **2020**, *156*, 734-743, doi:10.1016/j.ygyno.2019.12.030.

2

145.   Sasaki, T.; Hiroki, K.; Yamashita, Y. The role of epidermal growth factor receptor in cancer metastasis and microenvironment. *Biomed Res Int* **2013**, *2013*, 546318, doi:10.1155/2013/546318.

146.   Sigismund, S.; Avanzato, D.; Lanzetti, L. Emerging functions of the EGFR in cancer. *Mol Oncol* **2018**, *12*, 3-20, doi:10.1002/1878-0261.12155.

147.   Clinicaltrials.gov Cetuximab. Availabe online: https://clinicaltrials.gov/ct2/show/NCT00148109?term=cetuximab&cond=Soft+Tissue+Sarcoma&draw=3&rank=1 (accessed on 22 June 2020).

148.   Tummers, W.S.; Miller, S.E.; Teraphongphom, N.T.; Gomez, A.; Steinberg, I.; Huland, D.M.; Hong, S.; Kothapalli, S.R.; Hasan, A.; Ertsey, R., et al. Intraoperative Pancreatic Cancer Detection using Tumor-Specific Multimodality Molecular Imaging. *Ann Surg Oncol* **2018**, *25*, 1880-1888, doi:10.1245/s10434-018-6453-2.

149.   Miller, S.E.; Tummers, W.S.; Teraphongphom, N.; van den Berg, N.S.; Hasan, A.; Ertsey, R.D.; Nagpal, S.; Recht, L.D.; Plowey, E.D.; Vogel, H., et al. First-in-human intraoperative near-infrared fluorescence imaging of glioblastoma using cetuximab-IRDye800. *J Neurooncol* **2018**, *139*, 135-143, doi:10.1007/s11060-018-2854-0.

150.   Rosenthal, E.L.; Warram, J.M.; de Boer, E.; Chung, T.K.; Korb, M.L.; Brandwein-Gensler, M.; Strong, T.V.; Schmalbach, C.E.; Morlandt, A.B.; Agarwal, G., et al. Safety and Tumor Specificity of Cetuximab-IRDye800 for Surgical Navigation in Head and Neck Cancer. *Clin Cancer Res* **2015**, *21*, 3658-3666, doi:10.1158/1078-0432.Ccr-14-3284.

151.   Colman, R.W.; Pixley, R.A.; Sainz, I.M.; Song, J.S.; Isordia-Salas, I.; Muhamed, S.N.; Powell, J.A., Jr.; Mousa, S.A. Inhibition of angiogenesis by antibody blocking the action of proangiogenic high-molecular-weight kininogen. *J Thromb Haemost* **2003**, *1*, 164-170, doi:10.1046/j.1538-7836.2003.00025.x.

152.   Samkoe, K.S.; Gunn, J.R.; Marra, K.; Hull, S.M.; Moodie, K.L.; Feldwisch, J.; Strong, T.V.; Draney, D.R.; Hoopes, P.J.; Roberts, D.W., et al. Toxicity and Pharmacokinetic Profile for Single-Dose Injection of ABY-029: a Fluorescent Anti-EGFR Synthetic Affibody Molecule for Human Use. *Molecular imaging and biology* **2017**, *19*, 512-521, doi:10.1007/s11307-016-1033-y.

153.   Clinicaltrials.gov Panitumumab (Head&Neck Cancer). Availabe online: https://clinicaltrials.gov/ct2/show/NCT03405142?term=Panitumumab-IRDye800&draw=2&rank=4 (accessed on 22 June 2020).

154.   Clinicaltrials.gov Panitumumab (Lung Cancer). Availabe online: https://clinicaltrials.gov/ct2/show/NCT03582124?term=Panitumumab-IRDye800&draw=2&rank=3 (accessed on 22 June 2020).

155.   Clinicaltrials.gov Panitumumab. Availabe online: https://clinicaltrials.gov/ct2/show/NCT02415881?term=Panitumumab-IRDye800&draw=2&rank=2 (accessed on 22 June 2020).

156.   Clinicaltrials.gov Ganitumab. Availabe online: https://clinicaltrials.gov/ct2/show/NCT00819169?term=Ganitumab&cond=Soft+Tissue+Sarcoma&draw=2&rank=8, (accessed on 22 June 2020).

157.   Clinicaltrials.gov AMG-479. Availabe online: https://clinicaltrials.gov/ct2/show/NCT00562380?term=Ganitumab&cond=Soft+Tissue+Sarcoma&draw=2&rank=6 (accessed on 22 June 2020).

158.   Olmos, D.; Postel-Vinay, S.; Molife, L.R.; Okuno, S.H.; Schuetze, S.M.; Paccagnella, M.L.; Batzel, G.N.; Yin, D.; Pritchard-Jones, K.; Judson, I., et al. Safety, pharmacokinetics, and preliminary activity of the anti-IGF-1R antibody figitumumab (CP-751,871) in patients with sarcoma and Ewing's sarcoma: a phase 1 expansion cohort study. *Lancet Oncol* **2010**, *11*, 129-135, doi:10.1016/s1470-2045(09)70354-7.

159.   Pappo, A.S.; Vassal, G.; Crowley, J.J.; Bolejack, V.; Hogendoorn, P.C.; Chugh, R.; Ladanyi, M.; Grippo, J.F.; Dall, G.; Staddon, A.P., et al. A phase 2 trial of R1507, a monoclonal antibody to the insulin-like growth factor-1 receptor (IGF-1R), in patients with recurrent or refractory rhabdomyosarcoma, osteosarcoma, synovial sarcoma, and other soft tissue sarcomas: results of a Sarcoma Alliance for Research Through Collaboration study. *Cancer* **2014**, *120*, 2448-2456, doi:10.1002/cncr.28728.

160. Schoffski, P.; Adkins, D.; Blay, J.Y.; Gil, T.; Elias, A.D.; Rutkowski, P.; Pennock, G.K.; Youssoufian, H.; Gelderblom, H.; Willey, R., et al. An open-label, phase 2 study evaluating the efficacy and safety of the anti-IGF-1R antibody cixutumumab in patients with previously treated advanced or metastatic soft-tissue sarcoma or Ewing family of tumours. *Eur J Cancer* **2013**, *49*, 3219-3228, doi:10.1016/j.ejca.2013.06.010.

161. Zhang, H.; Zeng, X.; Li, Q.; Gaillard-Kelly, M.; Wagner, C.R.; Yee, D. Fluorescent tumour imaging of type I IGF receptor in vivo: comparison of antibody-conjugated quantum dots and small-molecule fluorophore. *British journal of cancer* **2009**, *101*, 71-79, doi:10.1038/sj.bjc.6605103.

162. Lai, Y.T.; Chao, H.W.; Lai, A.C.; Lin, S.H.; Chang, Y.J.; Huang, Y.S. CPEB2-activated PDGFRalpha mRNA translation contributes to myofibroblast proliferation and pulmonary alveologenesis. *J Biomed Sci* **2020**, *27*, 52, doi:10.1186/s12929-020-00643-0.

163. Andrae, J.; Gallini, R.; Betsholtz, C. Role of platelet-derived growth factors in physiology and medicine. *Genes Dev* **2008**, *22*, 1276-1312, doi:10.1101/gad.1653708.

164. Lin, L.H.; Lin, J.S.; Yang, C.C.; Cheng, H.W.; Chang, K.W.; Liu, C.J. Overexpression of Platelet-Derived Growth Factor and Its Receptor Are Correlated with Oral Tumorigenesis and Poor Prognosis in Oral Squamous Cell Carcinoma. *International journal of molecular sciences* **2020**, *21*, doi:10.3390/ijms21072360.

165. Andrick, B.J.; Gandhi, A. Olaratumab: A Novel Platelet-Derived Growth Factor Receptor α-Inhibitor for Advanced Soft Tissue Sarcoma. *Ann Pharmacother* **2017**, *51*, 1090-1098, doi:10.1177/1060028017723935.

166. Caudell, J.J.; Deavers, M.T.; Slomovitz, B.M.; Lu, K.H.; Broaddus, R.R.; Gershenson, D.M.; Ramondetta, L.M. Imatinib mesylate (gleevec)--targeted kinases are expressed in uterine sarcomas. *Applied immunohistochemistry & molecular morphology : AIMM* **2005**, *13*, 167-170.

167. Wang, J.; Coltrera, M.D.; Gown, A.M. Cell proliferation in human soft tissue tumors correlates with platelet-derived growth factor B chain expression: an immunohistochemical and in situ hybridization study. *Cancer research* **1994**, *54*, 560-564.

168. Gennatas, S.; Chamberlain, F.; Carter, T.; Slater, S.; Cojocaru, E.; Lambourn, B.; Stansfeld, A.; Todd, R.; Verrill, M.; Ali, N., et al. Real-world experience with doxorubicin and olaratumab in soft tissue sarcomas in England and Northern Ireland. *Clin Sarcoma Res* **2020**, *10*, 9, doi:10.1186/s13569-020-00131-x.

169. Piechutta, M.; Berghoff, A.S. New emerging targets in cancer immunotherapy: the role of Cluster of Differentiation 40 (CD40/TNFR5). *ESMO Open* **2019**, *4*, e000510, doi:10.1136/esmoopen-2019-000510.

170. Santilli, F.; Basili, S.; Ferroni, P.; Davi, G. CD40/CD40L system and vascular disease. *Intern Emerg Med* **2007**, *2*, 256-268, doi:10.1007/s11739-007-0076-0.

171. Vonderheide, R.H. Prospect of targeting the CD40 pathway for cancer therapy. *Clin Cancer Res* **2007**, *13*, 1083-1088, doi:10.1158/1078-0432.Ccr-06-1893.

172. Elmetwali, T.; Young, L.S.; Palmer, D.H. Fas-associated factor (Faf1) is a novel CD40 interactor that regulates CD40-induced NF-kappaB activation via a negative feedback loop. *Cell Death Dis* **2014**, *5*, e1213, doi:10.1038/cddis.2014.172.

173. Clinicaltrials.gov APX005M. Availabe online: https://clinicaltrials.gov/ct2/show/NCT03719430?term=APX005M&cond=Soft+Tissue+Sarcoma&draw=2&rank=1 (accessed on 22 June 2020).

174. Gu, L.; Ruff, L.E.; Qin, Z.; Corr, M.; Hedrick, S.M.; Sailor, M.J. Multivalent porous silicon nanoparticles enhance the immune activation potency of agonistic CD40 antibody. *Adv Mater* **2012**, *24*, 3981-3987, doi:10.1002/adma.201200776.

175. Ptaszyński, K.; Szumera-Ciećkiewicz, A.; Zakrzewska, K.; Tuziak, T.; Mrozkowiak, A.; Rutkowski, P. Her2, EGFR and TOPIIA gene amplification and protein expression in synovial sarcoma before and after combined treatment. *Pol J Pathol* **2009**, *60*, 10-18.

176.	Tap, W.D.; Wagner, A.J.; Schöffski, P.; Martin-Broto, J.; Krarup-Hansen, A.; Ganjoo, K.N.; Yen, C.C.; Abdul Razak, A.R.; Spira, A.; Kawai, A., et al. Effect of Doxorubicin Plus Olaratumab vs Doxorubicin Plus Placebo on Survival in Patients With Advanced Soft Tissue Sarcomas: The ANNOUNCE Randomized Clinical Trial. *Jama* **2020**, *323*, 1266-1276, doi:10.1001/jama.2020.1707.

177.	Yonemori, K.; Kodaira, M.; Satoh, T.; Kudo, T.; Takahashi, S.; Nakano, K.; Ando, Y.; Shimokata, T.; Mori, J.; Inoue, K., et al. Phase 1 study of olaratumab plus doxorubicin in Japanese patients with advanced soft-tissue sarcoma. *Cancer Sci* **2018**, *109*, 3962-3970, doi:10.1111/cas.13846.

178.	Wagner, A.J.; Kindler, H.; Gelderblom, H.; Schoffski, P.; Bauer, S.; Hohenberger, P.; Kopp, H.G.; Lopez-Martin, J.A.; Peeters, M.; Reichardt, P., et al. A phase II study of a human anti-PDGFRalpha monoclonal antibody (olaratumab, IMC-3G3) in previously treated patients with metastatic gastrointestinal stromal tumors. *Ann Oncol* **2017**, *28*, 541-546, doi:10.1093/annonc/mdw659.

179.	Schwartz, G.K.; Tap, W.D.; Qin, L.X.; Livingston, M.B.; Undevia, S.D.; Chmielowski, B.; Agulnik, M.; Schuetze, S.M.; Reed, D.R.; Okuno, S.H., et al. Cixutumumab and temsirolimus for patients with bone and soft-tissue sarcoma: a multicentre, open-label, phase 2 trial. *Lancet Oncol* **2013**, *14*, 371-382, doi:10.1016/s1470-2045(13)70049-4.

180.	Chisholm, K.M.; Chang, K.W.; Truong, M.T.; Kwok, S.; West, R.B.; Heerema-McKenney, A.E. β-Adrenergic receptor expression in vascular tumors. *Modern pathology : an official journal of the United States and Canadian Academy of Pathology, Inc* **2012**, *25*, 1446-1451, doi:10.1038/modpathol.2012.108.

181.	Federico, S.M.; Caldwell, K.J.; McCarville, M.B.; Daryani, V.M.; Stewart, C.F.; Mao, S.; Wu, J.; Davidoff, A.M.; Santana, V.M.; Furman, W.L., et al. Phase I expansion cohort to evaluate the combination of bevacizumab, sorafenib and low-dose cyclophosphamide in children and young adults with refractory or recurrent solid tumours. *Eur J Cancer* **2020**, *132*, 35-42, doi:10.1016/j.ejca.2020.03.010.

182.	Hong, D.S.; Garrido-Laguna, I.; Ekmekcioglu, S.; Falchook, G.S.; Naing, A.; Wheler, J.J.; Fu, S.; Moulder, S.L.; Piha-Paul, S.; Tsimberidou, A.M., et al. Dual inhibition of the vascular endothelial growth factor pathway: a phase 1 trial evaluating bevacizumab and AZD2171 (cediranib) in patients with advanced solid tumors. *Cancer* **2014**, *120*, 2164-2173, doi:10.1002/cncr.28701.

183.	Tap, W.D.; Federman, N.; Eilber, F.C. Targeted therapies for soft-tissue sarcomas. *Expert Rev Anticancer Ther* **2007**, *7*, 725-733, doi:10.1586/14737140.7.5.725.

184.	Petrus, P.; Fernandez, T.L.; Kwon, M.M.; Huang, J.L.; Lei, V.; Safikhan, N.S.; Karunakaran, S.; O'Shannessy, D.J.; Zheng, X.; Catrina, S.B., et al. Specific loss of adipocyte CD248 improves metabolic health via reduced white adipose tissue hypoxia, fibrosis and inflammation. *EBioMedicine* **2019**, *44*, 489-501, doi:10.1016/j.ebiom.2019.05.057.

185.	Vodanovich, D.A.; PF, M.C. Soft-tissue Sarcomas. *Indian J Orthop* **2018**, *52*, 35-44, doi:10.4103/ortho.IJOrtho_220_17.

186.	Human Protein Atlas. Availabe online: http://www.proteinatlas.org (accessed on 13 December 2020).

187.	Grothey, A.; Strosberg, J.R.; Renfro, L.A.; Hurwitz, H.I.; Marshall, J.L.; Safran, H.; Guarino, M.J.; Kim, G.P.; Hecht, J.R.; Weil, S.C., et al. A Randomized, Double-Blind, Placebo-Controlled Phase II Study of the Efficacy and Safety of Monotherapy Ontuxizumab (MORAb-004) Plus Best Supportive Care in Patients with Chemorefractory Metastatic Colorectal Cancer. *Clin Cancer Res* **2018**, *24*, 316-325, doi:10.1158/1078-0432.Ccr-17-1558.

188.	Coats, S.; Williams, M.; Kebble, B.; Dixit, R.; Tseng, L.; Yao, N.S.; Tice, D.A.; Soria, J.C. Antibody-Drug Conjugates: Future Directions in Clinical and Translational Strategies to Improve the Therapeutic Index. *Clin Cancer Res* **2019**, *25*, 5441-5448, doi:10.1158/1078-0432.Ccr-19-0272.

189.	Kersting, C.; Packeisen, J.; Leidinger, B.; Brandt, B.; von Wasielewski, R.; Winkelmann, W.; van Diest, P.J.; Gosheger, G.; Buerger, H. Pitfalls in immunohistochemical assessment of EGFR expression in soft tissue sarcomas. *J Clin Pathol* **2006**, *59*, 585-590, doi:10.1136/jcp.2005.028373.

Appendix A. Search Strategy.

("Sarcoma"[Mesh] OR "soft tissue sarcoma*"[tw]) AND ("Receptors, Vascular Endothelial Growth Factor"[Mesh] OR "VEGF"[tw] OR "vascular endothelial growth factor receptor"[tw] OR "EGFR"[tw] OR "epithelial growth factor receptor"[tw] OR "Endosialin"[tw] OR "TEM1"[tw] OR "CD248"[tw] OR "Receptors, Platelet-Derived Growth Factor"[Mesh] OR "Platelet-Derived Growth Factor Receptor*"[tw] OR "PDGFR"[tw] OR "programmed death ligand 1"[tw] OR "PD-L1"[tw] OR "Insulin-Like Growth Factor I"[Mesh] OR "Insulin-Like Growth Factor I"[tw] OR "IGF-1R"[tw] OR "TRAIL-R2"[tw] OR "CTLA-4 Antigen" [Mesh] OR "CTLA-4"[tw] OR "CD40 Antigens"[Mesh] OR "CD40"[tw] OR "Receptor Tyrosine Kinase-like Orphan Receptors"[Mesh] OR "Receptor Tyrosine Kinase-like Orphan Receptor*"[tw] OR "ROR2"[tw] OR "LRRC15"[tw]) NOT ("Animals" [Mesh] NOT "Humans"[Mesh])

Appendix B. Search Previously Imaged and Search Internalization.

("Spectroscopy, Near-Infrared"[Mesh] OR "Near-Infrared"[tw] OR "Near infrared"[tw] OR "NIR"[tw] OR "fluorescence"[MeSH] OR "fluorescence"[tw] OR "fluorescent"[tw] OR "imaging"[tw] OR "Positron Emission Tomography Computed Tomography"[tw] OR "PET-CT"[tw] OR "PET"[tw] OR "immune-pet"[tw] OR "tomography, emission-computed, single-photon"[MeSH] OR "spect"[tw] OR "radiolabelled"[tw] OR "radio-labelled"[tw] AND ("Receptors, Vascular Endothelial Growth Factor"[Mesh] OR "VEGF"[tw] OR "vascular endothelial growth factor receptor"[tw] OR "EGFR"[tw] OR "epithelial growth factor receptor"[tw] OR "Endosialin"[tw] OR "TEM1"[tw] OR "CD248"[tw] OR "Receptors, Platelet-Derived Growth Factor"[Mesh] OR "Platelet-Derived Growth Factor Receptor*"[tw] OR "PDGFR"[tw] OR "programmed death ligand 1"[tw] OR "PD-L1"[tw] OR "Insulin-Like Growth Factor I"[Mesh] OR "Insulin-Like Growth Factor I"[tw] OR "IGF-1R"[tw] OR "TRAIL-R2"[tw] OR "CTLA-4 Antigen" [Mesh] OR "CTLA-4"[tw] OR "CD40 Antigens"[Mesh] OR "CD40"[tw] OR "Receptor Tyrosine Kinase-like Orphan Receptors"[Mesh] OR "Receptor Tyrosine Kinase-like Orphan Receptor*"[tw] OR "ROR2"[tw] OR "LRRC15"[tw])

("Internalization"[tw] OR "Internalize"[tw] OR "Internalisation"[tw] OR "Internalise"[tw] OR "Endocytosis"[Mesh] OR "Endocytosis"[tw] OR "Endocyte"[tw]) AND ("Receptors, Vascular Endothelial Growth Factor"[Mesh] OR "VEGF"[tw] OR "vascular endothelial growth factor receptor"[tw] OR "EGFR"[tw] OR "epithelial growth factor receptor"[tw] OR "Endosialin"[tw] OR "TEM1"[tw] OR "CD248"[tw] OR "Receptors, Platelet-Derived Growth Factor"[Mesh] OR "Platelet-Derived Growth Factor Receptor*"[tw] OR "PDGFR"[tw] OR "programmed death ligand 1"[tw] OR "PD-L1"[tw] OR "Insulin-Like Growth Factor I"[Mesh] OR "Insulin-Like Growth Factor I"[tw] OR "IGF-1R"[tw] OR "TRAIL-R2"[tw] OR "CTLA-4 Antigen" [Mesh] OR "CTLA-4"[tw] OR "CD40 Antigens"[Mesh] OR "CD40"[tw] OR "Receptor Tyrosine Kinase-like Orphan Receptors"[Mesh] OR "Receptor Tyrosine Kinase-like Orphan Receptor*"[tw] OR "ROR2"[tw] OR "LRRC15"[tw])

Appendix C. STS Subtypes Examined for Each of the Top 7 Biomarkers.

Table 1. Overview of the studied STS subtypes for each of the top 7 biomarkers.

Biomarker	STS Subtypes
TEM1	Angiosarcoma, desmoplastic small round cell, epithelioid hemangioendothelioma, epithelioid sarcoma, fibrosarcoma, inflammatory myofibroblastic sarcoma, kaposi sarcoma, LMS, liposarcoma, MPNST, malignant solitary fibrous tumor, myxofibrosarcoma, RMS, spindle cell sarcoma NOS, synovial sarcoma, USTS, and uterine sarcoma
VEGFR-1	Alveolar STS, angiosarcoma, endometrial stromal sarcoma, Kaposi sarcoma, LMS, liposarcoma, MPNST, malignant solitary fibrous tumor, myxofibrosarcoma, myxoid liposarcoma, pulmonary artery sarcoma, RMS, sarcoma NOS, synovial sarcoma, and USTS
VEGFR-2	Alveolar STS, angiosarcoma, endometrial stromal sarcoma, epithelioid hemangioendotheliomas, fibrosarcoma, LMS, liposarcoma, MPNST, malignant solitary fibrous tumor, myxofibrosarcoma, pulmonary artery sarcoma, RMS, sarcoma NOS, synovial sarcoma, and USTS
EGFR	Acral myxoinflammatory fibroblastic sarcoma, alveolar soft part sarcoma, atypical fibroxanthoma, desmoplastic tumor, endometrial stromal sarcoma, epithelioid sarcoma, fibromatosis, fibromyxoid sarcoma, fibrosarcoma, follicular dendritic cell sarcoma, intimal sarcoma, liposarcoma, LMS, MPNST, myofibroblastic sarcoma, myxoinflammatory fibroblastic sarcoma, myxofibrosarcoma, myxoid liposarcoma, myxoid sarcoma, pleomorphic dermal sarcoma, RMS, sarcoma NOS, synovial sarcoma, undifferentiated endometrial sarcoma, USTS, and undifferentiated stromal sarcoma
IGF-1R	Alveolar STS, angiosarcoma, desmoplastic tumor, fibrosarcoma, LMS, liposarcoma, MPNST, myxofibrosarcoma, RMS, sarcoma NOS, spindle cell sarcoma, synovial sarcoma, and USTS
PDGFRα	Alveolar soft part sarcoma, Angiosarcoma, dermatofibrosarcoma protuberans, endometrial stromal sarcoma, fibromyxoid sarcoma, fibrosarcoma, liposarcoma, LMS, MPNST, myofibroblastic sarcoma, myxoinflammatory fibroblastic sarcoma, myxofibrosarcoma, myxoid liposarcoma, pulmonary artery sarcoma, RMS, sarcoma NOS, solitary fibrous tumor, synovial sarcoma, undifferentiated endometrial sarcoma, undifferentiated uterine sarcoma, undifferentiated stromal sarcoma, and USTS
CD40	Kaposi sarcoma, liposarcoma, LMS, MPNST, RMS, and USTS

Appendix D. Toxicity of Clinically Available Monoclonal Antibodies in Patients with STS.

Table 2. Overview of the Toxicity of Clinically Available Monoclonal Antibodies in STS Patients.

Clinical trial	Phase	Tumor type	Evaluable for toxicity	Median age (years)	Treatment	Most common adverse events	Percentage patients with ≥3 adverse events (vs placebo)	Most common grade ≥ 3 adverse events
TEM1 (Ontuxizumab)								
Jones et al. 2019	2	STS	209	55	Ontuxizumab 8mg/kg + G/D VS placebo + G/D[e]	Fatigue (74% vs 66%), anemia (61% vs 60%), nausea (56% vs 52%), diarrhea (44% vs 36%), and peripheral edema (42% vs 45%)	Not reported	Pyrexia (4% vs 0%) and anemia (1% vs 3%)[g]
IGF-1R (Teprotomumab, Figitumumab and Cixutumumab)								
Pappo et al. 2014	2	STS + osteosarcoma	163	31	Teprotumumab 9mg/kg; 1 dose per week	Fatigue (20.2%), nausea (14.1%), hyperglycemia (9.2%), and muscle spasms (8.6%)	10.4%	Hyperglycemia (2.5%), dehydration (1.8%), fatigue (1.8%), and hyponatremia (1.2%)
Olmos et al. 2010	1	STS + Ewing sarcoma + myxoid chondrosarcoma	29	30	Figitumumab 20mg/kg; 1 dose per 3-4 weeks	Hyperglycemia (17%), skin reactions (rash, urticaria, infection, eczema) (13.8%), increased GGT (10.3%), headache (10.3%), and fatigue (10.3%)	17.2%	Vomiting (3.4%), back pain (3.4%), DVT (3.4%), increased uric acid concentration (3.4%), and increased AST, ALT or GGT (3.4%)
Wagner et al. 2015	2	STS + Ewing sarcoma + osteosarcoma	44	14 – 18[1]	Cixutumumab 6mg/kg and Temsirolimus 8mg/m2; 1 dose per week	Mucositis, electrolyte disturbances and myelosuppression [f]	Not reported	Neutropenia (13.6%), thrombocytopenia (11.4%), hypokalemia (11.4%), oral mucositis (9.1%), and hypophosphatemia (9.1%)

2

Table 2. Overview of the Toxicity of Clinically Available Monoclonal Antibodies in STS Patients. *(continued)*

Clinical trial	Phase	Tumor type	Evaluable for toxicity	Median age (years)	Treatment	Most common adverse events	Percentage patients with ≥3 adverse events (vs placebo)	Most common grade ≥ 3 adverse events
Schöffski et al. 2013	2	STS + Ewing family of tumors	113	27.5 – 33[1]	Cixutumumab 10mg/kg; 1 dose per 2 weeks	Nausea (26.1%), fatigue (23.4%), diarrhea (22.5%), hyperglycemia (19.8%), and anorexia (17.1%)	Not reported	Hyperglycemia (5.4%), pain (5.4%), thrombocytopenia (4.5%), asthenia (4.5%), and anemia (3.6%)
Schwartz et al. 2013	2	STS + sarcoma of bone	174	Mean: 48.1	Cixutumumab 6mg/kg and Temsirolimus 25mg; 1 dose per week	Oral mucositis (71.3%), hypercalcemia (68.4%), fatigue (65.5%), thrombocytopenia (63.8%), and anemia (62.6%)	Not reported	Anemia (9%), hyperglycemia (10%), hypophosphatemia (9%), lymphopenia (14%), oral mucositis (11%), and thrombocytopenia (11%)
PDGFR (Olaratumab)								
Tap et al. 2020	3	STS	506	Mean: 56.9	Olaratumab 15 mg/kg + Doxorubicin 75 mg/m² vs. Placebo + Doxorubicin 75 mg/m²[d]	Nausea (59.5% vs. 66.7%), neutropenia (55.3% vs. 57.8%), fatigue (54.1% vs. 59%), alopecia (43.6% vs. 49.8%), and anemia (42.8% vs. 45.4%)	Not reported	Neutropenia (46.3% vs. 49%), leukopenia (23.3% vs. 23.7%), febrile neutropenia (17.5% vs. 16.5%), anemia (13.6% vs. 12.4%), and thrombocytopenia (9.3% vs. 8.4%)
Yonemori et al. 2018	1	STS	19	41.5–52[a]	Olaratumab 15 mg/kg + Doxorubicin 25-75 mg/m²[e]	ALT increased (52.6%), neutrophil count decreased (52.6%), WBC count decreased (47.4%), anemia (36.8%), and GGT increased (31.6%)	57.9%	Decreased neutrophil count (42.1%), decreased WBC count (42.1%), increased ALT (15.8%), anemia (10.5%), and febrile neutropenia (10.5%)

2

Table 2. Overview of the Toxicity of Clinically Available Monoclonal Antibodies in STS Patients. *(continued)*

Clinical trial	Phase	Tumor type	Evaluable for toxicity	Median age (years)	Treatment	Most common adverse events	Percentage patients with ≥3 adverse events (vs placebo)	Most common grade ≥ 3 adverse events
Tap et al. 2016	2	STS	133	58.5	Olaratumab 15 mg/kg + Doxorubicin 75 mg/m² vs. Doxorubicin [f]	Nausea (73.4% vs. 52.3%), fatigue (68.8% vs. 69.2%), neutropenia (57.8% vs. 35.4%), mucositis (53.1% vs. 35.4%), and alopecia (51.6% vs. 40%)	67% vs. 55%	Neutropenia (53.2% vs. 32.3%), leukopenia (36% vs. 16.9%), febrile neutropenia (12.5% vs. 13.8%), anemia (12.5% vs. 9.2%), and fatigue (9.4% vs. 3.1%)

Abbreviations: STS, soft tissue sarcoma; ALT, alanine aminotransferase; WBC, white blood cell; GGT, gamma-glutamyl transferase; DVT, deep venous thrombosis; AST, aspartate aminotransferase.

[a] These trials had several cohorts with each a separate median age. Reported in the table is the range of median ages.

[b] Full treatment schedule was: Olaratumab 20 mg/kg in cycle 1 and 15 mg/kg in subsequent cycles or placebo (days 1 and 8) combined with Doxorubicin 75 mg/m2 (day 1) for up to 8 21-day cycles, followed by Olaratumab/placebo monotherapy.

[c] Full treatment schedule was: Olaratumab 15 mg/kg (day 1 and 8) of each 21-day cycle until progressive disease (PD) or other discontinuation criteria were met. Patients in Cohort 3 received a 20 mg/kg loading dose of Olaratumab (Day 1 and 8) in Cycle 1. Doxorubicin was administered for up to 6 cycles (or a cumulative dose of 500 mg/ m2, whichever came later) until PD or other discontinuation criteria were met. Patients in Cohort 1 received doxorubicin 25mg/m2 (day 1, 2, and 3) in each cycle, Cohorts 2 and 3 received doxorubicin 75mg/m2 (day 1) in each cycle.

[d] Full treatment schedule was: Olaratumab 15mg/kg (day 1 and 8) combined with doxorubicin 75mg/m2 or doxorubicin alone 75mg/m2 (day 1) of each 21-day cycle for up to eight cycles.

[e] Full treatment schedule was: Ontuxizumab 8mg/kg (day 1 and 8) of a 21-day cycle or a placebo with G/D (G/D; 900 mg/m2 gemcitabine (day 1 and 8) and 75mg/m2 docetaxel (day 8))

[f] Percentages not reported.

[g] These are the serious adverse events instead of all grade ≥3 adverse events, as the latter was not reported.

3

IMMUNOHISTOCHEMICAL EVALUATION OF BIOMARKERS FOR FLUORESCENCE-GUIDED SURGERY OF MYXOFIBROSARCOMA

Z. Rijs[1], E. Belt[1], G.M. Kalisvaart[2], C.F.M. Sier[3], P.J. K. Kuppen[3], A.H.G. Cleven[4,5], A.L. Vahrmeijer[3], M.A.J. van de Sande[1], P.B.A.A. van Driel[6]

[1] Department of Orthopedic Surgery, Leiden University Medical Center, Leiden, The Netherlands
[2] Department of Radiology, Leiden University Medical Center, Leiden, The Netherlands
[3] Department of Surgery, Leiden University Medical Center, Leiden, The Netherlands
[4] Department of Pathology, Leiden University Medical Center, Leiden, The Netherlands
[5] Department of Pathology, University Medical Center Groningen, Groningen, The Netherlands
[6] Department of Orthopedic Surgery, Isala Hospital, Zwolle, The Netherlands

Abstract

Introduction: Myxofibrosarcoma (MFS) is the most common soft-tissue sarcoma subtype in elderly patients. Local recurrence (LR) remains a major concern as the lack of intraoperative guidance and an infiltrative growth pattern with long, slender tails hamper surgeons' ability to achieve adequate resection margins for MFS. Fluorescence-guided surgery (FGS) could overcome this concern by delineating tumor tissue during surgery. One of the most important steps to successful FGS is to define a tumor-specific biomarker that is highly overexpressed in tumor tissue while low or absent in adjacent healthy tissue. The aim of this study is to evaluate the expression of eight previously selected promising biomarkers for FGS in MFS tissue samples with adjacent healthy tissue using immunohistochemistry (IHC). Methods: The following eight biomarkers were stained in seventeen paraffin-embedded MFS samples: tumor endothelial marker-1 (TEM-1, also known as endosialin/CD248), vascular endothelial growth factor receptor-1 (VEGFR-1, also known as Flt-1), vascular endothelial growth factor receptor-2 (VEGFR-2, also known as Flk1), vascular endothelial growth factor-A (VEGF-A), epidermal growth factor receptor (EGFR), insulin-like growth factor-1 receptor (IGF-1R), platelet derived growth factor receptor-α (PDGFR-A), and cluster of differentiation 40 (CD40, also known as TNFRSF5). A pathologist specializing in sarcoma annotated the margin between the tumor and adjacent healthy tissue in each MFS tissue sample. Subsequently, we used an objective IHC scoring method to assess and compare the difference in staining intensity between the tumor and adjacent healthy tissue, which is crucial for the use of FGS. Results: TEM-1, VEGF-A, and PDGFR-α stained all MFS tumors, while the other biomarkers did not show expression in all MFS tumors. Ultimately, TEM-1 was identified as the most suitable biomarker for FGS in MFS based on higher tumor-to-background (TBR) staining intensity compared to VEGF-A and PDGFR-α, regardless of preoperative therapy. Conclusion: TEM-1-targeted FGS tracers should be further investigated to optimize MFS treatment.

Introduction

Myxofibrosarcoma (MFS) is the most common soft tissue sarcoma (STS) subtype in elderly patients, with a peak incidence in 60–69-year-old patients [1,2]. To optimize treatment, MFS patients are referred to specialized sarcoma centers, where treatment is discussed in multidisciplinary tumor boards before surgery [3,4]. Despite increased complication risks associated with radiotherapy, localized MFS is currently treated with (neo)adjuvant radiotherapy combined with often extensive surgery [5,6]. This is because local recurrence (LR) is a major concern, occurring in 28–40% of MFS cases within a 5 year follow-up period and often associated with inadequate surgical margins [7,8]. Inherently, surgical margins are a significant predictor of survival [9]. Yet, sarcoma surgeons still rely on preoperative imaging modalities, such as MRI and CT, to identify the exact tumor location and margins. Translation of these preoperative images to the operating theatre is challenging, as surgeons only have their hands and eyes to rely on during surgery. In addition, the position of soft tissue changes during surgery, and MFS has an infiltrative growth pattern with long, slender tails that are difficult to detect with preoperative imaging [10]. Consequently, the surgical margins are difficult to appreciate and manage during surgery [11]. Efforts have been made to unravel the pathogenesis and identify druggable targets with molecular analyses, and targeting the cell cycle in these tumors could be a powerful approach [12,13]. However, this has not yet led to improved outcomes; a recent cohort study including 908 MFS patients, diagnosed between 2002 and 2019, highlighted that LR rates (39%) and survival (five year overall survival of 68%) did not improve during the study period, emphasizing the need to improve treatment strategies [14].

An upcoming tool and a different approach to achieving adequate margins in surgical oncology is fluorescence-guided surgery (FGS), which is based on near-infrared fluorescence (NIRF). FGS real-time intraoperative imaging helps the surgeon to discriminate tumors from adjacent healthy tissue. It can be subdivided into non-targeted FGS and targeted (tumor-specific) FGS. Non-targeted FGS mostly uses the fluorescent dye indocyanine green (ICG). Once ICG is administered, it accumulates in tumors due to their leaky vascular capillaries, which is referred to as the enhanced permeability and retention (EPR) effect [15]. However, this EPR effect is known to be influenced by many factors, such as tumor type, size, presence of necrosis, location, inflammation, and vascular mediators, as has been demonstrated for sarcoma surgery [16]. Therefore, the signal intensity of ICG is unpredictable, and will vary greatly between heterogeneous sarcoma tumors. False negativity could occur in cases with very small nodules, nodules with extensive necrosis, or minimally viable tissue. False positivity could occur as well, for example, in tissues with reactive changes or high levels of vascular permeability mediators such as bradykinin and prostaglandin. This could lead to over-resection, resulting in more wound complications and increased functional impairments. Targeted FGS, which can be achieved by binding fluorophores to sarcoma-specific targeting moieties such as antibodies or peptides, could theoretically overcome these issues. Targeted

3

FGS has already been explored for various tumor types with promising results and has the potential to play an important role in future sarcoma surgery [17-19].

Three important parameters define successful targeted FGS: the tumor-specific biomarker, the targeting moiety conjugated to a fluorophore (tracer), and the dedicated FGS camera system. While the ideal tumor-specific biomarker is strongly and diffusely expressed on tumor cells and absent on adjacent healthy tissue, a minimum of 1.5x overexpression of the tumor-specific biomarker on tumor cells compared to adjacent healthy tissue is already enough to guide surgeons in their actions [20]. The biomarker should preferably be located on the cell surface of malignant cells to permit direct targeting and have the possibility of internalization to facilitate a long-lasting fluorescence signal. Ideally, this biomarker is still present on residual cells after preoperative therapy. Based on these criteria, promising clinically translatable tumor-specific biomarkers for MFS and other sarcomas have been identified in a recent systematic review [21]. Since several dedicated NIRF camera systems are already on the market, evaluating a suitable biomarker is currently one of the most important steps to orchestrating successful FGS in MFS [22]. Nevertheless, preclinical immunohistochemical (IHC) evaluation studies evaluating biomarkers for FGS in MFS are scarce and did not comprehensively compare biomarkers in tumor tissue with adjacent healthy tissue [23]. Therefore, this study aims to evaluate and compare the expression of eight previously selected promising biomarkers for FGS by IHC in MFS tissue samples with adjacent healthy tissue using an objective IHC scoring method. In addition, the effect of preoperative therapy on staining intensity is assessed to determine if this might influence the biomarker's suitability for FGS.

Materials and methods

Sample Selection and Ethical Approval
Tissue samples from MFS patients who gave informed consent for the use of their tissue at the time of surgery, were older than 18 years, and underwent surgical resection between 2008 and 2020 were eligible for this study. Slides of MFS tissue samples with tumor and adjacent healthy tissue were selected by a pathologist specializing in sarcoma. Subsequently, all available corresponding formalin-fixed paraffin-embedded (FFPE) whole tissue blocks were collected from the bone and soft tissue tumor biobank at the Leiden University Medical Center. Anonymized patient and tumor characteristics of the collected specimen were retrospectively reviewed to describe some of the patient and tumor characteristics. The study was performed with ethical approval from the institutional review board of Leiden-Den Haag-Delft (protocol number: 2020-7; METC number: B20.048) and in compliance with the Declaration of Helsinki.

Biomarkers
A total of eight biomarkers were selected for IHC evaluation based on their potential to detect FGS in MFS. Biomarkers were chosen based on a clinical trial that had already included MFS patients using vascular endothelial growth factor A (VEGF-A) as a target for

FGS and a systematic review that selected targets for FGS in soft tissue sarcomas [18,21]. Selected biomarkers were: tumor endothelial marker-1 (TEM-1), vascular endothelial growth factor receptor-1 (VEGFR-1), vascular endothelial growth factor receptor-2 (VEGFR-2), VEGF-A, epidermal growth factor receptor (EGFR), insulin-like growth factor-1 receptor (IGF-1R), platelet-derived growth factor receptor-α (PDGFR-α), and cluster of differentiation antigen 40 (CD40, also known as TNFRS5 or p50).

Immunohistochemistry procedure

The primary and secondary antibodies used for IHC evaluation were selected based on the literature and previous experience with antibodies for IHC staining in our lab [23] (Supplementary Table S1). FFPE whole tissue samples from MFS patients were collected, and 4 µm-thick sections were prepared using a microtome (Leica RM2235, Leica Biosystems, Nußloch, Germany). Next, sections were deparaffinized in xylene for 15 min, rehydrated in a series of 100%, 50%, and 25% ethanol dilutions, and rinsed in demineralized water. Subsequently, endogenous peroxidase was blocked with 0.3% hydrogen peroxide in demineralized water for 20 min. Afterwards, antigen retrieval was done as described in Supplementary Table S1 using the PT Link (Dako, Glostrup, Denmark), and two washing steps of 5 min in phosphate buffered saline (PBS) were performed. According to the protocol, sections were incubated in a humidified room with 150 µL primary antibodies using predetermined optimal solutions based on a series of test stainings for each biomarker on positive as well as negative controls (identified with the human protein atlas, Supplementary Table S1) [24]. Afterwards, slides were washed three times in PBS for 5 min and incubated with appropriate secondary antibodies (goat anti-mouse HRP conjugate for VEGF-A: catalog number K4001, Agilent Technologies, Santa Clara, CA, USA; and goat anti-rabbit HRP conjugate for all other biomarkers: catalog number K4003, Agilent Technologies, Santa Clara, CA, USA), followed by an additional washing step. Staining was visualized through incubation with 3,3-diaminobenzidine tetrahydrochloride solution (DAB, K3468, Agilent Technologies, Inc., Santa Clara, CA, USA) for 10 min at room temperature. Finally, sections were counterstained with Mayer's hematoxylin solution for 30 s (Sigma-Aldrich, St. Louis, MO, USA) and rinsed. After dehydration in an incubator for 1 h at 37°C, slides were mounted with Pertex (Leica Microsystems, Wetzlar, Germany). A negative (PBS) and conjugate control (only secondary antibody) were included to evaluate potential nonspecific staining. Slides were examined under a Zeiss AxioSkop 20 light microscope (Carl Zeiss, Jena, Germany), scanned using a PANNORAMIC 250 scanner (3DHISTECH Ltd., Budapest, Hungary), and viewed using CaseViewer (3DHISTECH Ltd., Budapest, Hungary).

Objective Immunohistochemistry Scoring Method

A pathologist specializing in sarcoma (who works in a tertiary referral center and has more than 10 years of experience) annotated the margin between tumor and adjacent healthy tissue in each hematoxylin and eosin (H&E)-stained MFS tissue sample using the CaseViewer application. Annotated images were saved and opened in ImageJ, an open platform for biomedical image analysis [25]. An objective and easy-to-use 5 step protocol was used to evaluate the difference in staining intensity between the tumor and adjacent healthy tissue

(Supplementary Protocol S1). In step 1, we select the tumor and adjacent healthy tissue as two separate regions of interest (ROI), based on manual annotations from the pathologist. In step 2, the non-DAB color spectra are filtered out by using the color deconvolution option (H&E DAB) [26]. In this way, only the relevant brown DAB staining that indicates biomarker staining intensity can be assessed. In step 3, the image data is converted from the tridimensional RGB color model into monochromous grayscale (pixel intensities ranging from 0 to 255) to reflect DAB staining density. In step 4, the image is inverted, so high pixel intensities represent high DAB staining density. Step 5 is the measurements step, where we measure the mean staining intensity and standard deviation in tumor tissue and adjacent healthy tissue. These values can be used for statistical analyses to indicate the difference in staining intensity between the tumor and adjacent healthy tissue and to calculate the tumor-to-background ratio (TBR, calculated as the mean staining intensity of the tumor ROI divided by the mean staining intensity of the adjacent healthy tissue ROI), which is crucial for assessing a biomarker's potential for FGS; a higher TBR indicates a greater potential for its use in FGS.

Statistical Analysis
Statistical analyses were performed using SPSS version 25 (IBM Corp., Armonk, NY, USA), and graphs were made using GraphPad PRISM (version 9, GraphPad Software, La Jolla, CA, USA). The mean and standard deviation were used because the distribution of our data was symmetric and there were no clear outliers. Descriptive statistics were used to report the TBR of each biomarker. A comparison of the mean staining intensity within one sample (tumor compared to adjacent healthy tissue) for biomarkers that showed good overall expression was performed using a paired t-test. A comparison of the mean staining intensity between two groups (with or without preoperative therapy) for biomarkers that showed good overall expression was performed using an unpaired t-test. Significance was set at a p-value ≤ 0.05.

Results

Patient Characteristics
Whole tissue blocks with vital tumor resection material and adjacent healthy tissue from seventeen MFS cases were included in this IHC evaluation study (Table 1). The total cohort had a mean age of 66 years; most of the included patients were male (n = 9; 53%); most tumors were located in the extremities (n = 14; 82%); most tumors had an intermediate or high histological grade according to the French Federation of Cancer Centers Sarcoma Group (FNCLCC) grading system (n = 13; 76%); most patients received preoperative therapy (n = 11; 65%); and the histopathological response according to the European Organization for Research and Treatment of Cancer-Soft Tissue and Bone Sarcoma Group (EORT-STBSG) was always E (≥50% stainable tumor cells; Table 1) [27,28].

Table 1. Patient and tumor characteristics.

Patient	Gender	Age	Tumor location	Histological Grade (FNCLCC)	Preoperative therapy	Response score (EORTC-STBSG)
1	Female	77	Upper extremity	2	None	Not applicable
2	Male	56	Upper extremity	1	None	Not applicable
3	Female	62	Lower extremity	1	Radiotherapy	E
4	Male	68	Trunk	1	None	Not applicable
5	Male	55	Lower extremity	2	None	Not applicable
6	Female	81	Trunk	3	None	Not applicable
7	Female	63	Upper extremity	2	None	Not applicable
8	Male	47	Lower extremity	1	Radiotherapy	E
9	Male	64	Upper extremity	2	Radiotherapy	E
10	Female	64	Upper extremity	3	Radiotherapy	E
11	Male	78	Lower extremity	2	Radiotherapy	E
12	Male	49	Lower extremity	2	Radiotherapy	E
13	Female	70	Lower extremity	2	Radiotherapy	E
14	Male	70	Trunk	2	Radiotherapy	E
15	Male	79	Lower extremity	3	Chemotherapy	E
16	Female	67	Upper extremity	2	Radiotherapy	E
17	Female	66	Upper extremity	2	Radiotherapy	E

Abbreviations: FNCLCC = French Federation of Cancer Centers Sarcoma Group classification system; 1 = low grade, 2 = intermediate grade, 3 = high grade. EORTC-STBSG = European Organization for Research and Treatment of Cancer-Soft Tissue and Bone Sarcoma Group; A = no stainable tumor cells, B = single stainable tumor cells or small clusters (overall below 1% of the whole specimen), C = ≥1% - <10% stainable tumor cells, D = ≥10% - < 50% stainable tumor cells, E = ≥50% stainable tumor cells.

Immunohistochemistry Results

Despite repeated scanning, annotating tumor tissue was impossible for two samples due to destructed IHC slides (loss of attachment) and bad imaging quality. We were able to include seventeen MFS cases in our IHC analyses. For the patients that had more than one FFPE sample, mean staining intensity values were averaged to ensure that each patient had one corresponding mean staining intensity value for the tumor tissue and one corresponding mean staining intensity value for the adjacent healthy tissue.

TEM-1, PDGFR-α, and VEGF-A Are Promising Biomarkers for FGS in MFS

Diffuse, strong TEM-1 expression was observed in all MFS (100%). For all TEM-1-stained samples, there was a mean staining intensity of 81 in tumor tissue (mean standard deviation 39) and a mean TBR of 3.1. Although TEM1 staining intensity values varied greatly between different samples, expression was always higher in tumors than in adjacent healthy tissue (Figure 1). For most cases, clear differences were observed between the tumor and adjacent muscle and fat tissue (Figures 2 and 3).

Diffuse, strong VEGF-A staining was also observed in all cases (100%), where the mean staining intensity of tumor tissue was 88 (mean standard deviation, 45). However, VEGF-A had a mean TBR of 2.4 because staining intensity was relatively high in adjacent healthy tissue. Moreover, in three samples, the staining intensity was higher in adjacent healthy tissue than in tumor tissue, resulting in a TBR < 1 (Figure 1).

For PDGFR-α, all MFS tumor cases (100%) also showed diffuse, strong expression, with a mean staining intensity of 64 (mean standard deviation, 36) and a mean TBR of 1.8. Similar to the VEGF-A staining, three samples had a higher staining intensity in adjacent healthy tissue compared to tumor tissue, resulting in a TBR < 1 (Figure 1).
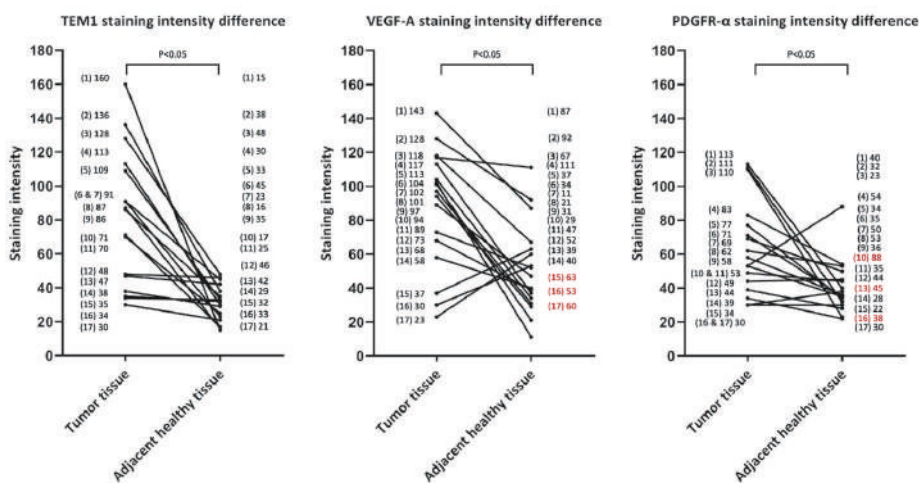
Figure 1. *Tissue intensity difference between tumor- and adjacent healthy tissue per myxofibrosarcoma-stained sample. Exact mean staining intensity values per case are displayed on the left- and right y-axis. TEM-1 displays the highest difference in tumor- versus adjacent healthy tissue staining intensity. For three cases, VEGF-A staining intensity and PDGFR-α staining intensity was higher in adjacent healthy tissue compared to tumor tissue (shown in red). Samples had a statistically significant higher staining intensity in tumor- compared to adjacent healthy tissue for the TEM-1, VEGF-A, and PDGFR-α staining groups (p<0.05).*
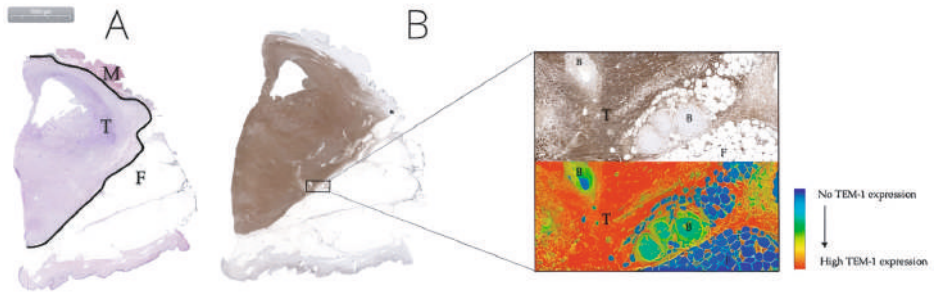
Figure 2. Grade 2 MFS located in the upper arm of a 63-year-old female. H&E staining of MFS tumor tissue (T), the tumor border (black line) and adjacent muscle tissue (M) (A). Corresponding TEM-1 staining (B): the upper right 10x enlarged image displays tumor tissue (T), the tumor border (black line), and adjacent healthy muscle tissue (M). The lower right corresponding image shows a gradient map of the same TEM-1 staining which clearly delineates tumor from adjacent healthy tissue.
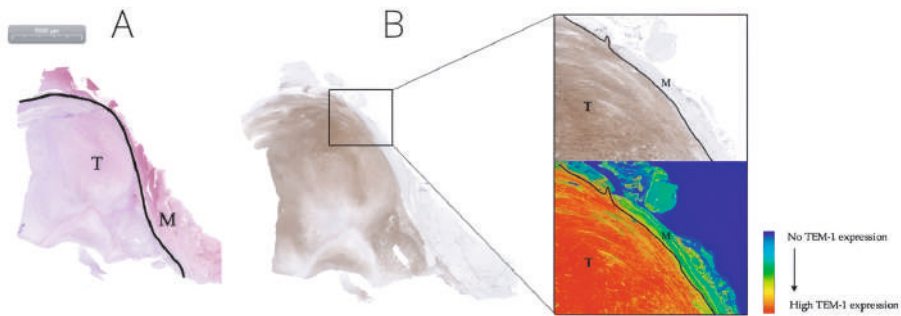
Figure 3. Grade 3 MFS tumor located in the upper arm of a 64-year-old female. H&E staining of MFS tumor tissue (T), the tumor border (black line) and adjacent muscle- and fat tissue (M and F) (A). Corresponding TEM-1 staining (B): the upper right 30x enlarged image displays tumor tissue (T), blood vessels (B), and adjacent fat tissue (F). The lower right corresponding image shows a gradient map of the same TEM-1 staining which clearly delineates tumor from adjacent healthy tissue.

VEGFR-1, VEGFR-2, EGFR, IGF-1R, and CD40 did not show good overall expression

Unfortunately, VEGFR-1, VEGFR-2, EGFR, IGF-1R, and CD40 was (Supplementary Figure S3) not expressed in 13/17 (76%) MFS cases (Supplementary Figures S1 – S3). Based on the 4 (24%) cases that showed biomarker expression, VEGFR-1 had a mean tumor staining intensity of 21, with a mean TBR of 1.5. In the same cases, mean tumor staining intensity was 25 for VEGFR-2 (mean TBR 0.7), 7 for EGFR (mean TBR 0.9), 7 for IGF-1R (mean TBR 0.5), and 18 for CD40 (mean TBR 2).

Preoperative therapy did not significantly affect TEM-1, PDGFR-α, and VEGF-A
expression

Six patients (35%) from the MFS tumor group did not receive any preoperative therapy. Subgroup analysis did not show statistically significant differences between mean tumor intensity and TBR values of TEM-1, VEGF-A and PDGFR-α when comparing groups of stained tissue samples with- or without preoperative therapy (Table 2). Surprisingly, mean tumor intensity scores were higher in the subgroup that received preoperative therapy compared to the group without preoperative therapy.

Table 2. Intensity scores and tumor-to-background ratios of TEM-1, VEGF-A, and PDGFR-α categorized by preoperative therapy.

	With preoperative therapy (n = 11)	**Without preoperative therapy (n = 6)**	*p*-Value
TEM-1			
Mean tumor intensity	85	74	0.60
Mean TBR	3.5	2.2	0.29
VEGF-A			
Mean tumor intensity	96	73	0.38
Mean TBR	2.7	1.8	0.19
PDGFR-α			
Mean tumor intensity	70	52	0.21
Mean TBR	1.9	1.5	0.41

Abbreviations: TBR = tumor-to-background ratio (calculated as mean staining intensity of the tumor- divided by mean staining intensity of the adjacent healthy tissue).

Discussion

FGS could improve adequate tumor resections by delineating tumor tissue from adjacent healthy tissue. This IHC study evaluated eight candidate biomarkers for FGS in seventeen MFS tumors in comparison with adjacent healthy tissue. A pathologist specializing in sarcomas annotated tumor tissue, and staining intensity was assessed using an objective scoring method. All MFS tissue samples showed expression of TEM-1, PDGFR-α, and VEGF-A. However, the mean TBR was higher for TEM-1 than for VEGF-A and PDGFR-α. Therefore, this study identified TEM-1 as the most suitable biomarker for FGS in MFS. Interestingly, no statistically significant differences were observed between the intensity scores of TEM-1, PDGFR-α, and VEGF-A with or without preoperative therapy, suggesting FGS based on these markers might still be feasible after preoperative therapy. Although IHC results might not directly correspond to clinical results, our findings align with the previous study published by de Gooyer et al. [23]. Here, 34 MFS tissue microarrays showed high expression for VEGF-A and TEM-1 and moderate expression for PDGFR-α. Additional H&E and TEM-1 stainings were performed on ten FFPE blocks with tumor and adjacent healthy tissue. Although results were not objectively

assessed, clear tumor- to-adjacent healthy tissue borders were reported in all TEM-1-stained sections. The added value of our study is the comprehensive and objective assessment of eight previously selected promising biomarkers for FGS in a higher amount (seventeen) of MFS tissue samples with adjacent healthy tissue. For each biomarker, this study described the number of MFS tissue samples that displayed expression, the mean tumor staining intensity, and the mean TBR. This broader approach gives a better understanding of which biomarker is most suitable for FGS in MFS. Steinkamp et al. could delineate several STS subtypes, including seven MFS, with Bevacizumab-800CW targeting VEGF-A in vivo [18]. In this paper, fluorescence TBRs of 2.0–2.5 were reported with doses of 10–25 mg tracer. Although overexpression of VEGF-A in STS has been described in several studies, the tumor-specificity of VEGF-A in MFS has not been reported [29-31]. Our study demonstrated three cases where VEGF-A was expressed more in adjacent healthy tissue compared to tumor tissue, which would be dramatic in the case of VEGF-A-based FGS as it could lead to over-resection with more wound complications and increased functional impairments as a consequence. Based on our IHC evaluation, this phenomenon seems less expected for TEM-1 because it has always been expressed more in tumor tissue compared to adjacent healthy tissue. Therefore, a TEM-1 targeting moiety, such as a humanized, clinically approved monoclonal antibody like Ontuxizumab or an anti-TEM-1 antibody fragment (1C1m) conjugated to a fluorophore, could be a more specific alternative than Bevacizumab-800CW [32,33].

This study has several strong points. The first strength is the inclusion of seventeen whole tissue samples with MFS tumor and adjacent healthy tissue assessed by a pathologist specializing in sarcoma. Second, the selected biomarkers in this IHC evaluation study had a scientifically robust basis because they were selected as promising biomarkers for FGS by a clinical trial that had already included MFS patients and a previous systematic review that selected targets for FGS in soft tissue sarcomas [18,21]. Another positive aspect, which should be the basis of IHC research with FFPE material, is the methodological transparency: optimal primary antibody solutions were predetermined based on a series of test stainings for each biomarker on positive as well as negative controls that were identified with the human protein atlas (Supplementary Table S1) [24]. Ambiguous staining results on control tissue were repeated with different antibody concentrations and sometimes on other positive or negative control tissues. Comparing IHC studies for the purpose of FGS should normally be done with caution due to the variability of results depending on the type of antibodies, dilutions, epitopes, clones, or staining protocols used [34]. However, by using the five step protocol (Supplementary Protocol S1), we were able to objectively quantify the intensity of each biomarker's staining, and our results depended less on subjective assessment by pathologists with interobserver variability [35]. Biomarker staining densities are still somewhat affected by pathology scanner characteristics and settings, color deconvolution algorithms, and variability in manual annotations. Negative aspects of the current objective scoring method are the lack of comparison with a manual scoring method, the lack of correction for cell density, and the fact that parts without tissue, such as empty fat vacuoles, were also part of the intensity measurements. Yet, we believe this method should be adopted

3

by others because it is unbiased, reproducible, and reliable in assessing the difference in a biomarker's staining intensity between tumor and adjacent healthy tissue for its potential in FGS. Limitations of the study include the lack of use of standard, semi-automated image annotation software to score the stained tissue. Automated image annotation algorithms, such as those that can be trained in QuPath, could also provide a more objective evaluation of biomarker expression [36]. Although QuPath has been previously used in our group, we decided not to do so because our cohort is relatively small, which complicates validation algorithms [37]. In addition, QuPath could also wrongly classify out-of-focus tissue areas and staining artifacts. Another limitation is the absence of diagnostic biopsy material from MFS patients to directly compare the preoperative therapy effect on biomarker expression. Response to neoadjuvant therapy could lead to decreased biomarker expression intensity if there is a large percentage of non-stainable tumor cells. All patients in our cohort had ≥50% stainable tumor cells (according to the EORTC-STBSG), which could explain why preoperative therapy did not significantly affect TEM-1, PDGFR-α, and VEGF-A expression [28]. From other types of cancer, such as breast and pancreatic cancer, we know that IHC staining patterns change after neoadjuvant therapy, but for TEM-1 in MFS, this remains largely unknown [38,39]. Although our analysis of the preoperative therapy effect did not have sufficient statistical power to draw conclusions, de Gooyer et al. also state that preoperative radiotherapy did not significantly influence TEM-1 expression in MFS tissue [23]. This observation could also be due to an increased expression with enhanced tumor grade and is particularly relevant as preoperative radiotherapy is currently advised for most intermediate- and high-grade MFS patients (21% of MFS patients in the Netherlands according to a recent epidemiological study) [5,14,30,40]. As briefly highlighted before, TEM-1 targeted tracer based on Ontuxizumab or 1C1m and conjugated to a fluorophore should be further investigated. For clinical translation, it is highly important that a targeted tracer against a promising biomarker (i.e., TEM-1 targeted tracer for MFS) is applicable to the majority of patients. Although our sample size is too small per subgroup to draw hard conclusions, we did not notice any association between staining intensity and tumor characteristics, like grade or location. Ideally, one universal FGS tracer should be implemented to improve clinical outcomes for all oncological patients. However, current literature provides mixed results concerning TEM-1 expression in other cancer subtypes. On one hand, TEM-1 is predominantly expressed by fibroblasts and a subset of pericytes associated with tumor vessels but not by tumor endothelium in melanoma, ovarian, lung, and brain cancer. On the other hand, several studies conclude that TEM-1 is strongly expressed on tumor cells, tumor vasculature, and stroma in the majority of soft tissue and bone sarcomas [41-47]. Future studies are needed to determine if TEM-1 is indeed expressed in other sarcomas and if TEM-1-specific tracers are suitable for FGS. For now, the main benefit of a TEM-1 targeted tracer seems to reside in delineating MFS from adjacent healthy tissue, which could theoretically lead to reduced LR and improved survival rates.

Conclusions

Fluorescence-guided surgery (FGS) has the potential to improve the surgical outcomes of myxofibrosarcoma (MFS) patients by delineating tumors from adjacent healthy tissue. This study evaluated eight biomarkers for their potential in FGS in seventeen MFS samples with adjacent healthy tissue. Expression of tumor endothelial marker-1 (TEM-1), vascular endothelial growth factor-A (VEGF-A), and platelet-derived growth factor receptor α (PDGFRα) was observed in all MFS tumors. However, TEM-1 was identified as the most promising biomarker for FGS in MFS because it had the highest tumor-to-background intensity ratio regardless of preoperative therapy. Therefore, TEM-1-targeted FGS tracers should be further investigated to optimize MFS treatment.

3

References

1. *International Agency for Research on Cancer. WHO Classification of Tumours Editorial Board. Soft tissue and bone tumours.*; Lyon, France, (WHO classification of tumours series, 5th ed.; vol. 3). 2020.

2. Huang, H.Y.; Lal, P.; Qin, J.; Brennan, M.F.; Antonescu, C.R. Low-grade myxofibrosarcoma: a clinicopathologic analysis of 49 cases treated at a single institution with simultaneous assessment of the efficacy of 3-tier and 4-tier grading systems. *Hum Pathol* **2004**, *35*, 612-621, doi:10.1016/j.humpath.2004.01.016.

3. Blay, J.Y.; Honoré, C.; Stoeckle, E.; Meeus, P.; Jafari, M.; Gouin, F.; Anract, P.; Ferron, G.; Rochwerger, A.; Ropars, M., et al. Surgery in reference centers improves survival of sarcoma patients: a nationwide study. *Ann Oncol* **2019**, *30*, 1143-1153, doi:10.1093/annonc/mdz124.

4. Blay, J.Y.; Soibinet, P.; Penel, N.; Bompas, E.; Duffaud, F.; Stoeckle, E.; Mir, O.; Adam, J.; Chevreau, C.; Bonvalot, S., et al. Improved survival using specialized multidisciplinary board in sarcoma patients. *Ann Oncol* **2017**, *28*, 2852-2859, doi:10.1093/annonc/mdx484.

5. Casali, P.G.; Abecassis, N.; Aro, H.T.; Bauer, S.; Biagini, R.; Bielack, S.; Bonvalot, S.; Boukovinas, I.; Bovee, J.; Brodowicz, T., et al. Soft tissue and visceral sarcomas: ESMO-EURACAN Clinical Practice Guidelines for diagnosis, treatment and follow-up. *Ann Oncol* **2018**, *29*, iv51-iv67, doi:10.1093/annonc/mdy096.

6. O'Sullivan, B.; Davis, A.M.; Turcotte, R.; Bell, R.; Catton, C.; Chabot, P.; Wunder, J.; Kandel, R.; Goddard, K.; Sadura, A., et al. Preoperative versus postoperative radiotherapy in soft-tissue sarcoma of the limbs: a randomised trial. *Lancet* **2002**, *359*, 2235-2241, doi:10.1016/s0140-6736(02)09292-9.

7. Look Hong, N.J.; Hornicek, F.J.; Raskin, K.A.; Yoon, S.S.; Szymonifka, J.; Yeap, B.; Chen, Y.L.; DeLaney, T.F.; Nielsen, G.P.; Mullen, J.T. Prognostic factors and outcomes of patients with myxofibrosarcoma. *Ann Surg Oncol* **2013**, *20*, 80-86, doi:10.1245/s10434-012-2572-3.

8. Odei, B.; Rwigema, J.C.; Eilber, F.R.; Eilber, F.C.; Selch, M.; Singh, A.; Chmielowski, B.; Nelson, S.D.; Wang, P.C.; Steinberg, M., et al. Predictors of Local Recurrence in Patients With Myxofibrosarcoma. *Am J Clin Oncol* **2018**, *41*, 827-831, doi:10.1097/coc.0000000000000382.

9. Sanfilippo, R.; Miceli, R.; Grosso, F.; Fiore, M.; Puma, E.; Pennacchioli, E.; Barisella, M.; Sangalli, C.; Mariani, L.; Casali, P.G., et al. Myxofibrosarcoma: prognostic factors and survival in a series of patients treated at a single institution. *Ann Surg Oncol* **2011**, *18*, 720-725, doi:10.1245/s10434-010-1341-4.

10. Yoo, H.J.; Hong, S.H.; Kang, Y.; Choi, J.Y.; Moon, K.C.; Kim, H.S.; Han, I.; Yi, M.; Kang, H.S. MR imaging of myxofibrosarcoma and undifferentiated sarcoma with emphasis on tail sign; diagnostic and prognostic value. *Eur Radiol* **2014**, *24*, 1749-1757, doi:10.1007/s00330-014-3181-2.

11. Bhangu, A.A.; Beard, J.A.; Grimer, R.J. Should Soft Tissue Sarcomas be Treated at a Specialist Centre? *Sarcoma* **2004**, *8*, 1-6, doi:10.1080/13577140410001679185.

12. Pauli, C.; De Boni, L.; Pauwels, J.E.; Chen, Y.; Planas-Paz, L.; Shaw, R.; Emerling, B.M.; Grandori, C.; Hopkins, B.D.; Rubin, M.A. A Functional Precision Oncology Approach to Identify Treatment Strategies for Myxofibrosarcoma Patients. *Mol Cancer Res* **2022**, *20*, 244-252, doi:10.1158/1541-7786.Mcr-21-0255.

13. Vanni, S.; De Vita, A.; Gurrieri, L.; Fausti, V.; Miserocchi, G.; Spadazzi, C.; Liverani, C.; Cocchi, C.; Calabrese, C.; Bongiovanni, A., et al. Myxofibrosarcoma landscape: diagnostic pitfalls, clinical management and future perspectives. *Ther Adv Med Oncol* **2022**, *14*, 17588359221093973, doi:10.1177/17588359221093973.

14. van der Horst, C.A.J.; Bongers, S.L.M.; Versleijen-Jonkers, Y.M.H.; Ho, V.K.Y.; Braam, P.M.; Flucke, U.E.; de Wilt, J.H.W.; Desar, I.M.E. Overall Survival of Patients with Myxofibrosarcomas: An Epidemiological Study. *Cancers (Basel)* **2022**, *14*, doi:10.3390/cancers14051102.

15. Matsumura, Y.; Maeda, H. A new concept for macromolecular therapeutics in cancer chemotherapy: mechanism of tumoritropic accumulation of proteins and the antitumor agent smancs. *Cancer Res* **1986**, *46*, 6387-6392.

16. Brookes, M.J.; Chan, C.D.; Nicoli, F.; Crowley, T.P.; Ghosh, K.M.; Beckingsale, T.; Saleh, D.; Dildey, P.; Gupta, S.; Ragbir, M., et al. Intraoperative Near-Infrared Fluorescence Guided Surgery Using Indocyanine Green (ICG) for the Resection of Sarcomas May Reduce the Positive Margin Rate: An Extended Case Series. *Cancers (Basel)* **2021**, *13*, doi:10.3390/cancers13246284.

17. Hernot, S.; van Manen, L.; Debie, P.; Mieog, J.S.D.; Vahrmeijer, A.L. Latest developments in molecular tracers for fluorescence image-guided cancer surgery. *Lancet Oncol* **2019**, *20*, e354-e367, doi:10.1016/s1470-2045(19)30317-1.

18. Steinkamp, P.J.; Pranger, B.K.; Li, M.F.; Linssen, M.D.; Voskuil, F.J.; Been, L.B.; van Leeuwen, B.L.; Suurmeijer, A.J.H.; Nagengast, W.B.; Kruijff, S., et al. Fluorescence-Guided Visualization of Soft-Tissue Sarcomas by Targeting Vascular Endothelial Growth Factor A: A Phase 1 Single-Center Clinical Trial. *J Nucl Med* **2021**, *62*, 342-347, doi:10.2967/jnumed.120.245696.

19. Wellens, L.M.; Deken, M.M.; Sier, C.F.M.; Johnson, H.R.; de la Jara Ortiz, F.; Bhairosingh, S.S.; Houvast, R.D.; Kholosy, W.M.; Baart, V.M.; Pieters, A., et al. Anti-GD2-IRDye800CW as a targeted probe for fluorescence-guided surgery in neuroblastoma. *Sci Rep* **2020**, *10*, 17667, doi:10.1038/s41598-020-74464-4.

20. Azargoshasb, S.; Boekestijn, I.; Roestenberg, M.; KleinJan, G.H.; van der Hage, J.A.; van der Poel, H.G.; Rietbergen, D.D.D.; van Oosterom, M.N.; van Leeuwen, F.W.B. Quantifying the Impact of Signal-to-background Ratios on Surgical Discrimination of Fluorescent Lesions. *Mol Imaging Biol* **2022**, 10.1007/s11307-022-01736-y, doi:10.1007/s11307-022-01736-y.

21. Rijs, Z.; Shifai, A.N.; Bosma, S.E.; Kuppen, P.J.K.; Vahrmeijer, A.L.; Keereweer, S.; Bovée, J.; van de Sande, M.A.J.; Sier, C.F.M.; van Driel, P. Candidate Biomarkers for Specific Intraoperative Near-Infrared Imaging of Soft Tissue Sarcomas: A Systematic Review. *Cancers (Basel)* **2021**, *13*, doi:10.3390/cancers13030557.

22. Barth, C.W.; Gibbs, S.L. Fluorescence Image-Guided Surgery - a Perspective on Contrast Agent Development. *Proc SPIE Int Soc Opt Eng* **2020**, *11222*, doi:10.1117/12.2545292.

23. de Gooyer, J.M.; Versleijen-Jonkers, Y.M.H.; Hillebrandt-Roeffen, M.H.S.; Frielink, C.; Desar, I.M.E.; de Wilt, J.H.W.; Flucke, U.; Rijpkema, M. Immunohistochemical selection of biomarkers for tumor-targeted image-guided surgery of myxofibrosarcoma. *Sci Rep* **2020**, *10*, 2915, doi:10.1038/s41598-020-59735-4.

24. Human Protein Atlas. Availabe online: http://www.proteinatlas.org (accessed on 4 Januari 2021).

25. Schindelin, J.; Rueden, C.T.; Hiner, M.C.; Eliceiri, K.W. The ImageJ ecosystem: An open platform for biomedical image analysis. *Mol Reprod Dev* **2015**, *82*, 518-529, doi:10.1002/mrd.22489.

26. Varghese, F.; Bukhari, A.B.; Malhotra, R.; De, A. IHC Profiler: an open source plugin for the quantitative evaluation and automated scoring of immunohistochemistry images of human tissue samples. *PLoS One* **2014**, *9*, e96801, doi:10.1371/journal.pone.0096801.

27. Guillou, L.; Coindre, J.M.; Bonichon, F.; Nguyen, B.B.; Terrier, P.; Collin, F.; Vilain, M.O.; Mandard, A.M.; Le Doussal, V.; Leroux, A., et al. Comparative study of the National Cancer Institute and French Federation of Cancer Centers Sarcoma Group grading systems in a population of 410 adult patients with soft tissue sarcoma. *J Clin Oncol* **1997**, *15*, 350-362, doi:10.1200/jco.1997.15.1.350.

28. Stevenson, M.G.; Hoekstra, H.J.; Song, W.; Suurmeijer, A.J.H.; Been, L.B. Histopathological tumor response following neoadjuvant hyperthermic isolated limb perfusion in extremity soft tissue sarcomas: Evaluation of the EORTC-STBSG response score. *Eur J Surg Oncol* **2018**, *44*, 1406-1411, doi:10.1016/j.ejso.2018.05.011.

29. Chao, C.; Al-Saleem, T.; Brooks, J.J.; Rogatko, A.; Kraybill, W.G.; Eisenberg, B. Vascular endothelial growth factor and soft tissue sarcomas: tumor expression correlates with grade. *Ann Surg Oncol* **2001**, *8*, 260-267, doi:10.1007/s10434-001-0260-9.

30. Kilvaer, T.K.; Valkov, A.; Sorbye, S.; Smeland, E.; Bremnes, R.M.; Busund, L.T.; Donnem, T. Profiling of VEGFs and VEGFRs as prognostic factors in soft tissue sarcoma: VEGFR-3 is an independent predictor of poor prognosis. *PLoS One* **2010**, *5*, e15368, doi:10.1371/journal.pone.0015368.

3

31.   Wanebo, H.J.; Argiris, A.; Bergsland, E.; Agarwala, S.; Rugo, H. Targeting growth factors and angiogenesis; using small molecules in malignancy. *Cancer Metastasis Rev* **2006**, *25*, 279-292, doi:10.1007/s10555-006-8508-2.

32.   Delage, J.A.; Faivre-Chauvet, A.; Fierle, J.K.; Gnesin, S.; Schaefer, N.; Coukos, G.; Dunn, S.M.; Viertl, D.; Prior, J.O. (177)Lu radiolabeling and preclinical theranostic study of 1C1m-Fc: an anti-TEM-1 scFv-Fc fusion protein in soft tissue sarcoma. *EJNMMI Res* **2020**, *10*, 98, doi:10.1186/s13550-020-00685-3.

33.   O'Shannessy, D.J.; Smith, M.F.; Somers, E.B.; Jackson, S.M.; Albone, E.; Tomkowicz, B.; Cheng, X.; Park, Y.; Fernando, D.; Milinichik, A., et al. Novel antibody probes for the characterization of endosialin/TEM-1. *Oncotarget* **2016**, *7*, 69420-69435, doi:10.18632/oncotarget.11018.

34.   Kersting, C.; Packeisen, J.; Leidinger, B.; Brandt, B.; von Wasielewski, R.; Winkelmann, W.; van Diest, P.J.; Gosheger, G.; Buerger, H. Pitfalls in immunohistochemical assessment of EGFR expression in soft tissue sarcomas. *J Clin Pathol* **2006**, *59*, 585-590, doi:10.1136/jcp.2005.028373.

35.   Adams, E.J.; Green, J.A.; Clark, A.H.; Youngson, J.H. Comparison of different scoring systems for immunohistochemical staining. *Journal of clinical pathology* **1999**, *52*, 75-77, doi:10.1136/jcp.52.1.75.

36.   Clinicaltrials.gov Ramucirumab. Availabe online: https://clinicaltrials.gov/ct2/show/NCT04145700?term=ramucirumab&cond=Soft+Tissue+Sarcoma&draw=2&rank=1 (accessed on 22 June 2020).

37.   Houvast, R.D.; Thijse, K.; Groen, J.V.; Chua, J.; Vankemmelbeke, M.; Durrant, L.G.; Mieog, J.S.D.; Bonsing, B.A.; Vahrmeijer, A.L.; Kuppen, P.J.K., et al. An Immunohistochemical Evaluation of Tumor-Associated Glycans and Mucins as Targets for Molecular Imaging of Pancreatic Ductal Adenocarcinoma. *Cancers (Basel)* **2021**, *13*, doi:10.3390/cancers13225777.

38.   Eurola, A.; Ristimäki, A.; Mustonen, H.; Nurmi, A.M.; Hagström, J.; Haglund, C.; Seppänen, H. Impact of histological response after neoadjuvant therapy on podocalyxin as a prognostic marker in pancreatic cancer. *Sci Rep* **2021**, *11*, 9896, doi:10.1038/s41598-021-89134-2.

39.   Shaaban, A.M.; Provenzano, E. Receptor Status after Neoadjuvant Therapy of Breast Cancer: Significance and Implications. *Pathobiology* **2022**, *89*, 297-308, doi:10.1159/000521880.

40.   Rouleau, C.; Smale, R.; Fu, Y.S.; Hui, G.; Wang, F.; Hutto, E.; Fogle, R.; Jones, C.M.; Krumbholz, R.; Roth, S., et al. Endosialin is expressed in high grade and advanced sarcomas: evidence from clinical specimens and preclinical modeling. *Int J Oncol* **2011**, *39*, 73-89, doi:10.3892/ijo.2011.1020.

41.   Christian, S.; Winkler, R.; Helfrich, I.; Boos, A.M.; Besemfelder, E.; Schadendorf, D.; Augustin, H.G. Endosialin (Tem1) is a marker of tumor-associated myofibroblasts and tumor vessel-associated mural cells. *Am J Pathol* **2008**, *172*, 486-494, doi:10.2353/ajpath.2008.070623.

42.   Davies, G.; Cunnick, G.H.; Mansel, R.E.; Mason, M.D.; Jiang, W.G. Levels of expression of endothelial markers specific to tumour-associated endothelial cells and their correlation with prognosis in patients with breast cancer. *Clin Exp Metastasis* **2004**, *21*, 31-37, doi:10.1023/b:clin.0000017168.83616.d0.

43.   Guo, Y.; Hu, J.; Wang, Y.; Peng, X.; Min, J.; Wang, J.; Matthaiou, E.; Cheng, Y.; Sun, K.; Tong, X., et al. Tumour endothelial marker 1/endosialin-mediated targeting of human sarcoma. *Eur J Cancer* **2018**, *90*, 111-121, doi:10.1016/j.ejca.2017.10.035.

44.   Kiyohara, E.; Donovan, N.; Takeshima, L.; Huang, S.; Wilmott, J.S.; Scolyer, R.A.; Jones, P.; Somers, E.B.; O'Shannessy, D.J.; Hoon, D.S. Endosialin Expression in Metastatic Melanoma Tumor Microenvironment Vasculature: Potential Therapeutic Implications. *Cancer Microenviron* **2015**, *8*, 111-118, doi:10.1007/s12307-015-0168-8.

45.   MacFadyen, J.R.; Haworth, O.; Roberston, D.; Hardie, D.; Webster, M.T.; Morris, H.R.; Panico, M.; Sutton-Smith, M.; Dell, A.; van der Geer, P., et al. Endosialin (TEM1, CD248) is a marker of stromal fibroblasts and is not selectively expressed on tumour endothelium. *FEBS Lett* **2005**, *579*, 2569-2575, doi:10.1016/j.febslet.2005.03.071.

46. Rouleau, C.; Curiel, M.; Weber, W.; Smale, R.; Kurtzberg, L.; Mascarello, J.; Berger, C.; Wallar, G.; Bagley, R.; Honma, N., et al. Endosialin protein expression and therapeutic target potential in human solid tumors: sarcoma versus carcinoma. *Clin Cancer Res* **2008**, *14*, 7223-7236, doi:10.1158/1078-0432.Ccr-08-0499.

47. Simonavicius, N.; Robertson, D.; Bax, D.A.; Jones, C.; Huijbers, I.J.; Isacke, C.M. Endosialin (CD248) is a marker of tumor-associated pericytes in high-grade glioma. *Mod Pathol* **2008**, *21*, 308-315, doi:10.1038/modpathol.3801006.

3

Supplementary Table S1. Antibodies used for immunohistochemical evaluation.

Antigen	Source	Clone	Manufacturer	Cat. Nr.	Positive control	Negative control	Dilution	Retrieval buffer	Retrieval method	Incubation temperature
TEM-1	Rabbit monoclonal	EPR17081	Abcam	204914	Breast and endometrium	Spleen	1:2000	pH high (EDTA)	Overnight	4°C
VEGFR-1	Rabbit monoclonal	Y103	Abcam	32152	Placenta	Liver	1:500	pH low (citrate)	Overnight	4°C
VEGFR-2	Rabbit monoclonal	55B11	Cell signaling technology	2479	Placenta and kidney	Skin	1:300	pH high (EDTA)	Overnight	4°C
VEGF-A	Mouse monoclonal	G153-694	BD Pharmingen	555036	Placenta and tonsil	Colon	1:400	pH low (citrate)	1 hour	RT
EGFR	Rabbit monoclonal	D38B1XP	Cell signaling technology	4267	Placenta	Tonsil	1:300	pH low (citrate)	1 hour	RT
IGF-1R	Rabbit monoclonal	D406W	Cell signaling technology	14534	Placenta	Skin	1:200	pH low (citrate)	Overnight	RT
PDGFR-α	Rabbit monoclonal	D13C6	Cell signaling technology	5241	Placenta and Skin	Spleen	1:100	pH high (EDTA)	Overnight	4°C
CD40	Rabbit monoclonal	D8W3N	Cell signaling technology	40868	Tonsil	Skin	1:100	pH high (EDTA)	Overnight	4°C

Abbreviations: TEM-1 = Tumor endothelial marker-1; VEGFR-1 = Vascular endothelial growth factor receptor-1; VEGFR-2 = Vascular endothelial growth factor receptor-2; VEGF-A = Vascular endothelial growth factor-A; EGFR = Epidermal growth factor receptor; IGF-1R = Insulin-like growth factor-1 receptor; PDGFR-α = Platelet derived growth factor receptor α; CD 40 = Cluster of differentiation 40; and RT = Room Temperature.

Supplementary protocol S2. New objective immunohistochemistry scoring method.

Step 1. Select the regions of interest.

Open the stained slide in ImageJ and select the regions of interest based on annotations from the pathologist. In ImageJ use "Analyze -> Tools -> ROI manager…" to select tumor tissue and adjacent healthy tissue (Figure 1).
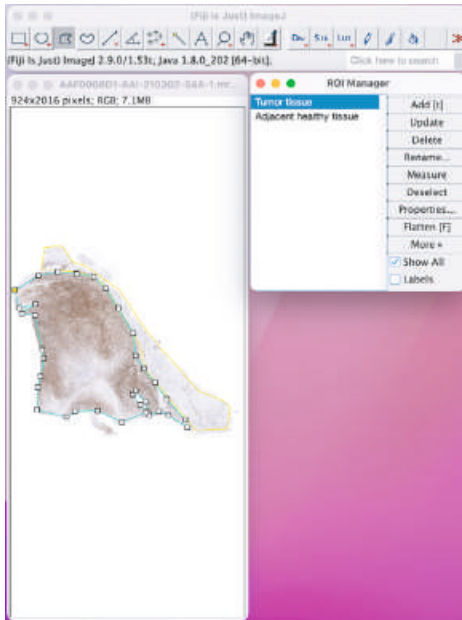
Figure 1. The regions of interest "Tumor tissue" and "Adjacent healthy tissue" have been selected.

Step 2. Filter out background colors using the "color deconvolution" option in ImageJ.

Select "Image -> Color -> Color deconvolution and select H&E DAB" in ImageJ to acquire the image that only shows the relevant brown DAB staining (Figure 2).
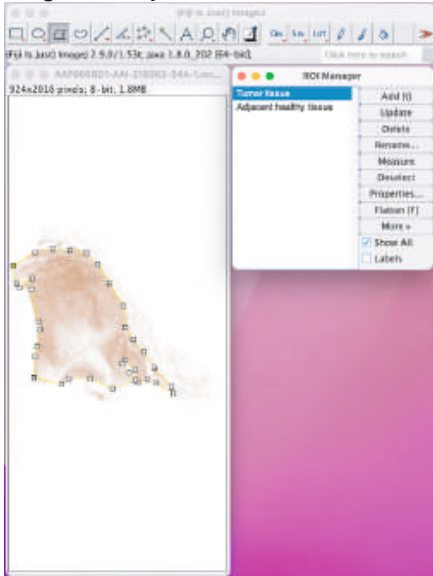
Figure 2. Only the relevant DAB staining is selected.

Step 3. Change color to greyscale

Select "Edit -> Options -> Conversions…" and tick the "Weighted RGB conversions" box and click "OK". Afterwards, select "Image -> Type -> 8-bit" to convert the brown DAB staining into grayscale.
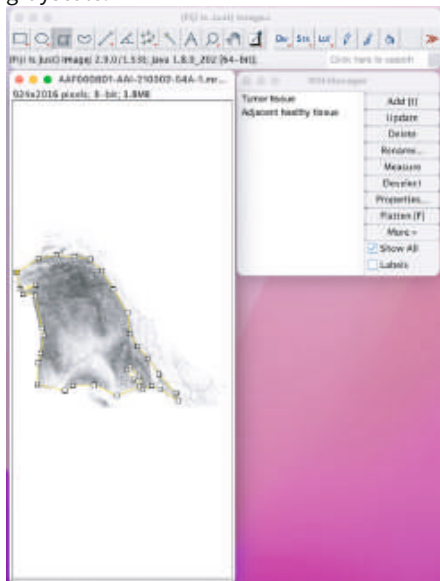
Figure 3. The image is converted into grayscale.

Step 4. Invert black and white

Select "Edit-> Invert" to invert the image. Now the pixel values correlate with staining intensity (Value black = 0 and value white = 255; Figure 4).
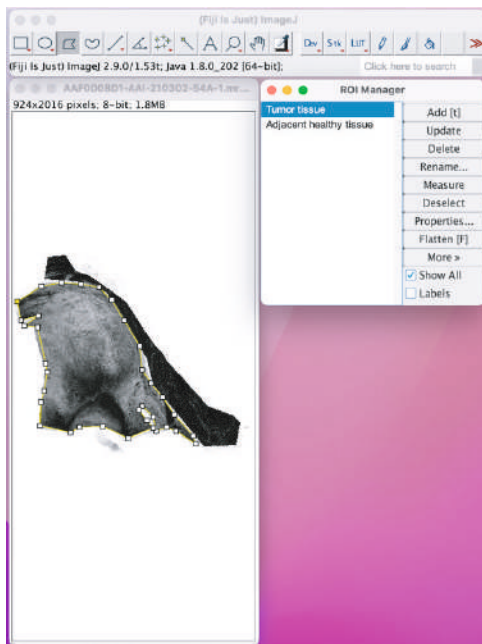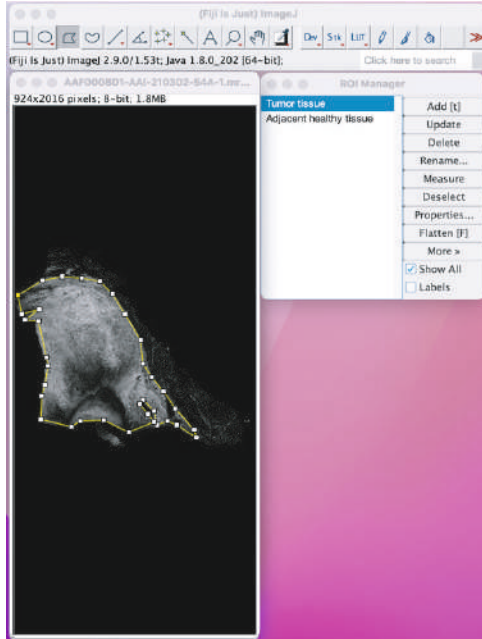
Figure 4. The whole image is inverted (left) or the selected regions are inverted (right); both options give the same result.

Step 5. Measure the mean pixel (staining) intensity value and the standard deviation

Select "Analyze -> Set Measurements…" and select "Mean gray value and Standard deviation". In ROI manager select measure (Figure 5).
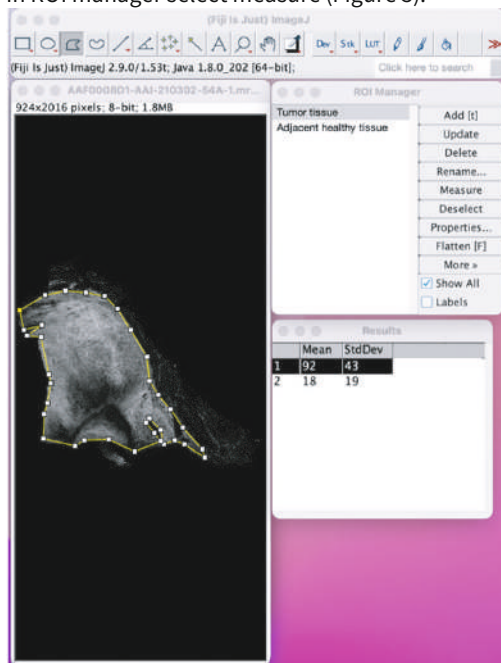
Figure 5. Mean intensity and standard deviation intensity values have been measured in "Tumor tissue (1)", and "Adjacent healthy tissue (2)".
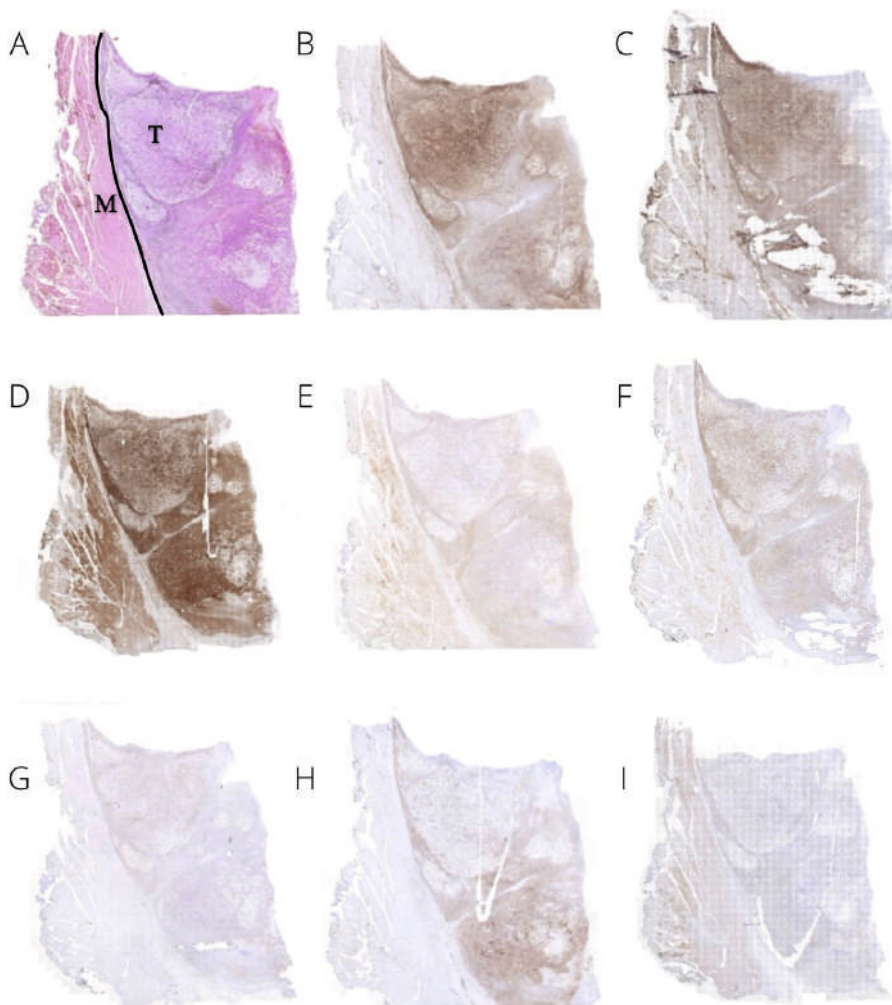
Supplementary Figure S3. MFS tumor located in the lower arm of a 64-year-old male who received pre-operative radiotherapy. H&E staining of MFS tumor tissue (T), the tumor border (black line) and adjacent muscle tissue (M) (A). Corresponding TEM-1 staining displays TEM-1 expression in MFS tumor tissue, while TEM-1 expression in adjacent muscle tissue was low (B). PDGFR-α and VEGF-A staining was strong in MFS tumor tissue, but adjacent muscle tissue was also stained positive (C, D). Expression of VEGFR-2, VEGFR-1, EGFR, CD40 and GF-1R was less evident in MFS tumor tissue (E up untill I).
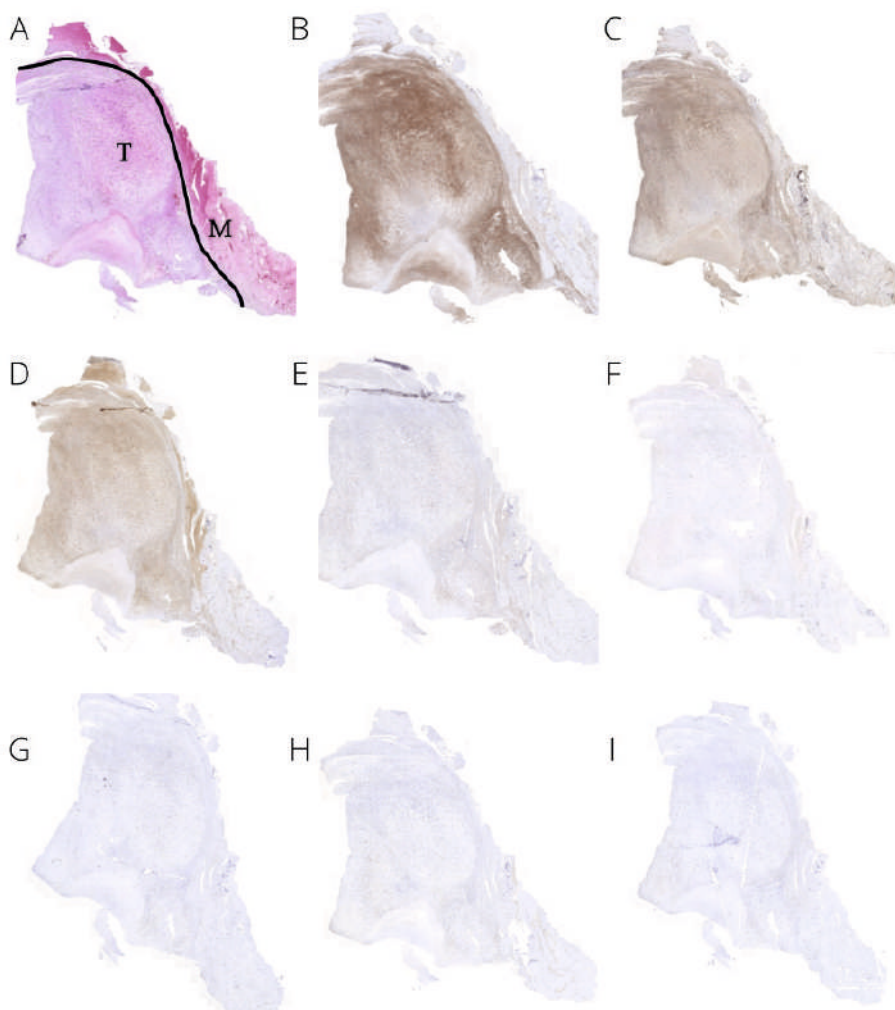
Supplementary Figure S4. Grade 2 MFS tumor located in the upper arm of a 63-year-old female. H&E staining of MFS tumor tissue (T), the tumor border (black line) and adjacent muscle tissue (M) (A). Corresponding TEM-1 staining shows strong TEM-1 expression in MFS tumor tissue, while TEM-1 expression in adjacent muscle tissue was low (B). PDGFR-α and VEGF-A staining was strong in MFS tumor tissue, but adjacent muscle tissue also stained positive (C, D). Although positive controls stained positive, there was virtually no expression of VEGFR-2, VEGFR-1, EGFR, CD40 and IGF-1R in MFS tumor tissue (E up untill I).
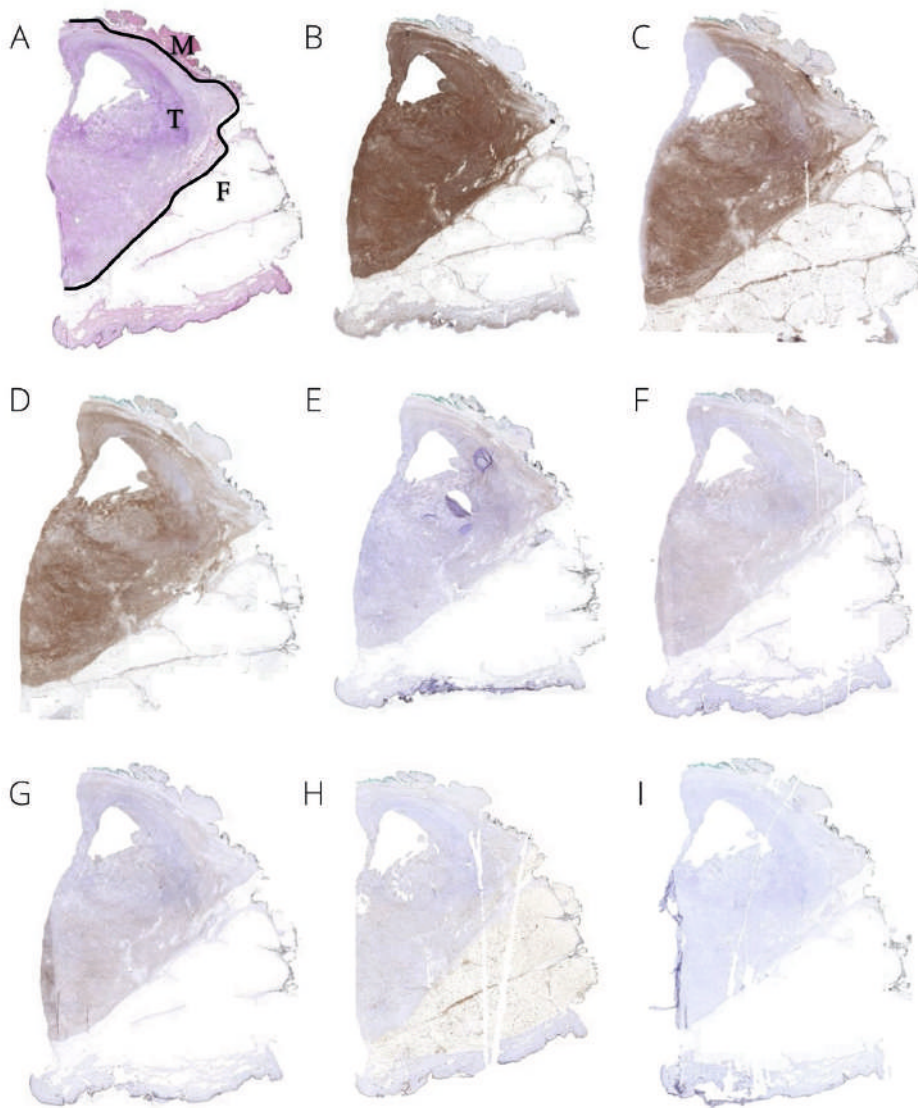
Supplementary Figure S5. Grade 3 MFS tumor located in the upper arm of a 64-year-old female. H&E staining of MFS tumor tissue (T), the tumor border (black line) and adjacent muscle- and fat tissue (M and F) (A). Corresponding TEM-1 staining displays TEM-1 expression in MFS tumor tissue, while TEM-1 expression in adjacent muscle- and fat tissue was low (B). PDGFR-α and VEGF-A staining was also strong in MFS tumor tissue, with little staining in adjacent muscle- and fat tissue (C, D). There was virtually no expression of VEGFR-2, VEGFR-1, EGFR, CD40 and IGF-1R (E up untill I).

3

4

INTRODUCING FLUORESCENCE-GUIDED SURGERY FOR PEDIATRIC EWING, OSTEO- AND RHABDOMYOSARCOMAS: A LITERATURE REVIEW

Z. Rijs[1,†], B. Jeremiasse[2,†], A. Naweed Shifai[1], H. Gelderblom[3], C.F.M. Sier[4], A.L Vahrmeijer[4], F.W.B. van Leeuwen[5], A.F.W. van der Steeg[2], M.A.J. van de Sande[1]
†Authors contributed equally

[1] Department of Orthopedic Surgery, Leiden University Medical Center, Leiden, The Netherlands
[2] Department of Surgery, Princess Maxima Center for Pediatric Oncology, Utrecht, The Netherlands
[3] Department of Medical Oncology, Leiden University Medical Center, Leiden, The Netherlands
[4] Department of Surgery, Leiden University Medical Center, Leiden, The Netherlands
[5] Interventional Molecular Imaging Laboratory, Department of Radiology, Leiden University Medical Center, Leiden, The Netherlands

Abstract

Sarcomas are a rare heterogeneous group of malignant neoplasms of mesenchymal origin which represent approximately 13% of all cancers in pediatric patients. The most prevalent pediatric bone sarcoma are osteosarcoma (OS) and Ewing sarcoma (ES). Rhabdomyosarcoma (RMS) is the most frequently occurring pediatric soft tissue sarcoma. The median age of OS and ES is approximately 17 years, so this disease is also commonly seen in adults while non-pleiomorphic RMS is rare in the adult population. The mainstay of all treatment regimens is multimodal treatment containing chemotherapy, surgical resection, and sometimes (neo)adjuvant radiotherapy. A clear resection margin improves both local control and overall survival and should be the goal during surgery with a curative intent. Real-time intraoperative fluorescence-guided imaging could facilitate complete resections by visualizing tumor tissue during surgery. This review evaluates whether non-targeted and targeted fluorescence-guided surgery (FGS) could be beneficial for pediatric OS, ES, and RMS patients. Necessities for clinical implementation, current literature, and the positive as well as negative aspects of non-targeted FGS using the NIR dye Indocyanine Green (ICG) were evaluated. In addition, we provide an overview of targets that could potentially be used for FGS in OS, ES, and RMS. Then, due to the time- and cost-efficient translational perspective, we elaborate on the use of antibody-based tracers as well as their disadvantages and alternatives. Finally, we conclude with recommendations for the experiments needed before FGS can be implemented for pediatric OS, ES, and RMS patients.

Introduction

Sarcomas are a rare heterogeneous group of malignant neoplasms of mesenchymal origin representing approximately 13% of all cancers in pediatric patients [1,2]. Sarcomas are generally subdivided into bone sarcomas and soft tissue sarcomas (STS) [3]. The most prevalent pediatric bone sarcoma is osteosarcoma (OS), with an annual incidence of 8-11 cases per million at 15-19 years of age [4], followed by Ewing sarcoma (ES), with an annual incidence of 9-10 cases per million at 10-19 years of age [5]. Rhabdomyosarcoma (RMS) is the most frequently occurring STS in the pediatric population representing approximately 40% of all STS with an annual incidence of five cases per million below the age of 2 [6].

OS, ES, and RMS are commonly treated with multimodality therapy comprising surgery and (neo)adjuvant chemotherapy with or without radiotherapy [7-11]. For surgery, the current standard has been moved from amputations (with radical or wide margins) towards limb-salvage surgery with free margins [12,13]. Hence, the accuracy of surgical resection is an important prognostic factor for local recurrence free and overall survival rates [7,14,15]. Although preoperative radiological imaging aids surgical planning, intra-operative margin assessment can be challenging, particularly when tumor tissue is surrounded by vital neurovascular structures or when tumors are located within deeper and more complex anatomical sites such as the pelvis or the head and neck region. Unfortunately, inadequate or positive resection margins are described in 10-40% of OS, 15-30% of ES, and in 20-30% of RMS [12,16-20]. Differences in local recurrence rates, 5-year overall survival, or 5-year event-free survival between adequate (defined as radical or wide) and inadequate (defined as marginal or intralesional) resection margins range from 20 to 25% in favor of adequate resection margins [7,12,14,17]. Apart from increasing local recurrence free and overall survival rates, complete resections help reduce total dosages of adjuvant chemo- and or radiotherapy [7,16]. This is particularly relevant for pediatric patients as survivors face risks of common cancer treatment-related side effects, such as impaired growth and development, organ dysfunction, and secondary malignancies [21,22].

The increased local recurrence and decreased survival rate on the one hand and the increased risk of treatment-related side effects on the other hand indicate the necessity for adequate surgical resections. The real-time intraoperative visualization of malignancies could improve resection accuracy by aiding the surgeon to discriminate between healthy and malignant tissue. Fluorescence-guided surgery (FGS) is one of the promising technological advances facilitating the visualization of tumors in real-time during surgery [23,24].

FGS exploits the advantages of near-infrared-I (NIR-I) light (750-1000nm) or NIR-II light (1000-1700nm), which have a tissue penetration of several millimeters to a centimeter deep [25]. Another advantage of NIR light is that almost no autofluorescence is exhibited in the NIR spectrum by biological tissue, which maximizes the potential tumor-to-background ratio of fluorescence when visualizing tumors [26,27]. In addition, the surgical field is generally not

altered by NIR light, as the human eye is insensitive to NIR wavelengths [28]. The two main requirements for FGS comprise a fluorescent tracer and a dedicated camera system which captures light emitted by the tracer upon excitation with an appropriate light source [27]. FGS camera systems are manufactured by several companies; systems for open-, endoscopic- and/ or robotic surgery were developed and are currently available [29].

Depending on which fluorescent tracers are applied, both non-targeted and targeted FGS is possible [28,30]. Indocyanine green (ICG) is the most used and investigated fluorescent dye for non-targeted FGS. Its benefits have been shown, amongst others, in assessing perfusion, identifying liver metastases, and visualizing sentinel lymph nodes [24,31]. Targeted tracers contain fluorophores conjugated to cancer-specific targeting moieties such as antibodies, peptides, or small molecule inhibitors [32,33]. While FGS has been investigated with promising results in various types of malignancies, information regarding its application in pediatric sarcomas such as OS, ES, and RMS is relatively scarce [34]. This review evaluates whether non-targeted and targeted FGS strategies hold promise for OS, ES, and RMS surgery. Necessities for clinical implementation, current literature, and the disadvantages of non-targeted FGS using ICG versus targeted FGS are evaluated. In addition, we provide an overview of tumor receptors that could be targeted in OS, ES, and RMS. Then, due to the time- and cost-efficient translational perspective, we elaborate on the use of antibody-based tracers as well as their disadvantages and alternatives. Lastly, we conclude with recommendations for the experiments needed before FGS can be implemented for pediatric OS, ES, and RMS patients.

Non-Targeted Fluorescence-Guided Surgery for OS, ES, and RMS Using Indocyanine Green

The indocyanine fluorescent dye ICG is already implemented for FGS in clinics. Currently, ICG is registered under two names: ICG-GREEN (Food and Drug Administration; FDA, Washington, D.C., USA) and Verdye (European Medicines Agency; EMA, Amsterdam, The Netherlands). It can be administered with a maximum intravenous dose of 1.25mg/kg for children aged 0-2 years, 2.5mg/kg for children aged 2-11 years, and 5mg/kg for children older than 11 years [35]. Once ICG is administered, it binds to plasma proteins, thereby increasing its hydrodynamic diameter to approximately 10nm [36]. These complexes accumulate in tumors due to their leaky vascular capillaries, referred to as the enhanced permeability and retention (EPR) effect [37]. Once in the tumor, these molecules remain there due to their general characteristics such as size, shape, charge, and polarity, rather than tumor cell-specific binding.

ICG has been shown to be safe and accurate for the intra-operative visual identification of several tumor types in adults, such as colorectal liver metastasis, hepatocellular carcinoma, and brain tumors [26].

Although not applied for sarcoma resections, there is experience with ICG-guided surgery for pediatric patients [38]. Esposito et al. reported their results in 76 laparoscopic and/or robotic procedures (40 left varicocelectomies, 13 renal procedures, 12 cholecystectomies, 5 tumor excisions, 3 lymphoma excisions, 3 thoracoscopic procedures, 2 lobectomies, and 1 lymph node biopsy). They concluded that ICG-guidance is useful because it is easy to apply, safe, and allows for the better identification of anatomical structures as well as easier surgical dissection or resection in challenging cases. The technology is now also used in trial settings for pediatric surgical oncology [39].

Indocyanine Green for Sarcoma Resections
Only one study describes the use of ICG for various sarcoma resections in 26- to 79-year-old adults [40]. They included eleven patients, among which were one OS patient and one pleomorphic RMS patient who received 75 mg ICG 16-24h before surgery. All sarcomas contained a fluorescent signal, except for the OS patient. However, this tumor was more than 90% necrotic due to neoadjuvant treatment. For the two patients, including the RMS patient, ICG fluorescence was of definite guidance, leading to extended tissue resection to improve the resection margin.

Multiple studies describe the use of ICG for the resection of pulmonary metastases, which also frequently occur in young sarcoma patients [41]. Predina et al. administered 5mg/kg ICG 24h preoperatively to 30 adult patients (23-79 years) suspected of pulmonary sarcoma metastases, including six OS patients, four ES patients, and two RMS patients [42]. They found that during thoracotomy or thoracoscopy, respectively, 88 and 89% of pulmonary sarcoma metastases showed fluorescence. Non-fluorescent (tumor-to-background ratio <2) lesions were located deeper than 2 cm, corresponding with the maximum tissue penetration of light at this wavelength (<1 cm). Furthermore, ICG fluorescence identified additional occult lesions among which 88% were confirmed metastases and the others lymphoid aggregates. In addition, Keating et al. administered 5 mg/kg ICG 24h preoperatively to eight adult patients (exact age not described) with the suspected pulmonary metastasis of various primary tumors including two OS patients [43]. Intraoperative thoracoscopic ICG fluorescence identified six of the eight preoperatively localized lesions. The missed nodules were the deepest from the pleural surface on the CT scan (1.8cm and 1.6cm). One additional nodule was identified by ICG fluorescence, which was a metastasis as confirmed by pathology. In addition, Okusanya et al. administered 5 mg/kg ICG 24h preoperatively to 18 adult patients (29-79 years) with solitary pulmonary nodules that required resection [44]. Intraoperative thoracotomic ICG fluorescence identified 16/18 primary nodules with a maximum depth of 1.3cm from the pleural surface. The two non-fluorescent nodules were identified by manual palpation and visual inspection. Additionally, ICG fluorescence also identified five additional subcentimeter nodules (minimum size 0.2cm) of which two were metastatic sarcomas and three were metastatic adenocarcinomas.

4

Despite these results, it must still be assessed for which pediatric sarcoma types, often biologically different from sarcomas in adult patients, the application of non-targeted FGS using ICG could be useful [45]. St. Jude Children's Research Hospital is currently performing a large phase 1 single-center trial for pediatric oncology patients, which will include 39 OS, 39 ES, and 39 RMS patients. The results of this trial (scheduled end-date December 2022) will represent a large step forward in unraveling whether FGS using ICG could be of additive value for pediatric OS, ES, and RMS patients.

Pros and Cons of Fluorescence-Guided Surgery and Indocyanine Green for Patient and Surgeon
In general, FGS has several advantages when compared to other intra-operative detection methods. As mentioned in the introduction, it has a tissue penetration of several millimeters up to a centimeter, depending on the tissue type. It is relatively harmless compared with intraoperative computed tomography or radio-active agents. In addition, NIR-light emitted by NIR fluorophores is invisible to the naked eye and thus does not contaminate the surgical field nor does it leave long lasting tattoos, as is the case with blue dye [46]. Moreover, unlike the intraoperative histopathological examination of the surgical margin, FGS does not interrupt the surgical workflow [47]. Additional advantages have been reported for ICG specifically. ICG is relatively cheap and immediate reinjections are possible to assess perfusion when the fluorescent signal has diminished [48]. Furthermore, ICG is shown to be safe with only minor risks of adverse events, i.e., a risk of less than 1 in 10,000 of an anaphylactic reaction. Finally, ICG for FGS is generally given 24h preoperatively, which is usually the moment patients are admitted to the hospital before undergoing tumor resection.

However, the general disadvantages of FGS include an additional investment for a dedicated camera system which may not be affordable for every hospital. In addition, bone tumors and nodules located deeper than 1cm could still be missed due to the limited depth penetration of NIR fluorescence [25,49]. For the use of ICG, additional caveats and disadvantages have been described. First, there is not much scientific evidence regarding tumor-specific resections. Therefore, there is no proof that the use of ICG for tumor resections is beneficial for patient outcomes such as functional outcome, disease-specific local recurrence, and/or disease-specific survival. Secondly, since ICG is dissolved in a solution containing iodine, its application is contraindicated in patients with an iodine allergy or thyroid abnormalities, such as a clinical manifest hyperthyroidism or autonomous thyroid adenoma iodine [50]. In addition, patients with renal insufficiency might have an increased risk of anaphylactic reactions. Therefore, the advantages of ICG for patients with renal insufficiency (estimated GFR of < 30ml/min/1.73 m^2) should be carefully weighed against the risk of potential adverse events. Additionally, for patients that would not be admitted 24h preoperatively, intravenous administration of ICG may be a burden from a logistical and financial point of view. Lastly, ICG fluorescence is associated with the EPR effect, which is known to be influenced by many factors, such as the tumor type, size, presence of necrosis, location, inflammation, and vascular mediators. Therefore, the signal intensity of ICG is unpredictable. False negativity could occur in cases

with very small nodules, nodules with extensive necrosis or minimally viable tissue. In addition, false positivity could occur as well, for example in tissue with reactive changes or high levels of vascular permeability mediators such as bradykinin and prostaglandin [51,52].

Targeted Fluorescence-guided Surgery for OS, ES, and RMS

Tumor-specific FGS does not depend on the tumor microenvironment, such as ICG with the EPR effect, but depends on tracers that bind to tumor-specific receptors. To select tumor-specific receptors that are appropriate for FGS, several characteristics have to be evaluated. The most important parameters for target selection are the following: targets should have been assessed in a large amount of tumor samples as this represents a measurement of evidence; a high percentage of tumor samples should actually express the tumor-specific target; when a tumor is positively stained, a high percentage of tumor cells should express the target; there should be a diffuse expression pattern of the tumor-specific target throughout the whole tumor and not in specific parts; the receptor should be preferably located on the cell surface of malignant cells to permit direct targeting with the possibility of internalization for a long-lasting signal; the tumor-specific receptor is still present after neoadjuvant therapy, which is important because neoadjuvant therapy is standard treatment for OS, ES, and non-pleiomorphic RMS; and the expression of the target should be absent or substantially less in adjacent normal tissue to adequately differentiate tumor from healthy tissue (Table 1).

Table 1. Important parameters for target selection.

Target expression is evaluated in a large amount of tumor samples as this represents a measurement of evidence
A high percentage of evaluated samples display positive staining
When a tumor is stained positively, a high percentage of tumor cells express the target
The target is expressed diffusely throughout the whole tumor
The target is located on the cell surface of malignant cells
Expression of the target persists after neoadjuvant therapy
Target is minimally or not expressed in adjacent healthy tissue

Promising Tumor Specific Fluorescent Agents for ES, OS, and RMS
Bosma et al. systematically reviewed 86 articles that studied 47 targets for FGS in primary ES tumors [53]. Cell surface protein expression was evaluated by Western blot or immunohistochemistry, and in descending order, the following nine targets were selected as the most promising for FGS: Cluster of differentiation 99 (CD99), C-X-C chemokine receptor type 4 (CXCR4), occludin, neuropeptide receptor Y1 (NPY1), LINGO-1, insulin like growth factor 1 receptor (IGF-1R), claudin-1, c-kit (also known as cluster of differentiation 117; CD117), and NOTCH receptor. Except for occludin, all previously mentioned targets have clinically available targeting moieties which in principle can be used for FGS in ES [53]. Still, further immunohistochemical studies that include both tumor and adjacent normal tissue should be

performed to choose the most optimal candidate. In addition, more recent diagnostic markers, such as NKX2.2, could also be evaluated for their potential in FGS [54]. Nevertheless, the first steps were made to explore the promising targets for FGS in ES patients.

Systematic reviews selecting promising tumor-specific targets for OS and RMS have not been published to date. Therefore, we evaluated the literature to identify targets for FGS of OS and RMS. First, clinically available antibodies and their respective targeting antigens for these tumor types were identified from PubMed and clinicaltrials.gov (Supplementary Tables S1 and S2). This search was restricted to therapeutic antibodies which have been previously or are currently evaluated in clinical trials because these antibodies can be relatively time- and cost-efficiently modified into fluorescent tracers [23,55]. Second, PubMed searches were performed to find important information for target selection (Appendix A). Here, we considered targets promising for FGS if the expression was evaluated in at least 20 tissue samples for a tumor subtype and more than 50% of the samples stained positive. When targets did not meet these two requirements, they were considered less promising. Although the remaining criteria in Table 1 are indeed important, solely data on sample size and the percentage of positive samples were available for each target. Therefore, only these two criteria could be assessed to determine the most promising targets.

Based on this strategy, the following seven targets were considered candidates for the FGS of OS: AXL receptor tyrosine kinase (AXL), B7 homolog 3 (B7-H3), cluster of differentiation 47 (CD47), disialoganglioside GD2 (GD2), transmembrane nonmetastatic melanoma protein B (gpNMB), IGF-1R, and vascular endothelial growth factor A (VEGF-A). Interestingly, all promising targets were demonstrated to internalize upon binding with an antibody (-derivative) in other tumor types, except for VEGF-A as it is not a cell-surface expressed receptor [56-60]. In contrast, three targets with clinically therapeutic antibodies were considered less promising for FGS. These were: human epidermal growth factor receptor 2 (HER2), programmed death-ligand 1 (PD-L1), and tumor endothelial marker 1 (TEM1) (Table 2).

An important nuance is that HER2, PD-L1, and VEGF-A were investigated in a large number of (pre)clinical studies. The remaining targets were evaluated considerably less. Publication bias might have had an impact on the published results concerning these targets.

Table 2. Characteristics of targets evaluated for fluorescence-guided surgery in Osteosarcoma.

Targets	Tissue samples	% Positive samples	% Positive cells	Expression altered after neo-adjuvant therapy	(Adjacent) healthy tissue	Internalization[1]	References
Promising targets[2]							
AXL	40 TMA (RM) + 6 TB	75-83%	N.D.	N.D.	TMA (RM): 20% of 40 weakly positive	Yes	[56,78,79]
B7-H3	61 PR	92%	Median: 90%	N.D.	61 case matched healthy tissue negative staining	Yes	[60,80]
CD47	20 RM	85%	N.D.	N.D.	WB: substantially lower protein levels in 6 healthy tissues compared to tumor tissue	Yes	[57,81]
GD2	55 TMA (from TB, PR, RR)	95-100%	N.D.	No, target expression remains	N.D.	Yes	[58,82,83]
gpNMB	67 TMA (from TB, PR, RR)	93%	>66% positive tumor cells in 37% of samples	Probably not[3]	N.D.	N.D.	[84]
IGF-1R	84 TS	86%	50-75% positive cells in 24% of samples	N.D.	WB: substantially lower protein levels in healthy tissue compared to tumor tissue	Yes	[59,85]

4

Table 2. Characteristics of targets evaluated for fluorescence-guided surgery in Osteosarcoma. *(continued)*

Targets	Tissue samples	% Positive samples	% Positive cells	Expression altered after neo-adjuvant therapy	(Adjacent) healthy tissue	Internalization[1]	References
VEGF-A	466 TMA (TB + RR) + TB + PR + RR	Average of 59.9% (range 15-96%)	>50% in 11-38.8% of samples	Uncertain, varying results in different studies	N.D.	No	[86-98]
Less promising targets[2]							
HER2	1 systematic review: 934 TB + PR + RR	Average 42% (range 13-60%)	<50%	N.D.	10 healthy bone samples from fractures were negative	Yes	[86,99-101]
PD-L1	418 TMA (TS) + TB + PR + RR	Average of 32.5% (range 0-85%)	<25%[4]	Yes, decreased[5]	N.D.	Yes	[65,102-110]
TEM1	11 TS	63.6%	N.D.	N.D.	N.D.	Yes	[111,112]

Abbreviations: TMA - tissue microarray; RM - Resection material not defined whether it was a primary tumor or a recurrence; TB - tissue biopsies; N.D. - Not described; WB - Western Blot; PR - Primary resection material; RR - Recurrence resection material; TS - Tissue samples not defined whether tissue biopsy or resection sample.

1. While not described in OS, it was demonstrated that AXL, CD47, GD2, IGF-1R, and B7-H3 were internalized upon binding with an antibody (derivative) in other tumor types [56-60].

2. Targets were considered promising for FGS, if the expression was evaluated in at least 20 tissue samples for a tumor subtype and more than 50% of the samples stained positive. When targets did not meet these two requirements, they were considered less promising.

3. The staining intensity was similar in tissues from biopsies and resection material. Since OS patients commonly receive neoadjuvant treatment, gpNMB expression is most likely not altered after neoadjuvant treatment.

4. One study described the percentage of positive tumor cells. 84 tissue slides were assessed of which 12 tissue slides were positive. In these, less than 25% of cells stained positive for PD-L1[5].

5. One study compared diagnostic biopsies with corresponding tissue from subsequent primary resections after neoadjuvant chemotherapy (methotrexate, cisplatin, and doxorubicin). While 53% of pre-neoadjuvant treatment biopsies stained positive for PD-L1, none of the resection samples did [65].

For RMS, less literature is published regarding the expression of targets with clinically available antibodies. Based on the criteria in Table 1, three promising targets were selected: the cluster of differentiation 56 (CD56), IGF-1R, and VEGF-A (Table 3). Of these, IGF-1R has been demonstrated to internalize [59]. Interestingly, all studies are mainly investigated alveolar RMS and/or embryonal RMS. These are the subtypes which most frequently occur in pediatric RMS patient. In contrast, B7-H3 and TEM1 were considered less promising for FGS in RMS (Table 3).

Combining the results from the systematic review by Bosma et al. with Tables 2 and 3, IGF-1R seems the only target that is simultaneously promising for OS, ES, and RMS [53]. This suggests that a fluorescent dye conjugated to a clinically available antibody targeting IGF-1R (Supplementary Tables S1 and S2) could be applicable for the majority of pediatric OS, ES, and RMS sarcoma patients.

Obstacles Regarding the Selection of Tumor Specific Targets for Fluorescence-Guided Surgery

Data presented in the previous paragraphs are based on immunohistochemical studies which have been performed for other purposes than FGS. Therefore, the interpretation of the results of those studies for FGS purposes should be done with caution. The comparison of immunohistochemical studies is complicated as large inconsistencies in reported target expression exist between various studies. This can be due to the application of different antibodies for the same target but against various epitopes, due to differences in staining protocols, or due to inter-/intra-tumoral heterogeneity [61-63]. Moreover, the use of immunohistochemical evaluation in formalin-fixed paraffin-embedded (FFPE) samples with the intention to target the same protein on living cells for imaging purposes has multiple disadvantages. A prominent cause of the loss of antigenicity is formalin fixation which generates crosslinks between adjacent proteins that result in the steric interference of antibody binding to the respective epitope [64]. Furthermore, bone tissue requires decalcification, which is known to impair antigen retrieval and alters the immunohistochemical staining intensity [65,66].

To overcome the aforementioned obstacles, studies with the aim of target evaluation for FGS should be performed. Here, the staining of undecalcified fresh frozen sections (FFS) could be advantageous [62,67,68]. Unfortunately, many clinical FFS specimens are not readily available in this form, which complicates acquiring large sample sizes; storage is expensive and requires an advanced infrastructure; and tissue morphology is less well preserved over time compared to FFPE [69-71].

Translational Perspective of Targeted Fluorescence-Guided Surgery for OS, ES, and RMS

The previous sections provide an overview of potential tumor-specific targets for OS, ES, and RMS. As fluorophores by themselves generally lack tumor specificity, they could be conjugated to a targeting moiety such as a monoclonal antibody, a peptide, or small molecule inhibitors

[33]. Antibody-based tracers are most often investigated for FGS as monoclonal therapeutic antibodies against a wide variety of targets are readily available and can be repurposed for FGS by fluorophore conjugation [27]. For this purpose, various fluorophores are available, and some are clinically approved, paving the way for implementing FGS to optimize surgical oncology [29].

Several therapeutic antibodies binding to candidate targets for OS, ES, and RMS are available (Supplementary Table S1). Additional therapeutic antibodies that are currently being investigated in clinical trials are described in Supplementary Table S2. Because most therapeutic antibodies are human or have been humanized, they are reported with tolerable safety profiles. Moreover, it should be noted that doses of antibodies injected for FGS are substantially (approximately 10-100x) lower compared to therapeutic doses. Consequently, the serum concentration of the antibody (conjugated to a fluorophore) is lower when used for FGS and little or no toxicity is expected [72]. Moreover, some of the therapeutic antibodies evaluated for therapy in pediatric OS, ES, and RMS patients have already been repurposed for FGS and accurately visualized tumor tissue in other cancer types [73-77]. Although it is important to notice that HER2 is considered a less promising target in OS (Table 2), Trastuzumab-IRDye800CW targeting HER2 has imaged breast cancer and could be tested in OS patients as well [75]. More encouragingly, Bevacizumab-IRDye800CW targeting VEGF-A was successful for FGS in adult soft tissue sarcoma patients [77]. Due to the presence of VEGF-A in pediatric OS and RMS (Tables 2 and 3), testing Bevacizumab-IRDye800CW is a relatively straightforward option which could pave the road towards the clinical implementation of FGS in pediatric OS and RMS patients.

Disadvantages of Using Antibodies for Fluorescence-Guided Surgery and Their Alternatives

Although antibodies bind to their target with high affinity and specificity, the large size of antibodies (150 kDa) is expected to limit tumor penetration and establish a long blood half-life. Therefore, the use of antibodies as targeted tracers for tumor-specific FGS necessitates a turnover time of several days to obtain an optimal tumor-to-background ratio [124]. For patients, this implicates an extra preoperative hospital visit for tracer administration. Apart from the extra costs and logistic planning, this leads to an extra burden for pediatric OS, ES, and RMS patients. Therefore, smaller targeting moiety alternatives such as antibody fragments, peptide conjugates and small molecule conjugates may be advantageous for FGS [32]. Briefly, tracers smaller than 60 kDa are generally cleared via the kidneys instead of via the liver, resulting in faster blood clearance from non-targeted tissues. Consequently, high tumor-to-background contrast can be attained within hours after the administration of a tumor-specific smaller targeting moiety alternative-based tracer [27,32,124].

Table 3. Characteristics of targets evaluated for fluorescence-guided surgery in Rhabdomyosarcoma.

Targets	Tissue samples	% Positive samples	% Positive cells	Expression altered after neo-adjuvant therapy	(Adjacent) healthy tissue	Internalization[1]	References
Promising targets[2]							
CD56	117 TMA (TS) + TS	Average 96% (range 90-100%)	>50% positive cells in >75% of sample	N.D.	N.D.	N.D.	[113-117]
IGF-1R	124 TB + RM	63-83%	N.D.	N.D.	N.D.	Yes	[59,118,119]
VEGF-A	145 TMA (PR) + PR + RR	59-70%	N.D.	N.D.	N.D.	N.D.	[120,121]
Less promising targets[2]							
B7-H3	4 patient-derived xenografts	100%	Average H-score 108 (range 49-150)[3]	N.D.	N.D.	Yes	[60,122]
TEM1	126 TMA (TB)	31%	N.D.	N.D.	N.D.	Yes	[112,123]

Abbreviations: TMA - tissue microarray; TS - Tissue samples not defined whether tissue biopsy or resection sample; N.D. - Not described; TB - tissue biopsies; RM – Resection material not defined whether it was a primary tumor or a recurrence; PR - Primary resection material; RR - Recurrency resection material.

1. While not described in RMS, it was demonstrated that CD56, TEM1 and B7-H3 internalized upon binding with an antibody (derivative) in a different tumor type [59].

2. Targets were considered promising for FGS, if the expression was evaluated in at least 20 tissue samples for a tumor subtype and more than 50% of the samples stained positive. When targets did not meet these two requirements, they were considered less promising.

3. The H-score is ranges from 0-300 and is a semiquantitative score obtained by determining the staining intensity score (ranging from 0-3) of each tumor cell and applying the formula [1 × (% cells 1+) + 2 × (% cells 2+) + 3 × (% cells 3+)].

4

As mentioned before, deeper located tumors could still be missed by these tracers [25,49]. To this end, hybrid radionuclear/fluorescence imaging combined into a single tracer is attractive. The nuclear component can be of added value for initial intra-operative navigation towards the tumor using a gamma-detecting probe. When the tumor is reached, fluorescence could provide high resolution visual guidance for precise resection [125]. The integration of both modalities onto a tracer can be effectuated in several ways. The conjugation of a fluorophore and chelator for radioactive labeling at different positions of the tracer is one option. Examples include colorectal carcinoma imaging using fluoresceinated monoclonal antibodies against carcinoembryonic antigen which were also labeled with 125I, and the conjugation of IRDye800CW and ^{111}In to Girentuximab for the visualization of clear-cell renal-cell carcinomas [126,127]. Combining the NIR fluorophore and the radiolabel into a single structure is another option [128]. This would be advantageous since this is in most cases a site-specific labeling method which implies that properties of the tracer cannot vary, creating a predictable tracer with regards to its biodistribution. In addition, this is often the only possibility when working with small peptides or chemical molecules, as multiple conjugation sites may not be available. An example of this technique is the hybrid nuclear and NIR fluorescent PSMA tracer in prostate cancer [129]. However, these single structures are more complex to design, as opposed to the more straightforward separate conjugation of the fluorophore and chelator to an antibody.

Future Perspective and Recommendations for Fluorescence-Guided Surgery in OS, ES, and RMS Patients

In general, the standard preclinical work preceding the application of FGS consists of the following: target selection, target evaluation, tracer development, *in vitro* evaluation, *in vivo* evaluation with animal experiments, and clinical in-human experiments. Because FGS for pediatric OS, ES, and RMS patients is still in its infancy, this review reveals an overview of promising targets as a basic first step. A follow-up would be to evaluate the expression of these targets with immunohistochemistry in a comparative setting using intra-patient sets of tumor and control tissue. Ideally, fresh surgically resected- or frozen tissue with representative intra- and intertumoral heterogeneity should be used to determine the level and diffusivity of target expression [130,131]. A possible advantage of frozen tissue would be that the antigenicity of its targets may be comparable to those on in-human tumors. The disadvantage is probably the logistics of obtaining these samples in a (large) representative cohort which would involve prospective sampling in a multicenter setting. Therefore, we recommend first evaluating the expression of targets with immunohistochemistry using FFPE samples, given its availability and relatively low cost. Subsequently, the expression of promising targets should be evaluated in fresh surgically resected- or frozen tissue. This enables the systematic, cost-effective, and valid selection of candidate targets for FGS. Then, fluorescent tracers should be developed based on the most favorable target evaluated by immunohistochemistry. Clinically available antibodies conjugated to fluorophores that bind to these targets allow faster and cost-efficient translation to clinics. Afterwards, preclinical (mouse) models can be used to show *in-vivo*

efficacy. However, the major disadvantages of genetically altered mice are the absence of human tumor microenvironment and the difficulty of mimicking intertumoral heterogeneity. Therefore, results cannot be directly extrapolated to the clinical setting. Ultimately, the assessment of the additive value of FGS can only be performed in humans.

Conclusions

We created an overview of the potential of non-targeted and targeted FGS for pediatric OS, ES, and RMS patients. Although ICG has been shown to be safe in pediatric patients, the results of an ongoing clinical trial (scheduled end-date of December 2022) will reveal whether FGS using ICG is accurate for the intra-operative visual identification of pediatric OS, ES, and RMS patients. As FGS using ICG is based on the EPR effect, false negative and false positive signals could occur. Therefore, targeted FGS might be a better alternative. We listed the promising tumor-specific targets for FGS in pediatric OS, ES, and RMS patients. The conjugation of fluorophores to clinically available antibodies that bind to these targets may result in safe and tumor-specific tracers that could improve tumor resection success rates. Evaluating the already clinically tested fluorescent-labeled antibody Bevacizumab-IRDye800CW in pediatric OS and RMS patients is a relatively straightforward option because this has already shown promising results in adult soft tissue sarcomas. However, the development of a fluorescent-labeled IGF-1R antibody would be ideal because this seems to be the only promising target for pediatric OS, ES, and RMS simultaneously. Due to disadvantages of antibody-based tracers, smaller targeting moiety alternatives for tracer development should be investigated. In addition, surgical navigation with the use of hybrid radionuclear/fluorescence tracers could be investigated to detect deeper located and hidden tumors. In conclusion, FGS has the potential to optimize OS, ES, and RMS treatment, but more research remains to be done before this promising technique can be implemented for OS, ES, and RMS patients.

References

1. Bompas, E.; Martin, V.; Meniai, F.; Toulmonde, M.; Marec-Berard, P.; Claude, L.; Ducimetiere, F.; Chargari, C.; Minard-Colin, V.; Corradini, N., et al. Management of sarcomas in children, adolescents and adults: Interactions in two different age groups under the umbrellas of GSF-GETO and SFCE, with the support of the NETSARC+ network. *Bulletin du cancer* **2021**, 10.1016/j.bulcan.2020.10.009, doi:10.1016/j.bulcan.2020.10.009.

2. Hernandez Tejada, F.N.; Zamudio, A.; Marques-Piubelli, M.L.; Cuglievan, B.; Harrison, D. Advances in the Management of Pediatric Sarcomas. *Current oncology reports* **2020**, *23*, 3, doi:10.1007/s11912-020-00995-8.

3. Stiller, C.A.; Trama, A.; Serraino, D.; Rossi, S.; Navarro, C.; Chirlaque, M.D.; Casali, P.G. Descriptive epidemiology of sarcomas in Europe: report from the RARECARE project. *European journal of cancer (Oxford, England : 1990)* **2013**, *49*, 684-695, doi:10.1016/j.ejca.2012.09.011.

4. Ritter, J.; Bielack, S.S. Osteosarcoma. *Annals of Oncology* **2010**, *21*, vii320-vii325, doi:https://doi.org/10.1093/annonc/mdq276.

5. Esiashvili, N.; Goodman, M.; Marcus, R.B., Jr. Changes in incidence and survival of Ewing sarcoma patients over the past 3 decades: Surveillance Epidemiology and End Results data. *J Pediatr Hematol Oncol* **2008**, *30*, 425-430, doi:10.1097/MPH.0b013e31816e22f3.

6. Chen, S.; Rudzinski, E.R.; Arnold, M.A. Challenges in the Diagnosis of Pediatric Spindle Cell/Sclerosing Rhabdomyosarcoma. *Surgical pathology clinics* **2020**, *13*, 729-738, doi:10.1016/j.path.2020.08.010.

7. Williams, R.F.; Fernandez-Pineda, I.; Gosain, A. Pediatric Sarcomas. *Surg Clin North Am* **2016**, *96*, 1107-1125, doi:10.1016/j.suc.2016.05.012.

8. Bernthal, N.M.; Federman, N.; Eilber, F.R.; Nelson, S.D.; Eckardt, J.J.; Eilber, F.C.; Tap, W.D. Long-term results (>25 years) of a randomized, prospective clinical trial evaluating chemotherapy in patients with high-grade, operable osteosarcoma. *Cancer* **2012**, *118*, 5888-5893, doi:10.1002/cncr.27651.

9. Goorin, A.M.; Schwartzentruber, D.J.; Devidas, M.; Gebhardt, M.C.; Ayala, A.G.; Harris, M.B.; Helman, L.J.; Grier, H.E.; Link, M.P. Presurgical chemotherapy compared with immediate surgery and adjuvant chemotherapy for nonmetastatic osteosarcoma: Pediatric Oncology Group Study POG-8651. *Journal of clinical oncology : official journal of the American Society of Clinical Oncology* **2003**, *21*, 1574-1580, doi:10.1200/jco.2003.08.165.

10. Crist, W.M.; Anderson, J.R.; Meza, J.L.; Fryer, C.; Raney, R.B.; Ruymann, F.B.; Breneman, J.; Qualman, S.J.; Wiener, E.; Wharam, M., et al. Intergroup rhabdomyosarcoma study-IV: results for patients with nonmetastatic disease. *J Clin Oncol* **2001**, *19*, 3091-3102, doi:10.1200/jco.2001.19.12.3091.

11. Bailey, K.; Cost, C.; Davis, I.; Glade-Bender, J.; Grohar, P.; Houghton, P.; Isakoff, M.; Stewart, E.; Laack, N.; Yustein, J., et al. Emerging novel agents for patients with advanced Ewing sarcoma: a report from the Children's Oncology Group (COG) New Agents for Ewing Sarcoma Task Force. *F1000Res* **2019**, *8*, doi:10.12688/f1000research.18139.1.

12. He, F.; Zhang, W.; Shen, Y.; Yu, P.; Bao, Q.; Wen, J.; Hu, C.; Qiu, S. Effects of resection margins on local recurrence of osteosarcoma in extremity and pelvis: Systematic review and meta-analysis. *International journal of surgery (London, England)* **2016**, *36*, 283-292, doi:10.1016/j.ijsu.2016.11.016.

13. Loh, A.H.; Wu, H.; Bahrami, A.; Navid, F.; McCarville, M.B.; Wang, C.; Wu, J.; Bishop, M.W.; Daw, N.C.; Neel, M.D., et al. Influence of bony resection margins and surgicopathological factors on outcomes in limb-sparing surgery for extremity osteosarcoma. *Pediatric blood & cancer* **2015**, *62*, 246-251, doi:10.1002/pbc.25307.

14. Donaldson, S.S. Ewing sarcoma: radiation dose and target volume. *Pediatric blood & cancer* **2004**, *42*, 471-476, doi:10.1002/pbc.10472.

15. Abed, R.; Grimer, R. Surgical modalities in the treatment of bone sarcoma in children. *Cancer treatment reviews* **2010**, *36*, 342-347, doi:10.1016/j.ctrv.2010.02.010.

16. Foulon, S.; Brennan, B.; Gaspar, N.; Dirksen, U.; Jeys, L.; Cassoni, A.; Claude, L.; Seddon, B.; Marec-Berard, P.; Whelan, J., et al. Can postoperative radiotherapy be omitted in localised standard-risk Ewing sarcoma? An observational study of the Euro-E.W.I.N.G group. *European journal of cancer (Oxford, England : 1990)* **2016**, *61*, 128-136, doi:10.1016/j.ejca.2016.03.075.

17. Bacci, G.; Longhi, A.; Briccoli, A.; Bertoni, F.; Versari, M.; Picci, P. The role of surgical margins in treatment of Ewing's sarcoma family tumors: experience of a single institution with 512 patients treated with adjuvant and neoadjuvant chemotherapy. *International journal of radiation oncology, biology, physics* **2006**, *65*, 766-772, doi:10.1016/j.ijrobp.2006.01.019.

18. Ozaki, T.; Hillmann, A.; Hoffmann, C.; Rübe, C.; Blasius, S.; Dunst, J.; Jürgens, H.; Winkelmann, W. Significance of surgical margin on the prognosis of patients with Ewing's sarcoma. A report from the Cooperative Ewing's Sarcoma Study. *Cancer* **1996**, *78*, 892-900, doi:10.1002/(sici)1097-0142(19960815)78:4<892::Aid-cncr29>3.0.Co;2-p.

19. Hawkins, W.G.; Hoos, A.; Antonescu, C.R.; Urist, M.J.; Leung, D.H.; Gold, J.S.; Woodruff, J.M.; Lewis, J.J.; Brennan, M.F. Clinicopathologic analysis of patients with adult rhabdomyosarcoma. *Cancer* **2001**, *91*, 794-803.

20. Seitz, G.; Dantonello, T.M.; Int-Veen, C.; Blumenstock, G.; Godzinski, J.; Klingebiel, T.; Schuck, A.; Leuschner, I.; Koscielniak, E.; Fuchs, J. Treatment efficiency, outcome and surgical treatment problems in patients suffering from localized embryonal bladder/prostate rhabdomyosarcoma: a report from the Cooperative Soft Tissue Sarcoma trial CWS-96. *Pediatric blood & cancer* **2011**, *56*, 718-724, doi:10.1002/pbc.22950.

21. Board, P.D.Q.P.T.E. Late Effects of Treatment for Childhood Cancer (PDQ®): Health Professional Version. In *PDQ Cancer Information Summaries*, National Cancer Institute (US): Bethesda (MD), 2002.

22. Paulino, A.C.; Simon, J.H.; Zhen, W.; Wen, B.C. Long-term effects in children treated with radiotherapy for head and neck rhabdomyosarcoma. *International journal of radiation oncology, biology, physics* **2000**, *48*, 1489-1495, doi:10.1016/s0360-3016(00)00799-9.

23. Rijs, Z.; Shifai, A.N.; Bosma, S.E.; Kuppen, P.J.K.; Vahrmeijer, A.L.; Keereweer, S.; Bovée, J.; van de Sande, M.A.J.; Sier, C.F.M.; van Driel, P. Candidate Biomarkers for Specific Intraoperative Near-Infrared Imaging of Soft Tissue Sarcomas: A Systematic Review. *Cancers (Basel)* **2021**, *13*, doi:10.3390/cancers13030557.

24. Egloff-Juras, C.; Bezdetnaya, L.; Dolivet, G.; Lassalle, H.P. NIR fluorescence-guided tumor surgery: new strategies for the use of indocyanine green. *International journal of nanomedicine* **2019**, *14*, 7823-7838, doi:10.2147/ijn.S207486.

25. Cao, J.; Zhu, B.; Zheng, K.; He, S.; Meng, L.; Song, J.; Yang, H. Recent Progress in NIR-II Contrast Agent for Biological Imaging. *Front Bioeng Biotechnol* **2019**, *7*, 487, doi:10.3389/fbioe.2019.00487.

26. Vahrmeijer, A.L.; Hutteman, M.; van der Vorst, J.R.; van de Velde, C.J.; Frangioni, J.V. Image-guided cancer surgery using near-infrared fluorescence. *Nature reviews. Clinical oncology* **2013**, *10*, 507-518, doi:10.1038/nrclinonc.2013.123.

27. Hernot, S.; van Manen, L.; Debie, P.; Mieog, J.S.D.; Vahrmeijer, A.L. Latest developments in molecular tracers for fluorescence image-guided cancer surgery. *Lancet Oncol* **2019**, *20*, e354-e367, doi:10.1016/s1470-2045(19)30317-1.

28. Schaafsma, B.E.; Mieog, J.S.; Hutteman, M.; van der Vorst, J.R.; Kuppen, P.J.; Löwik, C.W.; Frangioni, J.V.; van de Velde, C.J.; Vahrmeijer, A.L. The clinical use of indocyanine green as a near-infrared fluorescent contrast agent for image-guided oncologic surgery. *Journal of surgical oncology* **2011**, *104*, 323-332, doi:10.1002/jso.21943.

29. Barth, C.W.; Gibbs, S.L. Fluorescence Image-Guided Surgery - a Perspective on Contrast Agent Development. *Proc SPIE Int Soc Opt Eng* **2020**, *11222*, doi:10.1117/12.2545292.

4

30. Keereweer, S.; Kerrebijn, J.D.; van Driel, P.B.; Xie, B.; Kaijzel, E.L.; Snoeks, T.J.; Que, I.; Hutteman, M.; van der Vorst, J.R.; Mieog, J.S., et al. Optical image-guided surgery--where do we stand? *Molecular imaging and biology* **2011**, *13*, 199-207, doi:10.1007/s11307-010-0373-2.

31. Benson, R.C.; Kues, H.A. Fluorescence properties of indocyanine green as related to angiography. *Phys Med Biol* **1978**, *23*, 159-163, doi:10.1088/0031-9155/23/1/017.

32. Jiao, J.; Zhang, J.; Yang, F.; Song, W.; Han, D.; Wen, W.; Qin, W. Quicker, deeper and stronger imaging: A review of tumor-targeted, near-infrared fluorescent dyes for fluorescence guided surgery in the preclinical and clinical stages. *Eur J Pharm Biopharm* **2020**, *152*, 123-143, doi:10.1016/j.ejpb.2020.05.002.

33. Debie, P.; Hernot, S. Emerging Fluorescent Molecular Tracers to Guide Intra-Operative Surgical Decision-Making. *Front Pharmacol* **2019**, *10*, 510, doi:10.3389/fphar.2019.00510.

34. Baljer, B.C.; Kolhe, S.; Chan, C.D.; Nicoli, F.; Ghanbasha, A.; Brookes, M.J.; Gamie, Z.; Ghosh, K.M.; Beckingsale, T.B.; Saleh, D.B., et al. Advances in image enhancement for sarcoma surgery. *Cancer letters* **2020**, *483*, 1-11, doi:10.1016/j.canlet.2020.03.029.

35. Verdye. SAMENVATTING VAN DE PRODUCTKENMERKEN. **UK/H/0654/01**.

36. Bunschoten, A.; Buckle, T.; Kuil, J.; Luker, G.D.; Luker, K.E.; Nieweg, O.E.; van Leeuwen, F.W. Targeted non-covalent self-assembled nanoparticles based on human serum albumin. *Biomaterials* **2012**, *33*, 867-875, doi:10.1016/j.biomaterials.2011.10.005.

37. Matsumura, Y.; Maeda, H. A new concept for macromolecular therapeutics in cancer chemotherapy: mechanism of tumoritropic accumulation of proteins and the antitumor agent smancs. *Cancer Res* **1986**, *46*, 6387-6392.

38. Esposito, C.; Settimi, A.; Del Conte, F.; Cerulo, M.; Coppola, V.; Farina, A.; Crocetto, F.; Ricciardi, E.; Esposito, G.; Escolino, M. Image-Guided Pediatric Surgery Using Indocyanine Green (ICG) Fluorescence in Laparoscopic and Robotic Surgery. *Front Pediatr* **2020**, *8*, 314, doi:10.3389/fped.2020.00314.

39. Goldstein, S.D.; Heaton, T.E.; Bondoc, A.; Dasgupta, R.; Abdelhafeez, A.; Davidoff, A.M.; Lautz, T.B. Evolving applications of fluorescence guided surgery in pediatric surgical oncology: a practical guide for surgeons. *Journal of Pediatric Surgery* **2020**, 10.1016/j.jpedsurg.2020.10.013, doi:10.1016/j.jpedsurg.2020.10.013.

40. Nicoli, F.; Saleh, D.B.; Baljer, B.; Chan, C.D.; Beckingsale, T.; Ghosh, K.M.; Ragbir, M.; Rankin, K.S. Intraoperative Near-infrared Fluorescence (NIR) Imaging With Indocyanine Green (ICG) Can Identify Bone and Soft Tissue Sarcomas Which May Provide Guidance for Oncological Resection. *Ann Surg* **2021**, *273*, e63-e68, doi:10.1097/sla.0000000000003857.

41. Croteau, N.J.; Heaton, T.E. Pulmonary Metastasectomy in Pediatric Solid Tumors. *Children (Basel)* **2019**, *6*, doi:10.3390/children6010006.

42. Predina, J.D.; Newton, A.D.; Corbett, C.; Shin, M.; Sulfyok, L.F.; Okusanya, O.T.; Delikatny, E.J.; Nie, S.; Gaughan, C.; Jarrar, D., et al. Near-infrared intraoperative imaging for minimally invasive pulmonary metastasectomy for sarcomas. *J Thorac Cardiovasc Surg* **2019**, *157*, 2061-2069, doi:10.1016/j.jtcvs.2018.10.169.

43. Keating, J.; Newton, A.; Venegas, O.; Nims, S.; Zeh, R.; Predina, J.; Deshpande, C.; Kucharczuk, J.; Nie, S.; Delikatny, E.J., et al. Near-Infrared Intraoperative Molecular Imaging Can Locate Metastases to the Lung. *Ann Thorac Surg* **2017**, *103*, 390-398, doi:10.1016/j.athoracsur.2016.08.079.

44. Okusanya, O.T.; Holt, D.; Heitjan, D.; Deshpande, C.; Venegas, O.; Jiang, J.; Judy, R.; DeJesus, E.; Madajewski, B.; Oh, K., et al. Intraoperative near-infrared imaging can identify pulmonary nodules. *Ann Thorac Surg* **2014**, *98*, 1223-1230, doi:10.1016/j.athoracsur.2014.05.026.

45. Chen, Y.; Cruz, F.D.; Sandhu, R.; Kung, A.L.; Mundi, P.; Deasy, J.O.; Tannenbaum, A. Pediatric Sarcoma Data Forms a Unique Cluster Measured via the Earth Mover's Distance. *Sci Rep* **2017**, *7*, 7035, doi:10.1038/s41598-017-07551-8.

46. Govaert, G.A.; Oostenbroek, R.J.; Plaisier, P.W. Prolonged skin staining after intradermal use of patent blue in sentinel lymph node biopsy for breast cancer. *Eur J Surg Oncol* **2005**, *31*, 373-375, doi:10.1016/j.ejso.2004.12.009.

47. Nunez, A.; Jones, V.; Schulz-Costello, K.; Schmolze, D. Accuracy of gross intraoperative margin assessment for breast cancer: experience since the SSO-ASTRO margin consensus guidelines. *Sci Rep* **2020**, *10*, 17344, doi:10.1038/s41598-020-74373-6.

48. Kaneko, J.; Ishizawa, T.; Masuda, K.; Kawaguchi, Y.; Aoki, T.; Sakamoto, Y.; Hasegawa, K.; Sugawara, Y.; Kokudo, N. Indocyanine green reinjection technique for use in fluorescent angiography concomitant with cholangiography during laparoscopic cholecystectomy. *Surg Laparosc Endosc Percutan Tech* **2012**, *22*, 341-344, doi:10.1097/SLE.0b013e3182570240.

49. Shao, W.; Chen, G.; Kuzmin, A.; Kutscher, H.L.; Pliss, A.; Ohulchanskyy, T.Y.; Prasad, P.N. Tunable Narrow Band Emissions from Dye-Sensitized Core/Shell/Shell Nanocrystals in the Second Near-Infrared Biological Window. *J Am Chem Soc* **2016**, *138*, 16192-16195, doi:10.1021/jacs.6b08973.

50. Makek, M.; Grant, J.W. Epithelial-myoepithelial carcinoma of the parotid gland associated with a primary carcinoma of the lung. *Int J Oral Maxillofac Surg* **1988**, *17*, 134-137, doi:10.1016/s0901-5027(88)80168-1.

51. Holt, D.; Okusanya, O.; Judy, R.; Venegas, O.; Jiang, J.; DeJesus, E.; Eruslanov, E.; Quatromoni, J.; Bhojnagarwala, P.; Deshpande, C., et al. Intraoperative near-infrared imaging can distinguish cancer from normal tissue but not inflammation. *PLoS One* **2014**, *9*, e103342, doi:10.1371/journal.pone.0103342.

52. Tummers, Q.R.; Hoogstins, C.E.; Peters, A.A.; de Kroon, C.D.; Trimbos, J.B.; van de Velde, C.J.; Frangioni, J.V.; Vahrmeijer, A.L.; Gaarenstroom, K.N. The Value of Intraoperative Near-Infrared Fluorescence Imaging Based on Enhanced Permeability and Retention of Indocyanine Green: Feasibility and False-Positives in Ovarian Cancer. *PLoS One* **2015**, *10*, e0129766, doi:10.1371/journal.pone.0129766.

53. Bosma, S.E.; van Driel, P.B.; Hogendoorn, P.C.; Dijkstra, P.S.; Sier, C.F. Introducing fluorescence guided surgery into orthopedic oncology: A systematic review of candidate protein targets for Ewing sarcoma. *J Surg Oncol* **2018**, *118*, 906-914, doi:10.1002/jso.25224.

54. Russell-Goldman, E.; Hornick, J.L.; Qian, X.; Jo, V.Y. NKX2.2 immunohistochemistry in the distinction of Ewing sarcoma from cytomorphologic mimics: Diagnostic utility and pitfalls. *Cancer Cytopathol* **2018**, *126*, 942-949, doi:10.1002/cncy.22056.

55. Gao, R.W.; Teraphongphom, N.; de Boer, E.; van den Berg, N.S.; Divi, V.; Kaplan, M.J.; Oberhelman, N.J.; Hong, S.S.; Capes, E.; Colevas, A.D., et al. Safety of panitumumab-IRDye800CW and cetuximab-IRDye800CW for fluorescence-guided surgical navigation in head and neck cancers. *Theranostics* **2018**, *8*, 2488-2495, doi:10.7150/thno.24487.

56. Leconet, W.; Larbouret, C.; Chardès, T.; Thomas, G.; Neiveyans, M.; Busson, M.; Jarlier, M.; Radosevic-Robin, N.; Pugnière, M.; Bernex, F., et al. Preclinical validation of AXL receptor as a target for antibody-based pancreatic cancer immunotherapy. *Oncogene* **2014**, *33*, 5405-5414, doi:10.1038/onc.2013.487.

57. Guo, Z.; Liu, Y.; Zhou, H.; Zheng, K.; Wang, D.; Jia, M.; Xu, P.; Ma, K.; Cui, C.; Wang, L. CD47-targeted bismuth selenide nanoparticles actualize improved photothermal therapy by increasing macrophage phagocytosis of cancer cells. *Colloids Surf B Biointerfaces* **2019**, *184*, 110546, doi:10.1016/j.colsurfb.2019.110546.

58. Wang, C.H.; Huang, Y.J.; Chang, C.W.; Hsu, W.M.; Peng, C.A. In vitro photothermal destruction of neuroblastoma cells using carbon nanotubes conjugated with GD2 monoclonal antibody. *Nanotechnology* **2009**, *20*, 315101, doi:10.1088/0957-4484/20/31/315101.

59. Garofalo, C.; Mancarella, C.; Grilli, A.; Manara, M.C.; Astolfi, A.; Marino, M.T.; Conte, A.; Sigismund, S.; Carè, A.; Belfiore, A., et al. Identification of common and distinctive mechanisms of resistance to different anti-IGF-IR agents in Ewing's sarcoma. *Mol Endocrinol* **2012**, *26*, 1603-1616, doi:10.1210/me.2012-1142.

4

60. Wilson, K.E.; Bachawal, S.V.; Abou-Elkacem, L.; Jensen, K.; Machtaler, S.; Tian, L.; Willmann, J.K. Spectroscopic Photoacoustic Molecular Imaging of Breast Cancer using a B7-H3-targeted ICG Contrast Agent. *Theranostics* **2017**, *7*, 1463-1476, doi:10.7150/thno.18217.

61. Bauer, M.; Macdonald, J.; Henri, J.; Duan, W.; Shigdar, S. The Application of Aptamers for Immunohistochemistry. *Nucleic Acid Ther* **2016**, *26*, 120-126, doi:10.1089/nat.2015.0569.

62. Hira, V.V.V.; de Jong, A.L.; Ferro, K.; Khurshed, M.; Molenaar, R.J.; Van Noorden, C.J.F. Comparison of different methodologies and cryostat versus paraffin sections for chromogenic immunohistochemistry. *Acta Histochem* **2019**, *121*, 125-134, doi:10.1016/j.acthis.2018.10.011.

63. Kersting, C.; Packeisen, J.; Leidinger, B.; Brandt, B.; von Wasielewski, R.; Winkelmann, W.; van Diest, P.J.; Gosheger, G.; Buerger, H. Pitfalls in immunohistochemical assessment of EGFR expression in soft tissue sarcomas. *J Clin Pathol* **2006**, *59*, 585-590, doi:10.1136/jcp.2005.028373.

64. Stumptner, C.; Pabst, D.; Loibner, M.; Viertler, C.; Zatloukal, K. The impact of crosslinking and non-crosslinking fixatives on antigen retrieval and immunohistochemistry. *N Biotechnol* **2019**, *52*, 69-83, doi:10.1016/j.nbt.2019.05.003.

65. Chen, S.; Guenther, L.M.; Aronhalt, A.; Cardillo, L.; Janeway, K.A.; Church, A.J. PD-1 and PD-L1 Expression in Osteosarcoma: Which Specimen to Evaluate? *J Pediatr Hematol Oncol* **2020**, *42*, 482-487, doi:10.1097/mph.0000000000001685.

66. Forest, F.; Cote, G.; Laville, D.; Da Cruz, V.; Dal Col, P.; Camy, F.; Mobarki, M.; Clemenson, A.; Yvorel, V.; Péoc'h, M. Impact of delayed fixation and decalcification on PD-L1 expression: a comparison of two clones. *Virchows Arch* **2019**, *475*, 693-699, doi:10.1007/s00428-019-02613-w.

67. Boi, G.; Scalia, C.R.; Gendusa, R.; Ronchi, S.; Cattoretti, G. Disaccharides Protect Antigens from Drying-Induced Damage in Routinely Processed Tissue Sections. *J Histochem Cytochem* **2016**, *64*, 18-31, doi:10.1369/0022155415616162.

68. Fujihara, R.; Chiba, Y.; Nakagawa, T.; Murakami, R.; Matsumoto, K.; Kawauchi, M.; Fujii, T.; Shimono, R.; Yamamoto, T.; Ueno, M. Histomorphometry of ectopic mineralization using undecalcified frozen bone sections. *Microsc Res Tech* **2018**, *81*, 1318-1324, doi:10.1002/jemt.23140.

69. Rodig, S.J. Preparing Frozen Tissue Sections for Staining. *Cold Spring Harb Protoc* **2021**, *2021*, doi:10.1101/pdb.prot099655.

70. Ralton, L.D.; Murray, G.I. The use of formalin fixed wax embedded tissue for proteomic analysis. *J Clin Pathol* **2011**, *64*, 297-302, doi:10.1136/jcp.2010.086835.

71. Mathieson, W.; Marcon, N.; Antunes, L.; Ashford, D.A.; Betsou, F.; Frasquilho, S.G.; Kofanova, O.A.; McKay, S.C.; Pericleous, S.; Smith, C., et al. A Critical Evaluation of the PAXgene Tissue Fixation System: Morphology, Immunohistochemistry, Molecular Biology, and Proteomics. *Am J Clin Pathol* **2016**, *146*, 25-40, doi:10.1093/ajcp/aqw023.

72. Coats, S.; Williams, M.; Kebble, B.; Dixit, R.; Tseng, L.; Yao, N.S.; Tice, D.A.; Soria, J.C. Antibody-Drug Conjugates: Future Directions in Clinical and Translational Strategies to Improve the Therapeutic Index. *Clin Cancer Res* **2019**, *25*, 5441-5448, doi:10.1158/1078-0432.Ccr-19-0272.

73. de Jongh, S.J.; Tjalma, J.J.J.; Koller, M.; Linssen, M.D.; Vonk, J.; Dobosz, M.; Jorritsma-Smit, A.; Kleibeuker, J.H.; Hospers, G.A.P.; Havenga, K., et al. Back-Table Fluorescence-Guided Imaging for Circumferential Resection Margin Evaluation Using Bevacizumab-800CW in Patients with Locally Advanced Rectal Cancer. *J Nucl Med* **2020**, *61*, 655-661, doi:10.2967/jnumed.119.232355.

74. Harlaar, N.J.; Koller, M.; de Jongh, S.J.; van Leeuwen, B.L.; Hemmer, P.H.; Kruijff, S.; van Ginkel, R.J.; Been, L.B.; de Jong, J.S.; Kats-Ugurlu, G., et al. Molecular fluorescence-guided surgery of peritoneal carcinomatosis of colorectal origin: a single-centre feasibility study. *Lancet Gastroenterol Hepatol* **2016**, *1*, 283-290, doi:10.1016/s2468-1253(16)30082-6.

75. Korb, M.L.; Hartman, Y.E.; Kovar, J.; Zinn, K.R.; Bland, K.I.; Rosenthal, E.L. Use of monoclonal antibody-IRDye800CW bioconjugates in the resection of breast cancer. *J Surg Res* **2014**, *188*, 119-128, doi:10.1016/j.jss.2013.11.089.

76. Lamberts, L.E.; Koch, M.; de Jong, J.S.; Adams, A.L.L.; Glatz, J.; Kranendonk, M.E.G.; Terwisscha van Scheltinga, A.G.T.; Jansen, L.; de Vries, J.; Lub-de Hooge, M.N., et al. Tumor-Specific Uptake of Fluorescent Bevacizumab-IRDye800CW Microdosing in Patients with Primary Breast Cancer: A Phase I Feasibility Study. *Clin Cancer Res* **2017**, *23*, 2730-2741, doi:10.1158/1078-0432.Ccr-16-0437.

77. Steinkamp, P.J.; Pranger, B.K.; Li, M.F.; Linssen, M.D.; Voskuil, F.J.; Been, L.B.; van Leeuwen, B.L.; Suurmeijer, A.J.H.; Nagengast, W.B.; Kruijff, S., et al. Fluorescence-Guided Visualization of Soft-Tissue Sarcomas by Targeting Vascular Endothelial Growth Factor A: A Phase 1 Single-Center Clinical Trial. *J Nucl Med* **2021**, *62*, 342-347, doi:10.2967/jnumed.120.245696.

78. Zhang, Y.; Tang, Y.J.; Man, Y.; Pan, F.; Li, Z.H.; Jia, L.S. Knockdown of AXL receptor tyrosine kinase in osteosarcoma cells leads to decreased proliferation and increased apoptosis. *Int J Immunopathol Pharmacol* **2013**, *26*, 179-188, doi:10.1177/039463201302600117.

79. Rettew, A.N.; Young, E.D.; Lev, D.C.; Kleinerman, E.S.; Abdul-Karim, F.W.; Getty, P.J.; Greenfield, E.M. Multiple receptor tyrosine kinases promote the in vitro phenotype of metastatic human osteosarcoma cell lines. *Oncogenesis* **2012**, *1*, e34, doi:10.1038/oncsis.2012.34.

80. Wang, L.; Zhang, Q.; Chen, W.; Shan, B.; Ding, Y.; Zhang, G.; Cao, N.; Liu, L.; Zhang, Y. B7-H3 is overexpressed in patients suffering osteosarcoma and associated with tumor aggressiveness and metastasis. *PLoS One* **2013**, *8*, e70689, doi:10.1371/journal.pone.0070689.

81. Xu, J.F.; Pan, X.H.; Zhang, S.J.; Zhao, C.; Qiu, B.S.; Gu, H.F.; Hong, J.F.; Cao, L.; Chen, Y.; Xia, B., et al. CD47 blockade inhibits tumor progression human osteosarcoma in xenograft models. *Oncotarget* **2015**, *6*, 23662-23670, doi:10.18632/oncotarget.4282.

82. Poon, V.I.; Roth, M.; Piperdi, S.; Geller, D.; Gill, J.; Rudzinski, E.R.; Hawkins, D.S.; Gorlick, R. Ganglioside GD2 expression is maintained upon recurrence in patients with osteosarcoma. *Clin Sarcoma Res* **2015**, *5*, 4, doi:10.1186/s13569-014-0020-9.

83. Roth, M.; Linkowski, M.; Tarim, J.; Piperdi, S.; Sowers, R.; Geller, D.; Gill, J.; Gorlick, R. Ganglioside GD2 as a therapeutic target for antibody-mediated therapy in patients with osteosarcoma. *Cancer* **2014**, *120*, 548-554, doi:10.1002/cncr.28461.

84. Roth, M.; Barris, D.M.; Piperdi, S.; Kuo, V.; Everts, S.; Geller, D.; Houghton, P.; Kolb, E.A.; Hawthorne, T.; Gill, J., et al. Targeting Glycoprotein NMB With Antibody-Drug Conjugate, Glembatumumab Vedotin, for the Treatment of Osteosarcoma. *Pediatr Blood Cancer* **2016**, *63*, 32-38, doi:10.1002/pbc.25688.

85. Wang, Y.H.; Han, X.D.; Qiu, Y.; Xiong, J.; Yu, Y.; Wang, B.; Zhu, Z.Z.; Qian, B.P.; Chen, Y.X.; Wang, S.F., et al. Increased expression of insulin-like growth factor-1 receptor is correlated with tumor metastasis and prognosis in patients with osteosarcoma. *J Surg Oncol* **2012**, *105*, 235-243, doi:10.1002/jso.22077.

86. Aznab, M.; Khajevand Ahmady, M.; Jamshidi, K.; Madani, S.H.; Khazaei, S.; Shoushtaryzadeh, T.; Bagheri, A. Investigating the Relationship between of Vascular Endothelial Growth Factor and HER-2neu in IHC Staining with Metastasis and Mortality in Patients with Osteosarcoma. *Asian Pac J Cancer Prev* **2020**, *21*, 3005-3009, doi:10.31557/apjcp.2020.21.10.3005.

87. Lin, F.; Zheng, S.E.; Shen, Z.; Tang, L.N.; Chen, P.; Sun, Y.J.; Zhao, H.; Yao, Y. Relationships between levels of CXCR4 and VEGF and blood-borne metastasis and survival in patients with osteosarcoma. *Med Oncol* **2011**, *28*, 649-653, doi:10.1007/s12032-010-9493-4.

88. Lammli, J.; Fan, M.; Rosenthal, H.G.; Patni, M.; Rinehart, E.; Vergara, G.; Ablah, E.; Wooley, P.H.; Lucas, G.; Yang, S.Y. Expression of Vascular Endothelial Growth Factor correlates with the advance of clinical osteosarcoma. *Int Orthop* **2012**, *36*, 2307-2313, doi:10.1007/s00264-012-1629-z.

4

89.   Rossi, B.; Schinzari, G.; Maccauro, G.; Scaramuzzo, L.; Signorelli, D.; Rosa, M.A.; Fabbriciani, C.; Carlo, B. Neoadjuvant multidrug chemotherapy including high-dose methotrexate modifies VEGF expression in osteosarcoma: an immunohistochemical analysis. *BMC Musculoskelet Disord* **2010**, *11*, 34, doi:10.1186/1471-2474-11-34.

90.   Bajpai, J.; Sharma, M.; Sreenivas, V.; Kumar, R.; Gamnagatti, S.; Khan, S.A.; Rastogi, S.; Malhotra, A.; Bakhshi, S. VEGF expression as a prognostic marker in osteosarcoma. *Pediatr Blood Cancer* **2009**, *53*, 1035-1039, doi:10.1002/pbc.22178.

91.   Charity, R.M.; Foukas, A.F.; Deshmukh, N.S.; Grimer, R.J. Vascular endothelial growth factor expression in osteosarcoma. *Clin Orthop Relat Res* **2006**, *448*, 193-198, doi:10.1097/01.blo.0000205877.05093.c9.

92.   Ek, E.T.; Ojaimi, J.; Kitagawa, Y.; Choong, P.F. Does the degree of intratumoural microvessel density and VEGF expression have prognostic significance in osteosarcoma? *Oncol Rep* **2006**, *16*, 17-23.

93.   Kaya, M.; Wada, T.; Akatsuka, T.; Kawaguchi, S.; Nagoya, S.; Shindoh, M.; Higashino, F.; Mezawa, F.; Okada, F.; Ishii, S. Vascular endothelial growth factor expression in untreated osteosarcoma is predictive of pulmonary metastasis and poor prognosis. *Clin Cancer Res* **2000**, *6*, 572-577.

94.   Boulytcheva, I.V.; Soloviev, Y.N.; Kushlinskii, N.E.; Mahson, A.N. Expression of molecular markers in the tumor and survival prognosis in osteosarcoma. *Bull Exp Biol Med* **2010**, *150*, 237-242, doi:10.1007/s10517-010-1114-x.

95.   Becker, R.G.; Galia, C.R.; Morini, S.; Viana, C.R. Immunohistochemical expression of vegf and her-2 proteins in osteosarcoma biopsies. *Acta Ortop Bras* **2013**, *21*, 233-238, doi:10.1590/s1413-78522013000400010.

96.   Yang, J.; Zhao, L.; Tian, W.; Liao, Z.; Zheng, H.; Wang, G.; Chen, K. Correlation of WWOX, RUNX2 and VEGFA protein expression in human osteosarcoma. *BMC Med Genomics* **2013**, *6*, 56, doi:10.1186/1755-8794-6-56.

97.   Abdeen, A.; Chou, A.J.; Healey, J.H.; Khanna, C.; Osborne, T.S.; Hewitt, S.M.; Kim, M.; Wang, D.; Moody, K.; Gorlick, R. Correlation between clinical outcome and growth factor pathway expression in osteogenic sarcoma. *Cancer* **2009**, *115*, 5243-5250, doi:10.1002/cncr.24562.

98.   Qu, Y.; Xu, J.; Jiang, T.; Zhao, H.; Gao, Y.; Zheng, C.; Shi, X. Difference in pre- and postchemotherapy vascular endothelial growth factor levels as a prognostic indicator in osteosarcoma. *J Int Med Res* **2011**, *39*, 1474-1482, doi:10.1177/147323001103900436.

99.   Zhang, Q.; Liu, F.; Wang, B.; Li, Z.; Zhou, D.; Yang, Q.; Dong, J.; Li, J. HER-2 expression in biopsy and surgical specimen on prognosis of osteosarcoma: A systematic review and meta-analysis of 16 studies. *Medicine (Baltimore)* **2016**, *95*, e3661, doi:10.1097/md.0000000000003661.

100.   Abdou, A.G.; Kandil, M.; Asaad, N.Y.; Dawoud, M.M.; Shahin, A.A.; Abd Eldayem, A.F. The Prognostic Role of Ezrin and HER2/neu Expression in Osteosarcoma. *Appl Immunohistochem Mol Morphol* **2016**, *24*, 355-363, doi:10.1097/pai.0000000000000197.

101.   Chen, C.; Constantinou, A.; Chester, K.A.; Vyas, B.; Canis, K.; Haslam, S.M.; Dell, A.; Epenetos, A.A.; Deonarain, M.P. Glycoengineering approach to half-life extension of recombinant biotherapeutics. *Bioconjugate chemistry* **2012**, *23*, 1524-1533, doi:10.1021/bc200624a.

102.   Wunder, J.S.; Lee, M.J.; Nam, J.; Lau, B.Y.; Dickson, B.C.; Pinnaduwage, D.; Bull, S.B.; Ferguson, P.C.; Seto, A.; Gokgoz, N., et al. Osteosarcoma and soft-tissue sarcomas with an immune infiltrate express PD-L1: relation to clinical outcome and Th1 pathway activation. *Oncoimmunology* **2020**, *9*, 1737385, doi:10.1080/2162402x.2020.1737385.

103.   Hashimoto, K.; Nishimura, S.; Akagi, M. Characterization of PD-1/PD-L1 Immune Checkpoint Expression in Osteosarcoma. *Diagnostics (Basel)* **2020**, *10*, doi:10.3390/diagnostics10080528.

104.   Liu, P.; Xiao, Q.; Zhou, B.; Dai, Z.; Kang, Y. Prognostic Significance of Programmed Death Ligand 1 Expression and Tumor-Infiltrating Lymphocytes in Axial Osteosarcoma. *World Neurosurg* **2019**, *129*, e240-e254, doi:10.1016/j.wneu.2019.05.121.

105. Gomez-Brouchet, A.; Illac, C.; Gilhodes, J.; Bouvier, C.; Aubert, S.; Guinebretiere, J.M.; Marie, B.; Laroussserie, F.; Entz-Werlé, N.; de Pinieux, G., et al. CD163-positive tumor-associated macrophages and CD8-positive cytotoxic lymphocytes are powerful diagnostic markers for the therapeutic stratification of osteosarcoma patients: An immunohistochemical analysis of the biopsies from the French OS2006 phase 3 trial. *Oncoimmunology* **2017**, *6*, e1331193, doi:10.1080/2162402x.2017.1331193.

106. Torabi, A.; Amaya, C.N.; Wians, F.H., Jr.; Bryan, B.A. PD-1 and PD-L1 expression in bone and soft tissue sarcomas. *Pathology* **2017**, *49*, 506-513, doi:10.1016/j.pathol.2017.05.003.

107. Majzner, R.G.; Simon, J.S.; Grosso, J.F.; Martinez, D.; Pawel, B.R.; Santi, M.; Merchant, M.S.; Geoerger, B.; Hezam, I.; Marty, V., et al. Assessment of programmed death-ligand 1 expression and tumor-associated immune cells in pediatric cancer tissues. *Cancer* **2017**, *123*, 3807-3815, doi:10.1002/cncr.30724.

108. Liao, Y.; Chen, L.; Feng, Y.; Shen, J.; Gao, Y.; Cote, G.; Choy, E.; Harmon, D.; Mankin, H.; Hornicek, F., et al. Targeting programmed cell death ligand 1 by CRISPR/Cas9 in osteosarcoma cells. *Oncotarget* **2017**, *8*, 30276-30287, doi:10.18632/oncotarget.16326.

109. Koirala, P.; Roth, M.E.; Gill, J.; Piperdi, S.; Chinai, J.M.; Geller, D.S.; Hoang, B.H.; Park, A.; Fremed, M.A.; Zang, X., et al. Immune infiltration and PD-L1 expression in the tumor microenvironment are prognostic in osteosarcoma. *Sci Rep* **2016**, *6*, 30093, doi:10.1038/srep30093.

110. Kalim, M.; Wang, S.; Liang, K.; Khan, M.S.I.; Zhan, J. Engineered scPDL1-DM1 drug conjugate with improved in vitro analysis to target PD-L1 positive cancer cells and intracellular trafficking studies in cancer therapy. *Genetics and molecular biology* **2020**, *42*, e20180391, doi:10.1590/1678-4685-gmb-2018-0391.

111. Rouleau, C.; Curiel, M.; Weber, W.; Smale, R.; Kurtzberg, L.; Mascarello, J.; Berger, C.; Wallar, G.; Bagley, R.; Honma, N., et al. Endosialin protein expression and therapeutic target potential in human solid tumors: sarcoma versus carcinoma. *Clin Cancer Res* **2008**, *14*, 7223-7236, doi:10.1158/1078-0432.Ccr-08-0499.

112. Lange, S.E.; Zheleznyak, A.; Studer, M.; O'Shannessy, D.J.; Lapi, S.E.; Van Tine, B.A. Development of 89Zr-Ontuxizumab for in vivo TEM-1/endosialin PET applications. *Oncotarget* **2016**, *7*, 13082-13092, doi:10.18632/oncotarget.7552.

113. Gupta, S.; Sosa, C.P.; Kosari, F.; Folpe, A.; Bhinge, K.N.; Yang, L.; Agahi, A.; Johnson, S.H.; Frank, I.; Boorjian, S.A., et al. A comparison of adult rhabdomyosarcoma and high-grade neuroendocrine carcinoma of the urinary bladder reveals novel PPP1R12A fusions in rhabdomyosarcoma. *Hum Pathol* **2019**, *88*, 48-59, doi:10.1016/j.humpath.2019.03.007.

114. Sadikovic, B.; Graham, C.; Ho, M.; Zielenska, M.; Somers, G.R. Immunohistochemical expression and cluster analysis of mesenchymal and neural stem cell-associated proteins in pediatric soft tissue sarcomas. *Pediatr Dev Pathol* **2011**, *14*, 259-272, doi:10.2350/10-08-0890-oa.1.

115. Bahrami, A.; Gown, A.M.; Baird, G.S.; Hicks, M.J.; Folpe, A.L. Aberrant expression of epithelial and neuroendocrine markers in alveolar rhabdomyosarcoma: a potentially serious diagnostic pitfall. *Mod Pathol* **2008**, *21*, 795-806, doi:10.1038/modpathol.2008.86.

116. Mechtersheimer, G.; Staudter, M.; Möller, P. Expression of the natural killer cell-associated antigens CD56 and CD57 in human neural and striated muscle cells and in their tumors. *Cancer Res* **1991**, *51*, 1300-1307.

117. Thompson, L.D.R.; Jo, V.Y.; Agaimy, A.; Llombart-Bosch, A.; Morales, G.N.; Machado, I.; Flucke, U.; Wakely, P.E., Jr.; Miettinen, M.; Bishop, J.A. Sinonasal Tract Alveolar Rhabdomyosarcoma in Adults: A Clinicopathologic and Immunophenotypic Study of Fifty-Two Cases with Emphasis on Epithelial Immunoreactivity. *Head Neck Pathol* **2018**, *12*, 181-192, doi:10.1007/s12105-017-0851-9.

118. Karakuş, R.; Karakuş, E.; Emir, S.; Kaçar, A.; Özyörük, D. Insulin-like growth factor-1 receptor expression in pediatric tumors: a comparative immunohistochemical study. *Turk J Med Sci* **2018**, *48*, 419-423, doi:10.3906/sag-1801-233.

4

119. van Gaal, J.C.; Roeffen, M.H.; Flucke, U.E.; van der Laak, J.A.; van der Heijden, G.; de Bont, E.S.; Suurmeijer, A.J.; Versleijen-Jonkers, Y.M.; van der Graaf, W.T. Simultaneous targeting of insulin-like growth factor-1 receptor and anaplastic lymphoma kinase in embryonal and alveolar rhabdomyosarcoma: a rational choice. *Eur J Cancer* **2013**, *49*, 3462-3470, doi:10.1016/j.ejca.2013.06.022.

120. Miyoshi, K.; Kohashi, K.; Fushimi, F.; Yamamoto, H.; Kishimoto, J.; Taguchi, T.; Iwamoto, Y.; Oda, Y. Close correlation between CXCR4 and VEGF expression and frequent CXCR7 expression in rhabdomyosarcoma. *Hum Pathol* **2014**, *45*, 1900-1909, doi:10.1016/j.humpath.2014.05.012.

121. Krawczyk, M.A.; Styczewska, M.; Sokolewicz, E.M.; Kunc, M.; Gabrych, A.; Fatyga, A.; Izycka-Swieszewska, E.; Kazanowska, B.; Adamkiewicz-Drozynska, E.; Bien, E. Tumour expressions of hypoxic markers predict the response to neo-adjuvant chemotherapy in children with inoperable rhabdomyosarcoma. *Biomarkers* **2019**, *24*, 538-548, doi:10.1080/1354750x.2019.1606275.

122. Kendsersky, N.M.; Lindsay, J.; Kolb, E.A.; Smith, M.A.; Teicher, B.A.; Erickson, S.W.; Earley, E.J.; Mosse, Y.P.; Martinez, D.; Pogoriler, J., et al. The B7-H3-Targeting Antibody-Drug Conjugate m276-SL-PBD Is Potently Effective Against Pediatric Cancer Preclinical Solid Tumor Models. *Clin Cancer Res* **2021**, 10.1158/1078-0432.Ccr-20-4221, doi:10.1158/1078-0432.Ccr-20-4221.

123. Thway, K.; Robertson, D.; Jones, R.L.; Selfe, J.; Shipley, J.; Fisher, C.; Isacke, C.M. Endosialin expression in soft tissue sarcoma as a potential marker of undifferentiated mesenchymal cells. *Br J Cancer* **2016**, *115*, 473-479, doi:10.1038/bjc.2016.214.

124. Freise, A.C.; Wu, A.M. In vivo imaging with antibodies and engineered fragments. *Mol Immunol* **2015**, *67*, 142-152, doi:10.1016/j.molimm.2015.04.001.

125. van Leeuwen, F.W.B.; Schottelius, M.; Brouwer, O.R.; Vidal-Sicart, S.; Achilefu, S.; Klode, J.; Wester, H.J.; Buckle, T. Trending: Radioactive and Fluorescent Bimodal/Hybrid Tracers as Multiplexing Solutions for Surgical Guidance. *J Nucl Med* **2020**, *61*, 13-19, doi:10.2967/jnumed.119.228684.

126. Hekman, M.C.; Rijpkema, M.; Muselaers, C.H.; Oosterwijk, E.; Hulsbergen-Van de Kaa, C.A.; Boerman, O.C.; Oyen, W.J.; Langenhuijsen, J.F.; Mulders, P.F. Tumor-targeted Dual-modality Imaging to Improve Intraoperative Visualization of Clear Cell Renal Cell Carcinoma: A First in Man Study. *Theranostics* **2018**, *8*, 2161-2170, doi:10.7150/thno.23335.

127. Folli, S.; Wagnières, G.; Pèlegrin, A.; Calmes, J.M.; Braichotte, D.; Buchegger, F.; Chalandon, Y.; Hardman, N.; Heusser, C.; Givel, J.C., et al. Immunophotodiagnosis of colon carcinomas in patients injected with fluoresceinated chimeric antibodies against carcinoembryonic antigen. *Proc Natl Acad Sci U S A* **1992**, *89*, 7973-7977, doi:10.1073/pnas.89.17.7973.

128. Kuil, J.; Velders, A.H.; van Leeuwen, F.W. Multimodal tumor-targeting peptides functionalized with both a radio- and a fluorescent label. *Bioconjug Chem* **2010**, *21*, 1709-1719, doi:10.1021/bc100276j.

129. Hensbergen, A.W.; Buckle, T.; van Willigen, D.M.; Schottelius, M.; Welling, M.M.; van der Wijk, F.A.; Maurer, T.; van der Poel, H.G.; van der Pluijm, G.; van Weerden, W.M., et al. Hybrid Tracers Based on Cyanine Backbones Targeting Prostate-Specific Membrane Antigen: Tuning Pharmacokinetic Properties and Exploring Dye-Protein Interaction. *J Nucl Med* **2020**, *61*, 234-241, doi:10.2967/jnumed.119.233064.

130. Kopper, O.; de Witte, C.J.; Lõhmussaar, K.; Valle-Inclan, J.E.; Hami, N.; Kester, L.; Balgobind, A.V.; Korving, J.; Proost, N.; Begthel, H., et al. An organoid platform for ovarian cancer captures intra- and interpatient heterogeneity. *Nat Med* **2019**, *25*, 838-849, doi:10.1038/s41591-019-0422-6.

131. Jacob, F.; Salinas, R.D.; Zhang, D.Y.; Nguyen, P.T.T.; Schnoll, J.G.; Wong, S.Z.H.; Thokala, R.; Sheikh, S.; Saxena, D.; Prokop, S., et al. A Patient-Derived Glioblastoma Organoid Model and Biobank Recapitulates Inter- and Intra-tumoral Heterogeneity. *Cell* **2020**, *180*, 188-204.e122, doi:10.1016/j.cell.2019.11.036.

Appendix A. PubMed search strategy for clinical trials investigating antibodies in OS, RMS, or ES.
("Antibodies"[Mesh] OR "antibodies"[tw] OR "antibody"[tw] OR "Immunoglobu-lins"[Mesh] OR "Immunoglobulins"[tw] OR "Immunoglobulin"[tw] OR (("targeted"[All Fields] OR "target*"[tw]) AND ("therapy"[Subheading] OR "therapeutics"[MeSH] OR "therapy"[tw] OR "therap*"[tw])))

AND

("Rhabdomyosarcoma"[MeSH] OR "Rhabdomyosarcoma"[tw] OR "Rhabdomyo-sar*"[tw] OR "sarcoma, Ewing"[MeSH] OR "Ewing sarcoma"[tw] OR "Ewing's Sar-coma"[tw] OR "Ewings Sarcoma"[tw] OR "Ewing's Tumor"[tw] OR "Ewings Tumor"[tw] OR "Ewing tumor"[tw] OR "Osteosarcoma"[MeSH] OR "Osteosarcoma"[tw] OR "Oste-osarc*"[tw] OR "Osteogenic sarc*"[tw])

AND

("Child"[MeSH] OR "child"[tw] OR "child*"[tw] OR "infant"[MeSH] OR "infant"[tw] OR "infant*"[tw] OR "pediatrics"[MeSH] OR "pediatric"[tw] OR "pediatric*"[tw] OR "young adult"[tw] OR "young adult*"[tw] OR "young"[tw] OR "youth"[tw] OR "youth*"[tw] OR "adolescent"[MeSH] OR "adolescent"[tw] OR "adolescent*"[tw] OR "adolescence"[tw] OR "adolescen*"[tw] OR "teen"[tw] OR "teen*"[tw])

4

Supplementary Table S1. Published/completed trials with clinically available antibodies for Osteosarcoma-, Rhabdomyosarcoma- and Ewing Sarcoma patients.

Targets	Tumor type	Clinically available antibody (targeted therapy)	Age of the study population	Clinical trial phase	Safety	Literature (PMID/NCT)
HER2	Metastatic OS	Trastuzumab	<32-year-old patients	Phase 2	Safe	22665540
gpNMB	Recurrent OS	Glembatumumab vedotin	12–31-year-old patients	Phase 2	Safe	31586757
VEGF-A	OS, ES, and RMS	Bevacizumab	0.5-29-year-old patients	Pilot- and phase 2	Safe (one study reported wound complications)	28631382, 26461056, 23630159, 31513481, 28738258
IGF-1R	OS, ES, and RMS	Cixutumumab, Ganitumab, Teprotumumab, Figitumumab, Robatumumab and Dalotuzumab	1–85-year-old patients	Pilot-, phase 1 and phase 2	Safe	30351457, 22508822, 22025149, 20371689, 22465830, 25446280, 23956055, 22184397, 23477833, 22025154, 27362300, 24797726, 21127194, 23835252, 21750201, 27185573, 20036194
TRAIL-R2	Recurrent or progressive OS, ES, and RMS	Lexatumumab	2–21-year-old patients	Phase 1	Safe	23071222
TEM1	OS, recurrent or refractory ES and RMS	Ontuxizumab	3–21-year-old patients	Phase 1	Safe	29292843
B7-H3	Relapsed/refractory OS, ES, and RMS	Enoblituzumab	1–35-year-old patients	Phase 1	No statement on safety	NCT02982941

Supplementary Table S2. Ongoing/unpublished trials with clinically available antibodies for Osteosarcoma-, Rhabdomyosarcoma- and Ewing Sarcoma patients.

Targets	Tumor type	Clinically available antibody (targeted therapy)	Age of the study population	Clinical trial phase	Status	NCT-number
GD2	OS	Hu3F8-BsAb (humanized 3F8 bispecific antibody) and Dinutuximab	1–40-year-old patients	Phase 1 and phase 2	Recruiting Active, not recruiting Not yet recruiting	NCT02502786 and NCT03860207 NCT02484443 NCT04751383
HER2	OS	Trastuzumab Deruxtecan (ADC)	12 – 39-year-old patients	Phase 2	Recruiting	NCT04616560
PD-L1	OS	ZKAB001, Avelumab and Durvalimub	12–55-year-old patients	Phase 1, phase 2 and phase 3	Recruiting Active, not recruiting Not yet recruiting	NCT03676985 and NCT04668300 NCT03006848 NCT04359550
CD47 and GD2	OS	Magrolimab + Dinutuximab	1–35-year-old patients	1	Not yet recruiting	NCT04751383
semaphorin 4D	Recurrent or refractory OS	Pepinemab	1–30-year-old patients	1-2	Active, not recruiting	NCT03320330
AXL	OS and ES	CAB-ANTI-AXL-ADC	> 17-year-old patients	1-2	Recruiting	NCT03425279
IGF-1R	ES, Embryonal and Alveolar RMS	Ganitumab	> 1-year-old patients < 51-year-old patients	Phase 1, phase 2 and phase 3	Recruiting Active, not recruiting	NCT03041701 NCT02306161
CD56	RMS	Lorvotuzumab Mertansin (ADC)	1–30-year-old patients	2	Active, not recruiting	NCT02452554

4

5

EVALUATION OF POTENTIAL TARGETS FOR FLUORESCENCE-GUIDED SURGERY IN PEDIATRIC EWING SARCOMA: A PRECLINICAL PROOF-OF-CONCEPT STUDY

B. Jeremiasse[1,†], Z. Rijs[2,†], K.R. Angoelal[1], L.S. Hiemcke-Jiwa[3,4], E.A. de Boed[3], P.J.K. Kuppen[5], C.F.M. Sier[5], P.B.A.A. van Driel[6], M.A.J. van de Sande[1,2], M.H.W.A. Wijnen[1], A.C. Rios[7,8], A.F.W. van der Steeg[1]

[†]Authors contributed equally

[1] Department of Surgery, Princess Maxima Center for Pediatric Oncology, Utrecht, The Netherlands
[2] Department of Orthopedic Surgery, Leiden University Medical Center, Leiden, The Netherlands
[3] Department of Pathology, Princess Maxima Center for Pediatric Oncology, Utrecht, The Netherlands
[4] Department of Pathology, University Medical Center Utrecht, Utrecht, The Netherlands
[5] Department of Surgery, Leiden University Medical Center, Leiden, The Netherlands
[6] Department of Orthopedic Surgery, Isala Hospital, Zwolle, The Netherlands
[7] Research Department, Princess Maxima Center for Pediatric Oncology, Utrecht, The Netherlands
[8] Oncode Institute, Utrecht, The Netherlands

Simple Summary

The only cure for children with Ewing sarcoma (ES) is surgery. Unfortunately, surgeons are often not able to differentiate healthy from malignant tissue. Fluorescent imaging during the operation will facilitate recognition of malignant cells, but unfortunately there are no ES specific tracers available yet. We searched for proteins on ES cells that could be used as a target against which specific tracers could be developed. The most promising proteins, CD99, CD117, and GD2, were found in paraffin-embedded tissue samples collected from ES patients. Tracers against CD99 and CD117, consisting of monoclonal antibodies attached with a fluorescent dye, showed positive signals on cultured ES cells. In a proof-of-concept study, these tracers were topically applied on fresh ES tissue, showing a signal in the tumor. Our results indicate the applicability for fluorescence-guided surgery of ES-based tracers, but these data have to be confirmed in a larger cohort of pediatric ES patients.

Abstract

Fluorescence-guided surgery (FGS), based on fluorescent tracers binding to tumor-specific biomarkers, could assist surgeons to achieve complete tumor resections. This study evaluated potential biomarkers for FGS in pediatric Ewing sarcoma (ES). Immunohistochemistry (IHC) was performed to assess CD99, CXCR4, CD117, NPY-R-Y1, and IGF-1R expression in ES biopsies and resection specimens. LINGO-1 and GD2 evaluation did not work on the acquired tissue. Based on the immunoreactive scores, anti-CD99 and anti-CD117 were evaluated for binding specificity using flow cytometry and immunofluorescence microscopy. Anti-GD2, a tracer in the developmental phase, was also tested. These three tracers were topically applied to a freshly resected ES tumor and adjacent healthy tissue. IHC demonstrated moderate/strong CD99 and CD117 expression in ES tumor samples, while adjacent healthy tissue had limited expression. Flow cytometry and immunofluorescence microscopy confirmed high CD99 expression, along with low/moderate CD117 and low GD2 expression, in ES cell lines. Topical anti-CD99 and anti-GD2 application on ES tumor showed fluorescence, while anti-CD117 did not show fluorescence for this patient. In conclusion, CD99-targeting tracers hold promise for FGS of ES. CD117 and GD2 tracers could be potential alternatives. The next step towards development of ES-specific FGS tracers could be ex vivo topical application experiments on a large cohort of ES patients.

5

Introduction

Ewing sarcoma (ES) is a rare, aggressive, small blue round cell tumor that can occur in bone or, more rarely, in soft tissue [1,2]. It is the second most common primary osseous malignancy in children and young adults, after osteosarcoma [3]. Diagnostic workup involves plain radiographs, magnetic resonance imaging (MRI), sometimes with additional computed tomography (CT), followed by a biopsy, and (if possible) molecular confirmation [2,4,5]. Once confirmed, subsequent ES treatment is highly individualized, but generally consists of multimodality therapies comprising surgery and (neo)adjuvant chemotherapy with or without radiotherapy [2,6,7]. Clinical outcomes are highly dependent on surgical margins, as incomplete margins negatively affect both local recurrence (LR) and overall survival (OS) [8-10]. Moreover, incomplete resections often necessitate postoperative radiotherapy to reduce the risk for LR, while radiotherapy increases the risk for local complications [11]. This is especially relevant in the context of pediatric patients, as survivors are susceptible to encountering various (long-term) treatment-related side effects, including compromised growth and development, organ dysfunction, and secondary malignancies [12,13]. Therefore, improving complete resection rates is of paramount importance.

However, margin assessment is difficult due to the infiltrative and diffuse growth pattern of ES. Furthermore, preoperative imaging modalities, such as MRI and CT, which are used to identify the tumor location and extension, cannot be directly translated to the intraoperative setting for various reasons. First, these images are limited to a two-dimensional space, whereas the surgery is performed in a three-dimensional environment. Secondly, they do not precisely overlap with the intraoperative situation due to tissue manipulation and positioning. Hence, surgeons have to rely mostly on their tactile and visual feedback, which hinders intraoperative identification of the tumor border. As a consequence, incomplete resections occur in 20–30% of the ES patients [8,14].

Fluorescence-guided surgery (FGS) is an emerging tool that could help to increase the chance of complete tumor resections [15]. It has been developed to assist surgeons in accurately identifying critical anatomical structures, including tumors. By administering a fluorescent tracer, FGS enables real-time visualization of the structure of interest, facilitated by a dedicated camera system. FGS can be categorized into non-targeted and targeted (tumor-specific) FGS, which has been recently reviewed for pediatric ES [16]. Targeted FGS involves the use of tumor-specific tracers, such as antibodies or peptides conjugated to a fluorophore, to selectively recognize and bind to targets overexpressed on tumor cells. Currently, targeted FGS is being explored for various tumor types and has shown promising outcomes, presenting a potential avenue for improving ES surgery [17-21].

Targeted FGS can be implemented in two distinct ways: through intravenous (IV) administration of a near-infrared (NIR) fluorescent tracer or via topical application of a fluorescent tracer onto the resected specimen. Each method possesses its own advantages and disadvantages. The IV administration of a NIR fluorescent tracer is considered the preferred modality due to its

capability of providing real-time intraoperative fluorescence assessment of both malignant and surrounding healthy tissue, including the detection of possible satellite lesions in the tumor bed. However, the development of a NIR fluorescent tracer entails considerable costs and time investment. It necessitates comprehensive evaluation of toxicology and safety, determination of optimal dosage, window of imaging, and subsequent registration as an approved drug. Moreover, certain tracers may never become available due to significant side effects resulting from binding to healthy (distant) tissues. FGS by ex vivo topical application, on the other hand, can be a relatively feasible step towards the development of a FGS tracer for IV use, as it circumvents the need for expensive and time-consuming toxicology studies for human application [16]. Although the detection of potential satellite lesions is not possible, topical application can still yield clinical benefits by aiding in the intraoperative assessment of tumor margins. Furthermore, this method enables the analysis of fluorescence within the patient-specific tumor-associated stromal and vascular composition and facilitates the evaluation of inter- and intratumoral heterogeneity. Thus, it may reduce the reliance on animal experiments, which should be minimized by EC regulation, but also because they may not accurately reflect the human background fluorescence necessary for calculating the tumor-to-background ratio (TBR).

Three important parameters define successful targeted FGS: the tumor-specific biomarker (target), the targeting moiety conjugated to a fluorophore (tracer), and the dedicated camera system (of which several are already on the market) [22]. Encouragingly, Bosma et al. already identified some promising targets for ES, based on their overexpression on ES tumor tissue as assessed by immunohistochemistry (IHC) or flow cytometry [23]. The following targets were identified: Cluster of Differentiation 99 (CD99), C-X-C chemokine receptor type 4 (CXCR4 also known as CD184), Cluster of Differentiation 117 (CD117, also known as C-Kit), Neuropeptide Y receptor type 1 (NPY-R-Y1), Leucine rich repeat, Immunoglobin-like domain-containing protein 1 (LINGO-1), and insulin-like growth factor 1 receptor (IGF-1R) [23]. Additionally, disialoganglioside 2 (GD2) could be a promising target due to its known expression of 40–90% in ES biopsy samples and the clinical availability of an FGS tracer for neuroblastoma, which will soon be tested in a phase 1/2 clinical trial [24-27].

However, while these potential targets have shown overexpression in pediatric ES, their expression on healthy tissue surrounding the tumor has not been assessed. As a crucial step towards developing targeted FGS for ES, this study aims to evaluate the selected targets through IHC analysis conducted on biopsies and resection specimens, including adjacent healthy tissue. Including resection specimens with adjacent healthy tissue allows the evaluation of target expression after preoperative treatment and assessment of the differential expression between healthy and malignant tissue which will affect the TBR. Subsequently, three tracers with the highest potential for FGS were further evaluated with fluorescent tracers. Binding specificity of the tracers was assessed using cell-line-based flow cytometry and immunofluorescence microscopy experiments. Finally, as proof-of-concept, a topical application experiment with the three selected tracers was performed on freshly resected tissue from pediatric ES tumor and surrounding healthy tissue.

5

Materials and Methods

Sample Selection
ES patients who gave informed consent for the use of their tissue at the time of surgery and underwent surgical resection between 2018 and 2022 were eligible for this study. Biopsies and sections of ES tissue samples with tumor and adjacent healthy tissue were selected by a sarcoma pathologist. Subsequently, all available corresponding formalin-fixed paraffin-embedded (FFPE) biopsy material and resection specimens were collected from the biobank of the Princess Maxima Center for Pediatric Oncology, The Netherlands. Ethical approval for collecting FFPE tissue and for the use of freshly excised tissue was acquired from the institutional review board of the Princess Maxima Center for Pediatric Oncology (PMCLAB2022.317). The study was conducted in accordance with the Declaration of Helsinki.

Biomarkers
Seven biomarkers were selected for IHC evaluation based on their potential for FGS in ES, as reported in the literature [23]. The biomarkers CD99, CXCR4, CD117, NPY-R-Y1, LINGO-1, and IGF-1R were based on a systematic review that selected promising targets for FGS in ES [23]. GD2 was added for its known overexpression on ES and the availability of a clinically targeted tracer [23,24,26].

Immunohistochemistry
FFPE biopsies from 13 ES patients, and 8 corresponding resection specimens with adjacent healthy tissue, were included in the IHC evaluation. All of these selected cases received preoperative chemotherapy as standard treatment at the Princess Maxima Center for Pediatric Oncology (Table 1). Sections from FFPE blocks having a 4 µm thickness were cut, mounted on pre-coated slides, and dried for at least 30 min at 70°C. For IGF-1R, sections were manually deparaffinized in xylene for 15 min, rehydrated in a series of 100%, 50%, and 25% ethanol dilutions, and rinsed in demineralized water. Endogenous peroxidase was blocked with 0.3% hydrogen peroxide in demineralized water for 20 min. Antigen retrieval was performed using the PT Link (Dako, Glostrup, Denmark; Appendix A), and two washing steps of 5 min in phosphate buffered saline (PBS) were performed. Sections were incubated in a humidified room with 150 µL primary antibody using predetermined solutions based on test stainings on control tissue (Appendix A). Afterwards, slides were washed three times in PBS for 5 min and incubated with the appropriate secondary goat-anti rabbit HRP conjugate (catalog number K4003, Agilent Technologies, Santa Clara, CA, USA), followed by an additional washing step. Staining was visualized through incubation with 3,3-diaminobenzidine tetrahydrochloride solution (DAB, K3468, Agilent Technologies, Inc., Santa Clara, CA, USA) for 10 min at room temperature. For the other biomarkers, deparaffinization and IHC stains were performed with an automated BOND-RX system (Leica Microsystems, Wetzlar, Germany). Antigen retrieval was performed by boiling the sections in TRIS/EDTA (BOND Epitope Retrieval Solution 2, pH9; Leica Biosystems, Wetzlar, Germany) for 15 min for CXCR4, GD2, and LINGO-1, for 20 min for CD99 and CD117, and for 30 min for NPY-R-Y1. Primary and secondary antibodies used for IHC evaluation

were selected based on the literature (Appendix A). Endogenous peroxidase was blocked with 0.3% hydrogen peroxide in demineralized water for 5 min and the sections were incubated for 15 min at RT with the primary antibodies, except for LINGO-1 which was incubated for 30 min at RT. The sections were then incubated for 8 min with a post primary rabbit anti-mouse linker followed by incubation for 8 min with anti-rabbit horseradish-peroxidase-labeled polymer. After incubation for 10 min with diaminobenzidine, all slides were counterstained for 5 min with hematoxylin (BOND Polymer Refine Detection Kit; Leica Biosystems), dehydrated, cleared, and mounted. On each slide a positive and negative control tissue was included (identified with the human protein atlas; Appendix A) [28]. Stained sections were digitalized with the Aperio Scanner (Leica Biosystems, Wetzlar, Germany) and viewed with ImageScope Software (version 12.4.6, Aperio ePathology, Leica).

Table 1. Ewing sarcoma patient and tumor characteristics.

Patient	Gender	Age *	Preoperative Therapy	% Vital Tumor in Resection Specimen	cTNM
1	Female	13	VIDE	30%	cT1N0M0
2	Female	16	VIDE, Melphalan/Treosulfan, Irinotecan/ Temozolomide	N.A.	cTxN0M0
3	Male	14	VIDE, Dactinomycin, Melphalan/ Treosulfan	40%	cT2N1M1
4	Female	2	VIDE, VAI	N.A.	cT1N0M1
5	Male	5	VIDE, VAI	40%	cT1N0M0
6	Male	14	VIDE, VAC, Melphalan/Treosulfan	40%	cT2N1M0
7	Male	6	VIDE, VAI, Busulfan/Melphalan	80%	cT1N0M0
8	Male	5	Cyclofosfamide/Topotecan, Tremozolamide/Irinotecan, Treosulfan/ Melphalan, VIDE, VAI, Vinorelbine	N.A.	cT2N0M1
9	Male	6	VIDE, VAI	N.A.	cT2N0M0
10	Female	8	VIDE, Treosulfan/Melphalan	40%	cT2N1M0
11	Female	18	VIDE	N.A.	cT2N0M0
12	Male	16	VIDE, VAI, Treosulfan/Melphalan	50%	cT2N0M0
13	Male	14	VIDE, Treosulfan/Melphalan, VAC, Cyclofosfamide/topotecan	40%	cT2N0M1

* Age at diagnosis in years. Abbreviations: VIDE = Vincristine Ifosfamide Doxorubicin Etoposide; VAI = Vincristine Dactinomycin Ifosfamide; VAC = Vincristine, Doxorubicin, Cyclophosphamide; N.A. = Not applicable, since only biopsy material but no resection specimen was available.

Immunohistochemistry Scoring Method

IHC scoring was performed by a pathologist specialized in sarcomas. For assessment, an ordinal scale was used based on the percentage of stained cells and staining intensity (number of stained cells: $0 \leq 10\%$; $1 = 10–25\%$; $2 = 25–50\%$; $3 = 50–75\%$; and $4 \geq 75\%$; staining intensity:

0 = no staining; 1 = mild; 2 = moderate; 3 = strong). The two scores were then multiplied to create the final immunoreactive score (IRS) with a range from 0 to 12. The final expression score was the IRS subdivided into 3 categories (0–3 = weak expression; 4–8 = moderate expression, and 9–12 = strong expression). An example of the immunohistochemical scoring method in biopsies of ES tumors is depicted in Figure 1. Biomarkers with strong expression in the tumor and weak expression in adjacent healthy tissue were considered most suitable for FGS.
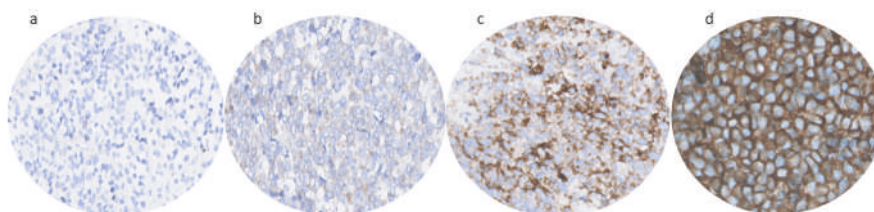

Figure 1. *Example of immunohistochemical scoring method in biopsies of ES tumors. An ordinal scale was used based on the percentage of stained cells and staining intensity. The two scores were then multiplied to create the final immunoreactive score (IRS); (a) ≤ 10% stained cells (=score 0) and no expression intensity (=score 0) creates an IRS of 0 (IGF-1R); (b) = 10–25% stained cells (=score 1) and mild intensity (=score 1) creates an IRS of 1 (CXCR4); (c) ≥ 75% stained cells (=score 4) and moderate intensity (=score 2) creates an IRS of 8 (CD117); (d) ≥ 75% stained cells (=score 4) and strong intensity (=score 3) creates an IRS of 12 (CD99).*

Human Cancer Lines

ES cell lines A673 and RD-ES were selected as cells to assess binding of the tracers, while neuroblastoma cell lines SK-N-BE and KCNR, and breast cancer organoid lines BC27T and BC62T served as positive or negative controls for the selected targets (Table 2). Controls were selected based on RNA expression for the targets of interest (Appendix B). ES cell lines were obtained from American Type Culture Collection (ATCC, Manassas, USA), neuroblastoma cell lines from cryopreservation at the Princess Maxima Center, The Netherlands, and breast cancer organoid lines were developed, with informed consent from all donors at Hubrecht Organoid Technology, Utrecht, The Netherlands. Short tandem repeat (STR) profiling was performed to ensure quality and integrity of the ES cell lines. A673 cells were cultured in Dulbecco's modified Eagle's medium (DMEM) containing high glucose, glutamine, phenol red, and sodium pyruvate (Gibco, Invitrogen, Carlsbad, USA), 10% Fetal Bovine Serum (FBS; Hyclone, Thermo Scientific, Rockford, IL, USA), and penicillin/streptomycin (PS, both 100 IU/mL; Invitrogen). RD-ES cells were cultured in RPMI-1640 medium (Invitrogen) with 10% FBS and PS. SK-N-BE and KCNR cells were cultured in DMEM4x medium, which consists of DMEM (Invitrogen) supplemented with high glucose, 2 mM L-glutamine (Invitrogen), Minimum Essential Medium (MEM) non-essential amino acids (Invitrogen), 10% FBS and PS. BC27T and 62T cells were received in 12-well suspension plates (Greiner Bio-One GmbH, Firckenhausen, Germany) seeded in basement membrane extract (Cultrex BME, R&D Systems, Minneapolis, USA) just before the experiment was conducted [29,30]. Absence of mycoplasma in all cell

lines was confirmed using polymerase chain reaction. Cells were grown to 90% confluence in a humidified incubator at 37 °C (5% CO2) and detached with trypLE/EDTA (Invitrogen).

Table 2. Human cancer lines selected as tested and positive and negative control lines for the three selected targets, CD99, CD117, and GD2.

Target	Tested Ewing Sarcoma Cell Lines	Positive Control	Negative Control
CD99	A673 and RD-ES	BC62T	SK-N-BE
CD117	A673 and RD-ES	BC62T	BC27T
GD2	A673 and RD-ES	KCNR	BC27T

Antibodies Used for Flow Cytometry and Immunofluorescence Microscopy

Mouse IgG2a kappa monoclonal CD99 antibody (3B2/TA8) labeled with FITC and mouse IgG1 kappa monoclonal CD117 antibody (YB5.B8) labeled with PE were bought from Invitrogen. Mouse IgG2a kappa isotype control (eBM2a) labeled with FITC and mouse IgG1 kappa isotype control (P3.6.2.8.1) labeled with PE (Invitrogen) were recommended (by Invitrogen) and used as isotype controls. A chimeric monoclonal antibody against GD2 (Dinutuximab-beta, Qarziba, Laupheim, Germany) was conjugated to Alexa Fluor™ NHS ester 647 (Invitrogen). The Alexa Fluor (AF) NHS esters were dissolved in anhydrous dimethylsulfoxide (DMSO) (Invitrogen, D12345, Carlsbad, USA), and the reaction was carried out in 0.5 M Hepes buffer (15630–056, Gibco, Carlsbad, USA), pH 8.0, at room temperature for two hours. 0.1 M Tris was added to quench the reaction. The antibody-fluorophore conjugate was purified twice using a gel filtration column (Zeba Spin Desalting Column, 40 MWKO, Thermo Fisher Scientific, Waltham, USA). The degree of labeling (DoL) was calculated by measuring the protein concentration and fluorophore concentration using the NanoDrop™ One (Thermo Fisher Scientific, Waltham, USA). A DoL around 1–1.5 was considered successful as this is generally recommended for FGS probes [31].

Flow Cytometry

After detachment, cells were adjusted to 0.3×10^6 viable cells/well in FACS buffer (10% FBS, ThermoFisher) in a 96-well U-bottom plate (Invitrogen). Cells were incubated on ice for 45–60 min, avoiding light exposure, with 5 μg/mL 3B2/TA8-FITC, 5 μg/mL YB5.B8-PE, and 1 μg/mL Dinutuximab-AF647 in FACS buffer containing live/dead staining (LIVE/DEAD™ Fixable Near-IR Dead Cell Stain, ThermoFisher). Apart from negative control cell lines, isotype controls (5 μg/mL eBM2a-FITC and 5 μg/mL P3.6.2.8.2-PE) were added to the cells in separate wells to assess binding specificity. Next, cells were washed twice, and flow cytometry measurements were performed using the CytoFLEX LX (Beckman Coulter, Brea, USA) using the lasers and detectors to measure FITC, PE, AF647, and the live/dead staining (respectively 525/40, 585/42, 695/40, and 763/43). Analysis was performed using FlowJo software (TreeStar, Woodburn, USA).

Immunofluorescence Microscopy

After detachment, cells were adjusted to 0.3×10^6 viable cells/well in culture medium in a Greiner 96-well glass-bottom plate (Sigma-Aldrich, St. Louis, USA). Cells were incubated for

45–60 min in a humidified incubator at 37°C and 5% CO_2 with similar antibody concentrations as described for flow cytometry. In addition, a cell membrane staining CellBrite 450 (Biotium, Fremont, USA) was added 1:1000 simultaneously with the antibodies. Next, imaging was performed with the SP8 Leica microscope (Leica Microsystems, Wetzlar, Germany) using a HC PL APO 10X/0.40 CS2 objective with zoom set to 1.0 and digitized in 16 bits per voxel. The 488 nm, 561 nm, and 633 nm lasers were used for FITC, PE, and AF647, respectively. For detection of every tracer, a separate photo-multiplier tube (PMT) detector was used with the minimum and maximum wavelengths set according to the reference spectra of FITC, PE, and AF647. Three-dimensional rendering was performed using Imaris x64 (10.0 Bitplane).

Topical Application and Imaging

Freshly resected tumor tissue and adjacent healthy (bone and muscle) tissue were derived from the proximal femur of a pediatric ES patient directly after surgery. A pathologist specialized in sarcoma, blinded for fluorescence, selected tissue samples from clinically relevant regions (with tumor and adjacent healthy tissues) based on visual inspection of the slides of the resection specimen. The acquired tissue was then cut into slices of approximately 0.5 cm × 0.5 cm × 0.2 cm. These tissues were immediately incubated for 45–60 min in a humidified incubator at 37°C and 5% CO_2 with CellBrite 450, 3B2/TA8-FITC, YB5.B8-PE, and Dinituximab-AF647 using the same concentrations as described for flow cytometry. Directly after incubation without any washing steps, multispectral imaging of the specimen was performed with the SP8 Leica microscope (Leica Microsystems, Wetzlar, Germany) using a HC PL APO 10X/0.40 CS2 objective with zoom set to 1.0 and digitized in 16 bits per voxel. Three-dimensional rendering was performed using Imaris x64 (10.0 Bitplane).

Statistical Analysis

Each biomarker's categorical IRS (0–3 = weak expression; 4–8 = moderate expression, and 9–12 = strong expression) was depicted with bar charts created by GraphPad Prism 9 (La Jolla, USA).

Results

Immunohistochemistry

In total, 13 patients (8 biopsies with corresponding post-chemotherapy resection specimen and 5 biopsies without) were included for the IHC evaluation. This cohort had a median age of 11 years (range: 2–19 years), most patients were male (n = 8/13; 62%), and all patients received preoperative chemotherapy (Table 1). IHC analysis showed high percentages of stained ES cells for CD99, CD117, and NPY-R-Y1, mostly with moderate/strong intensity, while expression on adjacent healthy tissue was limited (Figure 2). The tumor boundary was determined by a pathologist specialized in sarcoma using hematoxylin eosin (H&E) stained samples. The immunoreactive score was not utilized for differentiation between tumor and healthy tissues. Occasionally, false positive signals were observed in healthy tissue, posing

a risk of over-resection and potential loss of function. However, CD99 and CD117 showed relatively lower expression in healthy tissue compared to the tumor tissue. Despite some inter-tumor variability, both CD99 and CD117 were consistently expressed in both tumor biopsy and tumor resection specimens. For CD117, the average IRS score in post-chemotherapy resection specimen was lower compared to biopsies, which could mean that CD117 expression decreased after chemotherapy. For the other biomarkers, we did not observe this phenomenon as IRSs were comparable in the biopsy and corresponding resection specimen (Figure 3). For GD2 and LINGO-1, we could not establish a working IHC protocol for the acquired FFPE tissue.
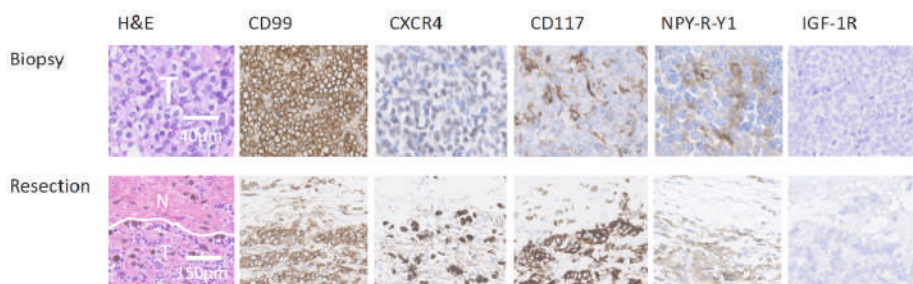
Figure 2. *Representative IHC staining of biopsy and corresponding post-chemotherapy resection specimen from an ES patient. The H&E staining shows tumor cells in biopsy material (T), and adjacent healthy "normal" tissue (N) as well as tumor tissue (T) in resection material. Overall, CD99, CD117, and NPY-R-Y1 showed high percentages of stained ES cells in biopsy and resection material, with moderate to strong intensity, while staining in adjacent healthy tissue was limited. In this case CXCR4 displayed a moderate percentage of stained cells with mild to strong intensity, while IGF-1R did not show any stained cells.*
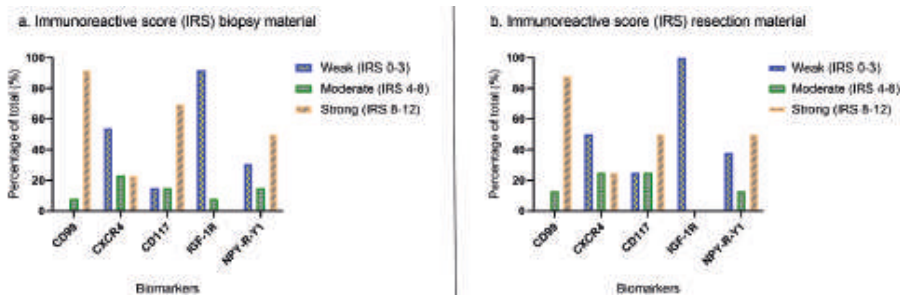
Figure 3. *Immunoreactive score (IRS) of the selected biomarkers divided into three categories; weak (IRS 0–3), moderate (IRS 4–8), and strong (IRS 8–12). Separate results are depicted for (a) biopsy material (n = 13) and (b) resection specimen (n = 8).*

Flow Cytometry and Immunofluorescence Microscopy

CD99 and CD117 were selected for cell line-based experiments based on their high IRS scores in ES tumor, but limited expression in adjacent healthy tissue. In addition, GD2 was investigated since an FGS tracer for this biomarker is in the developmental phase and previous literature reported relatively high GD2 expression (40–90%) in ES tissue [24-26]. First, binding

of anti-CD99 (3B2/TA8-FITC), anti-CD117 (Yb5.B8-PE), and anti-GD2 (Dinutuximab-AF647) was evaluated with flow cytometry. A673, RD-ES, BC62T, and SK-N-BE cells showed respectively high, high, moderate, and almost negative binding of anti-CD99 (Appendix C). A673, RD-ES, BC62T, and BC27T cells showed respectively low, moderate, moderate, and negative binding of anti-CD117 (Appendix C). A673, RD-ES, KCNR, and BC27T cells showed respectively low, moderate, high, and low binding of anti-GD2 (Appendix C). Next, immunofluorescence microscopy confirmed flow cytometry results; membranous binding of anti-CD99 and anti-CD117 was observed for all ES cells, while anti-GD2 only stained some ES cells (Figure 4).
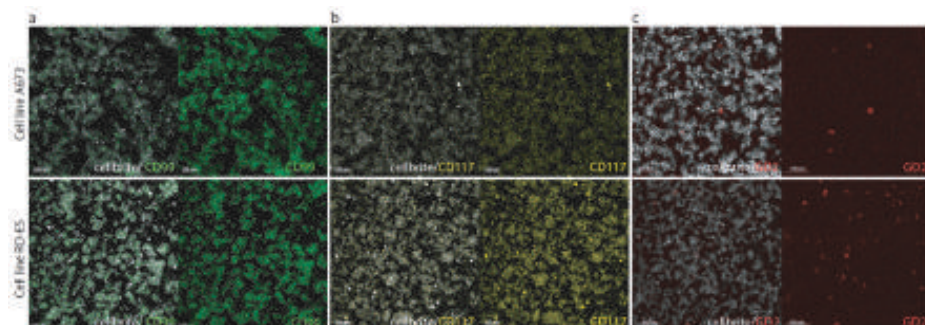
Figure 4. *Immunofluorescence analysis of (a) 3B2/TA8-FITC (anti-CD99); (b) Yb5.B8-PE (an-ti-CD117); and (c) Dinutuximab-AF647 (anti-GD2) binding to A673 and RD-ES cells. Anti-CD99, anti-CD117 and anti-GD2 are shown in green, yellow, and red, respectively. The cell membrane marker CellBrite 450 stained all cell membranes (white).*

Topical Application

Fresh tissue from a proximal femur resection specimen was collected directly after surgery (Figure 5). Tumor and adjacent healthy (bone and muscle) tissues were immediately incubated with CellBrite 450, anti-CD99, anti-CD117, and anti-GD2. Topical application of anti-CD99 and anti-GD2 on ES tumor showed fluorescence, while anti-CD117 did not. None of the tracers was fluorescent on neighboring healthy muscle or bone tissues (Figure 6).
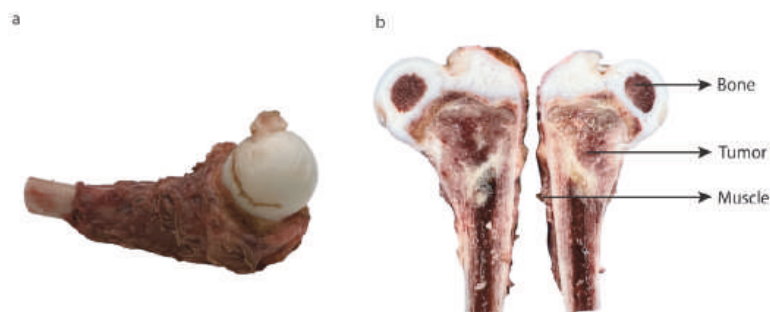
Figure 5. *Freshly resected ES: (a) left proximal femur of a 2-year-old child; (b) bisected specimen shows fresh tumor tissue with adjacent healthy bone and muscle (used for the topical application experiment).*
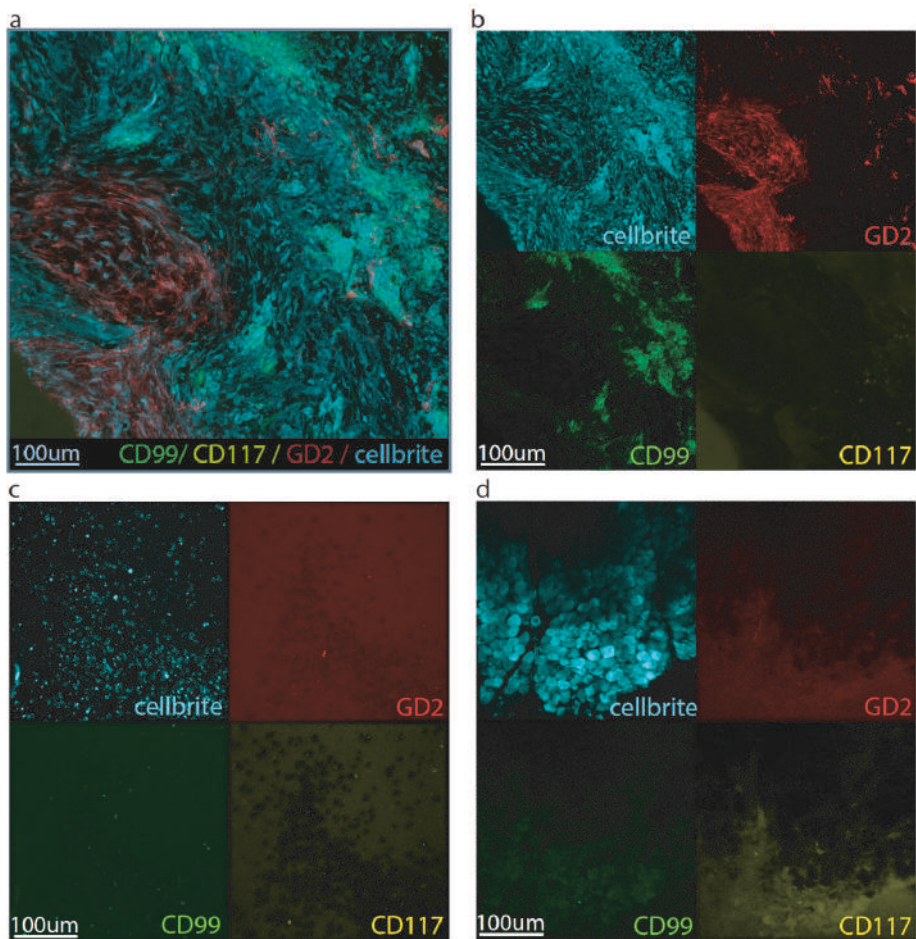
Figure 6. *Immunofluorescence evaluation of 3B2/TA8-FITC (anti-CD99, green), Yb5.B8-PE (an-ti-CD117, yellow), and Dinutuximab-AF647 (anti-GD2, red) binding to a freshly resected ES tumor (a, b) and adjacent healthy bone (c) and muscle (d) tissues ex vivo. Anti-CD99 and anti-GD2 showed fluorescent signal in the tumor explant, while anti-CD117 did not show fluorescent signal. No fluorescence was observed in adjacent healthy bone and muscle tissue. The cell membrane marker (CellBrite 450) clearly stained all cell membranes (cyan).*

5

Discussion

In this study, we first evaluated ES specific biomarkers on FFPE tumor and adjacent healthy tissue with IHC. Based on their IRS, CD99 and CD117 were considered the most promising targets for FGS in ES. In addition, GD2 was added as a promising biomarker based on previously reported high expression in ES and the exceptional availability of a clinical FGS tracer for pediatric patients (currently in clinical phase 1/2 trial for neuroblastoma) [26]. Next, flow cytometry and fluorescence microscopy experiments with fluorescent antibodies targeting CD99, CD117, and GD2 revealed, respectively, high, low/moderate, and low expression on living ES cells. Then, as proof-of-concept, an ex vivo topical application experiment was conducted on one freshly resected ES tumor and adjacent healthy tissue. Although not generalizable due to the small sample size, CD99 and GD2 targeting tracers showed fluorescent signal on the ES tumor, whereas anti-CD117 did not show fluorescence for this patient. Importantly for the intended application, none of the tracers showed fluorescence on adjacent healthy (bone and muscle) tissue.

We adhered to standard preclinical workup for the evaluation of biomarkers for targeted FGS. After the selection of potential targets by Bosma et al., we conducted IHC experiments including both healthy and malignant tissue [23]. While LINGO-1 and GD2 have demonstrated high expression in ES (40–91%), their expression in adjacent healthy tissue has not been characterized [24,32]. Unfortunately, we encountered difficulties in establishing a working IHC staining protocol for LINGO-1 and GD2 on FFPE tissue. GD2 is of particular interest due to the availability of a clinical tracer [26]. High GD2 expression has been reported in various pediatric tumor types, but inconsistencies in measured levels via IHC have been observed [24,26,33]. This discrepancy can be attributed to the solubility of GD2 in certain solvents, such as ethanol, which is required for FFPE tissue preparation [27,33]. Fresh frozen tissue could serve as an alternative, but flow cytometry on living cells also overcomes the limitations caused by sample processing [27,34]. Notably, Wingerter et al. employed flow cytometry to evaluate GD2 expression and, in line with our findings, reported low GD2 expression levels in the same commercially available ES cell lines (A673 and RD-ES) [27]. However, the percentage of GD2-positive cells in six primary (non-commercially available) ES cell lines ranged from low (1%) to high (98%) [27]. The heterogeneity in GD2 expression in ES cells could be attributed to the degree of tumor cell differentiation [28]. Therefore, GD2 expression might be specific to individual patients rather than tumor entities. Despite the low binding of anti-GD2 to ES cell lines A673 and RD-ES, as determined by flow cytometry and fluorescence microscopy, anti-GD2 exhibited a fluorescent signal in our topical application experiment. Together with the known heterogeneous GD2 expression in ES, this suggests that it should not be disregarded as a potential candidate for FGS.

We consider CD99 the most promising target for FGS in ES due to its consistent high tumor-specific expression demonstrated in both in vitro and ex vivo experiments. As emphasized in the introduction, the ex vivo topical application of a CD99-targeting tracer on resected

tumor specimens can serve as a practical initial approach for intraoperatively assessing tumor margins. This approach offers advantages such as bypassing the time-consuming and costly development of an intravenously administered tracer, while at the same time providing clinical benefits by aiding in intraoperative tumor margin assessment. Successful translation to IV use can be anticipated once ex vivo topical application consistently yields promising results, as demonstrated with EMI-137 targeting c-MET in penile squamous cell carcinoma [35]. However, multiple essential aspects need to be assessed before clinical translation of a targeted tracer, such as comprehensive evaluation of biodistribution, toxicology, determination of optimal dosage and safety, and subsequent registration as an approved drug. It is worth noting that fully humanized monoclonal antibodies and single-chain variable fragment (scFv) against CD99 are already available and have exhibited minimal toxicity to healthy peripheral blood cells [36]. Ideally, the smaller anti-CD99 scFv should be transformed into a clinical tracer by conjugation to a NIR fluorophore. This approach would enable the achievement of a high TBR within hours after IV administration, compared to days required for large-sized antibodies [16,36].

Ex vivo topical application experiments offer an additional advantage by enabling the simultaneous testing of multiple tracers when they are conjugated with fluorophores that have significantly different excitation and emission spectra. Considering tracers targeting CD117 and GD2 as potential alternatives to CD99, these could be included in the same trial. However, it is important to consider that the emission wavelength of the fluorophore may affect the penetration depth of the fluorescent signal and the level of autofluorescence. If the objective is to test only one tracer per patient using topical application, or when multiple tracers become available for IV use in the future, biopsies can be utilized to select the most promising patient-specific tracer. Our findings indicate that, except for CD117, the expression of the tested tracers for ES was relatively similar between biopsy and resection specimens. In cases where single tracers are unable to fully cover the tumor with fluorescence due to intratumoral heterogeneity, a possible solution would be to evaluate a combination of tracers [37].

This study has some limitations that should be acknowledged. Firstly, the rarity of ES resulted in a limited availability of FFPE samples. Additionally, despite our efforts, we were unable to establish a working ICH protocol for LINGO-1 and GD2 on the available FFPE tissue. In addition, comparing IHC stainings for the purpose of FGS should be undertaken with caution due to the variability of results depending on decalcification methods and the type of antibodies, dilutions, epitopes, clones, or staining protocols used [38]. Moreover, the IRS scoring can be seen as subjective due to intra- and inter-observer variability, and objective scoring methods using semi-automated imaging software such as ImageJ or QuPath could improve the quality of this study [39-41]. However, evaluation with QuPath required a test and validation set, which was unfeasible for our small cohort of ES samples. Additionally, scoring of our pathologist specialized in sarcoma (working in a tertiary referral center) is currently seen as the gold standard. Therefore, no further objective scoring was performed. Although we focused on the most promising targets, namely CD99, CD117, and GD2, we also found NPY-R-Y1 to be of interest and worthy of further investigation. Furthermore, the topical application was performed on

only one freshly resected ES bone specimen. The applicability for FGS of ES-based tracers has to be confirmed in a larger cohort of pediatric ES patients, preferably in a multicenter setting. This study was performed to showcase the proof-of-principle, and to encourage future studies to conduct topical application experiments with a large cohort of ES patients. Yet, the feasibility of targeted FGS in a large number of bone and soft tissue ES patients, as well as the possible applicability in non-Ewing SRCT, remains to be investigated. Ideally, FGS would be able to identify both bone and soft tissue margins. However, mainly the soft tissue expansion and the periosteal or subperiosteal expansion would be useful for visualization with FGS, as the osseous tumor margin could also be navigated with X-ray or computer-assisted surgery [42]. Nonetheless, with promising results obtained from IHC, in vitro experiments using two patient-derived ES cell lines (A673 and RD-ES), and a proof-of-principle experiment conducted on freshly resected ES tissue, we believe that this study demonstrates the potential of FGS for improving ES treatment in the future.

Conclusions

Based on the immunohistochemical evaluation, preclinical in vitro experiments, and ex vivo topical application experiment on freshly resected Ewing sarcoma and adjacent healthy tissue, our findings suggest that CD99-targeting tracers hold promise for fluorescence-guided surgery of Ewing sarcoma. Furthermore, tracers targeting CD117 and GD2 show potential as alternative options. As a next step towards the clinical implementation of intravenous tracers for targeted fluorescence-guided surgery in Ewing sarcoma, we recommend conducting an ex vivo topical application study on a large cohort of Ewing sarcoma patients. This study would provide valuable insights and pave the way for further advancements in the field of Ewing sarcoma treatment.

References

1. Esiashvili, N.; Goodman, M.; Marcus, R.B., Jr. Changes in incidence and survival of Ewing sarcoma patients over the past 3 decades: Surveillance Epidemiology and End Results data. *J Pediatr Hematol Oncol* **2008**, *30*, 425-430, doi:10.1097/MPH.0b013e31816e22f3.

2. Zöllner, S.K.; Amatruda, J.F.; Bauer, S.; Collaud, S.; de Álava, E.; DuBois, S.G.; Hardes, J.; Hartmann, W.; Kovar, H.; Metzler, M., et al. Ewing Sarcoma-Diagnosis, Treatment, Clinical Challenges and Future Perspectives. *J Clin Med* **2021**, *10*, doi:10.3390/jcm10081685.

3. Damron, T.A.; Ward, W.G.; Stewart, A. Osteosarcoma, chondrosarcoma, and Ewing's sarcoma: National Cancer Data Base Report. *Clin Orthop Relat Res* **2007**, *459*, 40-47, doi:10.1097/BLO.0b013e318059b8c9.

4. Daniel, A., Jr.; Ullah, E.; Wahab, S.; Kumar, V., Jr. Relevance of MRI in prediction of malignancy of musculoskeletal system--a prospective evaluation. *BMC Musculoskelet Disord* **2009**, *10*, 125, doi:10.1186/1471-2474-10-125.

5. Ulaner, G.; Hwang, S.; Lefkowitz, R.A.; Landa, J.; Panicek, D.M. Musculoskeletal tumors and tumor-like conditions: common and avoidable pitfalls at imaging in patients with known or suspected cancer: Part A: benign conditions that may mimic malignancy. *Int Orthop* **2013**, *37*, 871-876, doi:10.1007/s00264-013-1823-7.

6. Anderton, J.; Moroz, V.; Marec-Bérard, P.; Gaspar, N.; Laurence, V.; Martín-Broto, J.; Sastre, A.; Gelderblom, H.; Owens, C.; Kaiser, S., et al. International randomised controlled trial for the treatment of newly diagnosed EWING sarcoma family of tumours - EURO EWING 2012 Protocol. *Trials* **2020**, *21*, 96, doi:10.1186/s13063-019-4026-8.

7. Kreyer, J.; Ranft, A.; Timmermann, B.; Juergens, H.; Jung, S.; Wiebe, K.; Boelling, T.; Schuck, A.; Vieth, V.; Streitbuerger, A., et al. Impact of the Interdisciplinary Tumor Board of the Cooperative Ewing Sarcoma Study Group on local therapy and overall survival of Ewing sarcoma patients after induction therapy. *Pediatr Blood Cancer* **2018**, *65*, e27384, doi:10.1002/pbc.27384.

8. Bacci, G.; Longhi, A.; Briccoli, A.; Bertoni, F.; Versari, M.; Picci, P. The role of surgical margins in treatment of Ewing's sarcoma family tumors: experience of a single institution with 512 patients treated with adjuvant and neoadjuvant chemotherapy. *Int J Radiat Oncol Biol Phys* **2006**, *65*, 766-772, doi:10.1016/j.ijrobp.2006.01.019.

9. Ozaki, T.; Hillmann, A.; Hoffmann, C.; Rübe, C.; Blasius, S.; Dunst, J.; Jürgens, H.; Winkelmann, W. Significance of surgical margin on the prognosis of patients with Ewing's sarcoma. A report from the Cooperative Ewing's Sarcoma Study. *Cancer* **1996**, *78*, 892-900, doi:10.1002/(sici)1097-0142(19960815)78:4<892::Aid-cncr29>3.0.Co;2-p.

10. Sluga, M.; Windhager, R.; Lang, S.; Heinzl, H.; Krepler, P.; Mittermayer, F.; Dominkus, M.; Zoubek, A.; Kotz, R. The role of surgery and resection margins in the treatment of Ewing's sarcoma. *Clin Orthop Relat Res* **2001**, 10.1097/00003086-200111000-00051, 394-399, doi:10.1097/00003086-200111000-00051.

11. Dunst, J.; Schuck, A. Role of radiotherapy in Ewing tumors. *Pediatr Blood Cancer* **2004**, *42*, 465-470, doi:10.1002/pbc.10446.

12. Hamilton, S.N.; Carlson, R.; Hasan, H.; Rassekh, S.R.; Goddard, K. Long-term Outcomes and Complications in Pediatric Ewing Sarcoma. *Am J Clin Oncol* **2017**, *40*, 423-428, doi:10.1097/coc.0000000000000176.

13. Paulino, A.C. Late effects of radiotherapy for pediatric extremity sarcomas. *Int J Radiat Oncol Biol Phys* **2004**, *60*, 265-274, doi:10.1016/j.ijrobp.2004.02.001.

14. Foulon, S.; Brennan, B.; Gaspar, N.; Dirksen, U.; Jeys, L.; Cassoni, A.; Claude, L.; Seddon, B.; Marec-Berard, P.; Whelan, J., et al. Can postoperative radiotherapy be omitted in localised standard-risk Ewing sarcoma? An observational study of the Euro-E.W.I.N.G group. *Eur J Cancer* **2016**, *61*, 128-136, doi:10.1016/j.ejca.2016.03.075.

5

15. Vahrmeijer, A.L.; Hutteman, M.; van der Vorst, J.R.; van de Velde, C.J.; Frangioni, J.V. Image-guided cancer surgery using near-infrared fluorescence. *Nat Rev Clin Oncol* **2013**, *10*, 507-518, doi:10.1038/nrclinonc.2013.123.

16. Rijs, Z.; Jeremiasse, B.; Shifai, N.; Gelderblom, H.; Sier, C.F.M.; Vahrmeijer, A.L.; van Leeuwen, F.W.B.; van der Steeg, A.F.W.; van de Sande, M.A.J. Introducing Fluorescence-Guided Surgery for Pediatric Ewing, Osteo-, and Rhabdomyosarcomas: A Literature Review. *Biomedicines* **2021**, *9*, doi:10.3390/biomedicines9101388.

17. de Valk, K.S.; Deken, M.M.; Schaap, D.P.; Meijer, R.P.; Boogerd, L.S.; Hoogstins, C.E.; van der Valk, M.J.; Kamerling, I.M.; Bhairosingh, S.S.; Framery, B., et al. Dose-Finding Study of a CEA-Targeting Agent, SGM-101, for Intraoperative Fluorescence Imaging of Colorectal Cancer. *Ann Surg Oncol* **2021**, *28*, 1832-1844, doi:10.1245/s10434-020-09069-2.

18. Hernot, S.; van Manen, L.; Debie, P.; Mieog, J.S.D.; Vahrmeijer, A.L. Latest developments in molecular tracers for fluorescence image-guided cancer surgery. *Lancet Oncol* **2019**, *20*, e354-e367, doi:10.1016/s1470-2045(19)30317-1.

19. Hoogstins, C.E.; Tummers, Q.R.; Gaarenstroom, K.N.; de Kroon, C.D.; Trimbos, J.B.; Bosse, T.; Smit, V.T.; Vuyk, J.; van de Velde, C.J.; Cohen, A.F., et al. A Novel Tumor-Specific Agent for Intraoperative Near-Infrared Fluorescence Imaging: A Translational Study in Healthy Volunteers and Patients with Ovarian Cancer. *Clin Cancer Res* **2016**, *22*, 2929-2938, doi:10.1158/1078-0432.Ccr-15-2640.

20. Meijer, R.P.J.; de Valk, K.S.; Deken, M.M.; Boogerd, L.S.F.; Hoogstins, C.E.S.; Bhairosingh, S.S.; Swijnenburg, R.J.; Bonsing, B.A.; Framery, B.; Fariña Sarasqueta, A., et al. Intraoperative detection of colorectal and pancreatic liver metastases using SGM-101, a fluorescent antibody targeting CEA. *Eur J Surg Oncol* **2021**, *47*, 667-673, doi:10.1016/j.ejso.2020.10.034.

21. Steinkamp, P.J.; Pranger, B.K.; Li, M.F.; Linssen, M.D.; Voskuil, F.J.; Been, L.B.; van Leeuwen, B.L.; Suurmeijer, A.J.H.; Nagengast, W.B.; Kruijff, S., et al. Fluorescence-Guided Visualization of Soft-Tissue Sarcomas by Targeting Vascular Endothelial Growth Factor A: A Phase 1 Single-Center Clinical Trial. *J Nucl Med* **2021**, *62*, 342-347, doi:10.2967/jnumed.120.245696.

22. Barth, C.W.; Gibbs, S.L. Fluorescence Image-Guided Surgery - a Perspective on Contrast Agent Development. *Proc SPIE Int Soc Opt Eng* **2020**, *11222*, doi:10.1117/12.2545292.

23. Bosma, S.E.; van Driel, P.B.; Hogendoorn, P.C.; Dijkstra, P.S.; Sier, C.F. Introducing fluorescence guided surgery into orthopedic oncology: A systematic review of candidate protein targets for Ewing sarcoma. *J Surg Oncol* **2018**, *118*, 906-914, doi:10.1002/jso.25224.

24. Kailayangiri, S.; Altvater, B.; Meltzer, J.; Pscherer, S.; Luecke, A.; Dierkes, C.; Titze, U.; Leuchte, K.; Landmeier, S.; Hotfilder, M., et al. The ganglioside antigen G(D2) is surface-expressed in Ewing sarcoma and allows for MHC-independent immune targeting. *Br J Cancer* **2012**, *106*, 1123-1133, doi:10.1038/bjc.2012.57.

25. Spasov, N.J.; Dombrowski, F.; Lode, H.N.; Spasova, M.; Ivanova, L.; Mumdjiev, I.; Burnusuzov, H.; Siebert, N. First-line Anti-GD2 Therapy Combined With Consolidation Chemotherapy in 3 Patients With Newly Diagnosed Metastatic Ewing Sarcoma or Ewing-like Sarcoma. *J Pediatr Hematol Oncol* **2022**, *44*, e948-e953, doi:10.1097/mph.0000000000002488.

26. Wellens, L.M.; Deken, M.M.; Sier, C.F.M.; Johnson, H.R.; de la Jara Ortiz, F.; Bhairosingh, S.S.; Houvast, R.D.; Kholosy, W.M.; Baart, V.M.; Pieters, A., et al. Anti-GD2-IRDye800CW as a targeted probe for fluorescence-guided surgery in neuroblastoma. *Sci Rep* **2020**, *10*, 17667, doi:10.1038/s41598-020-74464-4.

27. Wingerter, A.; El Malki, K.; Sandhoff, R.; Seidmann, L.; Wagner, D.C.; Lehmann, N.; Vewinger, N.; Frauenknecht, K.B.M.; Sommer, C.J.; Traub, F., et al. Exploiting Gangliosides for the Therapy of Ewing's Sarcoma and H3K27M-Mutant Diffuse Midline Glioma. *Cancers (Basel)* **2021**, *13*, doi:10.3390/cancers13030520.

28. Human Protein Atlas. Availabe online: https://www.proteinatlas.org/ (accessed on 2 January 2023).

29. Dekkers, J.F.; van Vliet, E.J.; Sachs, N.; Rosenbluth, J.M.; Kopper, O.; Rebel, H.G.; Wehrens, E.J.; Piani, C.; Visvader, J.E.; Verissimo, C.S., et al. Long-term culture, genetic manipulation and xenotransplantation of human normal and breast cancer organoids. *Nat Protoc* **2021**, *16*, 1936-1965, doi:10.1038/s41596-020-00474-1.

30. Sachs, N.; de Ligt, J.; Kopper, O.; Gogola, E.; Bounova, G.; Weeber, F.; Balgobind, A.V.; Wind, K.; Gracanin, A.; Begthel, H., et al. A Living Biobank of Breast Cancer Organoids Captures Disease Heterogeneity. *Cell* **2018**, *172*, 373-386.e310, doi:10.1016/j.cell.2017.11.010.

31. Rijpkema, M.; Bos, D.L.; Cornelissen, A.S.; Franssen, G.M.; Goldenberg, D.M.; Oyen, W.J.; Boerman, O.C. Optimization of Dual-Labeled Antibodies for Targeted Intraoperative Imaging of Tumors. *Mol Imaging* **2015**, *14*, 348-355.

32. Town, J.; Pais, H.; Harrison, S.; Stead, L.F.; Bataille, C.; Bunjobpol, W.; Zhang, J.; Rabbitts, T.H. Exploring the surfaceome of Ewing sarcoma identifies a new and unique therapeutic target. *Proc Natl Acad Sci U S A* **2016**, *113*, 3603-3608, doi:10.1073/pnas.1521251113.

33. Sariola, H.; Terävä, H.; Rapola, J.; Saarinen, U.M. Cell-surface ganglioside GD2 in the immunohistochemical detection and differential diagnosis of neuroblastoma. *Am J Clin Pathol* **1991**, *96*, 248-252, doi:10.1093/ajcp/96.2.248.

34. Poon, V.I.; Roth, M.; Piperdi, S.; Geller, D.; Gill, J.; Rudzinski, E.R.; Hawkins, D.S.; Gorlick, R. Ganglioside GD2 expression is maintained upon recurrence in patients with osteosarcoma. *Clin Sarcoma Res* **2015**, *5*, 4, doi:10.1186/s13569-014-0020-9.

35. Vries, H.M.; Bekers, E.; van Oosterom, M.N.; Karakullukcu, M.B.; van, H.G.; Poel, D.; van Leeuwen, F.W.B.; Buckle, T.; Brouwer, O.R. c-MET Receptor-Targeted Fluorescence on the Road to Image-Guided Surgery in Penile Squamous Cell Carcinoma Patients. *J Nucl Med* **2022**, *63*, 51-56, doi:10.2967/jnumed.120.261864.

36. Romero, L.A.; Hattori, T.; Ali, M.A.E.; Ketavarapu, G.; Koide, A.; Park, C.Y.; Koide, S. High-valency Anti-CD99 Antibodies Toward the Treatment of T Cell Acute Lymphoblastic Leukemia. *J Mol Biol* **2022**, *434*, 167402, doi:10.1016/j.jmb.2021.167402.

37. van Beurden, F.; van Willigen, D.M.; Vojnovic, B.; van Oosterom, M.N.; Brouwer, O.R.; der Poel, H.G.V.; Kobayashi, H.; van Leeuwen, F.W.B.; Buckle, T. Multi-Wavelength Fluorescence in Image-Guided Surgery, Clinical Feasibility and Future Perspectives. *Mol Imaging* **2020**, *19*, 1536012120962333, doi:10.1177/1536012120962333.

38. Kersting, C.; Packeisen, J.; Leidinger, B.; Brandt, B.; von Wasielewski, R.; Winkelmann, W.; van Diest, P.J.; Gosheger, G.; Buerger, H. Pitfalls in immunohistochemical assessment of EGFR expression in soft tissue sarcomas. *J Clin Pathol* **2006**, *59*, 585-590, doi:10.1136/jcp.2005.028373.

39. Adams, E.J.; Green, J.A.; Clark, A.H.; Youngson, J.H. Comparison of different scoring systems for immunohistochemical staining. *J Clin Pathol* **1999**, *52*, 75-77, doi:10.1136/jcp.52.1.75.

40. Bankhead, P.; Loughrey, M.B.; Fernández, J.A.; Dombrowski, Y.; McArt, D.G.; Dunne, P.D.; McQuaid, S.; Gray, R.T.; Murray, L.J.; Coleman, H.G., et al. QuPath: Open source software for digital pathology image analysis. *Sci Rep* **2017**, *7*, 16878, doi:10.1038/s41598-017-17204-5.

41. Rijs, Z.; Belt, E.; Kalisvaart, G.M.; Sier, C.F.M.; Kuppen, P.J.K.; Cleven, A.H.G.; Vahrmeijer, A.L.; van de Sande, M.A.J.; van Driel, P. Immunohistochemical Evaluation of Candidate Biomarkers for Fluorescence-Guided Surgery of Myxofibrosarcoma Using an Objective Scoring Method. *Biomedicines* **2023**, *11*, doi:10.3390/biomedicines11030982.

42. Deng, Z.; Zhang, Q.; Hao, L.; Ding, Y.; Niu, X.; Liu, W. Accuracy of bony resection under computer-assisted navigation for bone sarcomas around the knee. *World J Surg Oncol* **2023**, *21*, 187, doi:10.1186/s12957-023-03071-0.

5

Appendix A.

Table appendix A. Antibodies used for immunohistochemical evaluation.

Antigen	Source	Clone	Manufacturer	Positive Control	Negative Control	Dilution	Retrieval Buffer
CD99	Rabbit monoclonal	CB1	Leica	Pancreas, tonsil, liver, and colon	None	1:40	pH high (Tris/EDTA)
CD117	Rabbit monoclonal	EP10	Leica	GIST, colon, skin	Liver	Ready to use	pH high (Tris/EDTA)
CXCR4	Mouse monoclonal	EP394	Cell Marque	Thymus, Hodgkin lymphoma, bone marrow, tonsil, spleen	Liver	1:60	pH high (Tris/EDTA)
NPY-R-Y1	Rabbit polyclonal	AB183108	Abcam	Brain and breast carcinoma	Liver	1:80	pH high (Tris/EDTA)
LINGO-1	Rabbit polyclonal	HPA074653	Sigma	Brain	Liver	1:80	pH high (Tris/EDTA)
IGF-1R	Rabbit monoclonal	D38B1XP	Cell signaling technology	Placenta	Skin	1:300	pH low (citrate)
GD2	Mouse monoclonal	14.G2a and H3F8	BD Pharmingen and Creative Biolabs	Brain and neuroblastoma	Kidney and liver	1:100 and 1:1000	Various antigen retrieval buffers were tested

Abbreviations: CD99 = Cluster of Differentiation 99; CXCR4 = C-X-C chemokine receptor type 4 (also known as CD184); CD117 = Cluster of Differentiation 117 (also known as C-Kit); NPY-R-Y1 = Neuropeptide Y receptor type1; LINGO-1 = Leucine rich repeat, Immunoglobin-like domain-containing protein 1; IGF-1R = Insulin-like growth factor 1 receptor; GD2 = Disialoganglioside GD2; GIST = Gastrointestinal stromal tumor.

Appendix B.

Table appendix B. RNA expression data for CD99, CD117, and GD2.

	BC27T	BC62T
CD99	2245	3463
CD117	1	5301
GD2	1	993
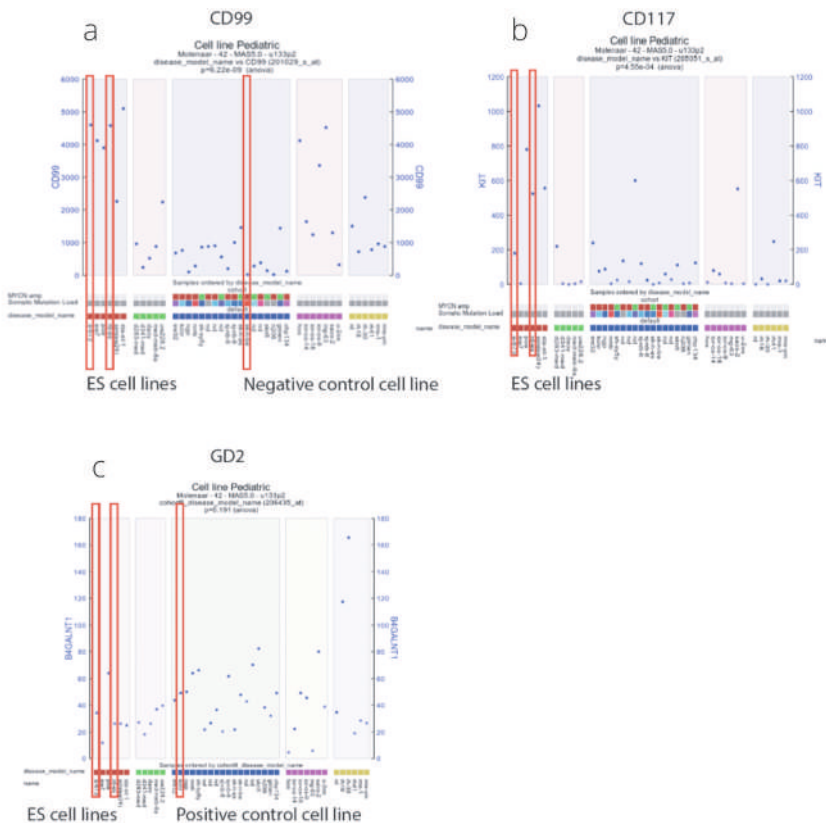
Appendix C.
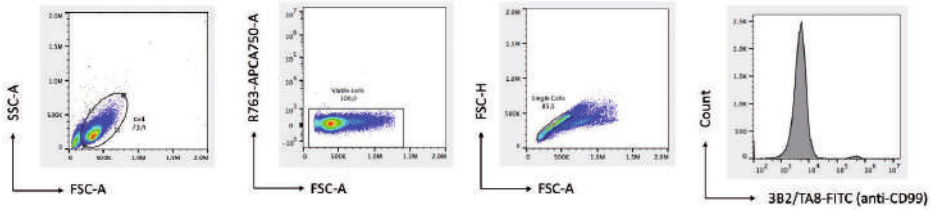
Figure C1. A standard FlowJo data processing protocol was used for the gating strategy during the assessment of CD99 expression. Briefly, unstained cells were used to distinguish cell debris from the cell population (a), viable cells were selected (b), and doublets were removed (c). Finally, the population is displayed on a histogram (d).
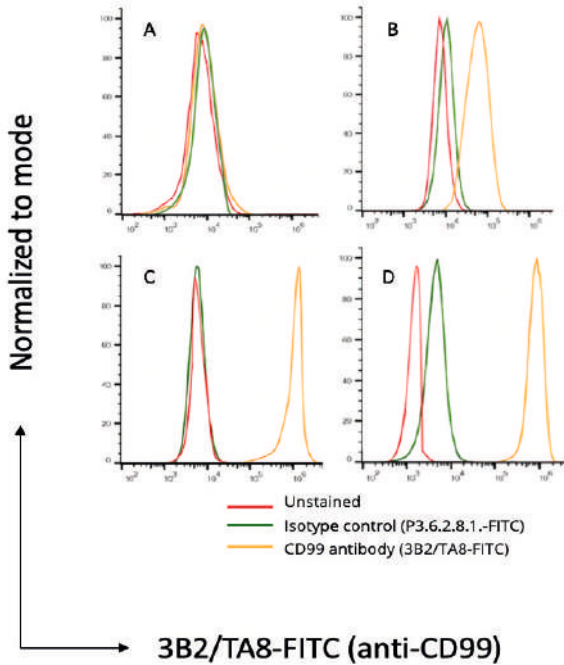
Figure C2. CD99 expression was assessed with flow cytometry on SK-N-BE (A: CD99 negative, Neuroblastoma), BC 62T (B: CD99 positive, Breast cancer organoid), and Ewing Sarcoma cell lines A673 and RD-ES (C and D). High CD99 expression was seen in both ES cell lines (C and D). Red line indicates the unstained cell line, green line indicates the cell line incubated with an isotype control, and orange line indicates the cell line incubated with the CD99 antibody.
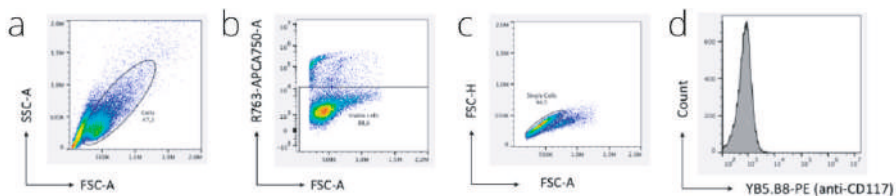
Figure C3. *A standard FlowJo data processing protocol was used for the gating strategy during the assessment of CD117 expression. Briefly, unstained cells were used to distinguish cell debris from the cell population (a), viable cells were selected (b), and doublets were removed (c). Finally, the population is displayed on a histogram (d).*
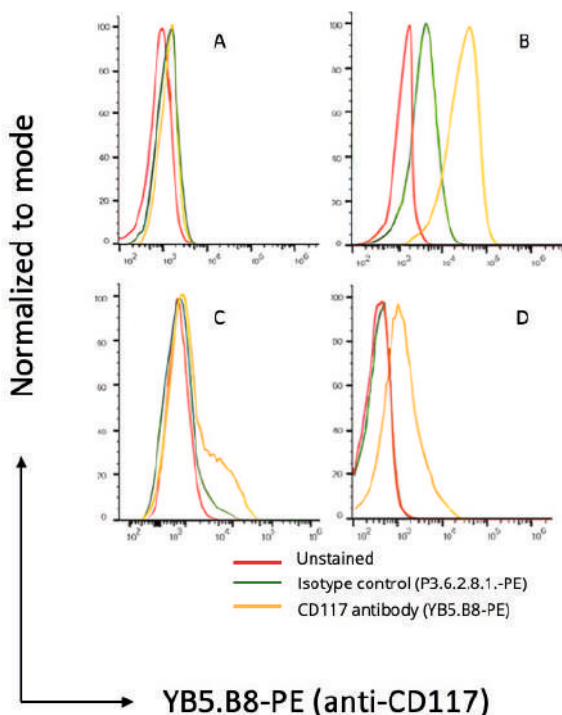
Figure C4. *CD117 expression was assessed with flow cytometry on BC 27T (A: CD117 negative, Breast cancer organoid), BC62T (B: CD117 positive, Breast cancer organoid), and Ewing Sarcoma cell lines A673 and RD-ES (C and D). Low/moderate CD117 expression was seen in ES cell lines (C and D). Red line indicates the unstained cell line, green line indicates the cell line incubated with an isotype control, and orange line indicates the cell line incubated with the CD117 antibody.*
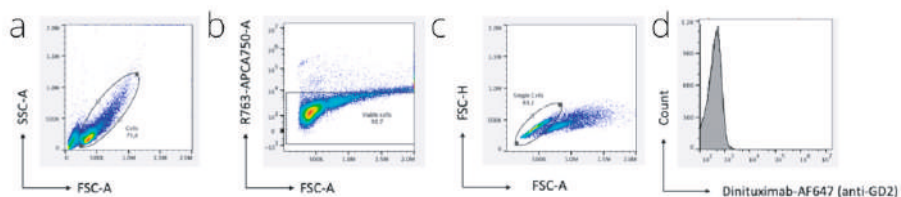
Figure C5. *A standard FlowJo data processing protocol was used for the gating strategy during the assessment of GD2 expression. Briefly, unstained cells were used to distinguish cell debris from the cell population (a), viable cells were selected (b), and doublets were removed (c). Finally, the population is displayed on a histogram (d).*
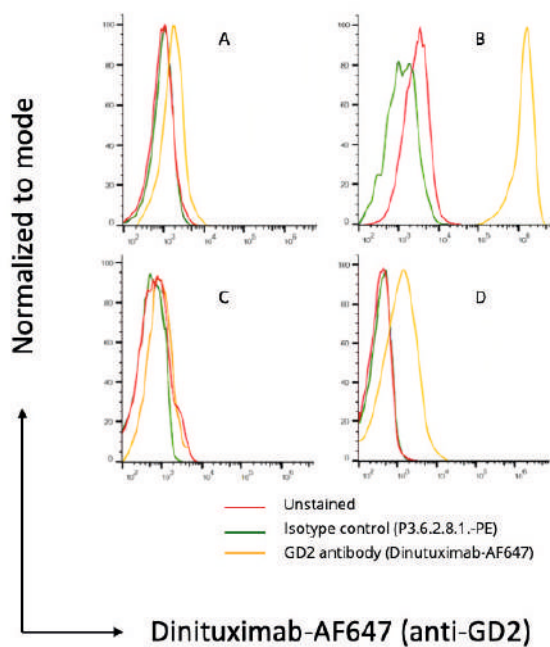
Figure C6. *GD2 expression was assessed on BC 27T (A: GD2 negative, Breast cancer organoid), KCNR (B: GD2 positive, Neuroblastoma), and Ewing Sarcoma cell lines A673 and RD-ES (C and D). Low/moderate GD2 expression was seen in ES cell lines (C and D). Red line indicates the unstained cell line, green line indicates the cell line incubated with an isotype control, and orange line indicates the cell line incubated with the GD2 antibody.*

5

PART II.

CARBON-FIBER IMPLANTS

6

COMPLICATIONS OF PATIENTS WITH BONE TUMORS TREATED WITH CARBON-FIBER PLATES: AN INTERNATIONAL MULTICENTER STUDY

Z. Rijs[1], A. Weekhout[1], S.A. Lozano-Calderon[2], O.Q. Groot[2], E. Berner[2], N. Merchan[2], C.M. Yeung[2], V. Oliveira[3], G. Bianchi[4], E. Staals[4], D. Lana[4], D. Donati[4], O. Segal[5], S. Marone[6], R. Piana[6], S. De Meo[6], P. Pellegrino[6], N. Ratto[6], C. Zoccali[7], M. Scorianz[8], C. Tomai[8], G. Scoccianti[8], D.A. Campanacci[8], L. Andreani[9], S. de Franco[9], M. Boffano[10], T. Cosker[11], V. Sethurajah[11], M.P. Pensado[12], I.B. Ruiz[12], E.H. Moreno[12], E.J. Ortiz-Cruz[12,13], M.A.J. van de Sande[1]

[1] Leiden University Medical Center, The Netherlands
[2] Massachusetts General Hospital | Harvard Medical School, United States of America
[3] Oporto University Hospital Center, Portugal
[4] Istituto Ortopedico Rizzoli, Italy
[5] Tel Aviv Sourasky Medical Center, Israel
[6] Centro Traumatologico Ortopedico Torino, Italy
[7] Regina Elena National Cancer Institute, Italy
[8] Azienda Ospedaliera Universitaria Careggi, Italy
[9] University Hospital of Pisa, Italy
[10] Regina Margherita Children's Hospital, Italy
[11] Nuffield Orthopaedic Centre, England
[12] La Paz University Hospital, Spain
[13] MD Anderson Cancer Center, Spain

Abstract

Carbon-fiber (CF) plates are a promising alternative to metal plates. However, reported experience in orthopedic oncology remains limited. The aim of this study was to identify complications of patients with bone tumors treated with CF plates. Between February 2015 and May 2021, 13 centers retrospectively registered patients with bone tumors that were reconstructed using CF plates. Complications were identified, and timing and etiology of complications were noted. Similar complications were tabulated and classified based on mechanical, non-mechanical and pediatric complications. Mechanical complications included: (1) aseptic loosening or graft-host non-union, and (2) structural complications. Non-mechanical complications included: (3) soft tissue complications, (4) infection and (5) tumor progression. Specific pediatric complications included (6) growth arrest resulting in longitudinal or angular deformity. Ninety-six patients were included with a median follow-up time of 35 months. In total, 22 (23%) patients had complications. Mechanical complications included: 1 (1%) aseptic loosening, 2 (2%) non-unions, and 7 (7%) structural complications. Nonmechanical complications included 1 (1%) soft tissue complication, 4 (4%) infections and 5 (5%) tumor progressions. Pediatric complications occurred in 2 (2%) patients. This study suggests CF plates are safe to use in demanding reconstructions after bone tumor resections, presenting a seemingly low complication profile.

Introduction

Metal has been the foundation of orthopedic implants. Advantages include high strength and stiffness, ease of machining, and low cost [1]. Many metals also offer good ductility allowing them to be manually bent intraoperatively to match the surface anatomy of the bone or reconstruction [1,2]. However, a major disadvantage for the oncological patient is its radiodensity which causes metal artifacts on radiographic imaging. This precludes accurate radiographic visualization for oncological follow-up or bone union and impedes precise radiation planning [3,4]. Besides, the stiffness of metal (200 gigapascal [GPa] for stainless steel and 110 GPa for titanium) is much higher than the human cortical bone (12 GPa) which may shield the underlying bone from stress and can lead to reduced bone quality [5,6]. Other disadvantages of metal implants include limited fatigue life, potential for generation of wear debris, cold welding, and corrosion [1,5,7]. Consequently, there is a demand for improved orthopedic implants. Carbon-fiber (CF), reinforced with polyetheretherketone, is one of the promising innovative implant materials in the field of orthopedic oncology. CF plates are increasingly used and offer several benefits compared with metal. First, CF's radiolucency allows for precise radiation planning and better radiologic visualization of local tumor recurrences and bone healing, thereby facilitating improved postoperative follow-up and surveillance for oncological patients (Figure 1) [8-11]. Second, the modulus of elasticity of CF (13 GPa) is closer to cortical bone (12GPa) [12]. Third, CF has the capability to withstand prolonged fatigue strength compared with current metal plates [12]. Therefore, biomechanical properties of CF should theoretically enhance bone healing and reduce complication risks. Lastly, other material-specific advantages include easier implant removal due to the metallic screws and polymeric plate (no cold welding) and the lack of metallic allergy [13]. Despite these advantages, CF composites have shown brittle failure in tension and flexural tests [14]. When this occurs, the material breaks into multiple solid fragments instead of deforming or straining under load. This was reported, under supra-physiological load in vitro, in 2 out of 12 simulated comminute distal fibula fractures treated with CF plates [15]. Additionally, intraoperative plate breakage occurred while inserting a screw to obtain fracture reduction by tightening the plate to the bone in 3 out of 78 proximal humerus CF plates in non-oncological patients [16]. Intraoperative plate breakage was also reported in 5 out of 110 distal radius fractures treated with volar CF plates [13]. Regarding oncological patients, one CF plate failure was reported 4 months after implantation in a 75-year-old patient with lymphoma, while the postoperative course of 2 CF plates was uneventful (77-year-old male with prostatic carcinoma metastasis in the humerus and 17-year-old patient with an intraosseous schwannoma in the tibia with 6 and 8 months of follow-up, respectively) [17,18].

Although CF plates are increasingly used in fracture care, reported experience in orthopedic oncology remains limited. Therefore, the purpose of this study was to identify complications of patients with bone tumors treated with CF plates.

6

Figure 1. *Giant cell tumor in the right distal femur treated with bone cement during curettage using a metal plate (a) and a carbon-fiber plate (b).*

Materials and methods

This retrospective study is based on the experience of the "Carbon-Fiber International Collaboration Initiative" research group which included 13 large academic and non-academic hospitals from Europe, the Middle East, the United Kingdom, and the United States of America (Figure 2). The study protocol was approved by the ethics committee Leiden (coordinating center), and each of the participating centers' institutional review board. Data exchange agreements were signed before patient inclusion started. Due to the observational nature of the study and with the aim to assess quality of the CF implants used, further ethical approval including informed consent was waived by the Medical Ethics Review Committee Leiden Den Haag Delft, reference G20.103. Data was collected through a centralized online Castor electronic data capture database [19]. The coordinating center (Leiden University Medical Center) had access to all data entered in Castor. All methods were performed in accordance with relevant guidelines and regulations.
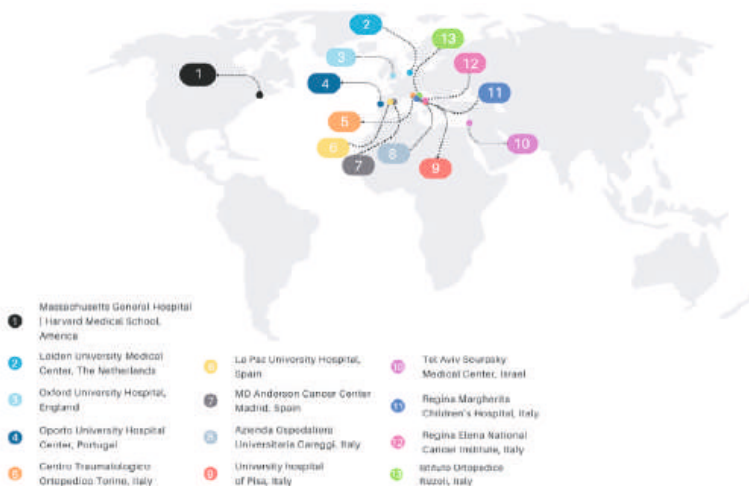
Figure 2. *World map showing all 13 participating centers.*

Participants and treatment details

Between February 2015 and May 2021, all sequential patients who received a CF plate were retrospectively included by each participating center without age restriction. Patients who received more than one CF plate during the same surgery were also included. Patients were excluded in case of (1) a combination of CF plate fixation with another surgical procedure of fixation such as intramedullary fixation, (2) non-malignancy, and (3) CF plate revisions. Only the first surgery was included if a patient had more than one qualifying surgery during the study period (Figure 3).

6
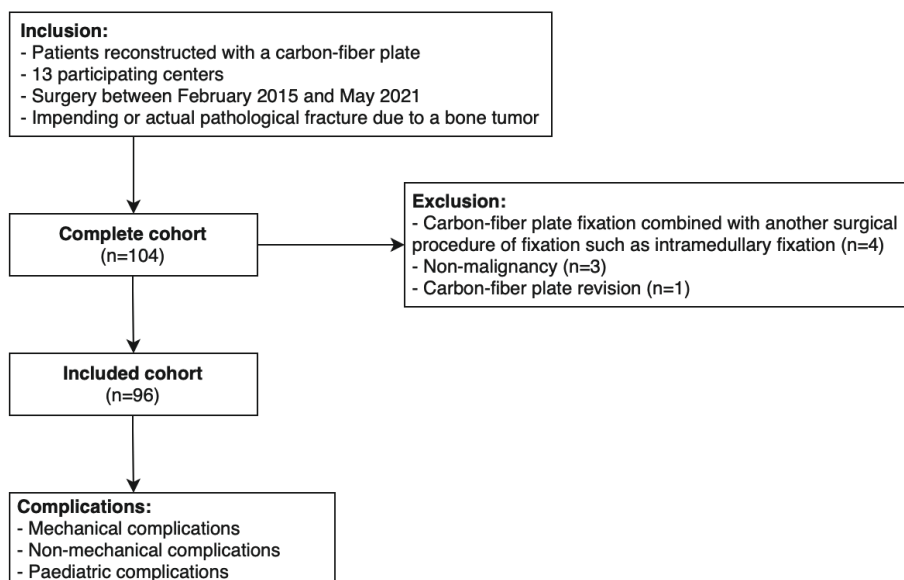
Figure 3. *Flow diagram illustrating patient selection and outcomes.*

The choice of treatment was made by shared decision making between the patient and surgeon. In general, surgery was recommended to oncological patients with impending or actual pathological fractures, mechanical axial loading pain, and no response to radiation therapy or oral narcotic pain medication. The choice of using a CF plate instead of a conventional metal plate was made by the operating surgeon. Length of the plates would not have been different between CF plates or conventional metal plates. Good candidates for CF plates were patients with standard anatomy because CF plates cannot easily be bend manually to match surface anatomy of individual bones. Therefore, surgeons must ensure good implant fit preoperatively. During this study, patients were treated with various FDA approved and CE marked CF plates with locking screw options (manufactured by CarboFix Orthopaedics; Herzeliya, Israel) (Figure 4). The surgical procedure, including positioning of the patient and surgical approach, depended on the surgeon's experience and preference. All oncological patients were clinically and radiographically evaluated postoperatively after 6-months, 1-year, and 2-years. Subsequent follow-up visits with radiographic evaluation were dependent on the patient's oncological status, and additional visits took place if needed. Patients were cleared for radiation therapy or chemotherapy 7-10 days after the surgical procedure and all patients adhered to weight bearing as tolerated after completion of surgery. The rate of loss to follow-up was 1% (1/96) at 6-months, 2% (2/96) at 1-year, and 5% (5/96) at 2-year. Five patients were lost to follow-up due to death of disease during the standard 2-year follow-up period. Follow-up was verified until July 8th, 2022.
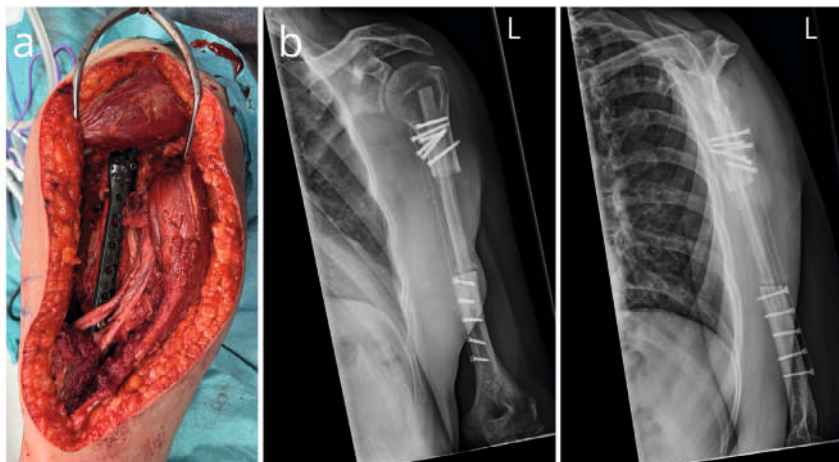
Figure 4. *Intraoperative picture after midshaft resection of the left humerus and partial resection of the triceps muscle due to an Ewing Sarcoma. Reconstruction was performed with a free vascularized fibula graft and a carbon-fiber humerus plate (a). Postoperative anteroposterior X-rays of the same patient (b).*

6

Variables and outcome measures

The following clinical variables were registered: sex; age; body mass index (BMI); smoking status (non-smoker was defined as stopped at least 6 months ago); American Society of Anesthesiologists (ASA) score; diagnosis/indication; tumor grade; preoperative chemotherapy; preoperative radiotherapy; postoperative chemotherapy within 6 months of surgery; postoperative radiotherapy within 6 months of surgery; date of surgery; surgical side; pathological fracture; location of surgery; location of bone; use of autograft, allograft, or cement; surgical margin; and type of CF plate.

Patients who had complications were identified, and timing and etiology of complications were noted. Similar complications were tabulated and classified based on mechanical, non-mechanical and pediatric complications. Mechanical complications included: (1) aseptic loosening or graft-host non-union in case of a biological reconstruction, and (2) structural complications such as periprosthetic fracture or plate breakage. Radiologic presence of mature bridging bone at graft-host junction site was considered bony union (Figure 5). Any patient failing to show bony union 1-year postoperatively or patients that required additional surgery to achieve healing was defined as having a non-union. Non-mechanical complications included: (3) soft tissue complications such as wound dehiscence, (4) infection and (5) tumor progression. Specific pediatric complications included (6) growth arrest resulting in longitudinal or angular deformity.
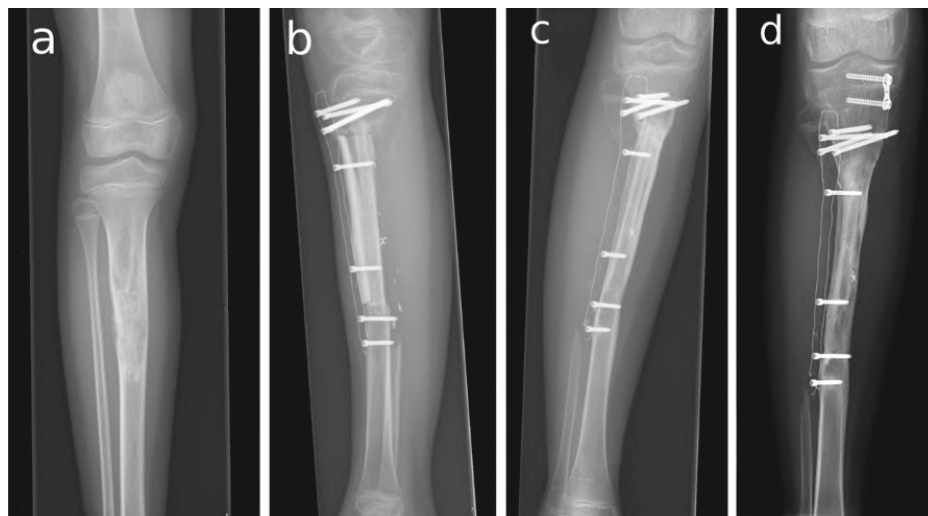
Figure 5. *Adamantinoma in the proximal tibia of a 10-year-old girl (a). Status after resection proximal tibia and reconstruction with humerus allograft, fibula transfer and carbon-fiber plate. Allograft-host junction healing at (a) 6 months, (b) 1-year, and (d) 2-years postoperatively. Additional surgery was performed to treat the valgus leg axis with an eight-plate 21 months after initial surgery (d).*

Statistical methods
Descriptive statistics were performed using SPSS v.24 (IBM Corp., Armonk, NY, USA). Baseline characteristics and surgical variables were shown using frequencies (percentages for categorical variables) and medians (interquartile ranges [IQR's] for continuous variables as they were not normally distributed based on histogram inspection).

Results

In total, 96 patients of which 59 female (61%) with a median age of 43 years (IQR; 19-54) were included with a median follow-up of 35 months (IQR; 21-49). The three most common indications included atypical cartilaginous tumors (34%), benign primary bone lesions (28%), and osteosarcomas (12%). Most lesions were located in the femur (70%), followed by the tibia (15%) and humerus (14%). The majority of surgical margins were intralesional (60%), followed by wide margins (19%), marginal margins (13%), no resection (5%), and not reported (3%). In total, 11 (12%) patients received an autograft, 43 (45%) received an allograft, and 43 (45%) received cement. Three (3%) patients received a diaphyseal and metaphyseal CF plate combined during the same surgical procedure (Table 1).

Table 1. Demographic features of included patients treated with carbon-fiber plates (n=96).

Baseline characteristics	n (%)
Female	59 (61%)
Age (years; median with IQR)	43 (19 – 54)
BMI (kg/m²;[a] median with IQR)	24 (20 – 27)
Smoking status[a]	17 (18%)
ASA score[a]	
1-2	81 (84%)
3-4	12 (13%)
Diagnosis/indication	
Atypical cartilaginous tumors	33 (34%)
Benign primary bone lesions	27 (28%)
Osteosarcoma	11 (12%)
Adamantinoma	10 (10%)
Metastasis	7 (7%)
Multiple myeloma	3 (3%)
Soft-tissue sarcoma with bone invasion	3 (3%)
Ewing Sarcoma	2 (2%)
Tumor grade[a] (excluded benign primary bone lesions[b])	
Low	44 (46%)
High	24 (25%)
Preoperative chemotherapy	17 (18%)
Preoperative radiotherapy to surgery site	4 (4%)
Postoperative chemotherapy	18 (19%)
Postoperative radiotherapy	7 (7%)
Surgical variables	
Surgical side	
Left	61 (64%)
Right	35 (36%)
Pathological fracture	14 (15%)
Location of surgery	67 (70%)
Femur	14 (15%)
Tibia	13 (14%)
Humerus	2 (2%)
Radius	
Location of bone	39 (41%)
Diaphyseal	38 (40%)
Metaphyseal	6 (6%)
Epiphyseal	7 (7%)
Diaphyseal and Metaphysial combined[c]	6 (6%)
Metadiaphyseal and Epiphyseal combined	
Cement	43 (45%)
Allograft	43 (45%)
Autograft	11 (12%)

Table 1. Demographic features of included patients treated with carbon-fiber plates (n=96). *(continued)*

Baseline characteristics	n (%)
Type of carbon-fiber plate	42 (44%)
Femoral condyle plate	22 (23%)
Diaphyseal broad femur plate	3 (3%)
Femoral condyle and diaphyseal broad plate combined[d]	4 (4%)
Diaphyseal narrow femur plate	23 (24%)
Proximal humerus plate	2 (2%)
Distal radius plate	
Surgical margin[a]	
Intralesional	58 (60%)
Marginal	12 (13%)
Wide	18 (19%)
No resection	5 (5%)

IQR= Interquartile range; ASA= American Society of Anesthesiologists; BMI=Body Mass Index.
a Missing data was present in BMI for 14/96 (15%); smoking status 13/96 (13%); ASA-score 3/96 (3%); Tumor grade 1/96 (1%); and surgical margin 3/96 (3%).
b Stage (latent, active, aggressive) of benign bone lesions was not reported.
c Three patients received a diaphyseal and metaphyseal plate combined during the same surgical procedure. Therefore, a total of 99 plates were placed in 96 patients.
d Type of carbon-fiber plate can be different to "location of surgery". For example, proximal humerus plates were used for lesions in the tibia (predominantly children) because carbon-fiber tibia plates were not yet available (FDA approved since October 2020).

In total, 22 (23%) patients endured complications (Table 2). Mechanical complications included 1 patient with aseptic loosening of the CF plate after 20 months, and 2 non-unions after biological reconstruction with an allograft (20 and 28 months postoperative). Structural complications occurred in 7 patients. These complications included 2 periprosthetic fractures (1 and 3 months postoperative), 1 traumatic proximal humerus plate breakage (14-year-old male fell off his bike 28 months after surgery) and 2 femoral condyle plate breakages without clear trauma (75-year-old female 5 months postoperative "stood up from bed", and 19-year-old male 2 months postoperative "while getting dressed") (Figure 6). In these cases, full weight bearing with incomplete bone healing and malalignment of the reconstruction was considered the cause of plate breakage. Further structural complications included 1 screw breakage (9 months postoperative), and 1 screw backing out (2 months postoperative). Non-mechanical complications included 1 patient with wound dehiscence within a month after surgery (this patient received preoperative radiotherapy with a total dose of 50 gray), 4 infections (less than a month, 1, 6 and 10 months postoperative); and 5 tumor progressions which lead to a transfemoral amputation in one case (5, 7, 17, 20 and 31 months postoperative). Specific pediatric complications occurred in 2 patients in which eight-plates were placed to treat valgus deformations (21 and 28 months postoperative). Interestingly, almost all mechanical complications, except for a traumatic humerus plate breakage, occurred in CF plates placed in the lower extremity. Non-mechanical complications were equally distributed between the upper- and lower extremity, and pediatric complications occurred in the lower extremity.

Besides, 5 of the CF plates were removed due to irritation/pain at the site of the implant after complete bone healing (after 12, 20, 21, 36, and 40 months).

Figure 6. *Carbon-fiber plate after pathological fracture of the left distal femur due to a diffuse large B-cell lymphoma (a). Plate breakage, exactly at the location of the pathological fracture at 5 months after surgery (b). Status after revision with a conventional retrograde femoral nail (c). Pseudoarthrosis remained, and this patient died of disease 1-year after the carbon-fiber plate revision with a conventional retrograde femoral nail. In general, an intramedullary osteosynthesis of lower extremity pathological fractures is preferred because steel plates are expected to break when fracture healing is not achieved.*

6

Table 2. Complications of patients with bone tumors treated with carbon-fiber plates.

	Time to complication (in months)	Etiology
Mechanical complications		
(1) Aseptic loosening or non-union in case of a biological reconstruction	20 20, 28	**1 (1%)** Aseptic loosening for which the CF plate was removed. **2 (2%)** Non-unions after reconstruction with an allograft. CF plate still in situ for both cases.
(2) Structural complications	1, 3 28 2, 5 9 2	**2 (2%)** Periprosthetic fractures without clear mechanism. CF plate was still in situ for both, one patient died. **1 (1%)** One traumatic plate breakage (14-year-old male fell off his bike). **2 (2%)** Plate breakages without clear trauma. Full weight bearing with incomplete bone healing and malalignment of the reconstruction identified as cause of plate breakage. CF plates were removed. **1 (1%)** Screw breakage. CF plate still in situ. **1 (1%)** Screw backed out and was removed without any difficulty. CF plate remained in situ.
Non-mechanical complications		
(3) Soft tissue complications	0	**1 (1%)** Wound dehiscence after preoperative radiotherapy (total dose 50 gray) requiring irrigation and removal of the CF plate.
(4) Infection	0, 1, 6, 10	**4 (4%)** infections: Two infections resulted in removal of the CF plate. The other two patients were successfully treated with debridement and long-lasting antibiotics.
(5) Tumor progression	5, 7, 17, 20, 31	**5 (5%)** Tumor progression: Two local recurrences resulted in CF plate removal, one of those patients was treated with a transfemoral amputation. Two other patients died of disease with the CF plate in situ and one local recurrence was successfully treated with thermoablation.
Pediatric complications		
(6) Growth arrest resulting in longitudinal or angular deformity	21, 28	**2 (2%)** Angular deformities. Both patients were treated with an eight-plate on the medial side of the proximal tibia for a valgus leg axis after resection of an adamantinoma. CF plates are still in situ.

Abbreviations: CF = Carbon-fiber

Discussion

Although CF plates are already used worldwide, reported experience in orthopedic oncology remains limited. Describing complications of patients with bone tumors treated with CF plates offers valuable information for orthopedic oncologists that may want to use CF plates. This international multicenter study evaluated 96 patients with bone tumors treated with CF plates. During the study period with a median follow-up of 35 months (IQR; 21-49), 22 (23%) patients were reported to have complications, which suggests CF plates are safe to use in patients with bone tumors that often require demanding reconstructions. Particularly the low percentage of nun-unions (2%) with high percentages of biological reconstructions (12% autograft and 45% allograft) are promising. To date, this is the largest CF plates cohort reporting on complications in an oncologic population.

The major disadvantage of CF plates is its inability to be manually bent to match surface anatomy of individual bones. Therefore, surgeons must ensure good implant fit preoperatively. CF plates could not be used during all reconstructive surgeries due to unique anatomy or complex mechanical problems. For some complex cases, conventional metal implants that can be bend, customizable orthopedic implants, or patient specific implants that can better match the reconstructed anatomy may be preferred [20]. However, patient specific implants are a time-consuming alternative, and it is still uncertain whether the theoretical biomechanical advantages carry true advantages in surgical outcomes when compared to standard procedures [20,21]. Secondly, while CF plate's radiolucency is beneficial for postoperative radiological imaging, determining the optimal plate position can be challenging. Thirdly, production costs and availability could be another disadvantage. However, CF reinforced composites have become more competitive and are widely used across industries like aerospace, wind energy, and automotive [22]. As a result, production costs have decreased, and the costs of CF plates are currently competitive with conventional metal plates.

Although study groups and surgical procedure are not always comparable, it may be noted that our study provides relatively low non-union rates (2%), even with a high percentage of biological reconstructions (12% autograft and 45% allograft). Wisanuyotin et al. reported 30% nonunion (mean time to union of 9.8 ± 2.9 months) for nonvascularized autograft (NA), and 32% nonunion (mean time to union of 11.5 ± 2.8 months) for allografts after resection and reconstruction of primary bone tumors [23]. In addition, Buecker et al. reported that locking plates for allograft-host junction fixation were associated with improved union rates compared with standard plates (75% union at an average of 13 months versus 56% at an average of 14 months, respectively) [24]. Moreover, the total rate of CF plate complications (23%) was low compared to conventional metal plate studies (complication range 42-76% with follow-up range of 35-112 months) [25-28]. When comparing our results with CF plates placed for trauma patients, we reported 12 (18%) CF femoral plate failures while Byun et al. and Mitchell et al. reported none (0%) and 1 (9%) failure in respectively 10 and 11 patients treated with CF femoral plates [29,30]. Although the number of failures is currently too small

6

to identify risk factors for plate complications, higher complication rates can be expected with more extensive treatment such as chemo- and/or radiotherapy and more complex surgery with auto-/allografts [27].

This study has several limitations. First, this remains a single-arm retrospective international multicenter study with inherent limitations associated with such a study design, including the lack of a comparison group and reliance on chart abstraction. As a result, our study was prone to selection bias. However, participating centers were asked to sequentially include patients according to a standard inclusion protocol. Centers were regularly contacted by the coordinating center to elaborate on cases if there were any questions, ambiguities, or missing data. Nevertheless, the authors acknowledge that the most scientifically robust study design to assess the added value of CF plates is a randomized controlled trial with clinical-, radiological-, and functional outcomes as primary endpoints. However, patients with bone tumors in this group were heterogeneous in terms of baseline characteristics and surgical variables. Therefore, acquiring a matching control group would be difficult and we recommend propensity score matching as the next best step for future research. Second, performance bias could have occurred because the surgical procedure and postoperative management also depended on the surgeon's experience and preference. Yet, no major differences in treatment outcomes between participating centers were observed.

Conclusion

Carbon-fiber (CF) implants offer several material specific benefits compared to the more common metal implants. To assess safety of CF plates, we performed an international multicenter study describing all complications occurring in orthopedic oncology patients that were treated with CF plates. Low complication rates are reported, and complications originated mainly from disease progression or infection. Although based on a very heterogenous retrospective multicenter database our results suggests that orthopedic oncologists may safely use CF plates in demanding reconstructions after bone tumor resections. However, studies of randomized or matched comparative nature are needed to assess the added clinical value of theoretical benefits of CF plates, such as precise radiation planning, improved bone healing, radiographic visualization of local recurrences and union.

References

1. Hak, D.J.; Banegas, R.; Ipaktchi, K.; Mauffrey, C. Evolution of plate design and material composition. *Injury* **2018**, *49 Suppl 1*, S8-s11, doi:10.1016/s0020-1383(18)30295-x.

2. Prasad, K.; Bazaka, O.; Chua, M.; Rochford, M.; Fedrick, L.; Spoor, J.; Symes, R.; Tieppo, M.; Collins, C.; Cao, A., et al. Metallic Biomaterials: Current Challenges and Opportunities. *Materials (Basel)* **2017**, *10*, doi:10.3390/ma10080884.

3. Ringel, F.; Ryang, Y.M.; Kirschke, J.S.; Müller, B.S.; Wilkens, J.J.; Brodard, J.; Combs, S.E.; Meyer, B. Radiolucent Carbon Fiber-Reinforced Pedicle Screws for Treatment of Spinal Tumors: Advantages for Radiation Planning and Follow-Up Imaging. *World Neurosurg* **2017**, *105*, 294-301, doi:10.1016/j.wneu.2017.04.091.

4. Soriani, A.; Strigari, L.; Petrongari, M.G.; Anelli, V.; Baldi, J.; Salducca, N.; Biagini, R.; Zoccali, C. The advantages of carbon fiber based orthopedic devices in patients who have to undergo radiotherapy. *Acta Biomed* **2020**, *91*, e2020057, doi:10.23750/abm.v91i3.7769.

5. Jockisch, K.A.; Brown, S.A.; Bauer, T.W.; Merritt, K. Biological response to chopped-carbon-fiber-reinforced peek. *J Biomed Mater Res* **1992**, *26*, 133-146, doi:10.1002/jbm.820260202.

6. Skinner, H.B. Composite technology for total hip arthroplasty. *Clin Orthop Relat Res* **1988**, 224-236.

7. Henderson, C.E.; Lujan, T.J.; Kuhl, L.L.; Bottlang, M.; Fitzpatrick, D.C.; Marsh, J.L. 2010 mid-America Orthopaedic Association Physician in Training Award: healing complications are common after locked plating for distal femur fractures. *Clin Orthop Relat Res* **2011**, *469*, 1757-1765, doi:10.1007/s11999-011-1870-6.

8. Baidya, K.P.; Ramakrishna, S.; Rahman, M.; Ritchie, A. Quantitative radiographic analysis of fiber reinforced polymer composites. *J Biomater Appl* **2001**, *15*, 279-289, doi:10.1106/bklq-e2yg-d2la-rg3r.

9. Feerick, E.M.; Kennedy, J.; Mullett, H.; FitzPatrick, D.; McGarry, P. Investigation of metallic and carbon fibre PEEK fracture fixation devices for three-part proximal humeral fractures. *Med Eng Phys* **2013**, *35*, 712-722, doi:10.1016/j.medengphy.2012.07.016.

10. Hak, D.J.; Mauffrey, C.; Seligson, D.; Lindeque, B. Use of carbon-fiber-reinforced composite implants in orthopedic surgery. *Orthopedics* **2014**, *37*, 825-830, doi:10.3928/01477447-20141124-05.

11. Li, C.S.; Vannabouathong, C.; Sprague, S.; Bhandari, M. The Use of Carbon-Fiber-Reinforced (CFR) PEEK Material in Orthopedic Implants: A Systematic Review. *Clin Med Insights Arthritis Musculoskelet Disord* **2015**, *8*, 33-45, doi:10.4137/cmamd.S20354.

12. Mugnai, R.; Tarallo, L.; Capra, F.; Catani, F. Biomechanical comparison between stainless steel, titanium and carbon-fiber reinforced polyetheretherketone volar locking plates for distal radius fractures. *Orthop Traumatol Surg Res* **2018**, *104*, 877-882, doi:10.1016/j.otsr.2018.05.002.

13. Tarallo, L.; Giorgini, A.; Novi, M.; Zambianchi, F.; Porcellini, G.; Catani, F. Volar PEEK plate for distal radius fracture: analysis of adverse events. *Eur J Orthop Surg Traumatol* **2020**, *30*, 1293-1298, doi:10.1007/s00590-020-02701-7.

14. Garcia-Gonzalez, D.; Rodriguez-Millan, M.; Rusinek, A.; Arias, A. Investigation of mechanical impact behavior of short carbon-fiber-reinforced PEEK composites. *Composite Structures* **2015**, *133*, 1116-1126, doi:https://doi.org/10.1016/j.compstruct.2015.08.028.

15. Wilson, W.K.; Morris, R.P.; Ward, A.J.; Carayannopoulos, N.L.; Panchbhavi, V.K. Torsional Failure of Carbon Fiber Composite Plates Versus Stainless Steel Plates for Comminuted Distal Fibula Fractures. *Foot Ankle Int* **2016**, *37*, 548-553, doi:10.1177/1071100715625291.

16. Rotini, R.; Cavaciocchi, M.; Fabbri, D.; Bettelli, G.; Catani, F.; Campochiaro, G.; Fontana, M.; Colozza, A.; De Biase, C.F.; Ziveri, G., et al. Proximal humeral fracture fixation: multicenter study with carbon fiber peek plate. *Musculoskelet Surg* **2015**, *99 Suppl 1*, S1-8, doi:10.1007/s12306-015-0371-2.

6

17.   Goudriaan, W.A.; Tordoir, R.L.; Broekhuis, D.; van der Wal, R.J.P. Early Failure of a Carbon-Fiber-Reinforced Polyetheretherketone Distal Femur Plate: A Case Report. *JBJS Case Connect* **2020**, *10*, e20.00041, doi:10.2106/jbjs.Cc.20.00041.

18.   Laux, C.J.; Hodel, S.M.; Farshad, M.; Müller, D.A. Carbon fibre/polyether ether ketone (CF/PEEK) implants in orthopaedic oncology. *World J Surg Oncol* **2018**, *16*, 241, doi:10.1186/s12957-018-1545-9.

19.   Castor Electronic Data Capture. Availabe online: https://castoredc.com/ (accessed on 8 July 2022).

20.   Haglin, J.M.; Eltorai, A.E.; Gil, J.A.; Marcaccio, S.E.; Botero-Hincapie, J.; Daniels, A.H. Patient-Specific Orthopaedic Implants. *Orthop Surg* **2016**, *8*, 417-424, doi:10.1111/os.12282.

21.   Willis, A.R.; Ippolito, J.A.; Patterson, F.R.; Benevenia, J.; Beebe, K.S. Customizable orthopaedic oncology implants: one institution's experience with meeting current IRB and FDA requirements. *Springerplus* **2016**, *5*, 967, doi:10.1186/s40064-016-2696-1.

22.   Hagnell, M.K.; Kumaraswamy, S.; Nyman, T.; Åkermo, M. From aviation to automotive - a study on material selection and its implication on cost and weight efficient structural composite and sandwich designs. *Heliyon* **2020**, *6*, e03716, doi:10.1016/j.heliyon.2020.e03716.

23.   Wisanuyotin, T.; Paholpak, P.; Sirichativapee, W.; Kosuwon, W. Allograft versus autograft for reconstruction after resection of primary bone tumors: a comparative study of long-term clinical outcomes and risk factors for failure of reconstruction. *Sci Rep* **2022**, *12*, 14346, doi:10.1038/s41598-022-18772-x.

24.   Buecker, P.J.; Berenstein, M.; Gebhardt, M.C.; Hornicek, F.J.; Mankin, H.J. Locking versus standard plates for allograft fixation after tumor resection in children and adolescents. *J Pediatr Orthop* **2006**, *26*, 680-685, doi:10.1097/01.bpo.0000230333.73286.06.

25.   Bus, M.P.; Dijkstra, P.D.; van de Sande, M.A.; Taminiau, A.H.; Schreuder, H.W.; Jutte, P.C.; van der Geest, I.C.; Schaap, G.R.; Bramer, J.A. Intercalary allograft reconstructions following resection of primary bone tumors: a nationwide multicenter study. *J Bone Joint Surg Am* **2014**, *96*, e26, doi:10.2106/jbjs.M.00655.

26.   Cara, J.A.; Laclériga, A.; Cañadell, J. Intercalary bone allografts. 23 tumor cases followed for 3 years. *Acta Orthop Scand* **1994**, *65*, 42-46, doi:10.3109/17453679408993716.

27.   Ortiz-Cruz, E.; Gebhardt, M.C.; Jennings, L.C.; Springfield, D.S.; Mankin, H.J. The results of transplantation of intercalary allografts after resection of tumors. A long-term follow-up study. *J Bone Joint Surg Am* **1997**, *79*, 97-106, doi:10.2106/00004623-199701000-00010.

28.   Donati, D.; Di Liddo, M.; Zavatta, M.; Manfrini, M.; Bacci, G.; Picci, P.; Capanna, R.; Mercuri, M. Massive bone allograft reconstruction in high-grade osteosarcoma. *Clin Orthop Relat Res* **2000**, 10.1097/00003086-200008000-00025, 186-194, doi:10.1097/00003086-200008000-00025.

29.   Byun, S.E.; Vintimilla, D.R.; Bedeir, Y.H.; Dean, C.S.; Parry, J.A.; Hak, D.J.; Mauffrey, C. Evaluation of callus formation in distal femur fractures after carbon fiber composite versus stainless steel plate fixation. *Eur J Orthop Surg Traumatol* **2020**, *30*, 1103-1107, doi:10.1007/s00590-020-02681-8.

30.   Mitchell, P.M.; Lee, A.K.; Collinge, C.A.; Ziran, B.H.; Hartley, K.G.; Jahangir, A.A. Early Comparative Outcomes of Carbon Fiber-Reinforced Polymer Plate in the Fixation of Distal Femur Fractures. *J Orthop Trauma* **2018**, *32*, 386-390, doi:10.1097/bot.0000000000001223.

7

CARBON-FIBER PLATES FOR TRAUMATIC AND (IMPENDING) PATHOLOGICAL FRACTURE FIXATION: WHERE DO WE STAND? A SYSTEMATIC REVIEW

Z. Rijs[1,†], A Weekhout[1,†], S. Daniel[1], J.W. Schoones[2], O.Q. Groot[3], S.A. Lozano-Calderon[3], M.A.J. van de Sande[1]
†Authors contributed equally

[1] Department of Orthopaedic Surgery, Leiden University Medical Center, Leiden, The Netherlands
[2] Directorate of Research Policy, Leiden University Medical Center, Leiden, The Netherlands
[3] Department of Orthopaedics, Massachusetts General Hospital—Harvard Medical School, Boston, USA

Abstract

Background

Carbon-fiber (CF) plates are increasingly used for fracture fixation. This systematic review evaluated complications associated with CF plate fixation. It also compared outcomes of patients treated with CF plates versus metal plates, aiming to determine if CF plates offered comparable results. The study hypothesized that CF plates display similar complication rates and clinical outcomes as metal plates for fracture fixation.

Methods

The study adhered to the Preferred Reporting Items for Systematic Reviews and Meta-Analyses guidelines. The following databases were searched from database inception until June 2023: PubMed, MEDLINE, Embase, Web of Science, Cochrane Library, Emcare, Academic Search Premier and Google Scholar. Studies reporting on clinical and radiological outcomes of patients treated with CF plates for traumatic fractures and (impending) pathological fractures were included. Study quality was assessed, and complications were documented as number and percentage per anatomic region.

Results

A total of 27 studies of moderate to very low quality of evidence were included. Of these, 22 studies (800 patients, median follow-up12 months) focused on traumatic fractures, and 5 studies (102 patients, median follow-up 12 months) on (impending) pathological fractures. A total of 11 studies (497 patients, median follow-up 16 months) compared CF plates with metal plates. Regarding traumatic fractures, the following complications were mostly reported: soft tissue complications (52 out of 391; 13%) for the humerus, structural complications (6 out of 291; 2%) for the distal radius, nonunion and structural complication (1 out of 34; 3%) for the femur, and infection (4 out of 104; 4%) for the ankle. For (impending) pathological fractures, the most frequently reported complications were reinfections (2 out of 14; 14%) for the humerus and structural complication (6 out of 86; 7%) for the femur/tibia. Comparative studies reported mixed results, although the majority (7 out of 11; 64%) reported no significant differences in clinical or radiological outcomes between patients treated with CF or metal plates.

Conclusion

This systematic review did not reveal a concerning number of complications related to CF plate fixation. Comparative studies showed no significant differences between CF plates and metal plates for traumatic fracture fixation. Therefore, CF plates appear to be a viable alternative to metal plates. However, high-quality randomized controlled trials (RCTs) with long-term follow-up are strongly recommended to provide additional evidence supporting the use of CF plates.

Introduction

Carbon-fiber (CF) plates, reinforced with polyetheretherketone, have gained increasing interest due to potential advantages compared to metal plates. For instance, CF plates offer radiolucency, which enables better radiographic visualization of postoperative fracture reduction, bone healing, and surveillance of tumor recurrence for oncological patients [1-4]. Furthermore, the absence of metallic artifacts allows for precise radiotherapy planning and accurate delivery after placement of CF implants [5-7]. Another advantage specific to CF plates may be reduced stress shielding, as their modulus of elasticity closely matches that of cortical bone; 13 gigapascal (GPa) for CF vs 12 GPa for cortical bone [8]. Additionally, *in-vitro* studies on CF plates have demonstrated superior fatigue strength compared to current metal plates, this may potentially enhance bone healing and reduce the risk of complications [8,9]. Finally, cold welding does not occur in CF plate constructs, which would facilitate easy implant removal [10].

Despite the increasing use of CF plates for fixating traumatic and (impending) pathological fractures, reported experience in the literature remains limited. Previous systematic reviews have primarily focused on comparative studies or specifically examined traumatic distal radius fracture fixation with CF plates [11-13]. In these studies, CF plates were considered as a valid alternative due to comparable results to metal plates [11-13]. However, cohort studies and case reports have identified several disadvantages associated with CF plates that were not mentioned in the afore mentioned systematic reviews. Drawbacks include the inability to deform the plate, plate breakage without clear trauma, and brittleness when plate breakage occurs [14-17]. Conducting a systematic review that includes all relevant existing evidence would provide a comprehensive overview and is crucial for assessing the safety and effectiveness of CF plates. Therefore, the aim of this systematic review was to evaluate complications associated with CF plate fixation for traumatic and (impending) fracture fixation. It also compared outcomes of patients treated with CF plates compared to metal plates, aiming to determine if CF plates offered comparable results. Based on the aforementioned systematic reviews, this study hypothesized that CF plates display similar complication rates and clinical outcomes as metal plates for (pathological) fracture fixation.

Methods

Search strategy and study selection
This systematic review was conducted in accordance with the Preferred Reporting Items for Systematic Reviews and Meta-Analyses (PRISMA) guidelines and followed a pre-registered PROSPERO protocol (CRD42021254603) [18]. A medical librarian assisted in developing the search strategy, which was based on the following PICO (population, intervention, comparison, outcome) algorithm: P = Patients with traumatic or (impending) pathological fractures, I = CF plate fixation, C = No specific controls or patients treated with metal plates, and O = radiological and/or clinical outcomes (including complications). Ultimately, the search

7

was divided into two parts: (1) CF plates used for traumatic fractures and (2) CF plates used for (impending) pathological fractures. The search contained keywords related to "carbon-fiber" and "fracture" for traumatic fractures, and "carbon-fiber" and "bone tumor" for (impending) pathological fractures (Appendix A). The following databases were reviewed from database inception up to June 2023: PubMed, MEDLINE, Embase, Web of Science, Cochrane Library, Emcare, Academic Search Premier and Google Scholar.

Eligibility criteria
Eligible study designs included randomized controlled trials (RCT's), cohort studies (with prospective and retrospective designs), case-control studies, cross-sectional studies, and case reports. Studies were included if they involved patients with traumatic or (impending) pathological fractures fixated with CF plates. Excluded were meeting abstracts, reviews, editorials, commentaries, surveys, animal-only, *in-vitro*, cadaver, or biomechanical studies. No filters or other constraints were used in the database search.

Study selection
After the retrieval of eligible studies, duplicates were removed. Out of the initial pool of 808 traumatic fracture records and 223 oncologic (bone tumor) records, a total of 335 studies on trauma fractures and 116 studies on (impending) pathological fractures remained. Abstracts were obtained and evaluated. Preliminary screening of titles and abstracts led to the exclusion of 311 studies for trauma fractures and 109 studies for (impending) pathological fractures. Subsequently, the full text of 24 studies on trauma fractures were reviewed, and two of them were excluded because a more recent third study used the same patient database. Similarly, two of the seven studies concerning (impending) pathological fractures were excluded after full text screening; one due to irrelevant outcome measurements and one because the same patient had been included in a more recent study (Figure 1).
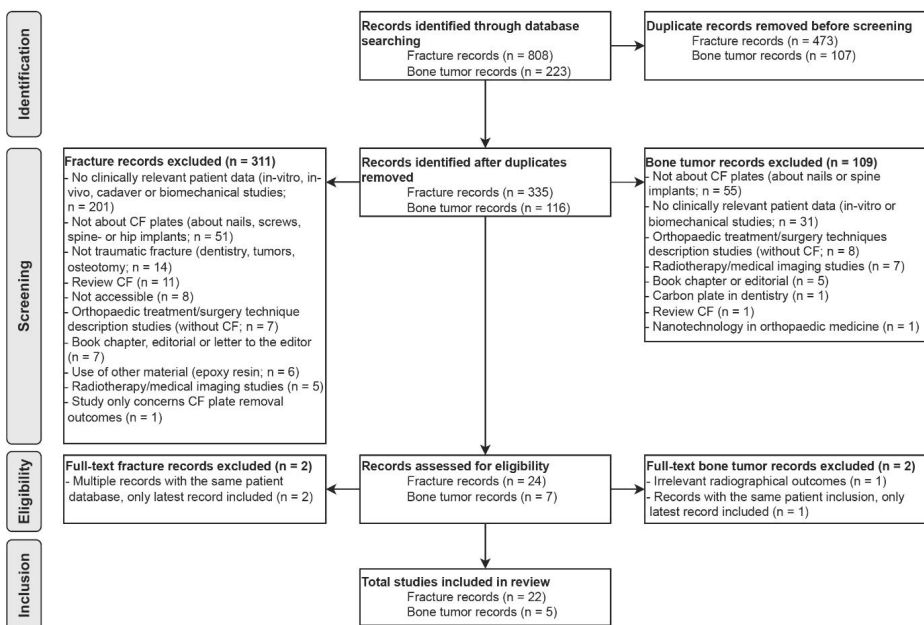
Figure 1. PRISMA flow diagram of the study. Abbreviations: CF = Carbon-fiber.

Quality assessment

Methodological quality assessment varied based on the study design. According to the Cochrane Handbook guidelines, the Risk of Bias II (RoB 2) tool was applied for RCT's, the Risk of Bias in Nonrandomized Studies of Intervention (ROBINS-I) tool for non-RCT's, and the Joanna Briggs Institute Checklist for case reports [19-21]. With the aid of these tools, various forms of bias were evaluated, including confounding bias, selection bias, bias in classification of intervention, bias due to deviations from intended interventions, bias due to missing data, bias in measurement of outcome, and bias in selection of the reported results [19-21]. In addition, the Grading of Recommendations Assessment, Development and Evaluation (GRADE) approach was utilized to grade quality of evidence, which is important for assessing appropriateness and trustworthiness of recommendations done in the evaluated studies [22]. Within GRADE the following quality of evidence options are possible: high, moderate, low, and very low. Randomized trials were initially rated high, observational studies low, and other levels of evidence very low. However, high quality evidence was downgraded if methodological flaws exist, and low quality evidence could be upgraded when large effect sizes exist. Three reviewers (Z.R., A.W., S.D.) independently assessed the risk of bias for the included studies, discrepancies were discussed, and the senior author (M.v.d.S.) was consulted in case of persistent disagreement.

7

Data extraction

A standard data extraction form was used to collect relevant data from the included studies. The extraction form captured study characteristics (author's, year of publication, country, setting, title, number of included patients, and level of evidence), patient characteristics (age, sex, smoking, body mass index (BMI), ASA classification, comorbidities, indication for CF plate fixation, and number of patients that received a CF plate), and outcomes (complications, union, clinical, radiological, and patient reported outcomes, as well as the duration of follow-up) [23].

Data analysis

To summarize the findings in a quantitative form, complications were subdivided per anatomical region, and presented separately for the upper and lower extremities, considering complications might depend on mechanical loading [24,25]. Descriptive statistics were performed using SPSS v.24 (IBM Corp., Armonk, NY, USA). Demographics of all included studies were shown using medians for continuous variables as demographic data contained outliers and skewed data due to the inclusion of case reports.

Results

Study characteristics

A total of 22 studies involving 800 patients with trauma fractures (median follow-up 12 months), and 5 studies involving 102 patients (median follow-up 12 months) with (impending) pathological fractures were included in the systematic review. Among them, 11 studies (497 patients, median follow-up 12 months), including three RCT's, compared CF plates with metal plates for trauma fractures (Table 1).

Table 1. Demographics of all included studies (n=27); for trauma fractures (n=22), of which 11 were comparative, and (impending) pathological fractures (n=5).

Parameter	Median (range) / % (n)
Trauma fracture studies (n=22; 800 patients)	
Number of patients	31 (1 – 160)
Patient age in years	58 (18 – 94)
Percentage of patient who were woman	66% (393)
BMI in kg/m^2 *	28 (16 – 44)
Follow-up in months *	12 (1 – 48)
(impending) pathological fracture studies (n=5; 102 patients)	
Number of patients	2 (1 – 96)
Patient age in years	30 (2 – 77)
Percentage of patient who were woman	61% (62)
BMI in kg/m^2 *	24 (20 – 27)
Follow-up in months *	12 (6 – 35)

Table 1. Demographics of all included studies (n=27); for trauma fractures (n=22), of which 11 were comparative, and (impending) pathological fractures (n=5). *(continued)*

Parameter	Median (range) / % (n)
Comparative studies (n=11; 497 patients)	
Number of patients	42 (22 – 87)
Patient age in years	59 (18 – 89)
Percentage of patient who were woman	64% (317)
BMI in kg/m^2 *	27 (19 – 48)
Follow-up in months *	16 (2 – 36)

* Not reported in all included studies.
Abbreviations: BMI=body mass index; kg/m2 = kilograms per square meter.

Study quality

The overall quality assessment score for RCT's, according to RoB 2 tool was "some concerns" for all included RCT's (n=3; Table 2). The ROBINS-I criteria score for non-comparative studies ranged from low to moderate (n=19; Table 3), and the mean score for case reports was 6/8 (n=5; Table 4). Following the GRADE approach, randomized trials were initially rated with a high certainty of evidence. However, due to the risk of bias of the included RCT's, scores were lowered in their certainty of evidence to moderate (Table 5). Observational studies and case reports were rated as with a low or very low certainty of evidence (Table 5). Consequently, recommendations of using CF plates for fixating fractures should be done with caution.

7

Table 2. Risk of Bias II (RoB 2) tool for RCT's. *Scoring: low risk, some concerns or high risk.*

Fracture studies	Randomization process	Deviations from intended interventions	Missing outcome data	Measurements of the outcome	Selection of the reported results	Overall bias judgement
Perugia [26]	Low	Low	Low	Low	Some concerns	Some concerns
Ziegler [27]	Some concerns	Low	Some concerns	Low	Some concerns	Some concerns
Berger-Groch [28]	Low	Low	Low	Low	Some concerns	Some concerns

Table 3. Risk of Bias in Nonrandomized Studies of Intervention (ROBINS-I) tool for non-RCT's.

Study	Confounding	Selection of participants	Classification of interventions	Deviation from intended interventions	Missing data	Measurements of outcomes	Selection of reported results	Overall
Baker et al. [29]	NI	Low	Moderate	Low	Low	Moderate	Low	Moderate
Rotini et al. [16]	NI	Low	Moderate	Low	Moderate	Moderate	Low	Moderate
Maggio et al. [30]	NI	Low	Moderate	Low	Moderate	Moderate	Low	Moderate
Pinter et al. [31]	Moderate	Low	Moderate	Low	Moderate	Moderate	Low	Moderate
Allemann et al. [32]	NI	Moderate	Moderate	Low	Low	Moderate	Low	Moderate
Tarallo et al. [10]	NI	Low	Moderate	Low	Moderate	Moderate	Low	Moderate
Guzzini et al. [33]	NI	Moderate	Moderate	Low	Moderate	Moderate	low	Moderate
Paracuollo et al. [34]	NI	Low	Moderate	Low	Low	Moderate	Low	Moderate
Caforio et al. [35]	NI	Moderate	Low	Low	Low	Moderate	Moderate	Moderate
Rijs et al. [36]	Moderate	Moderate	Moderate	Low	Low	Moderate	Low	Moderate
Schliemann et al. [37]	NI	Moderate	Moderate	Low	Low	Moderate	Low	Moderate
Guzzini et al. [38]	NI	Low	Low	Low	Moderate	Low	Low	Moderate
Katthagen et al. [39]	NI	Moderate	Low	Low	Low	Low	Low	Moderate
Mitchell et al. [40]	Moderate	Moderate	Moderate	Low	Low	Low	Low	Moderate
Padolino et al. [41]	Moderate	Moderate	Moderate	Low	Low	Low	Low	Moderate
Byun et al. [42]	Moderate	Moderate	Moderate	Low	Low	Low	Low	Moderate
Hazra et al. [43]	Moderate	Moderate	Moderate	Low	Low	Low	low	Moderate
Behrendt et al. [44]	Moderate	Moderate	Low	Low	Low	Low	Low	Moderate
Kimmeyer et al. [45]	Moderate	Low	Moderate	Low	Moderate	Moderate	Low	Moderate

Scoring: No information (NI) low, moderate, serious, or critical.

Table 4. Joanna Briggs Institute Critical Appraisal Checklist for Case Reports (n=5).

	Fracture	Tumor			
JBI checklist questions	Mellon [46]	Laux [47]	Barnds [48]	Zoccali [49]	Yeung [50]
1. Were patient's demographic characteristics clearly described?	Yes	Yes	Yes	Yes	Yes
2. Was the patient's history clearly described and presented as a timeline?	No	No	Yes	No	Yes
3. Was the current clinical condition of the patient on presentation clearly described?	Yes	Yes	Yes	Yes	Yes
4. Were diagnostic tests or assessment methods and the results clearly described?	Yes	Yes	Yes	Yes	Yes
5. Was the intervention(s) or treatment procedure(s) clearly described?	No	No	Yes	Yes	No
6. Was the post-intervention clinical condition clearly described?	Yes	Yes	Yes	Yes	Yes
7. Were adverse events (harms) or unanticipated events identified and described?	Yes	Yes	Yes	Yes	Yes
8. Does the case report provide takeaway lessons?	Yes	Yes	No	No	No
Overall appraisal	Included	Included	Included	Included	Included

Scoring: yes, no, unclear or not applicable.

7

Table 5. Reported complications.

Trauma fracture fixation						
Study	Study design	Level of evidence	Quality of evidence (GRADE)	Number of patients*	Age**	Gender
Dey Hazra [43]	RCS	III	Moderate	65 (30 CF)	61	22/30 Female
Katthagen [39]	PCS	III	Low	42 (21 CF)	67	14/21 Female
Kimmeyer [45]	RCS	III	Low	98	66	74/98 Female
Padolino [41]	RCS	III	Low	42 (21 CF)	57	12/21 Female
Rotini [16]	PCaS	III	Low	160	64	19/160 Female
Schliemann [37]	RCS	III	Low	58 (29 CF)	66	22/29 Female
Ziegler [27]	RCT	II	Moderate	63 (32 CF)	62	26/32 Female
Allemann [32]	RCaS	IV	Low	10	53	4/10 Female
Behrendt [44]	PCS	III	Low	26 (14 CF)	57	11/14 Female
Berger-Groch [28]	RCT	II	Moderate	31 (16 CF)	59	10/16 Female
Di Maggio [30]	RCaS	IV	Low	64	57	38/64 Female
Paracuollo [34]	RCaS	IV	Low	40	62	22/40 Female
Perugia [26]	RCT	II	Moderate	30 (15 CF)	57	10/15 Female
Tarallo [10]	RCaS	IV	Low	110	58	77/110 Female

Anatomic region of the plate	Indication	Follow up (in months)	Complications
Proximal humerus	Proximal humeral fracture	32	Structural complication (CF n=1 vs titanium n=1); Soft tissue complication (CF n=2 vs titanium n=0); Humeral head necrosis (CF n=0 vs titanium n=3)
Proximal humerus	Proximal humeral fracture	12	Soft tissue complications (CF n=4 vs titanium n=0)
Proximal humerus	Proximal humeral fracture	28	Avascular necrosis (n=12); head shaft malreduction (n=12); soft tissue complications (n=7); structural complications (n=5); tuberosity malreduction (n=5); malreduction of the fracture (n=3); tuberosity resorption/dislocation (n=2), secondary glenohumeral osteoarthritis (n=2); infection (n=1)
Proximal humerus	Proximal humeral fracture	31	Structural complication (CF n=2 vs titanium n=0); Humeral head necrosis (CF n=1 vs titanium n=1); Tuberosity resorption (>50%; CF n=3 vs titanium n=9); Varus/valgus malalignment (CF n=2 vs titanium n=0)
Proximal humerus	Proximal humeral fracture	24	Structural complication (n=15); Soft tissue complication (n=39); Humeral head necrosis (n=13); Reduction loss/tuberosity dislocation (n=7); Nonunion (n=2)
Proximal humerus	Proximal humeral fracture	24	Humeral head necrosis (CF n=1 vs metal n=3); Varus malalignment (CF n=4 vs metal n=7)
Proximal humerus	Proximal humeral fracture	6	None
Distal radius	Distal radius fracture	12	None
Distal radius	Distal radius fracture	2	None
Distal radius	Distal radius fracture	36	Soft tissue complications (CF n=1 vs titanium n=2)
Distal radius	Distal radius fracture	12	None
Distal radius	Distal radius fracture	12	None
Distal radius	Distal radius fracture	16	None
Distal radius	Distal radius fracture	48	Structural complication (n=5); Soft tissue complication (n=3); Infection (n=1)

Table 5. Reported complications. *(continued)*

Trauma fracture fixation

Study	Study design	Level of evidence	Quality of evidence (GRADE)	Number of patients*	Age**	Gender
Guzzini [33]	PCaS	III	Low	22	51	14/22 Female
Baker [29]	RCaS	IV	Low	12	78	*Not reported*
Byun [42]	RCS	III	Low	31 (10 CF)	50	3/10 Female
Mellon [46]	CR	IV	Very low	1	64	1/1 Female
Mitchell [40]	RCS	III	Low	22 (11 CF)	72	8/11 Female
Caforio [35]	PCaS	IV	Low	27	57	13/27 Female
Guzzini [38]	PCS	III	Low	87 (47 CF)	57	32/46 Female
Pinter [31]	RCaS	IV	Low	30	47	18/30 Female
(Impending) pathological fracture fixation						
Laux [47]	CR	IV	Very low	2	77	2/2 Male
Zoccali [49]	CR	IV	Very low	1	3	1/1 Female
Yeung [50]	CR	IV	Very low	2	60	2/2 Female
Rijs [36]	RCaS	IV	Low	96	43	59/96 Female
Barnds [48]	CR	IV	Very low	1	9	1/1 Male

*Number of patients treated with carbon-fiber plates between brackets; **Mean or median age (as reported in the study). Abbreviations: THA = Total Hip Arthroplasty; CF = Carbon-Fiber; RCS = Retrospective Cohort Study; RCaS = Retrospective Case Study; PCS = Prospective Cohort Study; PCaS = Prospective Case Study; CR = Case report(s); RCT = Randomized Controlled Trial.*

Anatomic region of the plate	Indication	Follow up (in months)	Complications
Distal radius	Distal radius fracture	12	Soft tissue complication (n=1)
Proximal femur	THA periprosthetic fracture	*Not reported*	Nonunion (n=1)
Distal femur	Distal femur fracture	6	None
Distal femur	Distal femur fracture	1	Structural complication (n=1)
Distal femur	Distal femur fracture	12	Structural complications (CF n=0 vs stainless steel n=4); Nonunion (CF n=1 vs stainless steel n=4)
Distal fibula + distal tibia	Ankle fracture	4	Soft tissue complication (n=1)
Distal fibula + distal tibia	Ankle fracture	24	Infection (CF n=3 vs stainless steel n=4)
Distal fibula	Unstable lateral malleolus fracture	20	Soft tissue complication (n=1); Infection (n=1); Nonunion (n=1)
Humerus and tibia	Pathological fracture and prophylactic plate after curettage	6 and 8	None
Femur	Plate fixation after reconstruction	12	None
Femur	Plate fixation after reconstruction	12 and 15	None
Femur (n=67), tibia (n=14), humerus (n=13), and radius (n=2)	(Impending) pathological fractures and plate fixation after reconstructions	35	Structural complication (n=7); Infection (n=4); Soft tissue complication (n=1); Tumor progression (n=5); Aseptic loosening (n=1); Nonunion (n=2); Angular deformation (n=2)
Tibia	Plate fixation after reconstruction	3	Structural complication (n=1)

7

Reported complications after CF plate fixation for trauma fractures

In the upper extremity, seven studies evaluated CF plate fixation after traumatic proximal humerus fractures, involving a total of 391 patients [16,27,37,39,41,43,45]. The most frequently reported complications were soft tissue complications (n=52; 13%), including impingement between plate and acromion (n=18), rotator cuff lesions (n=18), adhesive capsulitis/shoulder stiffness (n=15), and an intra-articular bicep tendon rupture (n=1). Avascular humeral head necrosis/collapse was also frequently reported (n=27; 7%). In addition, structural complications were frequently observed (n=23; 6%), which consisted of secondary screw perforation (n=12), screws backing out (n=5), plate breakages (n=4), and malpositioning of the plate (n=2). Furthermore, secondary loss of reduction or resorption (>50%) of tuberosity (n=17; 4%), varus/valgus malalignment (n=6; 2%), head shaft malreduction (n=12; 3%), malreduction of the fracture (n=3; 1%), nonunions (n=2; 1%), secondary glenohumeral osteoarthritis (n=2; 1%), and an infection (n=1; <1%) were documented as unfavorable events. Eight studies reported on traumatic distal radius fractures, with a total of 291 patients [10,26,28,30,32-34,44]. Complications for this group included structural complications (n=6; 2%), soft tissue complications (n=5; 2%), and an infection (n=1; <1%).

Regarding the lower extremity, four studies assessed traumatic femur fracture fixations with CF plates, encompassing a total of 34 patients [29,40,42,46]. Complications observed in this group included one nonunion (n=1; 3%), and one structural complication (plate breakage, n=1; 3%). Furthermore, three studies evaluated ankle fractures treated with CF plates [31,35,38], involving 104 patients in total. The most frequently reported complications included infections (n=4; 4%), soft tissue complication (n=2; 2%), and one nonunion (n=1; 1%) (Table 5).

Reported complications after CF plate fixation for (impending) pathological fractures

In the upper extremity, two studies evaluated pathological fractures involving 14 humerus and 2 distal radius CF plates [36,47]. Most frequently reported humerus complications included infections (n=2; 14%), a structural complication (traumatic plate breakage, n=1; 7%), and a tumor progression (n=1; 7%) for which the plate was removed. No complications were reported for the 2 distal radius CF plates.

Regarding the lower extremity, five studies encompassing a total of 86 patients investigated femoral- and/or tibial (impending) pathological fractures [36,47-50]. Complications included structural failures (n=6; 7%), consisting of plate breakages without clear trauma (n=2), periprosthetic fractures (n=2), screw breakage (n=1), and screw backing out (n=1). Additionally, documented complications consisted of tumor progressions (n=5; 6%), infections (n=4; 5%), nonunion (n=3; 4%), aseptic loosening (n=2; 3%), pediatric complications (valgus deformations treated with eight-plates, n=2; 3%), and a soft tissue complication (wound dehiscence after radiotherapy treatment, n=1; 2%) (Table 5).

Studies comparing CF plates with metal plates

Eleven studies have compared CF plates to metal plates, all focusing on traumatic fractures [26-28,37-44]. Among these studies, three were RCTs and the remaining eight were prospective (n=4) or retrospective (n=4) comparative studies. This study hypothesized that CF plates display similar complication rates and clinical outcomes as metal plates for fracture fixation.

In the upper extremity, five studies examined CF plates compared to metal plates for humerus fractures. Firstly, Dey Hazra et al. conducted a retrospective study comparing range of motion after 2 years after fixation using CF plates (n=30) or titanium plates (n=35) [43]. The CF group demonstrated significantly improved forward flexion, internal rotation, and abduction compared to the titanium group, with similar patient reported outcomes. Secondly, Katthagen et al. prospectively enrolled 21 CF treated patients and matched them with 21 titanium treated patients [39]. Although functional outcomes were comparable after 12 months, the titanium group required more revisions due to screw perforations (5 vs 0; *p=0.048*). Thirdly, Schliemann et al. conducted a prospective study comparing clinical and radiographic results of CF treated patients (n=29) to those treated with metal locking plates (n=29) [37]. After 2 years, patients treated with CF plates achieved significantly better Constant Murley and Oxford Shoulder scores (*p=0.038* and *0.029*, respectively), with fewer cases with loss of reduction or varus deformity in the CF group. Fourthly, Padolino et al. conducted a retrospective study comparing clinical and radiographic outcomes of CF treated patients (n=21) to those treated with titanium plates (n=21) [41]. Shoulder mobility, clinical- and pain scores were similar in both patient groups after 2-years, while cortical thinning was significantly greater in the CF group (*p=0.0003*). Besides, the metal group exhibited a significantly higher rate of tuberosity resorption (*p=0.040*). Lastly, Ziegler et al. performed an RCT comparing CF plates (n=32) with titanium plates (n=31), but reported no clinical or radiological differences after 6-months follow-up [27]. For distal radius fractures, three comparative studies consistently demonstrated similar clinical and radiological outcomes during follow-up evaluations spanning 2 weeks to 3 years [26,28,44].

In the lower extremity, two studies evaluated CF and metal plates for distal femur fractures. Mitchell et al. compared CF plates (n=11) with stainless steel plates (n=11), observing a trend towards better outcomes in the CF plate group, including less nonunion, less structural failures, and less reoperations (9% vs 36%; 0% vs 18%; and 9% vs 36%, respectively) [40]. Byun et al. also compared CF (n=10) with stainless steel (n=21), noting better callus formation at 3 months, although this effect diminished at 6 months [42]. Regarding ankle fractures, Guzzini et al. compared CF plates (n=47) with stainless steel plates (n=41), reporting no significant differences in terms of pain, radiographic and clinical outcomes at 6-, 12- and 24-month follow-up evaluations [38] (Table 5).

7

Discussion

As hypothesized, the findings of this systematic review indicate that utilization of CF plates for the fixation of traumatic and (impending) pathological fractures is associated with a comparable incidence of complications and clinical outcomes to conventional metal plates. CF implants have gained increasing interest due to their potential advantages over metal implants. These advantages include radiolucency which allows for improved visualization of bone healing and early detection of tumor recurrence, ensuring timely interventions if necessary. The absence of metallic artifacts on radiographic imaging enables more precise postoperative radiotherapy planning. Other advantages include reduced stress shielding which potentially leads to better bone quality, and the absence of cold welding which facilitates easier removal [1-6,8,10]. The reported complication data can serve as a valuable benchmark for clinicians and patients, helping manage expectations during CF plate treatment. Although existing evidence suggests CF plates are a viable addition to the surgeons' armamentarium, the quality of current evidence is moderate to weak. Hence, recommendations of utilizing CF plates instead of conventional metal plates should be done with caution.

Adoption of CF plates as standard care for fracture fixation may face challenges due to the well-established use of conventional metal plates and the surgeons' extensive training and experience with these conventional plates [51]. New technologies are often associated with a learning curve, as performance tends to improve over time [52,53]. Nevertheless, the surgical procedure in terms of operation time and accuracy of implant position was similar in CF plates compared to metal plates [44,45]. Moreover, comparable rates of reported complications suggest that implementation of CF plates does not necessitate additional training. Costs of innovations are another important factor for implementation. Although there is a lack of cost-effectiveness studies for CF plates, a recent study comparing CF nails to metal nails showed comparable cost profiles [54]. Yet, long-term evidence on safety and effectiveness needs to be further investigated before adaptation on a large scale is feasible. Rotini et al. and Tarallo et al. both described intraoperative plate breakages at an oval screw hole in the first-generation of CF plates [10,16]. This issue was not reported in more recent studies. Still, one of the drawbacks of CF is the inability to bend the plate to match the patient's surface anatomy during surgery. Therefore, good preoperative planning is recommended when using these implants. Importantly, patients should be involved in the decision making and evaluation of implant material, and other osteosynthesis methods, such as intramedullary nailing, should be considered before definitive treatment [55,56].

Three systematic reviews have previously evaluated CF plates for trauma fracture fixation. Firstly, Saracco et al. included seven studies on distal radius fractures, and reported CF as a potential alternative to conventional metal plates [12]. Secondly, Theivendran et al. evaluated CF fixation in a broader population with small improvements in functional recovery of CF plates after humerus fractures, while there was insufficient evidence to support its widespread use [13]. Thirdly, Choloros et al. (9 studies, 361 patients) states that, considering their high

union rates in extremity fracture fixation, CF seems to be a valid alternative to conventional metal plating [11]. Our systematic review (27 studies, 1297 patients), which also included pathological fractures, aligns with these previous results, and reported comparable material specific complications to their metal counterparts. However, high quality RCT's with long-term follow-up are strongly recommended to provide additional evidence supporting the use of CF plates, their hypothesized advantages, and possible contra-indications.

Limitations

This systematic review has several limitations. First, its quality is inherently related to the quality of the included studies. Level I or II comparative studies were limited, which represents a major limitation. In general, Level III and IV studies are more prone to selection bias (related to patient selection and/or uncontrolled confounders). The moderate to weak outcomes of the risk of bias assessment and GRADE approach to rate quality of evidence reflected our methodological concerns. However, all studies were still included because we wanted to provide a thorough overview of all available literature. Second, the lack of high-quality studies comparing CF and metal plates was a notable limitation. Especially for (impending) pathological fractures the absence of comparative studies is a drawback which invites future research. Third, due to the lack of homogenous (comparative) studies and heterogeneity in patient populations, cancer types, and complications, a meta-analysis was not performed. Pooling results with data on different complications and types of trauma or cancers would yield results with limited clinical validity. Fourth, there was a lack of clarity between minor and major (complications requiring surgical) interventions, which also limited our reporting about complications. Lastly, most of the included studies only reported short- or mid-term follow-up results, which hampers our ability to draw conclusions on the long-term safety and effectiveness of CF plates. Further research is needed to generate high-quality evidence on the long-term safety and effectiveness of CF plates compared to metal plates. Nevertheless, this review provides a comprehensive overview with a complete up-to-date summary on the complication profile of CF plates in traumatic and (impending) pathological fractures.

Conclusion

This systematic review hypothesized that CF plates display similar complication rates and clinical outcomes as metal plates for fracture fixation. Based on the available evidence, this systematic review concludes that CF plates are a viable alternative to metal plates for fracture fixation, without increased material-specific complications. However, more high-quality studies are needed to strengthen the evidence, especially for (impending) pathological fractures. In the meantime, the study's complication data can serve as a valuable benchmark for clinicians and patients, helping manage expectations during CF plate treatment.

References

1.	Gaspar, N.; Hawkins, D.S.; Dirksen, U.; Lewis, I.J.; Ferrari, S.; Le Deley, M.C.; Kovar, H.; Grimer, R.; Whelan, J.; Claude, L., et al. Ewing Sarcoma: Current Management and Future Approaches Through Collaboration. *J Clin Oncol* **2015**, *33*, 3036-3046, doi:10.1200/jco.2014.59.5256.

2.	Baidya, K.P.; Ramakrishna, S.; Rahman, M.; Ritchie, A. Quantitative radiographic analysis of fiber reinforced polymer composites. *J Biomater Appl* **2001**, *15*, 279-289, doi:10.1106/bklq-e2yg-d2la-rg3r.

3.	Feerick, E.M.; Kennedy, J.; Mullett, H.; FitzPatrick, D.; McGarry, P. Investigation of metallic and carbon fibre PEEK fracture fixation devices for three-part proximal humeral fractures. *Med Eng Phys* **2013**, *35*, 712-722, doi:10.1016/j.medengphy.2012.07.016.

4.	Hak, D.J.; Mauffrey, C.; Seligson, D.; Lindeque, B. Use of carbon-fiber-reinforced composite implants in orthopedic surgery. *Orthopedics* **2014**, *37*, 825-830, doi:10.3928/01477447-20141124-05.

5.	Takayanagi, A.; Siddiqi, I.; Ghanchi, H.; Lischalk, J.; Vrionis, F.; Ratliff, J.; Bilsky, M.; Hariri, O.R. Radiolucent Carbon Fiber-Reinforced Implants for Treatment of Spinal Tumors-Clinical, Radiographic, and Dosimetric Considerations. *World Neurosurg* **2021**, *152*, 61-70, doi:10.1016/j.wneu.2021.05.100.

6.	Tedesco, G.; Gasbarrini, A.; Bandiera, S.; Ghermandi, R.; Boriani, S. Composite PEEK/Carbon fiber implants can increase the effectiveness of radiotherapy in the management of spine tumors. *J Spine Surg* **2017**, *3*, 323-329, doi:10.21037/jss.2017.06.20.

7.	Depauw, N.; Pursley, J.; Lozano-Calderon, S.A.; Patel, C.G. Evaluation of Carbon Fiber and Titanium Surgical Implants for Proton and Photon Therapy. *Pract Radiat Oncol* **2023;13:256-262**, 10.1016/j.prro.2023.01.009, doi:10.1016/j.prro.2023.01.009.

8.	Mugnai, R.; Tarallo, L.; Capra, F.; Catani, F. Biomechanical comparison between stainless steel, titanium and carbon-fiber reinforced polyetheretherketone volar locking plates for distal radius fractures. *Orthop Traumatol Surg Res* **2018**, *104*, 877-882, doi:10.1016/j.otsr.2018.05.002.

9.	Bagheri, Z.S.; Tavakkoli Avval, P.; Bougherara, H.; Aziz, M.S.; Schemitsch, E.H.; Zdero, R. Biomechanical analysis of a new carbon fiber/flax/epoxy bone fracture plate shows less stress shielding compared to a standard clinical metal plate. *J Biomech Eng* **2014**, *136*, 091002, doi:10.1115/1.4027669.

10.	Tarallo, L.; Giorgini, A.; Novi, M.; Zambianchi, F.; Porcellini, G.; Catani, F. Volar PEEK plate for distal radius fracture: analysis of adverse events. *Eur J Orthop Surg Traumatol* **2020**, *30*, 1293-1298, doi:10.1007/s00590-020-02701-7.

11.	Chloros, G.D.; Prodromidis, A.D.; Wilson, J.; Giannoudis, P.V. Fracture fixation in extremity trauma with carbon fiber-reinforced polyetheretherketone (CFR-PEEK) plates: evidence today. *European Journal of Trauma and Emergency Surgery* **2022**, *48*, 2387-2406, doi:10.1007/s00068-021-01778-x.

12.	Saracco, M.; Fulchignoni, C.; Velluto, C.; Rocchi, L. SAFETY AND RELIABILITY OF CARBON-PEEK PLATE FOR THE TREATMENT OF DISTAL RADIUS FRACTURES: A REVIEW OF THE LITERATURE. *Orthop Rev (Pavia)* **2021**, *13*, 28362, doi:10.52965/001c.28362.

13.	Theivendran, K.; Arshad, F.; Hanif, U.K.; Reito, A.; Griffin, X.; Foote, C.J. Carbon fibre reinforced PEEK versus traditional metallic implants for orthopaedic trauma surgery: A systematic review. *J Clin Orthop Trauma* **2021**, *23*, 101674, doi:10.1016/j.jcot.2021.101674.

14.	Bagheri, Z.S.; El Sawi, I.; Schemitsch, E.H.; Zdero, R.; Bougherara, H. Biomechanical properties of an advanced new carbon/flax/epoxy composite material for bone plate applications. *J Mech Behav Biomed Mater* **2013**, *20*, 398-406, doi:10.1016/j.jmbbm.2012.12.013.

15.	Wilson, W.K.; Morris, R.P.; Ward, A.J.; Carayannopoulos, N.L.; Panchbhavi, V.K. Torsional Failure of Carbon Fiber Composite Plates Versus Stainless Steel Plates for Comminuted Distal Fibula Fractures. *Foot Ankle Int* **2016**, *37*, 548-553, doi:10.1177/1071100715625291.

16. Rotini, R.; Cavaciocchi, M.; Fabbri, D.; Bettelli, G.; Catani, F.; Campochiaro, G.; Fontana, M.; Colozza, A.; De Biase, C.F.; Ziveri, G., et al. Proximal humeral fracture fixation: multicenter study with carbon fiber peek plate. *Musculoskelet Surg* **2015**, *99 Suppl 1*, S1-8, doi:10.1007/s12306-015-0371-2.

17. Goudriaan, W.A.; Tordoir, R.L.; Broekhuis, D.; van der Wal, R.J.P. Early Failure of a Carbon-Fiber-Reinforced Polyetheretherketone Distal Femur Plate: A Case Report. *JBJS Case Connect* **2020**, *10*, e20.00041, doi:10.2106/jbjs.Cc.20.00041.

18. Page, M.J.; McKenzie, J.E.; Bossuyt, P.M.; Boutron, I.; Hoffmann, T.C.; Mulrow, C.D.; Shamseer, L.; Tetzlaff, J.M.; Akl, E.A.; Brennan, S.E., et al. The PRISMA 2020 statement: an updated guideline for reporting systematic reviews. *Bmj* **2021**, *372*, n71, doi:10.1136/bmj.n71.

19. Institute.;, T.J.B. JBI Critical Appraisal Checklist for Case Reports. Availabe online: https://jbi.global/sites/default/files/2019-05/JBI_Critical_Appraisal-Checklist_for_Case_Reports2017_0.pdf (accessed on

20. Sterne, J.A.; Hernán, M.A.; Reeves, B.C.; Savović, J.; Berkman, N.D.; Viswanathan, M.; Henry, D.; Altman, D.G.; Ansari, M.T.; Boutron, I., et al. ROBINS-I: a tool for assessing risk of bias in non-randomised studies of interventions. *Bmj* **2016**, *355*, i4919, doi:10.1136/bmj.i4919.

21. Sterne, J.A.C.; Savović, J.; Page, M.J.; Elbers, R.G.; Blencowe, N.S.; Boutron, I.; Cates, C.J.; Cheng, H.Y.; Corbett, M.S.; Eldridge, S.M., et al. RoB 2: a revised tool for assessing risk of bias in randomised trials. *Bmj* **2019**, *366*, l4898, doi:10.1136/bmj.l4898.

22. Guyatt, G.H.; Oxman, A.D.; Vist, G.E.; Kunz, R.; Falck-Ytter, Y.; Alonso-Coello, P.; Schünemann, H.J. GRADE: an emerging consensus on rating quality of evidence and strength of recommendations. *Bmj* **2008**, *336*, 924-926, doi:10.1136/bmj.39489.470347.AD.

23. Doyle, D.J.; Hendrix, J.M.; Garmon, E.H. American Society of Anesthesiologists Classification. In *StatPearls*, 2023.

24. Sundfeldt, M.; Carlsson, L.V.; Johansson, C.B.; Thomsen, P.; Gretzer, C. Aseptic loosening, not only a question of wear: a review of different theories. *Acta Orthop* **2006**, *77*, 177-197, doi:10.1080/17453670610045902.

25. Liverani, E.; Rogati, G.; Pagani, S.; Brogini, S.; Fortunato, A.; Caravaggi, P. Mechanical interaction between additive-manufactured metal lattice structures and bone in compression: implications for stress shielding of orthopaedic implants. *Journal of the Mechanical Behavior of Biomedical Materials* **2021**, *121*, 104608, doi:https://doi.org/10.1016/j.jmbbm.2021.104608.

26. Perugia, D.; Guzzini, M.; Mazza, D.; Iorio, C.; Civitenga, C.; Ferretti, A. Comparison between Carbon-Peek volar locking plates and titanium volar locking plates in the treatment of distal radius fractures. *Injury* **2017**, *48 Suppl 3*, S24-s29, doi:10.1016/s0020-1383(17)30653-8.

27. Ziegler, P.; Maier, S.; Stöckle, U.; Gühring, M.; Stuby, F.M. The Treatment of Proximal Humerus Fracture Using Internal Fixation with Fixed-angle Plates. *Dtsch Arztebl Int* **2019**, *116*, 757-763, doi:10.3238/arztebl.2019.0757.

28. Berger-Groch, J.; Stodtmeister, A.C.; Petersen, J.P.; Hoffmann, M. Palmar plating of distal radius fractures: 3-year follow-up with titanium and PEEK plates give similar outcomes. *Acta Orthop Belg* **2021**, *87*, 521-527.

29. Baker, D.; Kadambande, S.S.; Alderman, P.M. Carbon fibre plates in the treatment of femoral periprosthetic fractures. *Injury* **2004**, *35*, 596-598, doi:10.1016/j.injury.2003.10.014.

30. Di Maggio, B.; Sessa, P.; Mantelli, P.; Maniscalco, P.; Rivera, F.; Calori, G.M.; Bisogno, L.; Scaravilli, G.; Caforio, M. PEEK radiolucent plate for distal radius fractures: multicentre clinical results at 12 months follow up. *Injury* **2017**, *48 Suppl 3*, S34-s38, doi:10.1016/s0020-1383(17)30655-1.

31. Pinter, Z.W.; Smith, K.S.; Hudson, P.W.; Jones, C.W.; Hadden, R.; Elattar, O.; Shah, A. A Retrospective Case Series of Carbon Fiber Plate Fixation of Ankle Fractures. *Foot Ankle Spec* **2018**, *11*, 223-229, doi:10.1177/1938640017718343.

7

32. Allemann, F.; Halvachizadeh, S.; Rauer, T.; Pape, H.C. Clinical outcomes after carbon-plate osteosynthesis in patients with distal radius fractures. *Patient Saf Surg* **2019**, *13*, 30, doi:10.1186/s13037-019-0210-8.

33. Guzzini, M.; Lupariello, D.; Lanzetti, R.M.; Mazza, D.; Ferretti, A. Preliminary experience with triangular CarboFix "Piccolo" Distal Radius Plate in wrist fractures. Clinical and radiological results. *Acta Biomed* **2018**, *90*, 61-66, doi:10.23750/abm.v90i1-S.7697.

34. Paracuollo, M.; Coscione, A.V.; Coppola, A.; Pellegrino, G.; Pellegrino, A. Clinical and radiographic outcomes of distal radius fracture treatment with Carbon-Fiber-Reinforced- Polymer Volar Plates (CFRPEEK): analysis of 40 cases. *Lo Scalpello - Journal* **2022**, *36*, 185-190, doi:10.36149/0390-5276-224.

35. Caforio, M.; Perugia, D.; Colombo, M.; Calori, G.M.; Maniscalco, P. Preliminary experience with Piccolo Composite™, a radiolucent distal fibula plate, in ankle fractures. *Injury* **2014**, *45 Suppl 6*, S36-38, doi:10.1016/j.injury.2014.10.020.

36. Rijs, Z.; Weekhout, A.; Lozano-Calderon, S.A.; Groot, O.Q.; Berner, E.; Merchan, N.; Yeung, C.M.; Oliveira, V.; Bianchi, G.; Staals, E., et al. Complications of patients with bone tumors treated with carbon-fiber plates: an international multicenter study. *Scientific Reports* **2022**, *12*, 18969, doi:10.1038/s41598-022-23519-9.

37. Schliemann, B.; Hartensuer, R.; Koch, T.; Theisen, C.; Raschke, M.J.; Kösters, C.; Weimann, A. Treatment of proximal humerus fractures with a CFR-PEEK plate: 2-year results of a prospective study and comparison to fixation with a conventional locking plate. *J Shoulder Elbow Surg* **2015**, *24*, 1282-1288, doi:10.1016/j.jse.2014.12.028.

38. Guzzini, M.; Lanzetti, R.M.; Lupariello, D.; Morelli, F.; Princi, G.; Perugia, D.; Ferretti, A. Comparison between carbon-peek plate and conventional stainless steal plate in ankle fractures. A prospective study of two years follow up. *Injury* **2017**, *48*, 1249-1252, doi:10.1016/j.injury.2017.03.035.

39. Katthagen, J.C.; Ellwein, A.; Lutz, O.; Voigt, C.; Lill, H. Outcomes of proximal humeral fracture fixation with locked CFR-PEEK plating. *Eur J Orthop Surg Traumatol* **2017**, *27*, 351-358, doi:10.1007/s00590-016-1891-7.

40. Mitchell, P.M.; Lee, A.K.; Collinge, C.A.; Ziran, B.H.; Hartley, K.G.; Jahangir, A.A. Early Comparative Outcomes of Carbon Fiber-Reinforced Polymer Plate in the Fixation of Distal Femur Fractures. *J Orthop Trauma* **2018**, *32*, 386-390, doi:10.1097/bot.0000000000001223.

41. Padolino, A.; Porcellini, G.; Guollo, B.; Fabbri, E.; Kiran Kumar, G.N.; Paladini, P.; Merolla, G. Comparison of CFR-PEEK and conventional titanium locking plates for proximal humeral fractures: a retrospective controlled study of patient outcomes. *Musculoskelet Surg* **2018**, *102*, 49-56, doi:10.1007/s12306-018-0562-8.

42. Byun, S.E.; Vintimilla, D.R.; Bedeir, Y.H.; Dean, C.S.; Parry, J.A.; Hak, D.J.; Mauffrey, C. Evaluation of callus formation in distal femur fractures after carbon fiber composite versus stainless steel plate fixation. *Eur J Orthop Surg Traumatol* **2020**, *30*, 1103-1107, doi:10.1007/s00590-020-02681-8.

43. Dey Hazra, R.O.; Szewczyk, K.; Ellwein, A.; Blach, R.; Jensen, G.; Kühnapfel, A.; Lill, H.; Warnhoff, M. Minimum 2-year results of the second-generation CFR-PEEK locking plate on the proximal humeral fracture. *Eur J Orthop Surg Traumatol* **2022**, *33*, 1307-1314, doi:10.1007/s00590-022-03298-9.

44. Behrendt, P.; Kruse, E.; Klüter, T.; Fitschen-Oestern, S.; Weuster, M.; Menzdorf, L.; Finn, J.; Varoga, D.; Seekamp, A.; Müller, M., et al. Winkelstabile karbonverstärkte Polymerkompositplatte zur Versorgung einer distalen Radiusfraktur. *Der Unfallchirurg* **2017**, *120*, 139-146, doi:10.1007/s00113-015-0088-6.

45. Kimmeyer, M.; Schmalzl, J.; Rentschler, V.; Jessen, M.; Gerhardt, C.; Lehmann, L.J. Functional results and unfavorable events after treatment of proximal humerus fractures using a new locking plate system. *BMC Musculoskelet Disord* **2023**, *24*, 63, doi:10.1186/s12891-023-06176-5.

46. Mellon, M.B. Late recognition of an early catastrophic failure of a carbon fiber reinforced distal femoral plate: A case report. *Trauma Case Rep* **2021**, *34*, 100493, doi:10.1016/j.tcr.2021.100493.

47. Laux, C.J.; Hodel, S.M.; Farshad, M.; Müller, D.A. Carbon fibre/polyether ether ketone (CF/PEEK) implants in orthopaedic oncology. *World J Surg Oncol* **2018**, *16*, 241, doi:10.1186/s12957-018-1545-9.

48. Barnds, B.; Johnson, A.; Rosenthal, H.; Tilley, M. Ipsilateral rotational double-barrel fibula autograft for limb salvage in a pediatric patient with lower extremity intramedullary osteosarcoma: A case report. *Microsurgery* **2020**, *40*, 247-251, doi:10.1002/micr.30487.

49. Zoccali, C.; Careri, S.; Attala, D.; Florio, M.; Milano, G.M.; Giordano, M. A New Proximal Femur Reconstruction Technique after Bone Tumor Resection in a Very Small Patient: An Exemplificative Case. *Children (Basel)* **2021**, *8*, doi:10.3390/children8060442.

50. Yeung, C.M.; Bhashyam, A.R.; Patel, S.S.; Ortiz-Cruz, E.; Lozano-Calderón, S.A. Carbon Fiber Implants in Orthopaedic Oncology. *J Clin Med* **2022**, *11*, doi:10.3390/jcm11174959.

51. Uhthoff, H.K.; Poitras, P.; Backman, D.S. Internal plate fixation of fractures: short history and recent developments. *J Orthop Sci* **2006**, *11*, 118-126, doi:10.1007/s00776-005-0984-7.

52. Sarpong, N.O.; Herndon, C.L.; Held, M.B.; Neuwirth, A.L.; Hickernell, T.R.; Geller, J.A.; Cooper, H.J.; Shah, R.P. What Is the Learning Curve for New Technologies in Total Joint Arthroplasty? A Review. *Curr Rev Musculoskelet Med* **2020**, *13*, 675-679, doi:10.1007/s12178-020-09671-7.

53. Ramsay, C.R.; Grant, A.M.; Wallace, S.A.; Garthwaite, P.H.; Monk, A.F.; Russell, I.T. Assessment of the learning curve in health technologies. A systematic review. *Int J Technol Assess Health Care* **2000**, *16*, 1095-1108, doi:10.1017/s0266462300103149.

54. Herzog, L.N.; Traven, S.A.; Walton, Z.J.; Leddy, L.R. The Use of Carbon Fiber Implants for Impending or Existing Pathologic Fractures. *J Orthop Trauma* **2022**, *36*, e260-e264, doi:10.1097/bot.0000000000002320.

55. de Mik, S.M.L.; Stubenrouch, F.E.; Balm, R.; Ubbink, D.T. Systematic review of shared decision-making in surgery. *Br J Surg* **2018**, *105*, 1721-1730, doi:10.1002/bjs.11009.

56. Woudstra, K.; Tummers, M.; Rovers, M.M.; Reuzel, R. Innovators' views on involving users and patients in surgical device development: a qualitative interview study. *BMJ Open* **2021**, *11*, e050801, doi:10.1136/bmjopen-2021-050801.

7

Appendix A. Search strategy PubMed, search strategies other databases and their results are available upon request.

Fracture; 132 results in PubMed from database inception up until 20 June 2023.

(("carbon fiber reinforced polyetheretherketon plate"[tw] OR "carbon fiber reinforced polyetheretherketon plates"[tw] OR "carbon fiber reinforced polyetheretherketon"[tw] OR "carbon fiber reinforced polyether ether ketone"[tw] OR "carbon fiber reinforced poly ether ether ketone"[tw] OR "Carbon fiber reinforced poly etheretherketone"[tw] OR "CFR PEEK plates"[tw] OR "CFR PEEK plate"[tw] OR "CFR PEEK"[tw] OR "CFR PEEK*"[tw] OR "CFRPEEK"[tw] OR "CFRPEEK*"[tw] OR "Carbon Fiber Reinforced PEEK"[tw] OR "carbon peek"[tw] OR "Carbon fiber plates"[tw] OR "Carbon fiber plate"[tw] OR "CF plates"[tw] OR "CF plate"[tw] OR "Carbon fiber implants""[tw] OR "Carbon fiber implant"[tw] OR "CF implants"[tw] OR "CF implant"[tw] OR (("carbon fiber*"[tw] OR "carbonfiber*"[tw] OR "CFR"[tw]) AND ("polyetheretherketon*"[tw] OR "polyether ether keton*"[tw] OR "poly ether ether ketone"[tw] OR "poly etheretherketone"[tw] OR "PEEK"[tw])) OR (("Carbon Fiber"[Mesh] OR "Carbon"[Mesh] OR "carbon fiber"[tw] OR "carbon fibers"[tw] OR "carbon fibre"[tw] OR "carbon fibres"[tw]) AND ("Bone Plates"[Mesh] OR "bone plate"[tw] OR "bone plates"[tw] OR "bone plating"[tw] OR "plate"[ti] OR "plates"[ti]))) AND ("Fractures, Bone"[Mesh] OR "Fractures"[tw] OR "Fracture"[tw] OR "Fractur*"[tw] OR "break"[tw] OR "breaks"[tw] OR "broken"[tw] OR "broke"[tw] OR "malunion*"[tw] OR "mal union*"[tw] OR "nonunion*"[tw] OR "non union*"[tw]) NOT ("Animals"[mesh] NOT "Humans"[mesh]) AND english[la]).

Bone tumor; 44 results in PubMed from database inception up until 20 June 2023.

(("carbon fiber reinforced polyetheretherketon plate"[tw] OR "carbon fiber reinforced polyetheretherketon plates"[tw] OR "carbon fiber reinforced polyetheretherketon"[tw] OR "carbon fiber reinforced polyether ether ketone"[tw] OR "carbon fiber reinforced poly ether ether ketone"[tw] OR "Carbon fiber reinforced poly etheretherketone"[tw] OR "CFR PEEK plates"[tw] OR "CFR PEEK plate"[tw] OR "CFR PEEK"[tw] OR "CFR PEEK*"[tw] OR "CFRPEEK"[tw] OR "CFRPEEK*"[tw] OR "Carbon Fiber Reinforced PEEK"[tw] OR "carbon peek"[tw] OR "Carbon fiber plates"[tw] OR "Carbon fiber plate"[tw] OR "CF plates"[tw] OR "CF plate"[tw] OR "Carbon fiber implants"[tw] OR "Carbon fiber implant"[tw] OR "CF implants"[tw] OR "CF implant"[tw] OR (("carbon fiber*"[tw] OR "carbonfiber*"[tw] OR "CFR"[tw]) AND ("polyetheretherketon*"[tw] OR "polyether ether keton*"[tw] OR "poly ether ether ketone"[tw] OR "poly etheretherketone"[tw] OR "PEEK"[tw])) OR (("Carbon Fiber"[Mesh] OR "Carbon"[Mesh] OR "carbon fiber"[tw] OR "carbon fibers"[tw] OR "carbon fibre"[tw] OR "carbon fibres"[tw]) AND ("Bone Plates"[Mesh] OR "bone plate"[tw] OR "bone plates"[tw] OR "bone plating"[tw] OR "plate"[ti] OR "plates"[ti]))) AND ("Bone Neoplasms"[Mesh] OR "Neoplasms, Bone Tissue"[Mesh] OR "Bone Neoplasm"[tw] OR "Bone Neoplasms"[tw] OR "Bone Malignancy"[tw] OR "Bone Malignancies"[tw] OR "Orthopaedic oncology"[tw] OR "Orthopedic oncology"[tw] OR "Orthopedic tumor"[tw] OR "Orthopedic tumors"[tw] OR "Orthopaedic tumor"[tw] OR "Orthopaedic tumors"[tw] OR

"Orthopaedic tumour"[tw] OR "Orthopaedic tumours"[tw] OR "Bone tumor"[tw] OR "Bone tumors"[tw] OR "Bone tumour"[tw] OR "Bone tumours"[tw] OR "Bone cancer"[tw] OR "Bone cancers"[tw] OR "Adamantinoma"[tw] OR "Adamantinomas"[tw] OR "Osteochondroma"[tw] OR "Osteochondromas"[tw] OR "Giant cell tumor"[tw] OR "Giant cell tumors"[tw] OR "Giant cell tumour"[tw] OR "Giant cell tumours"[tw] OR "Osteoblastoma"[tw] OR "Osteoblastomas"[tw] OR "Ewing sarcoma"[tw] OR "Ewing sarcomas"[tw] OR "Ewings sarcomas"[tw] OR "Ewings sarcoma"[tw] OR "Ewing's sarcomas"[tw] OR "Ewing's sarcoma"[tw] OR "Soft tissue sarcoma"[tw] OR "Soft tissue sarcomas"[tw] OR "Osteosarcoma"[tw] OR "Osteosarcomas"[tw] OR "Femoral Neoplasm"[tw] OR "Femoral Neoplasms"[tw] OR "Femoral Tumor"[tw] OR "Femoral Tumors"[tw] OR "Femoral Tumour"[tw] OR "Femoral Tumours"[tw] OR "Jaw Cancer"[tw] OR "Jaw Malignancies"[tw] OR "Jaw Malignancy"[tw] OR "Jaw Neoplasm"[tw] OR "Jaw Neoplasms"[tw] OR "Jaw Tumor"[tw] OR "Jaw Tumors"[tw] OR "Jaw Tumour"[tw] OR "Jaw Tumours"[tw] OR "Mandibular Cancer"[tw] OR "Mandibular Malignancies"[tw] OR "Mandibular Malignancy"[tw] OR "Mandibular Neoplasm"[tw] OR "Mandibular Neoplasms"[tw] OR "Mandibular Tumor"[tw] OR "Mandibular Tumors"[tw] OR "Mandibular Tumour"[tw] OR "Mandibular Tumours"[tw] OR "Maxillary Cancer"[tw] OR "Maxillary Cancers"[tw] OR "Maxillary Malignancies"[tw] OR "Maxillary Malignancy"[tw] OR "Maxillary Neoplasm"[tw] OR "Maxillary Neoplasms"[tw] OR "Maxillary Tumor"[tw] OR "Maxillary Tumors"[tw] OR "Maxillary Tumour"[tw] OR "Maxillary Tumours"[tw] OR "Orbital Cancer"[tw] OR "Orbital Cancers"[tw] OR "Orbital Malignancies"[tw] OR "Orbital Malignancy"[tw] OR "Orbital Neoplasm"[tw] OR "Orbital Neoplasms"[tw] OR "Orbital Tumor"[tw] OR "Orbital Tumors"[tw] OR "Orbital Tumour"[tw] OR "Orbital Tumours"[tw] OR "Palatal Cancer"[tw] OR "Palatal Cancers"[tw] OR "Palatal Malignancies"[tw] OR "Palatal Neoplasm"[tw] OR "Palatal Neoplasms"[tw] OR "Palatal Tumor"[tw] OR "Palatal Tumors"[tw] OR "Palatal Tumour"[tw] OR "Palatal Tumours"[tw] OR "Skull Base Cancer"[tw] OR "Skull Base Cancers"[tw] OR "Skull Base Malignancies"[tw] OR "Skull Base Malignancy"[tw] OR "Skull Base Neoplasm"[tw] OR "Skull Base Neoplasms"[tw] OR "Skull Base Tumor"[tw] OR "Skull Base Tumors"[tw] OR "Skull Base Tumour"[tw] OR "Skull Base Tumours"[tw] OR "Skull Neoplasm"[tw] OR "Skull Neoplasms"[tw] OR "Skull Tumor"[tw] OR "Skull Tumors"[tw] OR "Skull Tumour"[tw] OR "Skull Tumours"[tw] OR "Spinal Cancer"[tw] OR "Spinal Malignancies"[tw] OR "Spinal Malignancy"[tw] OR "Spinal Neoplasm"[tw] OR "Spinal Neoplasms"[tw] OR "Spinal Tumor"[tw] OR "Spinal Tumors"[tw] OR "Spinal Tumour"[tw] OR "Spinal Tumours"[tw] OR "Spine Cancer"[tw] OR "Spine Cancers"[tw] OR "Spine Malignancy"[tw] OR "Spine Neoplasm"[tw] OR "Spine Neoplasms"[tw] OR "Spine Tumor"[tw] OR "Spine Tumors"[tw] OR "Spine Tumour"[tw] OR "Spine Tumours"[tw]) NOT ("Animals"[mesh] NOT "Humans"[mesh]) AND english[la]).

7

8

OUTCOMES OF LONG BONES TREATED WITH CARBON-FIBER NAILS FOR ONCOLOGIC INDICATIONS: INTERNATIONAL MULTI-INSTITUTIONAL STUDY

S.A. Lozano-Calderon[1], Z. Rijs[2], O.Q. Groot[1], M.W. Su[1], J.O. Werenski[1], N. Merchan[1], C.M. Yeung[1], A. Sodhi[1], E. Berner[1], V. Oliveira[3], G. Bianchi[4], E. Staals[4], D. Lana[4], D. Donati[4], O. Segal[5], S. Marone[6], R. Piana[6], S. De Meo[6], P. Pellegrino[6], N. Ratto[6], C. Zoccali[7], M. Scorianz[8], C. Tomai[8], G. Scoccianti[8], D.A. Campanacci[8], L. Andreani[9], S. de Franco[9], M. Boffano[10], M.P. Pensado[11], I.B. Ruiz[11], E.H. Moreno[11], E.J. Ortiz-Cruz[11,12], M.A.J. van de Sande[2]

[1] Massachusetts General Hospital | Harvard Medical School, United States of America
[2] Leiden University Medical Center, The Netherlands
[3] Oporto University Hospital Center, Portugal
[4] Istituto Ortopedico Rizzoli, Italy
[5] Tel Aviv Sourasky Medical Center, Israel
[6] Centro Traumatologico Ortopedico Torino, Italy
[7] Regina Elena National Cancer Institute, Italy
[8] Azienda Ospedaliera Universitaria Careggi, Italy
[9] University Hospital of Pisa, Italy
[10] Regina Margherita Children's Hospital, Italy
[11] La Paz University Hospital, Spain
[12] MD Anderson Cancer Center, Spain

Abstract

Background
Intramedullary nail fixation is commonly used for prophylactic stabilization of impending and fixation of complete pathological fractures of the long bones. However, metallic artifacts complicate imaging evaluation for bone healing or tumor progression and postoperative radiation planning. Carbon-fiber implants have gained popularity as an alternative, given their radiolucency and superior axial bending. This study evaluates incidences of mechanical and nonmechanical complications.

Methods
Adult patients (age 18 years and older) treated with carbon-fiber nails for impending/complete pathological long bone fractures secondary to metastases from 2013 to 2020 were analyzed for incidences and risk factors of mechanical and nonmechanical complications. Mechanical complications included aseptic screw loosening and structural failures of host bone and carbon-fiber implants. Deep infection and tumor progression were considered nonmechanical. Other complications/adverse events were also reported.

Results
A total of 239 patients were included; 47% were male, and 53% were female, with a median age of 68 (IQR, 59 to 75) years. Most common secondary metastases were related to breast cancer (19%), lung cancer (19%), multiple myeloma (18%), and sarcoma (13%). In total, 17 of 30 patients with metastatic sarcoma received palliative intramedullary nail fixation for impending/complete pathological fractures, and 13 of 30 received prophylactic nail stabilization of bone radiated preoperatively to manage juxta-osseous soft-tissue sarcomas, where partial resection of the periosteum or bone was necessary for negative margin resection. 33 (14%) patients had complications. Mechanical failures included 4 (1.7%) structural host bone failures, 7 (2.9%) implant structural failures, and 1 (0.4%) aseptic loosening of distal locking screws. Nonmechanical failures included 8 (3.3%) peri-implant infections and 15 (6.3%) tumor progressions with implant contamination. The 90-day and 1-year mortalities were 28% (61/239) and 53% (53/102), respectively. The literature reported comparable failure and mortality rates with conventional titanium treatment.

Conclusions
Carbon-fiber implants might be an alternative for treating impending and sustained pathological fractures secondary to metastatic bone disease. The seemingly comparable complication profile warrants further cohort studies comparing carbon-fiber and titanium nail complications.

Introduction

Intramedullary nail fixation has been a longstanding treatment for impending or complete pathologic fractures of the long bones secondary to metastatic bone disease [1-6]. With sustained increases in the lifespan of cancer patients with metastatic disease, the treatment of neoplastic pathologic fractures is gaining more importance as preservation of motion and function continues to become more needed in this patient population [1,6-9].

Recently, carbon-fiber (CF) has gained popularity as an alternative to conventional metal implants [10,11]. With good biocompatibility (referring to the ability to perform its desired function without eliciting any local or systemic adverse effects in the patient), low weight-to-strength ratio, and increased bending strength when compared to titanium, CF implants may be a more desirable treatment option for naturally unhealable pathologic fractures [10-14]. Additional benefits include CF's fatigue strength and closer modulus of elasticity to bone [15-17]. Its radiolucency and lack of scattering effect on MRI and CT are also appealing for imaging surveillance and theoretical treatment planning for postoperative radiation, as demonstrated in CF spinal implant papers (Figure 1) [10,13,18-20]. Although relatively high non-union rates were reported in a single center using 16 CF nails for diaphyseal correction osteotomy (11 limbs), shortening surgery (3 limbs), and diaphyseal closed tibia fractures (2 limbs), low non-union rates were reported in a multicenter study with 96 oncologic patients treated with CF plates [21,22]. As drawbacks, some argue that the lack of malleability makes using plates challenging in fracture care and question whether CF nails are more expensive than metal nails. However, costs are competitive with metal nails and bending of CF nails is often not necessary during surgery [23]. Despite the previously mentioned benefits, the literature is limited regarding complications, pitfalls, and pearls of using CF nails in metastatic cancer patients with osseous involvement. The present study is an early experience of the "Carbon-fiber International Collaboration Initiative" (CF-ICI) which includes 13 centers in Europe, the Middle East, the United Kingdom, and the United States, participating in an international, worldwide, prospective registry.

This study aims to assess implant complications categorized as structural and non-structural with their respective predictors concerning the use of CF femoral, tibial, and humeral nails for the management of impending or complete pathologic fractures of long bones secondary to metastatic bone disease or sarcoma treatment.

8
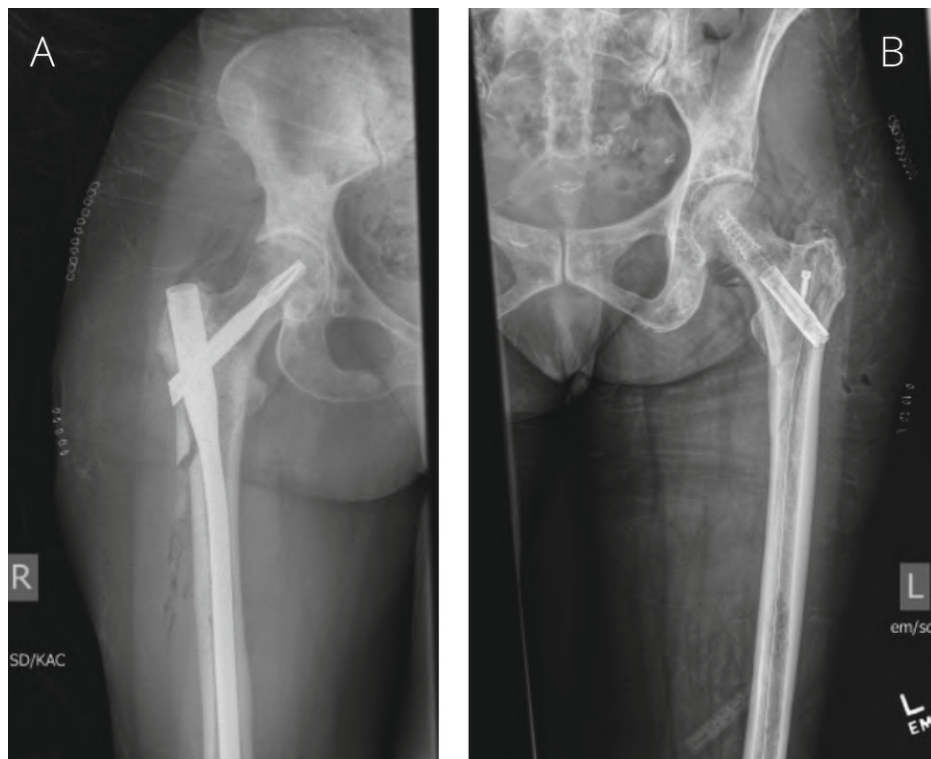
Figure 1. *A conventional titanium nail (A) and carbon-fiber nail (B) in the femur.*

Methods

Study design and setting

This is a multicenter, retrospective, international study approved by each of the 13 participating institutions' Institutional Review Boards. The data was collected from a prospective registry enrolling patients treated with CF implants. An online database created in Leiden (using Castor electronic data capture [EDC]), coordinated and hosted the prospective data registry for Europe, the Middle East, the United Kingdom, and the United States through data exchange agreements. This study adhered to the Strengthening Reporting of Observational Studies in Epidemiology (STROBE) guidelines [24]. None of the participating institutions received funding to support research focusing on CF implants. Investigators who have received fees as consultants or paid speakers declared their conflicts based on publication guidelines.

Participants/study subjects

Between 2013 and 2020, we included all adult patients (18 years or older) with impending or complete pathologic fractures to the long-bones secondary to metastatic bone disease,

with oligometastatic bone sarcoma or oligometastatic disease secondary to renal cell, breast, and papillary thyroid carcinoma who were treated with metastasectomy and reconstruction using a CF nail, and with soft tissue sarcomas treated with preoperative and/or postoperative radiation who required partial excision of bone or periosteum as part of the margin for oncologic treatment and were fixated prophylactically with a CF nail. Patients in the described groups were included in a registry that continues to prospectively include data to assess the long-term safety and effectiveness of CF implants. The choice of treatment was made by shared decision making between the patient and surgeon. In general, surgery was recommended for oncological patients with impending or actual pathological fractures, mechanical axial loading pain, and no response to radiation therapy or oral narcotic pain medication. The operating surgeon chose to use a CF plate instead of a megaprosthesis. Factors in the decision included tumor location and amount and quality of remaining bone available for intramedullary nail fixation. Exclusion criteria included patients younger than 18 years, surgery due to non-malignancy, and intramedullary fixation combined with any other surgical procedure of fixation, such as plates (Figures 2 and 3).
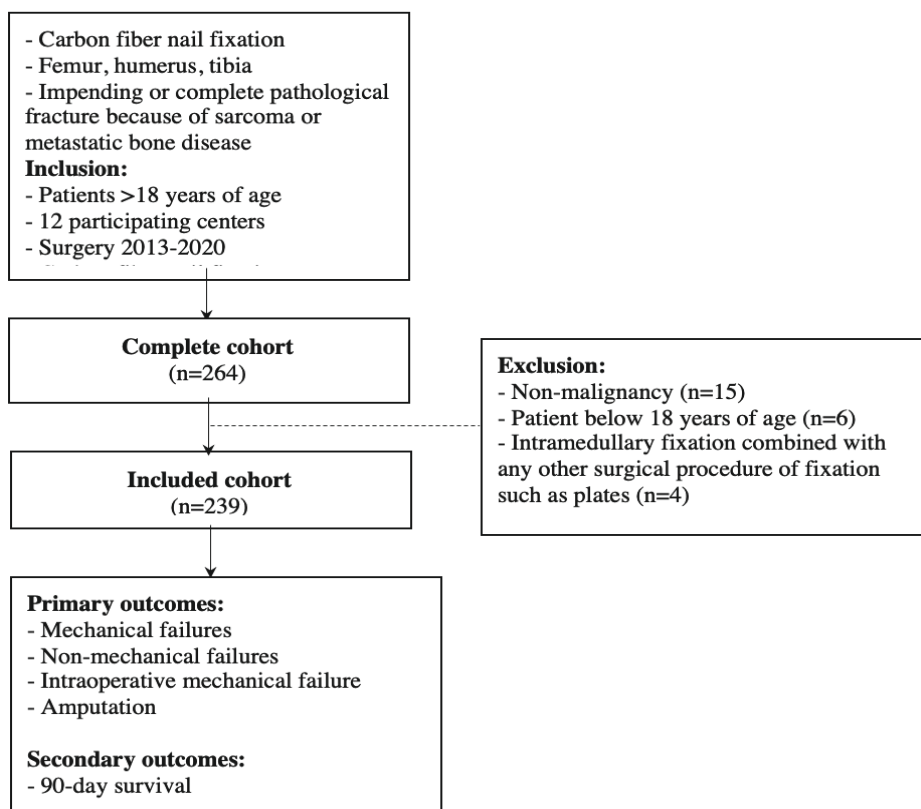
Figure 2. Flow diagram illustrating patient selection and outcomes.

8

Figure 3. *World map of all 13 participating institutions.*

Description of surgery

The choice of treatment was decided by mutual agreement between the patient and surgeon. The operating surgeon chose to use a CF nail. All patients with humeral lesions received the CarboFix long humeral nail, which is non-cannulated, 8.5mm in diameter, and has a locking mechanism consisting of two 4.5 mm proximal screws and up to three distal 3.5 mm screws. All patients with femoral lesions received the CarboFix long femoral nail with a trochanteric entry, which is cannulated and 11 to 12 mm in diameter and has a securing mechanism consisting of a 10.4 mm lag screw size 80 to 110 mm secured with a set screw and two distal femoral 4.0 mm screws. All patients treated with tibial nails received the CarboFix tibial nail, which is cannulated, 10 to 11 mm in diameter, and has a securing mechanism consisting of two proximal 5.0 mm screws, one 4.0 mm dynamic proximal screw, and three 4.0 mm distal locking screws. Most patients had two screws for distal fixation. Lateral or supine patient positioning varied depending on the surgeon's experience and preference. In general, surgery was recommended for patients with mechanical, axial-loading pain in the affected extremity, with no response to radiation therapy, or with high, oral-narcotic pain medication use. Patients with complete fractures were treated independently of previous symptomatology. At the 2-week, 6-week, 3-month, 6-month, and 1-year postoperative follow-ups, patients received clinical and radiographic evaluations (pending oncologic status). Patients were cleared for radiation therapy and/or chemotherapy 7 to 10 days after the surgical procedure. All patients were made weight bearing as tolerated after surgery.

Description of radiation therapy
The exact doses were not collected in this study because of protocol variation between institutions. Radiation oncology treatment was also not the focus of our investigation. Nevertheless, in general, patients with metastatic bone disease were treated with either 400 centigray (cGy) divided into 5 fractions or 300 cGy divided into 10 fractions. In patients treated for soft-tissue sarcomas, the radiation dose was 5,000-5,400 cGy divided into 25 fractions if delivered preoperatively or 6,000 cGy divided into 30 fractions if delivered postoperatively. Preoperative radiation patients that required a postoperative radiation boost, received a single dose between 1200 to 1600 cGy depending on preoperative radiation dose and tumor histology.

Outcome measures and explanatory variables
The primary outcome was measured by postoperative complications cataloged as mechanical or non-mechanical. Mechanical complications included[1] aseptic screw loosening,[2] structural failure of the host bone, such as peri-implant fractures or hip screw cut out,[3] and structural failures of the CF implant per se such as primary fracture of the implant or secondary to fracture nonunion or tumor progression. Non-mechanical complications included[4] deep infections requiring surgical treatment[5] and tumor progression with structural failure of the implant. Tumor progression causing implant failure, such as nail breakage, was counted as both, nonstructural failure (tumor progression) and structural failure, given that the implant ultimately broke. Complications related to implant use, such as superficial wound dehiscence, superficial wound infection, thromboembolic events, perioperative adverse events, and implant-use related deaths were also reported. The secondary outcome measures were 90-day and 1-year mortality by any cause after surgery.

The following clinical factors were obtained: age; sex; smoking status; American Society of Anesthesiologists (ASA) score; primary tumor type, prognosis (as classified by Katagiri, et al.[25]), and grade; additional bone metastases to surgical site; preoperative chemotherapy and/or radiation therapy; postoperative chemotherapy and/or radiation therapy within 3 months of surgery; pathological fracture; surgical site; location of bone; use of cement; allograft or autograft; surgical margin; and implant type.

Accounting for all patients
Of the 264 patients with CF nails, 9.5% (20/264) were excluded because of non-malignancy (n = 15), age less than 18 (n = 6), and another implant concomitantly used (n = 4). The remaining 239 patients were included. Loss to follow-up was 8.8% (21/239) at 90-days and 19% (45/239) at 1 year. Missing patients were at random. The median follow-up time was 17 months (IQR, 4 to 49). Follow-up was verified until June 1, 2021.

Statistical analysis
Variables are presented as frequencies (percentages for categoric variables) and medians (IQRs for continuous variables as they were not normally distributed based on histogram inspection).

8

No comparative analyses were performed between the complication profile in our study cohort and from the literature given the heterogeneity in the conventional titanium nail literature of study populations, selection criteria, and outcomes. Bivariate logistic regression was used to assess explanatory variables associated with four groupings of mechanical and non-mechanical complications:[1] overall complications without time constraint,[2] overall complications within 1-year of surgery,[3] complications without nonstructural type tumor progression and no time constraint,[4] and complications without non-structural type tumor progression within 1-year. The results were presented as odds ratios (OR) with 95% confidence intervals. Multiple chained imputation (n = 40) was used to estimate missing values for smoking in 39 patients (16%), ASA scores in 17 patients (7.1%), preoperative chemotherapy in 19 patients (7.9%), preoperative radiation therapy at surgery site in 19 patients (7.9%), postoperative chemotherapy in 42 patients (18%), and postoperative radiation therapy in 21 patients (8.8%). Of the 239 patients, 132 patients (55%) had a date of death. Of the remaining 107 patients (44%), the median follow-up time was 424 days (IQR, 142 to 894 days). A two-tailed P-value of < 0.05 was considered significant. Bonferroni correction was used for multiple comparisons. All statistical analyses were performed using Stata 15.0 (StataCorp LP).

Results

Study population

This study included 239 patients: 47% were male and 53% were female, with a median age of 68 years (IQR, 59 to 75; Table 1). Most patients had an ASA score of 3 to 4 (75%). The most common primary tumors included those related to breast cancer (19%), lung cancer (19%), multiple myeloma (18%), and sarcoma (13%; Table 2). Of the 239 surgical margins, 65% were intralesional, 6.7% wide, 2.5% marginal, and 26% had no resection. The location of surgery included the femur (55%), humerus (36%), and tibia (8.4%). The 90-day mortality was 28% (61/239) and 1-year mortality was 53% (53/102) which is comparable with patients treated with conventional titanium nails in the literature [26] (Supplementary tables 1 and 2).

Complications

In total, 33 patients (14%) had structural and non-structural events defined as complications, of which 22 (9.2%) occurred within 1 year. Mechanical failures included 1 (0.4%) with aseptic loosening of the distal locking screws within 2 years (1 femoral nail), 4 (1.7%) with host bone structural failures, and 7 (2.9%) with implant structural failures (5 femoral nails and 2 humeral nails) (Figure 4). One of the humeral nail failures occurred in a patient who required an intercalary resection because of a synovial sarcoma single bone metastasis and reconstruction with a cement spacer because of concerns for infection and need to complete systemic therapy. This failure was at the interface between the bone and cement spacer, suggesting that the failure was secondary to a modulus of elasticity mismatch (Figure 5). Non-mechanical failures occurred in 22 patients (9.2%), including 8 (3.3%) peri-implant infections requiring surgical treatment and 15 (6.3%) tumor progressions with implant contamination. One patient required

intraoperative removal of the CF nail as the metal thread of the head screw disassembled from its CF body. There is no tool to remove this metal thread as all instruments attach to the CF core of the screw. After several attempts with pliers, the metal thread could not be removed from the femoral neck/head. The patient received a proximal femoral replacement because a new nail could not be inserted (Figure 6). Two patients required amputations. One of them is a patient with thigh pleomorphic sarcoma with recurrence who sustained a peri-implant femoral fracture without nail structural failure. The second amputation was for the management of a failed free flap in a patient with oligometastatic bone disease secondary to uterine cancer affecting the tibia. Two incidences of non-infectious wound dehiscence occurred (Table 3). Subgroup analyses between prophylactic stabilization of impending and fixation of complete pathological fractures showed similar failure results. No other subgroup analyses were performed due to limited numbers in each group.

Table 1. Characteristics of patients treated surgically with carbon-fiber nails for impending or pathological fracture (n=239).

Variables	% (n)
Age (years) - median (IQR)	68 (59-75)
Male	47 (113)
Smoking[a]	26 (51)
ASA score[a]	
1-2	25 (56)
3-4	75 (166)
Underlying disease	
Metastatic carcinoma	87 (209)
Soft tissue sarcoma	13 (30)
Primary tumor group	
Good prognosis+	38 (90)
Poor prognosis	62 (149)
Tumor grade	
Low	14 (33)
High	86 (206)
Additional bone metastases to surgery site	82 (197)
Preoperative chemotherapy[a]	61 (134)
Preoperative radiotherapy to surgery site[a]	14 (30)
Postoperative chemotherapy[a]	52 (103)
Postoperative radiotherapy[a]	45 (99)
Surgical variables	
Surgical side	
Left	52 (125)
Right	48 (114)
Pathological fracture	49 (116)
Location of surgery	

Table 1. Characteristics of patients treated surgically with carbon-fiber nails for impending or pathological fracture (n=239). *(continued)*

Variables	% (n)
Femur	55 (132)
Humerus	36 (87)
Tibia	8.4 (20)
Location of bone	
Diaphyseal	66 (157)
Metadiaphyseal	28 (68)
Combined	5.9 (14)
Cement[b]	11 (27)
Allograft[c]	0.4 (1)
Autograft[c]	0.4 (1)
Surgical margin	
Intralesional	65 (156)
Marginal[d]	2.5 (6)
Wide	6.7 (16)
No resection	26 (61)
Primary total knee prosthesis[e]	0.8 (2)

IQR=interquartile range; ASA= American Society of Anesthesiologists. a Missing data was present in smoking for 16% (39/239) Non-Smoker was defined as stopped at least 6 months before surgery; ASA score in 7.1% (17/329); preoperative chemotherapy in 7.9% (19/239); preoperative radiotherapy in 7.9% (19/239); postoperative chemotherapy in 18% (42/239); and postoperative radiotherapy in 8.8% (21/239). b All 11 patients had metastatic disease. c Both patients had soft-tissue sarcomas. d Marginal surgical margin occurred in 5 patients with soft-tissue sarcoma and 1 patient with renal metastases. e 2 patients had a primary total knee replacement before they received a femoral carbon fiber nail in the same leg. + Good prognosis group includes patients with lymphoma, multiple myeloma, breast cancer, kidney cancer, prostate cancer, or thyroid cancer. Poor prognosis includes patients with lung cancer, colon cancer, rectal cancer, bladder cancer, esophageal cancer, liver cancer, melanoma, gastric cancer or other cancers.

Table 2. Characteristics of tumors (n=239).

Tumor grade	% (n)
Breast	19 (46)
Lung	19 (45)
Multiple myeloma	18 (42)
Soft tissue sarcoma	13 (30)
Kidney	7.5 (18)
Other	7.1 (17)
Colorectal	2.9 (7)
Prostate	2.5 (6)
Liver	2.5 (6)
Endometrium	2.5 (6)
Thyroid	1.7 (4)

Table 2. Characteristics of tumors (n=239). *(continued)*

Tumor grade	% (n)
Melanoma	1.3 (3)
Lymphoma	1.3 (3)
Ovary	0.4 (1)
Oropharyngeal	0.4 (1)
Gastric	0.4 (1)
Urothelial	0.4 (1)
Unknown	0.8 (2)

Table 3. Outcomes of patients treated surgically with carbon-fiber nails for impending or pathological fracture (n=239).

Outcomes	% (n)
Mechanical failures	5.0 (12)
Aseptic loosening of the implant screws	0.4 (1)
Structural failures of the host bone -peri-implant fractures, hip screw out	1.7 (4)
Structural failures of the carbon fiber implant	2.9 (7)
Femur	2.1 (5)
Humerus	0.8 (2)
Non-mechanical failures	9.6 (23)
Deep infections requiring surgical treatment	3.3 (8)
Tumor progression	6.3 (15)
Mortality[a]	
90-day	28 (61)
180-days	40 (84)
1-year	53 (102)
Intraoperative mechanical failure	1.3 (3)
Amputation	0.8 (2)
Soft tissue failure due to aseptic wound dehiscence	0.8 (2)

a Loss to follow-up was 8.8% (21/239) for 90-day mortality, 13% (31/239) for 180-day mortality, and 19% (45/239) for 1-year mortality. Median follow-up time was 199 days (interquartile range: 53 - 588 days).

8

Figure 4. Radiographs showing a 83-year-old male patient with metastatic renal cell carcinoma and impending pathological fracture of the left femur because of visceral load of disease and brain metastasis who received a carbon-fiber nail for prophylactic stabilization (A). Despite systemic treatment, there was notable disease progression (B) with ultimate implant fracture (C). The patient required revision to proximal femur replacement (D).
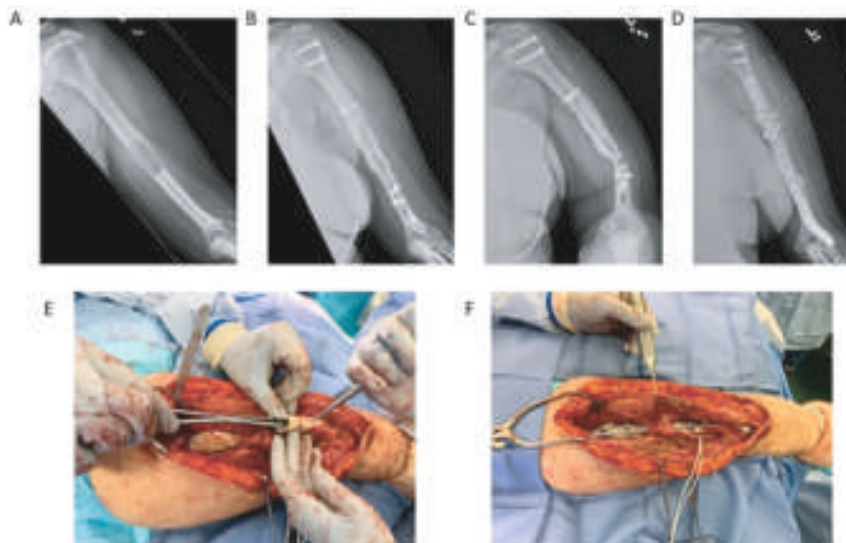
Figure 5. Radiographs showing a 38-year-old female patient with oligometastatic disease secondary to synovial sarcoma. Preoperative radiograph demonstrating an isolated intramedullary left humeral lesion (A). Six months after intercalary reconstruction with cemented spacer and carbon-fiber nail because of concern of infection (B). Complete failure of implant at host bone-cement interface (C). Revision surgery with plate augmentation and fixation after removal of the distal portion of nail (D). Intraoperative removal of distal portion of broken nail (E) and after revision surgery with metal plate augmentation (F).
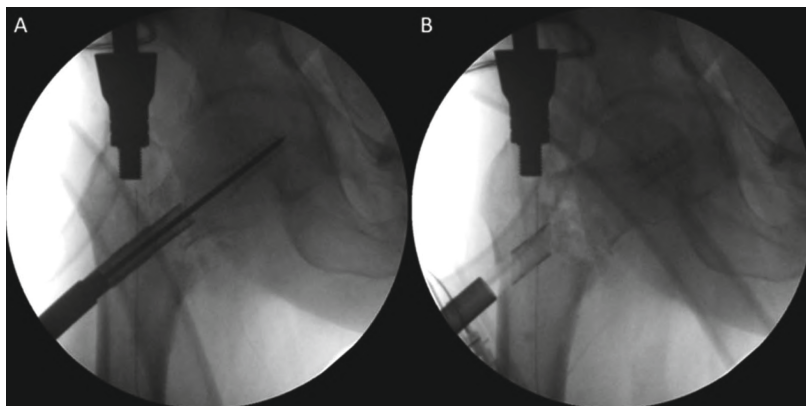
Figure 6. *Images showing insertion of screw under fluoroscopy (A) and disassembly from guidewire (B).*

Implant failure risk factors

Preoperative radiation therapy at the surgical site and femur surgery were associated with increased complication risk in all groups after adjusting for confounders during the analysis (overall complications without time constraint: OR, 4.35; 95% CI: 1.85 to 10.25; P = 0.001 and OR, 3.15; 95% CI: 1.24 to 8.05; P = 0.02, respectively; Supplementary Table 2). Additional bone metastases to the surgical site were associated with an increased risk of implant failures in overall complications without time constraints and without tumor progression within 1 year, but not in the other two groupings. The primary tumor group with good prognosis appeared to be associated with an increased risk of implant failures when no time constraint was applied. However, that association disappeared when we investigated only the events within 1 year. The follow-up time and 1-year survival for patients with a good tumor prognosis were considerably longer and better than those with poor tumor prognosis (median follow-up time: 333 (IQR, 91 to 693) days versus 93 (IQR, 28 to 239) days; 1-year survival: 64% versus 23%). The competing risk of death may explain why patients with "good prognosis" tumors had more failures as they had more time to develop them than patients with poor prognoses who died earlier and had shorter follow-up times.

Discussion

Intramedullary nails are part of the traditional treatment armamentarium for metastatic disease in the long bones (impending or complete pathological fractures). Although fixation with traditional titanium implants reports satisfactory clinical and functional outcomes, oncology patients are more critically affected by their drawbacks. Some of the limitations include metal scattering on MRI and/or CT, lack of similarity to bone elastic moduli, and scattering effect in radiation therapy planning [14,20,27]. The radiolucency of CF theoretically facilitates surveillance and radiation therapy planning using MRI or CT scans, respectively

8

[27]. Especially in the subset of patients treated with surgical curative intent, that is, the localized sarcoma group, who undergo regular MRI surveillance for recurrence. Despite the absent literature about early detection of recurrence or tumor progression on CT or MRI in long bones, there are some reports highlighting the benefit in planning of radiotherapy, at least in cadaver studies [17,28,29]. Finally, more reflective bone elastic moduli in CF implants may decrease host bone/implant mismatch when compared to their titanium counterparts. In theory, this may reduce midthigh pain reported by patients treated with titanium femoral nails suffering from host bone/implant modulus mismatch. CF implants also maintain higher ex-vivo biomechanical profiles, potentially reducing implant structural complications secondary to fracture non-healing or disease progression modeled by loading with axial or lateral bending forces [10]. However, previous studies reported mixed results regarding the fatigue strength and durability of CF implants [16,17,21]. Although CF nails may have reduced risks of fatigue failure, some nails still failed.

Compared with historic data, complication rate seems to be comparable in terms of mechanical implant failures between CF and titanium implants, although the titanium rates variated and had non-uniform definitions in the literature [2,3,30]. Acquiring more data is of utmost importance to provide insights into failure mechanisms. Our international multicenter database is designed to include patients treated with CF implants continuously and could facilitate data for future studies to identify risk factors for nail failures. Altogether, these insights could lead to ideas on improving implant material and/or usage in a specific subset of patients to optimize patient care. Although CF implants report comparable rates of wound dehiscence and superficial infections, thromboembolic events, failure because of disease progression, and rates of adverse events, their unique radiographic and biomechanical properties encourage further research [16,23,30-35]. For example, a more effective and controlled delivery of radiation therapy because of lack of scattering effect may translate in lower soft-tissue and wound complications. Still, previous studies report mixed results with relatively high non-union rates in a single center using 16 CF nails for diaphyseal correction osteotomy (11 limbs), shortening surgery (3 limbs), and diaphyseal closed tibia fractures (2 limbs), and low non-union rates in a multicenter study with 96 oncologic patients treated with CF plates [21,22]. Besides, a single institutional study in 2017 investigated 53 CF nails in oncological patients of which one nail developed a stress fracture proximally to the distal static screw, and a more recent single institutional case-control study (with 36 titanium nails and 36 CF nails) demonstrated no differences between both groups regarding operating time, surgical wound infection, and survival [35,36]. Our findings, together with the above studies, highlight an acceptable mechanical failure rate in the oncologic population, which has also been reported for titanium nails (supplementary table 3). Failure predictors are similar for both and depend on patients' disease progression, the burden of metastatic disease, and tumor location [2,3]. The time-constrained analysis seems to have no effect on the nature, incidence, and rate of complications.

Complications were found to be associated with nail type. Humeral and femoral nails had structural failures while tibial nails did not. Humeral nails fixing distal humeral diaphyseal segmental defects were more likely to break. The stress caused by the difference in elastic moduli between the cement spacer filling the diaphyseal defect and the distal humerus fragment apparently generated point forces in the distal third of the nail, causing the fracture of the implant at that level. For the remaining ones, the mismatch apparently was between the distal diaphysis and distal metaphysis. Theoretically, such fractures may be prevented by increasing humeral nail diameter or by opting for intercalary allografts instead of cement spacers. Alternatively, metal plate constructs and traditional megaprosthesis might be used instead with their own benefits and complications. For femoral nails, failure occurred with impending and complete pathologic fractures where neoplastic tissue was not removed or only curetted. Fractures occurred at the proximal metadiaphyseal junction or the diaphyseal portion of the nail. It is important to highlight that at least one of the failures was due to disease progression, and the nail was left in place until it failed because of plans of not stopping systemic treatment (Figure 4). All patients underwent revision surgery without complications. Table 4 summarizes implant structural failures.

The study is limited by its retrospective design, lack of patient matching, and potential heterogeneity in institutional patient data collection. This study should be interpreted in the context of its retrospective design and inherent shortcomings. However, the effect of the retrospective nature was deemed minimal as the survival and failure outcomes are incontrovertible. There was no direct comparison with patients that received non-CF nails at the participating institutions. Ideally, a randomized controlled trial (RCT) or propensity score-matched study may be a better option. However, this would have been difficult given the relatively small population of patients with long-bone metastases and the large size of this multicenter cohort, the biggest of its kind to our knowledge. This design should serve as the platform for a future prospective study randomizing patients to each nail type. This study also depended on each participating center to fill in their own data. Although we believe each institution filled in their data to the prospective registry to the best of their ability, following clearly defined criteria and extraction sheets, inconsistencies may still be present. If additional relevant information was required, the primary surgeon was contacted to clarify any discrepancies discovered during patient record review to minimize selection and recall bias. Finally, the sample size prevented us from performing subgroup analyses to detect any differences between, for example, soft-tissue sarcoma and metastatic carcinoma. Nevertheless, to our knowledge, this is the largest CF implant cohort determining complication profiles in patients treated surgically with CF nails for impending or complete pathologic fractures. By our international, multicenter effort, our study provides valuable insights into the use of CF nails in orthopedic oncology care.

8

Table 4. Patient characteristics for structural failures (n=7).

Gender	Age	ASA	Bone	Primary tumor	Location	Type of fracture	Resection	Postoperative day
Female	54	2	Femur	Lung	Metadiaphyseal	Impending	Intralesional	186
Male	65	3	Femur	Multiple myeloma	Diaphyseal	Fracture	No resection	654
Male	78	3	Femur	Kidney	Diaphyseal	Fracture	No resection	84
Male	77	3	Femur	Other	Metadiaphyseal	Impending	Intralesional	18
Female	64	2	Femur	Other	Metadiaphyseal	Fracture	Intralesional	69
Male	57	3	Humerus	Kidney	Diaphyseal	Fracture	Marginal	214
Male	71	3	Humerus	Kidney	Diaphyseal	Fracture	Intralesional	34

Conclusion

CF implants might be an alternative treatment option for impending and complete pathological fractures secondary to bone metastases. Their complications and failure rates seem to be comparable to those historically reported in titanium and stainless-steel implants. Given their radiolucency, good biocompatibility, bone-like elastic moduli, lack of scattering effect on MRI and CT, and strength on axial loading and bending forces, CF may particularly benefit oncology patient populations requiring frequent imaging follow-ups with MRI and/or CT scans and careful planning for postoperative radiation therapy treatment plans. Additional studies of randomized, comparative nature are needed to confirm the similar complication profiles for these implants. Relevant future research studies comparing the prospective benefits of early detection on imaging studies of local recurrence and/or tumor progression, as well as optimization of radiation therapy planning will help affirm the future standard of care for pathological fracture management in orthopedic oncology patients. Owing to the rarity of these events, international, multi-institutional collaborations are required to facilitate these studies.

8

References

1.   Bongers, M.E.R.; Groot, O.Q.; Thio, Q.; Bramer, J.A.M.; Verlaan, J.J.; Newman, E.T.; Raskin, K.A.; Lozano-Calderon, S.A.; Schwab, J.H. Prospective study for establishing minimal clinically important differences in patients with surgery for lower extremity metastases. *Acta Oncol* **2021**, *60*, 714-720, doi:10.1080/028 4186x.2021.1890333.

2.   Bonnevialle, P.; Descamps, J.; Niglis, L.; Lebaron, M.; Falguieres, J.; Mericq, O.; Fabre, T.; Reina, N.; Sailhan, F. Surgical treatment of tibial metastases: Retrospective, multicenter, observational study of 25 patients. *Orthop Traumatol Surg Res* **2020**, *106*, 1039-1045, doi:10.1016/j.otsr.2019.07.017.

3.   Brockett, C.L.; John, G.; Williams, S.; Jin, Z.; Isaac, G.H.; Fisher, J. Wear of ceramic-on-carbon fiber-reinforced poly-ether ether ketone hip replacements. *J Biomed Mater Res B Appl Biomater* **2012**, *100*, 1459-1465, doi:10.1002/jbm.b.32664.

4.   Damron, T.A.; Mann, K.A. Fracture risk assessment and clinical decision making for patients with metastatic bone disease. *J Orthop Res* **2020**, *38*, 1175-1190, doi:10.1002/jor.24660.

5.   Errani, C.; Mavrogenis, A.F.; Cevolani, L.; Spinelli, S.; Piccioli, A.; Maccauro, G.; Baldini, N.; Donati, D. Treatment for long bone metastases based on a systematic literature review. *Eur J Orthop Surg Traumatol* **2017**, *27*, 205-211, doi:10.1007/s00590-016-1857-9.

6.   Forsberg, J.A.; Wedin, R.; Boland, P.J.; Healey, J.H. Can We Estimate Short- and Intermediate-term Survival in Patients Undergoing Surgery for Metastatic Bone Disease? *Clin Orthop Relat Res* **2017**, *475*, 1252-1261, doi:10.1007/s11999-016-5187-3.

7.   Janssen, S.J.; Kortlever, J.T.; Ready, J.E.; Raskin, K.A.; Ferrone, M.L.; Hornicek, F.J.; Lozano-Calderon, S.A.; Schwab, J.H. Complications After Surgical Management of Proximal Femoral Metastasis: A Retrospective Study of 417 Patients. *J Am Acad Orthop Surg* **2016**, *24*, 483-494, doi:10.5435/jaaos-d-16-00043.

8.   Janssen, S.J.; Paulino Pereira, N.R.; Raskin, K.A.; Ferrone, M.L.; Hornicek, F.J.; van Dijk, C.N.; Lozano-Calderón, S.A.; Schwab, J.H. A comparison of questionnaires for assessing physical function in patients with lower extremity bone metastases. *J Surg Oncol* **2016**, *114*, 691-696, doi:10.1002/jso.24400.

9.   Janssen, S.J.; Pereira, N.R.P.; Thio, Q.; Raskin, K.A.; Bramer, J.A.M.; Lozano-Calderon, S.A.; Schwab, J.H. Physical function and pain intensity in patients with metastatic bone disease. *J Surg Oncol* **2019**, *120*, 376-381, doi:10.1002/jso.25510.

10.   Janssen, S.J.; Teunis, T.; Hornicek, F.J.; Bramer, J.A.; Schwab, J.H. Outcome of operative treatment of metastatic fractures of the humerus: a systematic review of twenty three clinical studies. *Int Orthop* **2015**, *39*, 735-746, doi:10.1007/s00264-014-2584-7.

11.   Janssen, S.J.; Teunis, T.; Hornicek, F.J.; van Dijk, C.N.; Bramer, J.A.; Schwab, J.H. Outcome after fixation of metastatic proximal femoral fractures: A systematic review of 40 studies. *J Surg Oncol* **2016**, *114*, 507-519, doi:10.1002/jso.24345.

12.   Janssen, S.J.; van Dijke, M.; Lozano-Calderón, S.A.; Ready, J.E.; Raskin, K.A.; Ferrone, M.L.; Hornicek, F.J.; Schwab, J.H. Complications after surgery for metastatic humeral lesions. *J Shoulder Elbow Surg* **2016**, *25*, 207-215, doi:10.1016/j.jse.2015.08.009.

13.   Jockisch, K.A.; Brown, S.A.; Bauer, T.W.; Merritt, K. Biological response to chopped-carbon-fiber-reinforced peek. *J Biomed Mater Res* **1992**, *26*, 133-146, doi:10.1002/jbm.820260202.

14.   Zimel, M.N.; Hwang, S.; Riedel, E.R.; Healey, J.H. Carbon fiber intramedullary nails reduce artifact in postoperative advanced imaging. *Skeletal Radiol* **2015**, *44*, 1317-1325, doi:10.1007/s00256-015-2158-9.

15.   Hak, D.J.; Mauffrey, C.; Seligson, D.; Lindeque, B. Use of carbon-fiber-reinforced composite implants in orthopedic surgery. *Orthopedics* **2014**, *37*, 825-830, doi:10.3928/01477447-20141124-05.

16. Li, C.S.; Vannabouathong, C.; Sprague, S.; Bhandari, M. The Use of Carbon-Fiber-Reinforced (CFR) PEEK Material in Orthopedic Implants: A Systematic Review. *Clin Med Insights Arthritis Musculoskelet Disord* **2015**, *8*, 33-45, doi:10.4137/cmamd.S20354.

17. Steinberg, E.L.; Rath, E.; Shlaifer, A.; Chechik, O.; Maman, E.; Salai, M. Carbon fiber reinforced PEEK Optima--a composite material biomechanical properties and wear/debris characteristics of CF-PEEK composites for orthopedic trauma implants. *J Mech Behav Biomed Mater* **2013**, *17*, 221-228, doi:10.1016/j.jmbbm.2012.09.013.

18. Fleege, C.; Makowski, M.; Rauschmann, M.; Fraunhoffer, K.L.; Fennema, P.; Arabmotlagh, M.; Rickert, M. Carbon fiber-reinforced pedicle screws reduce artifacts in magnetic resonance imaging of patients with lumbar spondylodesis. *Sci Rep* **2020**, *10*, 16094, doi:10.1038/s41598-020-73386-5.

19. Takayanagi, A.; Siddiqi, I.; Ghanchi, H.; Lischalk, J.; Vrionis, F.; Ratliff, J.; Bilsky, M.; Hariri, O.R. Radiolucent Carbon Fiber-Reinforced Implants for Treatment of Spinal Tumors-Clinical, Radiographic, and Dosimetric Considerations. *World Neurosurg* **2021**, *152*, 61-70, doi:10.1016/j.wneu.2021.05.100.

20. Tedesco, G.; Gasbarrini, A.; Bandiera, S.; Ghermandi, R.; Boriani, S. Composite PEEK/Carbon fiber implants can increase the effectiveness of radiotherapy in the management of spine tumors. *J Spine Surg* **2017**, *3*, 323-329, doi:10.21037/jss.2017.06.20.

21. Fragomen, A.T.; Teplensky, J.; Robert Rozbruch, S. Carbon-Fiber-Reinforced Polymer Intramedullary Nails Perform Poorly in Long-Bone Surgery. *Hss j* **2019**, *15*, 109-114, doi:10.1007/s11420-018-9634-4.

22. Group, C.-F.I.C.I.R. Complications of patients with bone tumors treated with carbon-fiber plates: an international multicenter study. *Sci Rep* **2022**, *12*, 18969, doi:10.1038/s41598-022-23519-9.

23. Herzog, L.N.; Traven, S.A.; Walton, Z.J.; Leddy, L.R. The Use of Carbon Fiber Implants for Impending or Existing Pathologic Fractures. *J Orthop Trauma* **2022**, *36*, e260-e264, doi:10.1097/bot.0000000000002320.

24. von Elm, E.; Altman, D.G.; Egger, M.; Pocock, S.J.; Gøtzsche, P.C.; Vandenbroucke, J.P. Strengthening the Reporting of Observational Studies in Epidemiology (STROBE) statement: guidelines for reporting observational studies. *Bmj* **2007**, *335*, 806-808, doi:10.1136/bmj.39335.541782.AD.

25. Katagiri, H.; Okada, R.; Takagi, T.; Takahashi, M.; Murata, H.; Harada, H.; Nishimura, T.; Asakura, H.; Ogawa, H. New prognostic factors and scoring system for patients with skeletal metastasis. *Cancer Med* **2014**, *3*, 1359-1367, doi:10.1002/cam4.292.

26. Thio, Q.; Karhade, A.V.; Bindels, B.J.J.; Ogink, P.T.; Bramer, J.A.M.; Ferrone, M.L.; Calderón, S.L.; Raskin, K.A.; Schwab, J.H. Development and Internal Validation of Machine Learning Algorithms for Preoperative Survival Prediction of Extremity Metastatic Disease. *Clin Orthop Relat Res* **2020**, *478*, 322-333, doi:10.1097/corr.0000000000000997.

27. Depauw, N.; Pursley, J.; Lozano-Calderon, S.A.; Patel, C.G. Evaluation of Carbon Fiber and Titanium Surgical Implants for Proton and Photon Therapy. *Pract Radiat Oncol* **2023**, *13*, 256-262, doi:10.1016/j.prro.2023.01.009.

28. Soriani, A.; Strigari, L.; Petrongari, M.G.; Anelli, V.; Baldi, J.; Salducca, N.; Biagini, R.; Zoccali, C. The advantages of carbon fiber based orthopedic devices in patients who have to undergo radiotherapy. *Acta Biomed* **2020**, *91*, e2020057, doi:10.23750/abm.v91i3.7769.

29. Steensma, M.; Healey, J.H. Trends in the surgical treatment of pathologic proximal femur fractures among Musculoskeletal Tumor Society members. *Clin Orthop Relat Res* **2013**, *471*, 2000-2006, doi:10.1007/s11999-012-2724-6.

30. Tanaka, T.; Imanishi, J.; Charoenlap, C.; Choong, P.F. Intramedullary nailing has sufficient durability for metastatic femoral fractures. *World J Surg Oncol* **2016**, *14*, 80, doi:10.1186/s12957-016-0836-2.

31. Mavrogenis, A.F.; Angelini, A.; Vottis, C.; Pala, E.; Calabrò, T.; Papagelopoulos, P.J.; Ruggieri, P. Modern Palliative Treatments for Metastatic Bone Disease: Awareness of Advantages, Disadvantages, and Guidance. *Clin J Pain* **2016**, *32*, 337-350, doi:10.1097/ajp.0000000000000255.

8

32.   Miller, K.D.; Fidler-Benaoudia, M.; Keegan, T.H.; Hipp, H.S.; Jemal, A.; Siegel, R.L. Cancer statistics for adolescents and young adults, 2020. *CA Cancer J Clin* **2020**, *70*, 443-459, doi:10.3322/caac.21637.

33.   Moon, B.S.; Dunbar, D.J.; Lin, P.P.; Satcher, R.L.; Bird, J.E.; Lewis, V.O. Is It Appropriate to Treat Sarcoma Metastases With Intramedullary Nailing? *Clin Orthop Relat Res* **2017**, *475*, 212-217, doi:10.1007/s11999-016-5069-8.

34.   Ofluoglu, O.; Erol, B.; Ozgen, Z.; Yildiz, M. Minimally invasive treatment of pathological fractures of the humeral shaft. *Int Orthop* **2009**, *33*, 707-712, doi:10.1007/s00264-008-0540-0.

35.   Piccioli, A.; Piana, R.; Lisanti, M.; Di Martino, A.; Rossi, B.; Camnasio, F.; Gatti, M.; Maniscalco, P.; Gherlinzoni, F.; Spinelli, M.S., et al. Carbon-fiber reinforced intramedullary nailing in musculoskeletal tumor surgery: a national multicentric experience of the Italian Orthopaedic Society (SIOT) Bone Metastasis Study Group. *Injury* **2017**, *48 Suppl 3*, S55-s59, doi:10.1016/s0020-1383(17)30659-9.

36.   Yeung, C.M.; Bhashyam, A.R.; Groot, O.Q.; Merchan, N.; Newman, E.T.; Raskin, K.A.; Lozano-Calderón, S.A. Comparison of carbon fibre and titanium intramedullary nails in orthopaedic oncology. *Bone Jt Open* **2022**, *3*, 648-655, doi:10.1302/2633-1462.38.Bjo-2022-0092.R1.

Supplementary Table 1. Summary of study characteristics that evaluate patients who underwent intramedullary nail fixation for metastatic bone disease.

Author	Years	Patients	Location	Type	Follow-up	Age
Willeumier, 2018	2000-2015	212 (228 nails)	Femur	Gamma nail: 164 (72%), PFN/PFNa: 21 (9%), IMHS: 24 (11%), TFN: 9 (4%), T2-Recon: 6 (3%), UFN/CFN: 4 (2%)	0.1-175 months, mean 14.4	29-93 years, mean 65
Piccioli, 2014	2000-2010	80	Femur	PFN/PFN-A: 26 (32.5%), AFN: 54 (67.5%)	1-48 months, mean 22	39-81 years, mean 61.2
Tanaka, 2016	2003-2013	75 (80 nails)	Femur	Trigen System: NA, Alta CFx IM rod system: NA	1-77 months, mean 11.4 months	20-80 years, mean 60.1
Kotian, 2018	2005-2017	138	Femur	NA	NA	13-90 years, mean 60, median 61
Moon, 2017	1996-2014	34 (40 nails)	Femur: 24, Humerus: 15, Tibia: 1	NA	0.3-86 months, median 13	27-81 years, median 52
Ofluoglu, 2009	2002-2006	23 (24 nails)	Humerus	Titanium: 16, Stainless steel: 8	6-44 months, mean 17	43-81 years, median 63
Bonnevialle, 2020	2001-2017	25 (8 nails, 14 plates, 2 cementoplasty only, 1 knee arthroplasty)	Tibia	NA	Minimum 6 months for all patients	Mean 66 years

PFN/PFNa=proximal femoral nail/proximal femoral nail helical blade; IMHS=intramedullary hip screw; TFN=titanium trochanteric fixation nail; UFN/CFN=unreamed/cannulated femoral nail; AFN=antegrade femoral nail; NA=not available

	Gender	Underlying Disease	Primary tumor	Chemotherapy	Radiotherapy
	84 men (40%)	Metastatic carcinoma	Breast: 76 (36%), lung: 51 (24%), kidney: 24 (11%), prostate: 23 (11%), other: 38 (18%)	NA	Neoadjuvant: 39, Adjuvant: 124
	42 men (52.5%)	Metastatic carcinoma	Breast: 23, prostate: 12, lung: 8, colon: 6, thyroid: 4, kidney: 2, myeloma: 16, lymphoma: 4, bladder: 3, liver: 2.	NA	Neoadjuvant: NA, Adjuvant: 100
	37 men (49%)	Metastatic carcinoma	Lung: 24 (32%), breast: 18 (24%), melanoma: 11 (14.7%), renal: 5 (6.7%), prostate: 5 (6.7%), unknown: 4 (5.3%), other: 8 (10.6%)	Neoadjuvant: NA, Adjuvant: yes (NA)	Neoadjuvant: NA, Adjuvant: 74
	57 men (41%)	Metastatic carcinoma	Breast: 29 (21%), plasma cell/ multiple myeloma: 29 (21%), lung: 21 (15%), renal cell: 12 (9%), prostate: 7 (5%), thyroid: 5 (4%), other: 35 (25%)	Neoadjuvant: NA, Adjuvant: 124	NA
	NA	Sarcoma	Osteosarcoma: 4, hemangiopericytoma: 5, leiomyosarcoma: 5, alveolar soft parts sarcoma: 4, angiosarcoma: 3, spindle cell sarcoma: 3, undifferentiated pleomorphic sarcoma: 2, liposarcoma: 2, fibrosarcoma: 1, myxofibrosarcoma: 1, epithelioid hemangioendothelioma: 1, synovial sarcoma: 1, Ewing's sarcoma: 1, neurofibrosarcoma: 1	29 total neoadjuvant and adjuvant	11 total neoadjuvant and adjuvant
	19 men	Metastatic carcinoma	Lung: 11, breast: 5, renal cell: 3, myeloma: 2, mesothelioma: 1, unknown: 1	Neoadjuvant: 15, Adjuvant: 12	Neoadjuvant: NA, Adjuvant: 23
	15 men (60%)	Metastatic carcinoma	Kidney: 10, lung: 4, other: 11	NA	NA

8

Supplementary Table 2. Summary of complication and survival rates in studies where patients underwent intramedullary nail fixation for metastatic bone disease.

Author	Survival	Complications	Complication Definition
Willeumier, 2018	6-month: 49%, 1-year: 33%, 2-year: 19%, Median OS: 6 months	Local complications: 28 (12%)	Local complications: persisting pain, tumor progression, implant breakage; Implant breakage: nail and screw fractures, migrations, deformations or malplacements, and peri-implant fractures
Piccioli, 2014	1-year: 40%, 2-year: 25%, 3-year: 15%, Mean OS: 10 months	NA	NA
Tanaka, 2016	2-year: 14.2%, 3-year: 8.4%	NA	NA
Kotian, 2018	Median OS: 8.4 months	Within 30 days: 18 (13%)	Major medical complications: DVT, PE, pneumonia, MI, arrhythmia, cerebrovascular accident, and renal failure; Wound complications: surgical site infection, hematoma
Moon, 2017	0.3-80 months, Median OS: 5 months	NA	NA
Ofluoglu, 2009	1-38 months, Mean OS: 11.4 months	4	NA
Bonnevialle, 2020	Median OS: 14 months	Nail group: 0	NA

OS=overall survival; DVT=deep venous thrombosis; PE=pulmonary embolism; MI=myocardial infarction; NA=not available

Mechanical vs. Non-Mechanical Definition	Complication Defined	Mechanical Complications	Non-mechanical Complications
NA	Implant breakage: 18 (8%) in 28 nails (12%), Persisting pain: 5 (2%), Tumor progression: 9 (4%), Revision: 12 (5%)	NA	NA
NA	DVT: 11 (13.75%), Superficial wound infection: 6 (7.5%), Pneumonia: 2 (2.5%)	NA	NA
NA	Implant breakage: 3 (3.8%), Early postoperative death via respiratory failure: 3 (3.8%)	NA	NA
NA	Major medical complications: 16 (12%), Wound complications: 3 (2.2%)	NA	NA
NA	Infection: 1 (3%), Amputation: 1 (3%), Tumor progression: 3 (9%), Distal cortex of femur penetration during nailing: 1 (3%), Fracture at tip of humeral nail: 1 (3%), Postoperative death via cardiovascular collapse: 1 (3%)	NA	NA
NA	Fixation failure: 1, Proximal locking screw loosening: 1, Tumor progression: 1, Tumor seeding at nail: 1	NA	NA
NA	None	NA	NA

8

Supplementary Table 3. Bivariate logistic regression analysis for (1) overall failure events, (2) overall failure events within 1 year, (3) failure events without type tumor progression, and (4) failure events without tumor progression within 1 year using chained multiple imputation (imputations=40).

Explanatory variables	Overall failures (events=33)			Overall failures within 1-year (events=22)		
	Odds ratio (95% CI)	Standard Error	p-value	Odds ratio (95% CI)	Standard Error	p-value
Age (years)	0.99 (0.97-1.02)	0.014	0.66	1.02 (0.98-1.05)	0.018	0.36
Male	0.85 (0.41-1.77)	0.318	0.67	0.63 (0.27-1.51)	0.281	0.31
Smoking	0.57 (0.19-1.68)	0.314	0.31	0.51 (0.15-1.81)	0.330	0.30
ASA score						
1-2	*Ref*			*Ref*		
3-4	0.69 (0.31-1.54)	0.283	0.36	0.72 (0.28-1.84)	0.345	0.49
Primary tumor group						
Good prognosis	2.27 (0.98-5.24)	0.969	0.06	1.53 (0.61-3.84)	0.718	0.37
Poor prognosis	*Ref*			*Ref*		
Tumor grade						
Low	*Ref*			*Ref*		
High	0.95 (0.34-2.67)	0.500	0.93	1.85 (0.41-8.28)	1.415	0.42
Additional bone metastases to surgery site	0.39 (0.0.17-0.88)	0.161	**0.02**	0.47 (0.18-1.22)	0.229	0.12
Preoperative chemotherapy	1.62 (0.72-3.67)	0.678	0.25	1.12 (0.45-2.76)	0.516	0.81
Preoperative radiotherapy to surgery site	4.35 (1.85-10.25)	1.902	**0.001**	5.23 (2.02-13.49)	2.528	**0.001**
Postoperative chemotherapy	0.80 (0.38-1.68)	0.304	0.55	0.76 (0.32-1.79)	0.331	0.53
Postoperative radiotherapy	1.04 (0.49-2.21)	0.401	0.93	0.92 (0.39-2.19)	0.408	0.85
Surgical side						
Left	1.26 (0.61-2.59)	0.464	0.54	2.41 (0.96-6.04)	1.129	0.06
Right	*Ref*			*Ref*		
Pathological fracture	0.67 (0.32-1.38)	0.248	0.28	0.89 (0.38-2.07)	0.383	0.78
Location of surgery						
Femur	3.15 (1.24-8.05)	1.507	**0.02**	2.59 (1.04-7.26)	1.362	**0.05**
Humerus	*Ref*			*Ref*		
Tibia	3.38 (0.85-13.37)	2.366	0.08	0.86 (0.10-7.82)	0.971	0.90

	Failures without tumor progression (events=20)			Failures without tumor progression within 1 year (events=16)		
	Odds ratio (95% CI)	Standard Error	p-value	Odds ratio (95% CI)	Standard Error	p-value
	1.02 (0.99-1.06)	0.020	0.20	0.99 (0.97-1.02)	0.014	0.66
	1.37 (0.57-3.30)	0.614	0.61	0.85 (0.41-1.77)	0.318	0.67
	0.44 (0.12-1.54)	0.281	0.20	0.57 (0.19-1.68)	0.314	0.31
	Ref			Ref		
	0.89 (0.33-2.40)	0.451	0.82	0.69 (0.31-1.54)	0.283	0.36
	0.168 (0.63-4.48)	0.840	0.30	2.27 (0.98-5.24)	0.969	0.06
	Ref			Ref		
	Ref			Ref		
	1.67 (0.37-7.49)	1.278	0.51	0.95 (0.34-2.67)	0.500	0.93
	0.53 (0.19-1.45)	0.272	0.22	0.39 (0.17-0.88)	0.161	**0.02**
	1.42 (0.56-3.65)	0.684	0.46	1.62 (0.72-3.67)	0.676	0.25
	4.69 (1.76-12.46)	2.338	**0.002**	4.35 (1.85-10.25)	1.902	**0.001**
	0.71 (0.29-1.77)	0.330	0.46	0.80 (0.38-1.68)	0.304	0.55
	1.21 (0.50-2.92)	0.545	0.68	1.04 (0.49-2.21)	0.401	0.93
	1.10 (0.46-2.66)	0.496	0.83	1.26 (0.61-2.59)	0.464	0.54
	Ref			Ref		
	1.07 (0.44-2.56)	0.477	0.89	0.67 (0.32-1.38)	0.248	0.28
	3.86 (1.09-13.68)	2.492	**0.04**	3.15 (1.24-8.05)	1.507	**0.02**
	Ref			Ref		
	4.94 (0.92-26.59)	4.243	0.06	3.38 (0.85-13.34)	2.366	0.08

8

Supplementary Table 3. Bivariate logistic regression analysis for (1) overall failure events, (2) overall failure events within 1 year, (3) failure events without type tumor progression, and (4) failure events without tumor progression within 1 year using chained multiple imputation (imputations=40). *(continued)*

	Overall failures (events=33)			Overall failures within 1-year (events=22)		
Location of bone						
Diaphyseal	*Ref*			*Ref*		
Metadiaphyseal	0.58 (0.24-1.41)	0.262	0.23	0.80 (0.30-2.12)	0.397	0.65
Combined	0.84 (0.18-3.98)	0.666	0.83	0.63 (0.08-5.15)	0.677	0.67
Surgical margin						
Intralesional	*Ref*			*Ref*		
Marginal	3.40 (0.58-19.78)	3.055	0.17	5.07 (0.85-30.19)	4.616	0.07
Wide	3.09 (0.97-9.83)	1.824	0.06	2.34 (0.59-9.21)	1.636	0.22
No resection	1.03 (0.43-2.47)	0.460	0.95	0.91 (0.31-2.63)	0.493	0.86

*CI=confidence interval; Ref=reference value. A 'reference' category is so titled because it serves as a point of comparison for the other categories. In other words, the other categories are evaluated in relation to the reference. For example, if you wanted to predict probability of 'Location of surgery', you will set the baseline (i.e., reference level) to one category and in this case "humerus". Missing values are listed in Table 1 and follow-up times in Table 2. **Bold** p-values are <0.05.*

	Failures without tumor progression (events=20)			Failures without tumor progression within 1 year (events=16)		
	Ref			*Ref*		
	0.85 (0.32-2.28)	0.428	0.75	0.58 (0.24-1.41)	0.262	0.23
	no value			0.84 (0.18-3.98)	0.666	0.83
	Ref			*Ref*		
	6.00 (0.99-36.18)	5.500	0.051	3.4 0(0.58-19.78)	3.055	0.17
	2.77 (0.69-11.08)	1.959	0.15	3.09 (0.97-9.83)	1.824	0.06
	1.07 (0.36-3.18)	0.595	0.90	1.03 (0.43-2.47)	0.460	0.95

8

9

EVALUATION OF COMPUTED TOMOGRAPHY ARTEFACTS OF CARBON-FIBER AND TITANIUM IMPLANTS IN PATIENTS WITH SPINAL OLIGOMETASTATIC DISEASE UNDERGOING STEREOTACTIC ABLATIVE RADIOTHERAPYY

Z. Rijs[1*], K.A. Kawsar[2], P. Saha[3], M.A.J. van de Sande[1], D. Lui[3]

[1] Department of Orthopedic Surgery, Leiden University Medical Center, Leiden, The Netherlands
[2] Department of Neurosurgery, Queen Elizabeth Hospital, Birmingham, United Kingdom
[3] Department of Orthopedic and Spinal Surgery, St. George's Hospital, London, United Kingdom

Abstract

This study evaluated artifacts on computed tomography (CT) images using Hounsfield units (HU) in patients with spinal oligometastatic disease who received carbon-fiber (CF; n=11) or titanium (n=11) spine implants and underwent stereotactic ablative radiotherapy (SABR). Pre- and postoperative HU were measured at the vertebral body, pedicle, and spinal cord at three different levels: the lower instrumented vertebra, the level of metastatic spinal cord compression, and an uninvolved level. Areas measured at each level were delicately matched pre- and postoperatively. Significant differences in HU were observed at the vertebral body, the pedicle, and the spinal cord at the lowest instrumented vertebra level for both CF and titanium (average increase 1.54-fold and 5.11-fold respectively). At the metastatic spinal cord compression level, a trend towards a higher HU-increase was observed in titanium compared with CF treated patients (average increase 2.51-fold and 1.43-fold respectively). The relatively high postoperative HU-increase after insertion of titanium implants indicated CT artifacts, while the relatively low HU-increase of CF implants was not associated with artifacts. Less CT artifacts could facilitate an easier contouring phase in radiotherapy planning. In addition, we propose a CT artifact grading system based on postoperative HU-increase. This system could serve as a valuable tool in future research to assess if less CT artifacts lead to time savings during radiotherapy treatment planning and, potentially, to better tumoricidal effects and less adverse effects if particle therapy would be administered.

Introduction

Spinal metastases are common in oncological care as approximately 70% of all bony metastasized cancers are located in the spine [1,2]. Spinal oligometastatic disease (OMD) is defined as a subgroup of patients with limited (≤ 5) metastatic lesions in the spine where all metastatic sites are safely treatable [3,4]. Treatment of spinal OMD is a multidisciplinary team effort, and management must be individualized for each patient. Factors that impact treatment strategy include histology, tumor location, symptoms, radiosensitivity, and prior treatment [5]. Surgery can be performed in case of mechanical pain, decompression, correction of instability or deformity, and with the purpose of oncological cytoreduction [6]. In patients with limited spinal OMD, surgery combined with postoperative radiotherapy (RT) to improve local control is an established practice [7].

Conventional external beam radiation therapy (EBRT) to the entire spine has been the golden standard for decades due to its excellent palliative effect. However, EBRT doses are too low to ensure long term local control, and raising the dose is not an option because the spinal cord is often at risk [8]. Fortunately, stereotactic ablative radiotherapy (SABR) is an emerging noninvasive approach for the treatment of spinal OMD [9]. It has drastically changed the treatment from palliative to curative care for several (early detected) cancers, including lung-, liver-, prostate-, breast-, and spine cancer [10-13]. SABR can precisely deliver tumoricidal radiation doses to the tumor(s), while sparing adjacent tissues, thereby achieving durable local tumor control with low complication rates [10]. This is a delicate procedure that highly depends on accuracy, not only because the dose must be high enough to be toxic to tumor cells, but also because it requires high precision as the spinal cord is often right next to the area being treated [14]. Therefore, precise SABR planning with computed tomography (CT), or magnetic resonance imaging (MRI), is essential to ensure optimal treatment for spinal OMD [15]. Several prospective trials have already demonstrated that SABR is an effective tool for treating spinal OMD [16-20].

Although very promising, a major challenge in the delivery of SABR to spinal OMD is the proximity of the spinal cord. Despite technical evolutions such as surface-guided monitoring systems, metal artifact reduction, and couch corrections in all six degrees of freedom, SABR treatment can be hampered when spinal tumors are treated with titanium (or other metallic) implants [21]. Commonly used titanium implant materials produce substantial artifacts on CT images [22]. Consequently, these implants pose problems with respect to (time-consuming) radiation planning and accurate delivery of the calculated dose [22]. This could lead to complications such as spinal cord radio necrosis, progressive myelopathy, spinal hemorrhage, and fractures [23,24]. Tedesco et al. reported that scattering of radiotherapy from titanium spine implants can compromise the therapeutic effect and lead to unwanted radiation to adjacent healthy tissue [25]. In addition, titanium (or other metallic) artifacts also interfere with postoperative radiologic surveillance used to track bone healing and identify recurrences [26].

9

A possible improvement for spinal OMD treatment with SABR is to change traditional titanium (or other metallic) implants to innovative carbon-fiber (CF) implants. CF materials have good biocompatibility, chemical stability, good mechanical properties, and a modulus of elasticity which is similar to human bone and theoretically leads to better bone quality [27]. Besides, clinical studies have not shown an increase in complications with implementation of CF implants [25,28-30]. Therefore, CF implants could improve SABR planning and lead to more accurate delivery of the calculated dose compared to traditional implants [31]. Several CF spine implants have shown promising results with regards to reducing artifacts, better radiation planning, and potentially greater safety and quality of radiotherapy [25,32,33]. However, it has been difficult to quantify the difference in CT artifacts after implementation of CF and titanium implants. In the current study, we utilized a quantitative technique to perform a pre- and postoperative comparison of CT artifacts produced by CF and titanium implants in patients with spinal OMD undergoing postoperative SABR. In addition, we propose an artifact grading system to classify CT artifacts.

Materials and methods

This retrospective single center study included patients ≥18 years with spinal OMD who received CF or titanium spinal implants (including pedicles, screws, and rods) between 2018 and 2020. A closely matched gender and age group of patients that received CF and titanium implants was selected because gender- and age-related osteoporotic changes in bone density could potentially influence CT artifact measurements. Patients with traumatic or inflammatory conditions, or previous fusion surgery were not eligible. Additionally, patients that received bone cement (i.e., polymethyl methacrylate or PMMA) at the level of metastasis or instrumented level were excluded because this could potentially interfere with CT artifact measurements. The study protocol was approved by the local ethics committee (St George's Research Ethics Committee, clinical audit registration number AUDI003026), and informed consent was obtained from all subjects and/or their legal guardians. All methods were performed in accordance with relevant guidelines and regulations.

Surgery was recommended as a curative treatment strategy in patients with spinal OMD. Most patients presented with pain, some with spinal cord compression, and response to non-surgical treatment was insufficient. Decompression and fixation surgery was predominantly performed for those cases, and there was no standardized protocol to choose for CF implants instead of titanium implants. Therefore, the choice between CF or titanium was made by shared decision making and the preference of the operating surgeon. During this study, patients were treated with various FDA approved and CE marked CF (CarboFix Orthopedics; Herzliya, Israel) and titanium implants (Stryker Corporation, Michigan, United States of America).

Outcomes assessment

Artifacts on CT images were measured preoperatively and within the first postoperative week using Hounsfield units (HU), which were determined by a picture archiving and communication system (PACS) integrated software (Phillips Medical Systems, Eindhoven, The Netherlands). An unmodified standard care CT spine protocol (median tube potential 140kVp, median tube current 60mA, 2.5mm slice thickness) was used to measure the artifacts; the software measured the density of a region of interest (ROI), which electronically overlaid the image, and calculated the corresponding HU. ROI were selected by a neurosurgeon (K.A.K.) and checked by an orthopedic surgeon specialized in spine surgery (D.L.). Pre- and postoperative HU measurements were performed at the vertebral body, pedicle, and spinal cord at three different levels: the lower instrumented vertebra, the level of metastatic spinal cord compression, and at an uninvolved level. These locations were chosen because the lower instrumented vertebra received the implant. The level of metastatic spinal cord compression was chosen because this is the level where radiotherapy is directed, and usually no screws are inserted at this level which means that HU changes come from scattering from different levels. Additionally, an uninvolved level served as internal control. Areas were measured as a circle in the vertebral body and spinal canal, while an ellipse was used for the pedicle (Figure 1). CT images were analyzed for the CF as well as the titanium implant group, and HU areas measured at each level were delicately matched between pre- and postoperative images (<10% difference in the examined area measured in cm^2). In addition, a CT artifact grading system was developed based on the postoperative HU change.
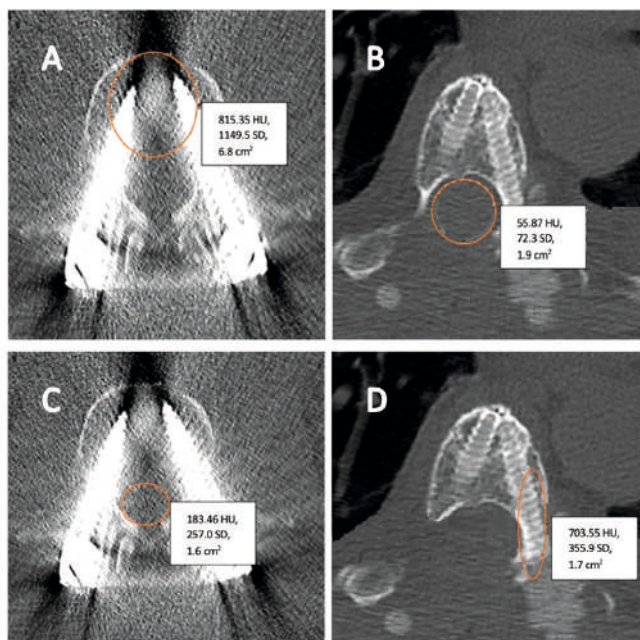
9

Figure 1. *Hounsfield unit measurement of the vertebral body of the lower instrumented vertebra with bright and dark artifacts after treatment with a titanium implant (A), measurements of the spinal cord near the lower instrumented vertebra with carbon-fiber (B), measurements of the spinal cord near the lower instrumented vertebra with titanium (C), and an elliptical measurement of the pedicle of the lower instrumented vertebra with carbon-fiber without bright or dark artifacts (D).*

Statistical analysis

Statistical analyses were performed using SPSS version 25 (IBM Corp, Somer, NY, USA). For continuous data, the Kolmogorov-Smirnov test was used to assess the normal distribution assumption. Mean HU were calculated for each group pre- and postoperatively. These mean HU values were used because the distribution of our data was symmetric without clear outliers, and a paired t-test was used to compare the mean HU pre- versus postoperatively. Significance was set as a p-value ≤ 0.05.

Results

In total, 22 patients were included. Six males and five females (n=11) were included in the CF implant group, with a mean age of 54 years (range 20 - 70 years). The titanium group consisted of five males and six females (n=11), with a mean age of 56 years (range 36 - 66 years). Although two patients in the CF group were primary spine tumors, most of the lesions were spinal metastasis, and the involved location was mostly at the thoracic level of the spine (Table 1).

Table 1. Demographic features of included patients treated with carbon-fiber or titanium implants.

Baseline characteristics	Carbon-fiber implant group (n=11)	Titanium implant group (n=11)
Female % (n of total)	45% (n=5)	55% (n=6)
Age (years; mean with range)	54 (20 – 70)	56 (36 – 66)
Primary tumor		
Primary spine tumor	18% (n=2)	0% (n=0)
Metastasis*	82% (n=9)	100% (n=11)
Level of the lesion	9% (n=1)	9% (n=1)
Cervical		
Thoracic	64% (n=7)	55% (n=6)
Lumbar	27% (n=3)	36% (n=4)

Metastasis most frequently originated from renal cell carcinoma (n=3) and lung cancer (n=3), followed by breast-, prostate-, and thyroid cancer (n=2 per group) and a group of other types of cancer including bladder cancer, gastric cancer, melanoma, ovarian cancer, plasmacytoma, and sarcoma (n=1 per type of cancer)

Pre- versus postoperative HU comparison for carbon fiber implants

The average HU of the vertebral body, pedicle, and spinal cord at the level of the lower instrumented vertebra, at the metastatic spinal cord compression level, and at the uninvolved level was compared before and after insertion of the CF implants. CF instrument scatter artifacts were observed with higher postoperative HU. Although HU only increased with a maximum of 1.67-fold compared to its preoperative value, there was a significant increase at the vertebral body-, pedicle-, and spinal cord at the lowest instrumented vertebra level (p=0.012, 0.015, and 0.014 respectively; Table 2). No statistically significant HU-increase was observed at the metastatic spinal cord compression level (generally no instrumentation at the tumor level) and at the uninvolved level (internal control) (Table 2).

9

Table 2. Hounsfield unit comparison within the carbon-fiber group.

Level	Preoperative HU*	Postoperative HU*	fold increase	p-value
LIV VB	163.19	267.67	1.64	**.012**
LIV ped	298.20	493.88	1.65	**.015**
LIV SC	36.27	47.81	1.32	**.014**
MSCC VB	236.46	394.63	1.67	.089
MSCC Ped	230.05	367.93	1.60	.910
MSCC SC	49.92	50.82	1.02	.125
Uninvolved level VB	137.26	141.77	1.03	.667
Uninvolved level Ped	282.86	286.37	1.01	.376
Uninvolved level SC	30.11	34.57	1.15	.261

Average values of all included patients are reported. Abbreviations: LIV=Lowest Instrumented Vertebra; VB=Vertebral Body; SC=Spinal Cord; Ped=Pedicle; MSCC=metastatic spinal cord compression, HU=Hounsfield unit

Pre- versus postoperative HU comparison for titanium implants

The average HU of the vertebral body, pedicle, and spinal cord at the level of the lower instrumented vertebra, at the metastatic spinal cord compression level, and at the uninvolved level was compared before and after insertion of the titanium implants. Titanium instrument scatter artifacts were observed with higher postoperative HU. The same trend was observed as with CF implants, with significantly increased HU postoperatively (maximum 5.65-fold increase) at the vertebral body-, pedicle-, and spinal cord at the lowest instrumented vertebra level (p-values of 0.00, 0.00, and 0.24 respectively; Table 3). Although not statistically significant, a trend towards higher HU was observed in titanium implants (average 2.51-fold HU-increase) at the metastatic spinal cord compression level. As expected, no significant HU-increase was observed at the uninvolved level (internal control).

Table 3. Hounsfield unit comparison within the titanium group.

Level	Preoperative HU*	Postoperative HU*	x increase	p-value
LIV VB	166.69	790.28	4.74	**.000**
LIV ped	249.49	1386.78	5.56	**.000**
LIV SC	29.37	147.49	5.02	**.024**
MSCC VB	174.39	530.01	3.04	.155
MSCC Ped	263.47	419.09	1.59	.058
MSCC SC	35.91	103.92	2.89	.243
Uninvolved level VB	195.02	177.18	0.91	.151
Uninvolved level Ped	295.26	283.86	0.96	.053
Uninvolved level SC	30.35	38.05	1.25	.082

Average values of all included patients are reported. Abbreviations: LIV=Lowest Instrumented Vertebra; VB=Vertebral Body; SC=Spinal Cord; Ped=Pedicle; MSCC=metastatic spinal cord compression, HU=Hounsfield unit

Artifact grading system to classify CT artifacts

Based on our observations the postoperative HU-increase was associated with an increase in CT artifacts. Therefore, we propose a CT artifact grading system where grade 0 = no increase (i.e., bone allografts), grade 1 = 1-1.3-fold (differences in study planes), grade 2 = 1.3-2-fold increase (CF), grade 3 = 2-4-fold increase (i.e., CF with cement), and 5 = >4-fold increase (titanium) (Table 4). This grading system provides information on the ability to assess anatomically relevant structures and could be used in future studies to assess if less CT artifacts indeed facilitate an easier contouring phase in radiotherapy planning and possibly lead to better tumoricidal effects and decreased adverse outcomes in cases where newer forms of radiotherapy, such as particle therapy, would be considered.

Table 4. CT artifact grading system based on postoperative HU-increase.

Grade	Fold increase of HU	Description, assessment of anatomically relevant structures
Grade 0	Less than 1	Bone allografts, perfect assessment
Grade 1	1 – 1.3	Differences in study planes, very good assessment
Grade 2	1.3 – 2	Carbon fiber implants, good assessment
Grade 3	2 - 4	Cement was observed to increase HU, moderate assessment
Grade 4	4 and above	Titanium implants, poor assessment

Discussion

In this study, we utilized a quantitative technique to perform a pre- versus postoperative comparison of HU produced by CF and titanium implants in patients with spinal OMD undergoing postoperative SABR. Significant increases in HU were observed at the vertebral body, the pedicle, and the spinal cord at the lowest instrumented vertebra level for both CF and titanium implants (average 1.54-fold and 5.11-fold HU-increase, respectively). At the metastatic spinal cord compression level, a trend towards a higher HU-increase was observed in titanium implants compared with CF implants (average 2.51-fold and 1.43-fold HU-increase respectively). In general, no screws are inserted at this level, which means the HU-increase comes from the scatter of a cage or rods posteriorly. As expected, no postoperative HU-increase was observed at the uninvolved level for both CF and titanium. Based on our observations, the HU-increase indicates an increase in CT artifacts. Therefore, we propose a CT artifact grading system based on postoperative HU-increase, which provides information on the ability to assess anatomically relevant structures and could be used in future long term follow up studies. These studies could assess if less CT artifacts (low grade artifacts) indeed lead to time savings during radiotherapy planning and, potentially, to enhanced tumoricidal effects with less adverse outcomes in cases where particle therapy would be administered.

9

A recent in vitro study of Krätzig et al. evaluated the susceptibility of artifacts in CT and MRI of titanium and CF screw-rod constructs for posterior spinal stabilization using a standardized in vitro model [34]. Here, similar manually placed 2D ROI were defined for each image, and CT imaging with typical implant configuration for thoracic stabilization demonstrated a significant artifact reduction in CF compared with titanium implants for the evaluation of index structures, such as the spinal cord and the vertebra. Coherently, Depauw et al. used a water phantom as a human tissue equivalent and reported no imaging artifacts and minimal dose perturbation of CF compared with titanium [35]. In addition, Fleege et al. reported reduced artifacts of CF pedicle screws in MRI scans of patients with lumbar spondylodesis [36]. The authors calculated the surface of the artifact free vertebral body area as percentage of the total vertebral body, and CF displayed significantly less artifacts than titanium (67.1 ± 5.6% vs. 48.3 ± 5.0%; *p≤0.01*, respectively). Furthermore, Ringel et al. reported reduced artifacts of CF spine implants compared with titanium implants and conclude that CF spine implants are a valuable and feasible option in spine tumors where postoperative imaging and radiation

planning are necessary [26]. Our findings, together with the previously mentioned studies, highlight that CF spine implants show reduced artifacts compared to titanium.

The clinical relevance of the reduced artifacts after CF implementation instead of titanium remains to be further elucidated. New treatment planning systems, which outline metallic materials and associate an atomic number which is used for dose calculation purposes (the density override method), correct for metallic artifacts. Therefore, metallic implants are unlikely to impact the tumoricidal effects of SABR. However, the density override method no longer needs to be applied with CF implants, which results in a simpler method and therefore time savings, as well as an accurate dose distribution [37]. Besides, radiation oncologists are increasingly interested in CF spinal instrumentation because it enables the use of particle therapy, such as proton beam therapy, in a group of patients where it was previously impossible due to the imaging artifacts and perturbation effect of metallic instrumentation [38]. Several studies have shown that the use of CF is favorable to titanium instrumentation for the use in particle therapy. Nevelsky et al. investigated the perturbation effect of CF screws compared to titanium screws and found a perturbation effect of less than 5% for CF screws, compared to greater than 30% for titanium screws [39]. Mastella et al. evaluated the dosimeric perturbation caused by CF screws compared to titanium screws and found less dose degradation caused by CF screws, making CF more suitable for particle therapy [40]. Ultimately, this might help achieving the goal of durable tumor control with low complication rates.

Drawbacks of CF implants include its potential challenging surgery due to its radiolucency. However, recent research has shown CT-guided navigation of pedicle screws is possible for instrumentation and precision assessment across the thoraco-lumbar spine [41]. Besides, long-term postoperative results of CF implants, including the effect of radiation on the properties of CF implants, remain to be investigated. Some also question whether availability and costs of CF implants could be a disadvantage. Although we are not aware of its availability, production costs have decreased as CF composites are widely used across other industries, and current costs of CF nails are competitive with conventional metal nails [42].

This study has several limitations. First, our objective quantitative assessment using HU is not a perfect measurement of artifacts. Although several studies have used HU to predict osteoporosis and artifacts, we acknowledge that HU values depend on CT scanner configurations, depth of the measurement, location of the measurement, tissue type, implant material and artifacts due to motion during the scan can all influence HU [34,43]. Artifacts can be bright (high HU) or dark (low HU). Therefore, postoperative HU differences, such as our CT artifact grading system based on postoperative HU-increase, might only be a surrogate marker for CT artifacts. Nevertheless, this real life setting with standard clinical protocols provides relevant clinical insights; the relatively high HU-increase after insertion of titanium implants indicated CT artifacts, while the relatively low HU-increase after insertion of CF implants was not associated with artifacts. A qualitative assessment by a musculoskeletal radiologist could contribute to the validity and reliability of our study because this is generally

seen as the ground-truth. Although not performed in this study, a qualitative analysis of post-operative artifact-free vertebrae surface area and its ratio to pre-operative vertebrae surface area, as done by Fleege et al., would presumably show better results in patients treated with CF implants [36]. Another limitation is that our proposed CT artifacts grading system is solely based on 11 patients receiving CF implants and 11 patients receiving titanium implants. Validation is needed to assess if this HU based classification system holds promise for assessing CT artifacts in future studies. Furthermore, our retrospective study design is inherently susceptible to several forms of bias, including selection- and assessor bias, and causal differences should be interpreted with caution. However, we objectively measured carefully matched ROI and compared the hardware against itself (in different levels) and against its own control (pre- and postoperatively). Postoperative HU differences which are clinically relevant for the ability to assess anatomically relevant structures or metastasis/ residual tumor, improve planning (time savings) and accurate administration of newer forms of radiotherapy, such as particle therapy, should be further examined.

Conclusion

It has been difficult to quantify the difference in computed tomography (CT) artifacts after implementation of carbon-fiber (CF) and titanium implants. This study utilized a quantitative technique to compare pre- and postoperative CT artifacts produced by CF and titanium implants in patients with spinal oligometastatic disease (OMD) undergoing stereotactic ablative radiotherapy (SABR). A greater increase in Hounsfield units (HU) was observed in the group treated with titanium spine implants than in the group treated with CF spine implants. This relatively high postoperative HU-increase after insertion of titanium implants indicated CT artifacts, while the relatively low HU-increase of CF implants was not associated with artifacts. Therefore, we propose a CT artifact grading system based on postoperative HU-increase. This could be used in future studies to assess if less CT artifacts due to treatment with CF implants lead to time savings during radiotherapy treatment planning and, potentially, better tumoricidal effects and decreased adverse effects if particle therapy would be administered.

9

References

1. Ecker, R.D.; Endo, T.; Wetjen, N.M.; Krauss, W.E. Diagnosis and treatment of vertebral column metastases. *Mayo Clin Proc* **2005**, *80*, 1177-1186, doi:10.4065/80.9.1177.

2. Wong, D.A.; Fornasier, V.L.; MacNab, I. Spinal metastases: the obvious, the occult, and the impostors. *Spine (Phila Pa 1976)* **1990**, *15*, 1-4.

3. Hellman, S.; Weichselbaum, R.R. Oligometastases. *J Clin Oncol* **1995**, *13*, 8-10, doi:10.1200/jco.1995.13.1.8.

4. Lievens, Y.; Guckenberger, M.; Gomez, D.; Hoyer, M.; Iyengar, P.; Kindts, I.; Méndez Romero, A.; Nevens, D.; Palma, D.; Park, C., et al. Defining oligometastatic disease from a radiation oncology perspective: An ESTRO-ASTRO consensus document. *Radiother Oncol* **2020**, *148*, 157-166, doi:10.1016/j.radonc.2020.04.003.

5. Chang, S.Y.; Mok, S.; Park, S.C.; Kim, H.; Chang, B.S. Treatment Strategy for Metastatic Spinal Tumors: A Narrative Review. *Asian Spine J* **2020**, *14*, 513-525, doi:10.31616/asj.2020.0379.

6. Barzilai, O.; Boriani, S.; Fisher, C.G.; Sahgal, A.; Verlaan, J.J.; Gokaslan, Z.L.; Lazary, A.; Bettegowda, C.; Rhines, L.D.; Laufer, I. Essential Concepts for the Management of Metastatic Spine Disease: What the Surgeon Should Know and Practice. *Global Spine J* **2019**, *9*, 98s-107s, doi:10.1177/2192568219830323.

7. Gerszten, P.C.; Mendel, E.; Yamada, Y. Radiotherapy and radiosurgery for metastatic spine disease: what are the options, indications, and outcomes? *Spine (Phila Pa 1976)* **2009**, *34*, S78-92, doi:10.1097/BRS.0b013e3181b8b6f5.

8. Yazici, G.; Sari, S.Y.; Yedekci, F.Y.; Yucekul, A.; Birgi, S.D.; Demirkiran, G.; Gultekin, M.; Hurmuz, P.; Yazici, M.; Ozyigit, G., et al. The dosimetric impact of implants on the spinal cord dose during stereotactic body radiotherapy. *Radiat Oncol* **2016**, *11*, 71, doi:10.1186/s13014-016-0649-z.

9. Glicksman, R.M.; Tjong, M.C.; Neves-Junior, W.F.P.; Spratt, D.E.; Chua, K.L.M.; Mansouri, A.; Chua, M.L.K.; Berlin, A.; Winter, J.D.; Dahele, M., et al. Stereotactic Ablative Radiotherapy for the Management of Spinal Metastases: A Review. *JAMA Oncol* **2020**, *6*, 567-577, doi:10.1001/jamaoncol.2019.5351.

10. Barzilai, O.; Fisher, C.G.; Bilsky, M.H. State of the Art Treatment of Spinal Metastatic Disease. *Neurosurgery* **2018**, *82*, 757-769, doi:10.1093/neuros/nyx567.

11. Barzilai, O.; Versteeg, A.L.; Sahgal, A.; Rhines, L.D.; Bilsky, M.H.; Sciubba, D.M.; Schuster, J.M.; Weber, M.H.; Pal Varga, P.; Boriani, S., et al. Survival, local control, and health-related quality of life in patients with oligometastatic and polymetastatic spinal tumors: A multicenter, international study. *Cancer* **2019**, *125*, 770-778, doi:10.1002/cncr.31870.

12. David, S.; Tan, J.; Savas, P.; Bressel, M.; Kelly, D.; Foroudi, F.; Loi, S.; Siva, S. Stereotactic ablative body radiotherapy (SABR) for bone only oligometastatic breast cancer: A prospective clinical trial. *Breast* **2020**, *49*, 55-62, doi:10.1016/j.breast.2019.10.016.

13. Zeng, K.L.; Tseng, C.L.; Soliman, H.; Weiss, Y.; Sahgal, A.; Myrehaug, S. Stereotactic Body Radiotherapy (SBRT) for Oligometastatic Spine Metastases: An Overview. *Front Oncol* **2019**, *9*, 337, doi:10.3389/fonc.2019.00337.

14. Cox, B.W.; Spratt, D.E.; Lovelock, M.; Bilsky, M.H.; Lis, E.; Ryu, S.; Sheehan, J.; Gerszten, P.C.; Chang, E.; Gibbs, I., et al. International Spine Radiosurgery Consortium consensus guidelines for target volume definition in spinal stereotactic radiosurgery. *Int J Radiat Oncol Biol Phys* **2012**, *83*, e597-605, doi:10.1016/j.ijrobp.2012.03.009.

15. Billiet, C.; Vingerhoed, W.; Van Laere, S.; Joye, I.; Mercier, C.; Dirix, P.; Nevens, D.; Vermeulen, P.; Meijnders, P.; Verellen, D. Precision of image-guided spinal stereotactic ablative radiotherapy and impact of positioning variables. *Phys Imaging Radiat Oncol* **2022**, *22*, 73-76, doi:10.1016/j.phro.2022.04.006.

16. Billiet, C.; Joye, I.; Mercier, C.; Depuydt, L.; De Kerf, G.; Vermeulen, P.; Van Laere, S.; Van de Kelft, E.; Meijnders, P.; Verellen, D., et al. Outcome and toxicity of hypofractionated image-guided SABR for spinal oligometastases. *Clin Transl Radiat Oncol* **2020**, *24*, 65-70, doi:10.1016/j.ctro.2020.06.011.

17. Ryu, S.; Jin, J.Y.; Jin, R.; Rock, J.; Ajlouni, M.; Movsas, B.; Rosenblum, M.; Kim, J.H. Partial volume tolerance of the spinal cord and complications of single-dose radiosurgery. *Cancer* **2007**, *109*, 628-636, doi:10.1002/cncr.22442.

18. Sahgal, A.; Myrehaug, S.D.; Siva, S.; Masucci, G.L.; Maralani, P.J.; Brundage, M.; Butler, J.; Chow, E.; Fehlings, M.G.; Foote, M., et al. Stereotactic body radiotherapy versus conventional external beam radiotherapy in patients with painful spinal metastases: an open-label, multicentre, randomised, controlled, phase 2/3 trial. *Lancet Oncol* **2021**, *22*, 1023-1033, doi:10.1016/s1470-2045(21)00196-0.

19. Sahgal, A.; Weinberg, V.; Ma, L.; Chang, E.; Chao, S.; Muacevic, A.; Gorgulho, A.; Soltys, S.; Gerszten, P.C.; Ryu, S., et al. Probabilities of radiation myelopathy specific to stereotactic body radiation therapy to guide safe practice. *Int J Radiat Oncol Biol Phys* **2013**, *85*, 341-347, doi:10.1016/j.ijrobp.2012.05.007.

20. Yamada, Y.; Bilsky, M.H.; Lovelock, D.M.; Venkatraman, E.S.; Toner, S.; Johnson, J.; Zatcky, J.; Zelefsky, M.J.; Fuks, Z. High-dose, single-fraction image-guided intensity-modulated radiotherapy for metastatic spinal lesions. *Int J Radiat Oncol Biol Phys* **2008**, *71*, 484-490, doi:10.1016/j.ijrobp.2007.11.046.

21. Boriani, S.; Tedesco, G.; Ming, L.; Ghermandi, R.; Amichetti, M.; Fossati, P.; Krengli, M.; Mavilla, L.; Gasbarrini, A. Carbon-fiber-reinforced PEEK fixation system in the treatment of spine tumors: a preliminary report. *Eur Spine J* **2018**, *27*, 874-881, doi:10.1007/s00586-017-5258-5.

22. Jia, Y.; Zhao, L.; Cheng, C.W.; McDonald, M.W.; Das, I.J. Dose perturbation effect of metallic spinal implants in proton beam therapy. *J Appl Clin Med Phys* **2015**, *16*, 333-343, doi:10.1120/jacmp.v16i5.5566.

23. Béhin, A.; Delattre, J.Y. Complications of radiation therapy on the brain and spinal cord. *Semin Neurol* **2004**, *24*, 405-417, doi:10.1055/s-2004-861535.

24. Furuya, T.; Lee, Y.K.; Archibald-Heeren, B.R.; Byrne, M.; Bosco, B.; Phua, J.H.; Shimizu, H.; Hashimoto, S.; Tanaka, H.; Sahgal, A., et al. Evaluation of multi-institutional end-to-end testing for post-operative spine stereotactic body radiation therapy. *Phys Imaging Radiat Oncol* **2020**, *16*, 61-68, doi:10.1016/j.phro.2020.09.005.

25. Tedesco, G.; Gasbarrini, A.; Bandiera, S.; Ghermandi, R.; Boriani, S. Composite PEEK/Carbon fiber implants can increase the effectiveness of radiotherapy in the management of spine tumors. *J Spine Surg* **2017**, *3*, 323-329, doi:10.21037/jss.2017.06.20.

26. Ringel, F.; Ryang, Y.M.; Kirschke, J.S.; Müller, B.S.; Wilkens, J.J.; Brodard, J.; Combs, S.E.; Meyer, B. Radiolucent Carbon Fiber-Reinforced Pedicle Screws for Treatment of Spinal Tumors: Advantages for Radiation Planning and Follow-Up Imaging. *World Neurosurg* **2017**, *105*, 294-301, doi:10.1016/j.wneu.2017.04.091.

27. Xin-ye, N.; Xiao-bin, T.; Chang-ran, G.; Da, C. The prospect of carbon fiber implants in radiotherapy. *J Appl Clin Med Phys* **2012**, *13*, 3821, doi:10.1120/jacmp.v13i4.3821.

28. Complications of patients with bone tumors treated with carbon-fiber plates: an international multicenter study. *Sci Rep* **2022**, *12*, 18969, doi:10.1038/s41598-022-23519-9.

29. Joerger, A.K.; Seitz, S.; Lange, N.; Aftahy, A.K.; Wagner, A.; Ryang, Y.M.; Bernhardt, D.; Combs, S.E.; Wostrack, M.; Gempt, J., et al. CFR-PEEK Pedicle Screw Instrumentation for Spinal Neoplasms: A Single Center Experience on Safety and Efficacy. *Cancers (Basel)* **2022**, *14*, doi:10.3390/cancers14215275.

30. Rijs, Z.; Weekhout, A.; Lozano-Calderon, S.A.; Groot, O.Q.; Berner, E.; Merchan, N.; Yeung, C.M.; Oliveira, V.; Bianchi, G.; Staals, E., et al. Complications of patients with bone tumors treated with carbon-fiber plates: an international multicenter study. *Scientific Reports* **2022**, *12*, 18969, doi:10.1038/s41598-022-23519-9.

9

31. Sakaura, H.; Hosono, N.; Mukai, Y.; Ishii, T.; Yonenobu, K.; Yoshikawa, H. Outcome of total en bloc spondylectomy for solitary metastasis of the thoracolumbar spine. *J Spinal Disord Tech* **2004**, *17*, 297-300, doi:10.1097/01.bsd.0000096269.75373.9b.

32. Takayanagi, A.; Siddiqi, I.; Ghanchi, H.; Lischalk, J.; Vrionis, F.; Ratliff, J.; Bilsky, M.; Hariri, O.R. Radiolucent Carbon Fiber-Reinforced Implants for Treatment of Spinal Tumors-Clinical, Radiographic, and Dosimetric Considerations. *World Neurosurg* **2021**, *152*, 61-70, doi:10.1016/j.wneu.2021.05.100.

33. Neal, M.T.; Richards, A.E.; Curley, K.L.; Patel, N.P.; Ashman, J.B.; Vora, S.A.; Kalani, M.A. Carbon fiber-reinforced PEEK instrumentation in the spinal oncology population: a retrospective series demonstrating technique, feasibility, and clinical outcomes. *Neurosurg Focus* **2021**, *50*, E13, doi:10.3171/2021.2.Focus20995.

34. Krätzig, T.; Mende, K.C.; Mohme, M.; Kniep, H.; Dreimann, M.; Stangenberg, M.; Westphal, M.; Gauer, T.; Eicker, S.O. Carbon fiber–reinforced PEEK versus titanium implants: an in vitro comparison of susceptibility artifacts in CT and MR imaging. *Neurosurgical Review* **2021**, *44*, 2163-2170, doi:10.1007/s10143-020-01384-2.

35. Depauw, N.; Pursley, J.; Lozano-Calderon, S.A.; Patel, C.G. Evaluation of Carbon Fiber and Titanium Surgical Implants for Proton and Photon Therapy. *Pract Radiat Oncol* **2023**, 10.1016/j.prro.2023.01.009, doi:10.1016/j.prro.2023.01.009.

36. Fleege, C.; Makowski, M.; Rauschmann, M.; Fraunhoffer, K.L.; Fennema, P.; Arabmotlagh, M.; Rickert, M. Carbon fiber-reinforced pedicle screws reduce artifacts in magnetic resonance imaging of patients with lumbar spondylodesis. *Sci Rep* **2020**, *10*, 16094, doi:10.1038/s41598-020-73386-5.

37. Akyol, O.; Dirican, B.; Toklu, T.; Eren, H.; Olgar, T. Investigating the effect of dental implant materials with different densities on radiotherapy dose distribution using Monte-Carlo simulation and pencil beam convolution algorithm. *Dentomaxillofac Radiol* **2019**, *48*, 20180267, doi:10.1259/dmfr.20180267.

38. Gaito, S.; Marvaso, G.; Ortiz, R.; Crellin, A.; Aznar, M.C.; Indelicato, D.J.; Pan, S.; Whitfield, G.; Alongi, F.; Jereczek-Fossa, B.A., et al. Proton Beam Therapy in the Oligometastatic/Oligorecurrent Setting: Is There a Role? A Literature Review. *Cancers (Basel)* **2023**, *15*, doi:10.3390/cancers15092489.

39. Nevelsky, A.; Borzov, E.; Daniel, S.; Bar-Deroma, R. Perturbation effects of the carbon fiber-PEEK screws on radiotherapy dose distribution. *J Appl Clin Med Phys* **2017**, *18*, 62-68, doi:10.1002/acm2.12046.

40. Mastella, E.; Molinelli, S.; Magro, G.; Mirandola, A.; Russo, S.; Vai, A.; Mairani, A.; Choi, K.; Fiore, M.R.; Fossati, P., et al. Dosimetric characterization of carbon fiber stabilization devices for post-operative particle therapy. *Phys Med* **2017**, *44*, 18-25, doi:10.1016/j.ejmp.2017.11.008.

41. Hubertus, V.; Wessels, L.; Früh, A.; Tkatschenko, D.; Nulis, I.; Bohner, G.; Prinz, V.; Onken, J.; Czabanka, M.; Vajkoczy, P., et al. Navigation accuracy and assessability of carbon fiber-reinforced PEEK instrumentation with multimodal intraoperative imaging in spinal oncology. *Sci Rep* **2022**, *12*, 15816, doi:10.1038/s41598-022-20222-7.

42. Herzog, L.N.; Traven, S.A.; Walton, Z.J.; Leddy, L.R. The Use of Carbon Fiber Implants for Impending or Existing Pathologic Fractures. *J Orthop Trauma* **2022**, *36*, e260-e264, doi:10.1097/bot.0000000000002320.

43. Zaidi, Q.; Danisa, O.A.; Cheng, W. Measurement Techniques and Utility of Hounsfield Unit Values for Assessment of Bone Quality Prior to Spinal Instrumentation: A Review of Current Literature. *Spine (Phila Pa 1976)* **2019**, *44*, E239-e244, doi:10.1097/brs.0000000000002813.

9

10

GENERAL DISCUSSION AND FUTURE PERSPECTIVES

Although sarcomas are rare, they are associated with significant morbidity and mortality [1,2]. Epidemiological studies show that recurrence rates and survival did not improve over the last decade [3]. Moreover, mortality is predicted to increase in 2025, highlighting insufficient advancements in sarcoma treatment [4]. Consequently, innovative treatment strategies are required to improve patient care. An emerging technique to guide surgeon's decision making and optimize margins is fluorescence-guided surgery (FGS), which has been explored in various tumor types and is examined for its potential use in sarcoma surgery in part I of this thesis [5]. Once adequate tumor resection has been achieved, the next phase involves reconstruction and fixation as tumor resections can cause large residual osseous defects and loss of soft tissue stabilizers. In part II of this thesis, carbon-fiber (CF) implants are evaluated as an innovative solution for stable fixation. CF offers several material specific advantages over traditional metal implants, particularly for the oncological population [6]. This chapter will discuss FGS and the use of CF implants, both innovative treatment strategies in orthopedic oncology. Initially, the clinical need and a scientifically robust workup for the implementation of FGS in sarcoma surgery will be addressed, along with the associated challenges and future perspectives. Subsequently, the focus will shift to the clinical need for CF implants, their anticipated impact, and future perspectives on orthopedic oncology treatment.

Clinical need for the implementation of FGS in sarcoma surgery

The success of surgical treatment for localized sarcomas highly depends on complete tumor resection as positive margins are associated with increased local recurrence (LR) and decreased overall survival [7]. Yet, determining the surgical margin during surgery remains a major challenge, particularly when tumor tissue is surrounded by vital or critical structures, in deeper or complex anatomical regions, or in sarcoma subtypes with a highly infiltrative growth pattern. Consequently, technologies that facilitate intraoperative decision-making to optimize margins is becoming an urgent need. From an industry perspective, interest in such technologies has grown substantially over the years. In 2022, the medical imaging market was valued at 40 billion United-States dollar, and is expected to grow at a 5.5% mean annual growth rate from 2023 to 2032, driven by technological innovations and advancements [8]. With the first randomized controlled trial for non-targeted FGS in sarcoma patients currently in the recruitment phase (expected end date on August 30, 2026), the field is at the doorstep of breakthroughs that could guide the surgeon's decision making during surgery [9].

Workup for the implementation of FGS in sarcoma surgery

Achieving a clear contrast between tumor and surrounding healthy (background) tissue is crucial for FGS. The threshold of such a tumor-to-background ratio (TBR) should at least be 1.5 to allow for tumor identification [10]. While non-targeted FGS can illuminate some sarcomas, the signal intensity is unreliable due to the variability of the enhanced permeability and retention effect [11]. Hence, targeted FGS is preferred. Selecting targets overexpressed on sarcomas, as performed in Chapter 2, is the first step for targeted FGS. IHC evaluation of these targets in a comparative setting using intra-patient sets of tumor and adjacent normal tissue, as shown in Chapter 3, is an important second step. Further in vitro evaluation, as depicted

in Chapter 5, can confirm binding specificity of a tracer directed to the selected target. Next, topical application of the tumor-specific tracer on freshly resected tumor and adjacent healthy tissue (Chapter 5) is a practical approach to assess tumor margins, as it circumvents the need for expensive and time-consuming toxicology studies for human application [12]. Topical tracers can be applied as a cream or spray to facilitate pathologists in assessing resection margins and perform inter- and intratumoral TBR analysis [13]. Successful translation to intravenous (IV) use can be anticipated once ex vivo topical application consistently yields promising results. However, evaluation of biodistribution, toxicology, optimal dosage and safety, and registration as an approved drug are required before implementation. The subsequent clinical success depends on evidence-based effectiveness, meaning better patient outcomes and/or an improved surgical workflow at a reasonable cost [14]. In this regard, patient benefits should be scored by looking at short-term complication rates and long-term outcomes across cohorts with and without use of FGS. In order to improve success rates, characterization of the patient's tumor surface antigen expression should become routine at diagnosis to decide which tracer is best for FGS for each specific case before surgical resection.

Challenges and future perspectives for FGS in sarcoma surgery
The ultimate goal for targeted FGS is to identify a single target consistently expressed across all cancer types, with minimal or no expression in adjacent healthy tissue. However, achieving this for sarcomas is already challenging due to the significant inter- and intra-tumor heterogeneity across subtypes [15]. Consequently, the current focus should be on specific sarcoma subtypes that grow infiltratively, have high percentages of positive margins and high local recurrence rates. Myxofibrosarcoma (MFS) is such an example with positive margins of 20% and LR rates of 40% (with 10-year follow-up) [16,17]. IHC studies demonstrated that tumor endothelial marker 1 (TEM1) was the most suitable biomarker for targeted FGS in MFS, regardless of preoperative therapy [18,19]. Therefore, we recommend developing a TEM1 specific tracer by conjugating a fluorescent dye to a clinically available monoclonal antibody (mAb) such as Ontuxizumab or 1C1m (mAb fragment) [20,21]. This tracer could be a more specific alternative than Bevacizumab-800CW, a tracer that has already been tested after IV administration in MFS patients with promising results, but room for improvement [22]. Translating clinically approved mAbs to tracers is cost- and time-efficient as biodistribution, toxicology, and dosing studies have already been performed. Moreover, a recent review emphasizes that several "off-the shelf" targeted tracers are already available [23]. However, the large size of mAbs (150kDa) limits tumor penetration and necessitates over 24 hours to obtain an optimal TBR [24]. In this regard, new-generation small molecules could be adopted to increase tumor penetration and provide an optimal TBR within hours after administration [25,26]. Still, FGS is limited by a maximum tissue penetration depth of approximately 1 centimeter of the emitted fluorescent light [27]. Hence, options to use another camera or detection system, such as ultrasound-based photoacoustic three dimensional in depth imaging, are being investigated while using the same tracer as for FGS [28]. Besides, integrating FGS with radio- or magnetic guidance using hybrid or bi-model tracers can facilitate the detection and excision of tumors situated deeper than 1 centimeter [29]. Yet, the combination of these technologies is complex and

10

requires collaboration of multidisciplinary expert teams (including surgeons, pathologists, radiologists, nuclear medicine physicians, technology orientated chemists and engineers) to achieve precise intraoperative guidance and complete tumor resection [30].

Clinical need for innovative implants

Adequate tumor resections can result in osseous defects and loss of soft tissue stabilizers, affecting function and viability of the resected site [31]. Reconstruction with biological constructs, such as autografts and allografts, and/or orthopedic implants are often required to maintain limb function and bone strength [32]. Traditionally, implants are made from stainless steel and titanium alloys. However, a major disadvantage of these metal implants is their radiodensity, which precludes accurate radiographic visualization for oncological follow-up and impedes precise postoperative radiation planning and delivery [33]. Moreover, the stiffness of metal (200 gigapascal [GPa] for stainless steel and 110 GPa for titanium) is much higher than the human cortical bone (12 GPa) which shields the underlying bone from stress and leads to reduced bone quality [34]. The introduction of CF implants, with several material specific advantages over metal implants, represents a new option for multidisciplinary oncology teams.

Anticipated impact of CF implants in orthopedic oncology and future perspectives

CF's radiolucency enhances the radiological evaluation of anatomical structures and allows for earlier detection of tumor recurrences [35]. Besides, it enables postoperative image-guided percutaneous interventions, such as pain palliation injections or ablation procedures [36]. For radiation oncologists, CF implants are beneficial in treating primary bone tumors, which necessitate high radiation doses for local control. In these cases, proton beam radiation therapy (PBRT) is essential to safely deliver therapeutic doses while respecting the tolerance of critical anatomical structures such as the spinal cord [36]. The presence of metal artifacts poses significant challenges for the planning and delivery, and metal implants were an independent predictor of local failure in patients with spinal chordoma treated with PBRT [37,38]. In contrast, CF implants minimize artifacts (Chapter 9), improve radiotherapy planning, and ensure adequate dose distribution [39]. From a surgical perspective, CF plates, nails, and spinal implants are safe for demanding reconstructions after tumor resections (Chapter 6 – 8) [40]. No significant differences in operation time, perioperative bleeding, complications, and average survival time underscore that CF is a viable alternative to metal implants [40-42]. Additionally, the modulus of elasticity of CF (13 GPa) is close to that of cortical bone, reducing stress shielding and enhancing bone quality [43]. Despite these advantages, adaptation of CF as standard care may face challenges due to the familiarity with metal implants and technical challenges. For example, the inability to bend CF implants necessitates careful preoperative planning. Yet, custom 3D printed CF instrumentation has been introduced and may become a valuable option for challenging reconstructions [44]. Besides, CF's radiolucency can complicate minimally invasive surgeries which rely heavily on fluoroscopic support for bone and implant visualization, but radiopaque markers have been incorporated to resolve this potential problem. Despite CF's clear potential, future comparative international multicenter

randomized controlled trials and cost-effectiveness studies are warranted to investigate the impact of using CF implants, particularly focusing on the benefits of improved bone quality, better follow-up, and the radiotherapeutic effect. For now, we recommend choosing CF implants when postoperative radiotherapy is needed at the site of the operation and for tumors with good prognosis for which imaging surveillance for LR is anticipated.

Overall conclusions

This thesis explored innovative treatment options in musculoskeletal tumor surgery. Fluorescence-guided surgery (FGS) was evaluated for margin optimization in sarcoma patients. Preclinical evaluation studies identified promising targets for targeted FGS. Additionally, a scientific robust workflow is provided to enable a successful and cost-efficient clinical translation of tracers for targeted FGS. With the first randomized controlled trial for non-targeted FGS in sarcoma patients currently in the recruitment phase, the field is at the doorstep of breakthroughs that could guide the surgeon's decision making during surgery. Following adequate tumor resection, the next phase involves reconstruction and fixation. In this context, the use of carbon-fiber (CF) implants presents an innovative option with several material specific advantages over conventional metal implants. Given their comparable safety profile and benefits such as radiolucency, reduced stress shielding, and lack of scattering artifacts, CF implants may become part of the standard treatment armamentarium, offering significant advantages for oncology patients.

10

References

1. Bergovec, M.; Kubat, O.; Smerdelj, M.; Seiwerth, S.; Bonevski, A.; Orlic, D. Epidemiology of musculoskeletal tumors in a national referral orthopedic department. A study of 3482 cases. *Cancer Epidemiol* **2015**, *39*, 298-302, doi:10.1016/j.canep.2015.01.015.

2. Ferguson, J.L.; Turner, S.P. Bone Cancer: Diagnosis and Treatment Principles. *Am Fam Physician* **2018**, *98*, 205-213.

3. van der Horst, C.A.J.; Bongers, S.L.M.; Versleijen-Jonkers, Y.M.H.; Ho, V.K.Y.; Braam, P.M.; Flucke, U.E.; de Wilt, J.H.W.; Desar, I.M.E. Overall Survival of Patients with Myxofibrosarcomas: An Epidemiological Study. *Cancers (Basel)* **2022**, *14*, doi:10.3390/cancers14051102.

4. Pizzato, M.; Collatuzzo, G.; Santucci, C.; Malvezzi, M.; Boffetta, P.; Comandone, A.; Levi, F.; La Vecchia, C.; Bertuccio, P.; Negri, E. Mortality patterns of soft-tissue sarcomas worldwide up to 2018, with predictions for 2025. *Eur J Cancer Prev* **2023**, *32*, 71-80, doi:10.1097/cej.0000000000000768.

5. Hernot, S.; van Manen, L.; Debie, P.; Mieog, J.S.D.; Vahrmeijer, A.L. Latest developments in molecular tracers for fluorescence image-guided cancer surgery. *Lancet Oncol* **2019**, *20*, e354-e367, doi:10.1016/s1470-2045(19)30317-1.

6. Yeung, C.M.; Bhashyam, A.R.; Patel, S.S.; Ortiz-Cruz, E.; Lozano-Calderón, S.A. Carbon Fiber Implants in Orthopaedic Oncology. *J Clin Med* **2022**, *11*, doi:10.3390/jcm11174959.

7. Jang, W.Y.; Kim, H.S.; Han, I. Impact of surgical margin on survival in extremity soft tissue sarcoma: A systematic review and meta-analysis. *Medicine (Baltimore)* **2021**, *100*, e24124, doi:10.1097/md.0000000000024124.

8. GM., I. Medical Imaging Market - by Product (X-Ray Devices, Magnetic Resonance Imaging (MRI), Ultrasound, Computed Tomography, Nuclear Imaging, Mammography), by End-Use (Hospitals, Diagnostic Centers) & Forecast, 2022–2030; 2022. Availabe online: https://www.gminsights.com/industry-analysis/medical-imaging-market (accessed on 24-06-2024).

9. UK, C.R. A trial of fluorescence guided surgery for sarcoma (sarcoSIGHT). Availabe online: https://www.cancerresearchuk.org/about-cancer/find-a-clinical-trial/a-trial-of-fluorescence-guided-surgery-for-sarcoma-sarcosight#undefined (accessed on 26-06-2024).

10. Azargoshasb, S.; Boekestijn, I.; Roestenberg, M.; KleinJan, G.H.; van der Hage, J.A.; van der Poel, H.G.; Rietbergen, D.D.D.; van Oosterom, M.N.; van Leeuwen, F.W.B. Quantifying the Impact of Signal-to-background Ratios on Surgical Discrimination of Fluorescent Lesions. *Mol Imaging Biol* **2023**, *25*, 180-189, doi:10.1007/s11307-022-01736-y.

11. Brookes, M.J.; Chan, C.D.; Nicoli, F.; Crowley, T.P.; Ghosh, K.M.; Beckingsale, T.; Saleh, D.; Dildey, P.; Gupta, S.; Ragbir, M., et al. Intraoperative Near-Infrared Fluorescence Guided Surgery Using Indocyanine Green (ICG) for the Resection of Sarcomas May Reduce the Positive Margin Rate: An Extended Case Series. *Cancers (Basel)* **2021**, *13*, doi:10.3390/cancers13246284.

12. Buckle, T.; van Alphen, M.; van Oosterom, M.N.; van Beurden, F.; Heimburger, N.; van der Wal, J.E.; van den Brekel, M.; van Leeuwen, F.W.B.; Karakullukcu, B. Translation of c-Met Targeted Image-Guided Surgery Solutions in Oral Cavity Cancer-Initial Proof of Concept Data. *Cancers (Basel)* **2021**, *13*, doi:10.3390/cancers13112674.

13. Slooter, M.D.; Handgraaf, H.J.M.; Boonstra, M.C.; van der Velden, L.A.; Bhairosingh, S.S.; Que, I.; de Haan, L.M.; Keereweer, S.; van Driel, P.; Chan, A., et al. Detecting tumour-positive resection margins after oral cancer surgery by spraying a fluorescent tracer activated by gamma-glutamyltranspeptidase. *Oral Oncol* **2018**, *78*, 1-7, doi:10.1016/j.oraloncology.2017.12.006.

14. Lauwerends, L.J.; van Driel, P.; Baatenburg de Jong, R.J.; Hardillo, J.A.U.; Koljenovic, S.; Puppels, G.; Mezzanotte, L.; Löwik, C.; Rosenthal, E.L.; Vahrmeijer, A.L., et al. Real-time fluorescence imaging in intraoperative decision making for cancer surgery. *Lancet Oncol* **2021**, *22*, e186-e195, doi:10.1016/s1470-2045(20)30600-8.

15. Board, W.C.o.T.E. *Tissue and Bone Tumours: WHO Classification of Tumours*, 5 ed.; 2020; Vol. 3.

16. Look Hong, N.J.; Hornicek, F.J.; Raskin, K.A.; Yoon, S.S.; Szymonifka, J.; Yeap, B.; Chen, Y.L.; DeLaney, T.F.; Nielsen, G.P.; Mullen, J.T. Prognostic factors and outcomes of patients with myxofibrosarcoma. *Ann Surg Oncol* **2013**, *20*, 80-86, doi:10.1245/s10434-012-2572-3.

17. Odei, B.; Rwigema, J.C.; Eilber, F.R.; Eilber, F.C.; Selch, M.; Singh, A.; Chmielowski, B.; Nelson, S.D.; Wang, P.C.; Steinberg, M., et al. Predictors of Local Recurrence in Patients With Myxofibrosarcoma. *Am J Clin Oncol* **2018**, *41*, 827-831, doi:10.1097/coc.0000000000000382.

18. de Gooyer, J.M.; Versleijen-Jonkers, Y.M.H.; Hillebrandt-Roeffen, M.H.S.; Frielink, C.; Desar, I.M.E.; de Wilt, J.H.W.; Flucke, U.; Rijpkema, M. Immunohistochemical selection of biomarkers for tumor-targeted image-guided surgery of myxofibrosarcoma. *Sci Rep* **2020**, *10*, 2915, doi:10.1038/s41598-020-59735-4.

19. Rijs, Z.; Belt, E.; Kalisvaart, G.M.; Sier, C.F.M.; Kuppen, P.J.K.; Cleven, A.H.G.; Vahrmeijer, A.L.; van de Sande, M.A.J.; van Driel, P. Immunohistochemical Evaluation of Candidate Biomarkers for Fluorescence-Guided Surgery of Myxofibrosarcoma Using an Objective Scoring Method. *Biomedicines* **2023**, *11*, doi:10.3390/biomedicines11030982.

20. Delage, J.A.; Faivre-Chauvet, A.; Fierle, J.K.; Gnesin, S.; Schaefer, N.; Coukos, G.; Dunn, S.M.; Viertl, D.; Prior, J.O. (177)Lu radiolabeling and preclinical theranostic study of 1C1m-Fc: an anti-TEM-1 scFv-Fc fusion protein in soft tissue sarcoma. *EJNMMI Res* **2020**, *10*, 98, doi:10.1186/s13550-020-00685-3.

21. O'Shannessy, D.J.; Smith, M.F.; Somers, E.B.; Jackson, S.M.; Albone, E.; Tomkowicz, B.; Cheng, X.; Park, Y.; Fernando, D.; Milinichik, A., et al. Novel antibody probes for the characterization of endosialin/TEM-1. *Oncotarget* **2016**, *7*, 69420-69435, doi:10.18632/oncotarget.11018.

22. Steinkamp, P.J.; Pranger, B.K.; Li, M.F.; Linssen, M.D.; Voskuil, F.J.; Been, L.B.; van Leeuwen, B.L.; Suurmeijer, A.J.H.; Nagengast, W.B.; Kruijff, S., et al. Fluorescence-Guided Visualization of Soft-Tissue Sarcomas by Targeting Vascular Endothelial Growth Factor A: A Phase 1 Single-Center Clinical Trial. *J Nucl Med* **2021**, *62*, 342-347, doi:10.2967/jnumed.120.245696.

23. Giuliani, S.; Paraboschi, I.; McNair, A.; Smith, M.; Rankin, K.S.; Elson, D.S.; Paleri, V.; Leff, D.; Stasiuk, G.; Anderson, J. Monoclonal Antibodies for Targeted Fluorescence-Guided Surgery: A Review of Applicability across Multiple Solid Tumors. *Cancers (Basel)* **2024**, *16*, doi:10.3390/cancers16051045.

24. Freise, A.C.; Wu, A.M. In vivo imaging with antibodies and engineered fragments. *Mol Immunol* **2015**, *67*, 142-152, doi:10.1016/j.molimm.2015.04.001.

25. Jiao, J.; Zhang, J.; Yang, F.; Song, W.; Han, D.; Wen, W.; Qin, W. Quicker, deeper and stronger imaging: A review of tumor-targeted, near-infrared fluorescent dyes for fluorescence guided surgery in the preclinical and clinical stages. *Eur J Pharm Biopharm* **2020**, *152*, 123-143, doi:10.1016/j.ejpb.2020.05.002.

26. Shou, K.; Qu, C.; Sun, Y.; Chen, H.; Chen, S.; Zhang, L.; Xu, H.; Hong, X.; Yu, A.; Cheng, Z. Multifunctional biomedical imaging in physiological and pathological conditions using a NIR-II probe. *Adv Funct Mater* **2017**, *27*, doi:10.1002/adfm.201700995.

27. Keiser, G. *Biophotonics: Concepts to Applications*; 2016.

28. Baart, V.M.; van der Horst, G.; Deken, M.M.; Bhairosingh, S.S.; Schomann, T.; Sier, V.Q.; van der Mark, M.H.; Iamele, L.; de Jonge, H.; Resnati, M., et al. A multimodal molecular imaging approach targeting urokinase plasminogen activator receptor for the diagnosis, resection and surveillance of urothelial cell carcinoma. *Eur J Cancer* **2021**, *146*, 11-20, doi:10.1016/j.ejca.2021.01.001.

10

29.   van Leeuwen, F.W.B.; Schottelius, M.; Brouwer, O.R.; Vidal-Sicart, S.; Achilefu, S.; Klode, J.; Wester, H.J.; Buckle, T. Trending: Radioactive and Fluorescent Bimodal/Hybrid Tracers as Multiplexing Solutions for Surgical Guidance. *J Nucl Med* **2020**, *61*, 13-19, doi:10.2967/jnumed.119.228684.

30.   van Leeuwen, F.W.B.; Buckle, T.; Rietbergen, D.D.D.; van Oosterom, M.N. The realization of medical devices for precision surgery - development and implementation of 'stop-and-go' imaging technologies. *Expert Rev Med Devices* **2024**, *21*, 349-358, doi:10.1080/17434440.2024.2341102.

31.   Salzer, M.; Knahr, K. Resection of malignant bone tumors. *Recent Results Cancer Res* **1976**, 10.1007/978-3-642-80997-2_21, 239-256, doi:10.1007/978-3-642-80997-2_21.

32.   Zhao, Z.; Yan, T.; Guo, W.; Yang, R.; Tang, X.; Wang, W. Surgical options and reconstruction strategies for primary bone tumors of distal tibia: A systematic review of complications and functional outcome. *J Bone Oncol* **2019**, *14*, 100209, doi:10.1016/j.jbo.2018.100209.

33.   Laux, C.J.; Villefort, C.; Ehrbar, S.; Wilke, L.; Guckenberger, M.; Müller, D.A. Carbon Fiber/Polyether Ether Ketone (CF/PEEK) Implants Allow for More Effective Radiation in Long Bones. *Materials (Basel)* **2020**, *13*, doi:10.3390/ma13071754.

34.   Jockisch, K.A.; Brown, S.A.; Bauer, T.W.; Merritt, K. Biological response to chopped-carbon-fiber-reinforced peek. *J Biomed Mater Res* **1992**, *26*, 133-146, doi:10.1002/jbm.820260202.

35.   Baidya, K.P.; Ramakrishna, S.; Rahman, M.; Ritchie, A. Quantitative radiographic analysis of fiber reinforced polymer composites. *J Biomater Appl* **2001**, *15*, 279-289, doi:10.1106/bklq-e2yg-d2la-rg3r.

36.   Long, J.R.; Kalani, M.A.; Goulding, K.A.; Ashman, J.B.; Flug, J.A. Carbon-fiber-reinforced polyetheretherketone orthopedic implants in musculoskeletal and spinal tumors: imaging and clinical features. *Skeletal Radiol* **2023**, *52*, 393-404, doi:10.1007/s00256-022-04069-7.

37.   Jia, Y.; Zhao, L.; Cheng, C.W.; McDonald, M.W.; Das, I.J. Dose perturbation effect of metallic spinal implants in proton beam therapy. *J Appl Clin Med Phys* **2015**, *16*, 333-343, doi:10.1120/jacmp.v16i5.5566.

38.   Rutz, H.P.; Weber, D.C.; Sugahara, S.; Timmermann, B.; Lomax, A.J.; Bolsi, A.; Pedroni, E.; Coray, A.; Jermann, M.; Goitein, G. Extracranial chordoma: Outcome in patients treated with function-preserving surgery followed by spot-scanning proton beam irradiation. *Int J Radiat Oncol Biol Phys* **2007**, *67*, 512-520, doi:10.1016/j.ijrobp.2006.08.052.

39.   Soriani, A.; Strigari, L.; Petrongari, M.G.; Anelli, V.; Baldi, J.; Salducca, N.; Biagini, R.; Zoccali, C. The advantages of carbon fiber based orthopedic devices in patients who have to undergo radiotherapy. *Acta Biomed* **2020**, *91*, e2020057, doi:10.23750/abm.v91i3.7769.

40.   Schmidt Morgen, S.; Alfthan Madsen, E.B.; Skive Weiland, A.; Dahl, B.; Gehrchen, M. Carbon Instrumentation in Patients with Metastatic Spinal Cord Compression. *Cancers (Basel)* **2024**, *16*, doi:10.3390/cancers16040736.

41.   Behrendt, P.; Kruse, E.; Klüter, T.; Fitschen-Oestern, S.; Weuster, M.; Menzdorf, L.; Finn, J.; Varoga, D.; Seekamp, A.; Müller, M., et al. [Fixed angle carbon fiber reinforced polymer composite plate for treatment of distal radius fractures : Pilot study on clinical applications]. *Unfallchirurg* **2017**, *120*, 139-146, doi:10.1007/s00113-015-0088-6.

42.   Yeung, C.M.; Bhashyam, A.R.; Groot, O.Q.; Merchan, N.; Newman, E.T.; Raskin, K.A.; Lozano-Calderón, S.A. Comparison of carbon fibre and titanium intramedullary nails in orthopaedic oncology. *Bone Jt Open* **2022**, *3*, 648-655, doi:10.1302/2633-1462.38.Bjo-2022-0092.R1.

43.   Bagheri, Z.S.; Tavakkoli Avval, P.; Bougherara, H.; Aziz, M.S.; Schemitsch, E.H.; Zdero, R. Biomechanical analysis of a new carbon fiber/flax/epoxy bone fracture plate shows less stress shielding compared to a standard clinical metal plate. *J Biomech Eng* **2014**, *136*, 091002, doi:10.1115/1.4027669.

44.   Shen, F.H.; Gasbarrini, A.; Lui, D.F.; Reynolds, J.; Capua, J.; Boriani, S. Integrated Custom Composite Polyetheretherketone/Carbon fiber (PEEK/CF) Vertebral Body Replacement (VBR) in the Treatment of Bone Tumors of the Spine: A Preliminary Report From a Multicenter Study. *Spine (Phila Pa 1976)* **2022**, *47*, 252-260, doi:10.1097/brs.0000000000004177.

10

11

SUMMARY

The objective of this thesis is to improve the treatment for patients with musculoskeletal tumors. **Part I** explores the potential of optimizing margins using fluorescence-guided surgery (FGS) for sarcomas, and, after tumor resection, **Part II** focuses on achieving adequate reconstruction and stable fixation with carbon-fiber (CF) implants.

In **Chapter 2**, a systematic literature review is conducted to identify candidate biomarkers that can be used for targeted FGS. Based on a target selection scoring system, the search revealed 7 biomarkers that are abundantly present on soft tissue sarcoma tumor cells. More specifically, tumor endothelial marker 1 (TEM1), platelet derived growth factor α (PDGFRα), and epidermal growth factor receptor (EGFR) are identified as most promising cell surface-expressed biomarkers for tumor-specific FGS in Myxofibrosarcoma (MFS), Undifferentiated Soft Tissue Sarcoma (USTS), and Synovial Sarcoma (SS). Important for cost- and time-efficient clinical translation, clinically approved monoclonal antibodies targeting the aforementioned biomarkers are present. These antibodies can be conjugated to a fluorophore for imaging purposes as they are expected to be safe for their use in FGS. However, biomarker expression on adjacent healthy tissue had not been investigated yet.

In **Chapter 3**, an immunohistochemical (IHC) evaluation of the previously selected biomarkers was performed on seventeen paraffin-embedded MFS samples with adjacent healthy tissue. An objective scoring method is developed and demonstrates that TEM1 was the most suitable biomarker for targeted FGS in MFS. This is based on a higher tumor-to-normal staining intensity compared to other biomarkers, regardless of preoperative therapy.

In **Chapter 4**, FGS using Indocyanine Green (ICG) as well as targeted FGS were reviewed for three prevalent pediatric sarcomas: Osteosarcoma (OS), Ewing Sarcoma (ES), and Rhabdomyosarcoma (RMS). Although ICG is relatively cheap and safe, intravenous administration might be a burden from a logistical point of view as it has to be administered 24 hours before surgery. Moreover, ICG's signal intensity is unpredictable. False negativity and false positivity could occur, potentially leading to under- or over-resection, resulting in incomplete tumor resections, or increased functional impairments and wound complications. Targeted FGS could theoretically overcome these disadvantages and might therefore be seen as a next step towards successful intraoperative tumor delineation. An overview of potential tumor-specific targets for OS, ES, and RMS is provided.

In **Chapter 5**, ES is the subject of further investigation. IHC evaluation of potential targets is performed on a total of thirteen ES patients. Based on relatively high tumor-to-normal expression, two proteins located on the tumor cell membrane, cluster of differentiation 99 (CD99), and cluster of differentiation 117 (CD117) are selected as most promising targets. Additionally, disialoganglioside 2 (GD2) is considered as a promising target due to its known high expression in ES biopsy samples and the clinical availability of an FGS tracer. Next, anti-CD99, anti-CD117, and anti-GD2 tracers are evaluated for binding specificity using flow cytometry and immunofluorescence microscopy. These experiments confirm high CD99

expression, along with low/moderate CD117 and low GD2 expression, in Ewing Sarcoma cell lines. To demonstrate the proof-of-principle, these tracers are topically applied on freshly resected ES tumor- and adjacent healthy tissue. We conclude that CD99-targeting tracers hold most promise for FGS in ES, while CD117 and GD2 tracers could be potential alternatives.

In **Chapter 6**, 13 centers retrospectively registered 96 oncological patients with a median follow up of 35 months, who are reconstructed with CF plates between 2015 and 2021. In total, 22 (23%) patients had complications. Mechanical complications included: 1 (1%) aseptic loosening, 2 (2%) non-unions, and 7 (7%) structural complications such as periprosthetic fractures or screw/plate breakages. Non-mechanical complications included 1 (1%) soft tissue complication which was a wound dehiscence, 4 (4%) infections and 5 (5%) tumor progressions. Pediatric complications occurred in 2 (2%) patients with a growth arrest resulting in longitudinal or angular deformity. Due to the relatively low complication profile, this study suggests CF plates are safe to use in demanding reconstructions after bone tumor resections.

In **Chapter 7**, a systematic review includes 27 studies reporting on clinical and radiological outcomes of patients treated with CF plates. The review does not reveal a concerning number of complications related to CF plate fixation. Therefore, CF plates appear to be a viable alternative to metal plates. However, high-quality randomized controlled trials with long-term follow-up are strongly recommended to provide additional evidence supporting the use of CF plates.

In **Chapter 8**, 239 patients treated with CF nails for impending or complete pathological fractures between 2013 and 2020 are analyzed for incidences and risk factors of mechanical and non-mechanical complications with a median follow up of 17 months. Thirty-three (14%) patients had complications. Mechanical failures included 4 (2%) structural host-bone failures, 7 (3%) implant-structural failures, and 1 (<1%) aseptic loosening of distal locking screws. Non-mechanical failures included 8 (3%) peri-implant infections and 15 (6%) tumor progressions. Preoperative radiation therapy at the surgical site and femur surgery are associated with increased complication risk in all groups after adjusting for confounders in the multivariate analysis. The 90-day and 1-year mortalities are 28% and 53%, respectively. The literature reports comparable failure and mortality rates to conventional titanium implants, suggesting CF nails might be a viable alternative.

In **Chapter 9**, artefacts on CT images in 11 patients treated with CF spinal implants are compared with 11 patients treated with titanium spinal implants. Both patient groups showed spinal oligometastatic disease and underwent stereotactic ablative radiotherapy. Less CT artefacts are observed in patients treated with CF spinal implants, which could facilitate an easier contouring phase in radiotherapy planning. Yet, future studies of randomized or matched comparative nature are needed to assess the added clinical value of the theoretical benefits of CF implants, such as precise radiation planning, improved bone healing, and improved radiographic visualization of local recurrences.

11
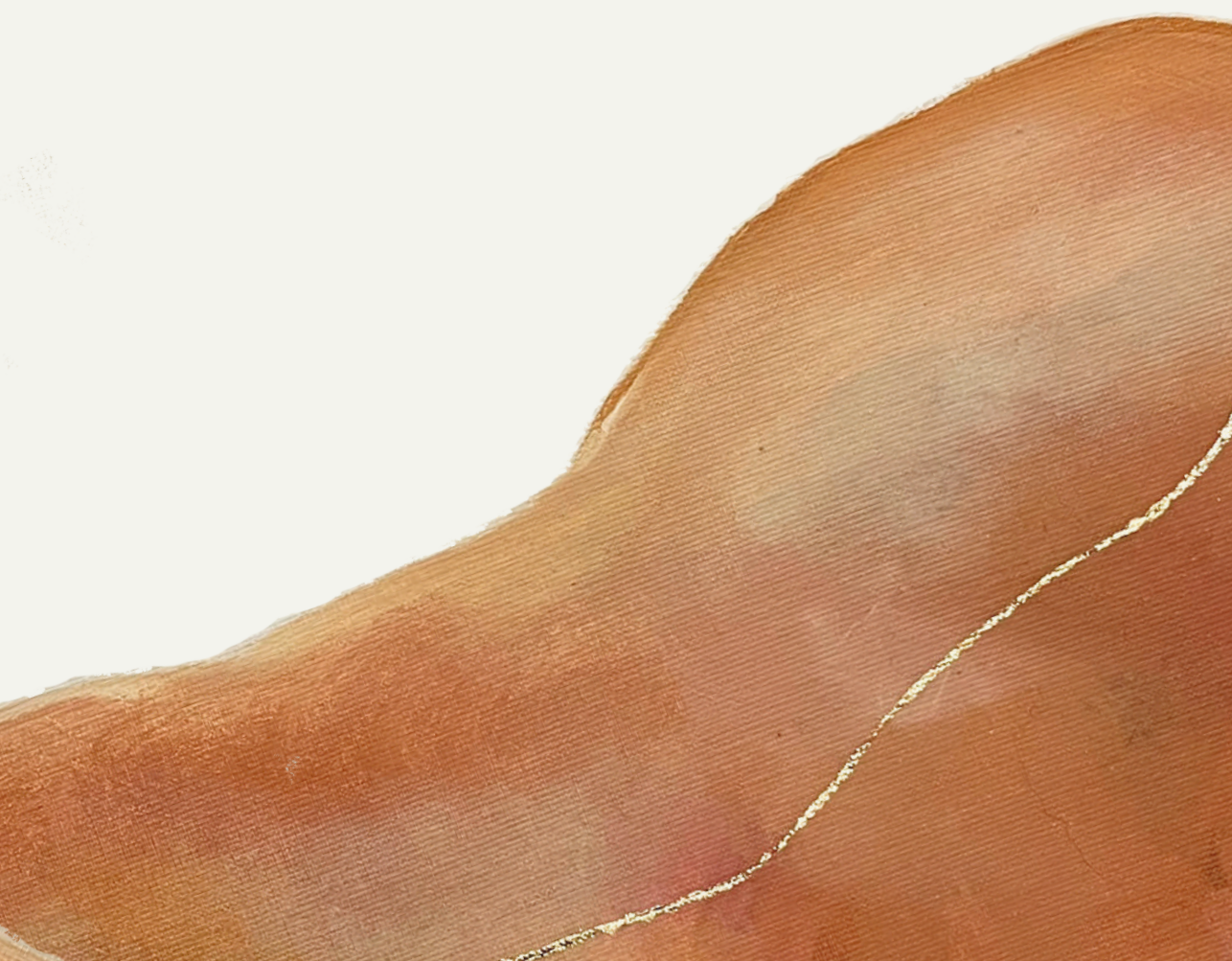
Appendices

Appendix A

Dutch Summary – Nederlandse Samenvatting

Het doel van dit proefschrift is om de behandeling voor patiënten met musculoskeletale tumoren te verbeteren. In **Deel I** (hoofdstuk 2 - 5) wordt onderzocht hoe chirurgische marges geoptimaliseerd kunnen worden met behulp van fluorescentie-geleide chirurgie (FGS) bij kwaadaardige musculoskeletale tumoren (sarcomen). Bij de resectie van musculoskeletale tumoren kunnen botdefecten en verlies van omliggend weefsel (zoals spieren en zenuwen) optreden, wat de functie van een lichaamsdeel kan beïnvloeden. Na een resectie volgt de reconstructie en fixatie, vaak met behulp van implantaten. In **Deel II** (hoofdstuk 6 - 9) wordt het gebruik van innovatieve koolstofvezel (CF) implantaten onderzocht wegens mogelijke materiaal specifieke voordelen die CF biedt ten opzichte van conventionele metalen implantaten.

In **Hoofdstuk 2** wordt een systematisch literatuuronderzoek uitgevoerd om biomarkers te identificeren die gebruikt kunnen worden voor tumor-specifieke FGS. Op basis van een scoresysteem worden 7 biomarkers geïdentificeerd die geschikt kunnen zijn voor FGS bij wekedelensarcomen. Specifiek worden "Tumor endothelial marker 1" (TEM1), "Platelet-derived growth factor receptor α" (PDGFRα) en "Epidermal growth factor receptor" (EGFR) als meest veelbelovende biomarkers geïdentificeerd voor Myxofibrosarcoom (MFS), ongedifferentieerd weke delen sarcoom (USTS) en synoviaal sarcoom (SS). Voor deze biomarkers zijn al klinisch goedgekeurde monoklonale antilichamen beschikbaar, wat belangrijk is voor kosten- en tijdefficiënte klinische translatie. Deze therapeutische antilichamen kunnen namelijk relatief gemakkelijk worden gebruikt voor FGS door ze te conjugeren met een fluorofoor, en er kan worden verwacht dat ze veilig zijn. De expressie van de door ons geselecteerde biomarkers op omliggend normaal weefsel is echter nog niet onderzocht.

In **Hoofdstuk 3** wordt een immunohistochemische (IHC) evaluatie van de geselecteerde biomarkers uitgevoerd op zeventien in paraffine ingebedde MFS-tumoren met omliggend gezond weefsel. Een door ons ontwikkelde objectieve scoringsmethode toont aan dat TEM1 de meest geschikte biomarker is voor tumor-specifieke FGS, gebaseerd op een hogere tumor-naar-normale kleurintensiteit vergeleken met andere biomarkers, ongeacht preoperatieve therapie.

In **Hoofdstuk 4** worden zowel niet-tumor-specifieke als tumor-specifieke FGS beoordeeld voor drie veelvoorkomende pediatrische sarcomen: Osteosarcoom (OS), Ewing-sarcoom (ES) en Rhabdomyosarcoom (RMS). Hoewel niet-tumor-specifieke FGS met behulp van Indocyanine Green (ICG) relatief goedkoop en veilig is, kan intraveneuze toediening logistiek gezien lastig zijn, omdat het ongeveer 24 uur vóór de operatie moet worden toegediend. Daarnaast is de signaalintensiteit van ICG onvoorspelbaar, wat kan leiden tot vals negatieve en vals

positieve signalen. Dit kan vervolgens leiden tot resectie van te weinig of te veel weefsel, waardoor onvolledige tumorverwijdering of verhoogde functionele beperkingen en meer kans op wondcomplicaties kunnen ontstaan. Tumor-specifieke FGS zou deze nadelen kunnen ondervangen en zien wij daarom als een volgende stap naar het verbeteren van chirurgische tumor resecties. Tot slot geven wij een overzicht van potentiële tumor-specifieke biomarkers voor OS, ES en RMS.

In **Hoofdstuk 5** wordt ES verder onderzocht. IHC-evaluaties van potentiële biomarkers voor tumor-specifieke FGS worden uitgevoerd op materiaal van dertien ES-patiënten. Op basis van de relatief hoge tumor-tot-normale expressie worden twee celmembraan eiwitten, "cluster van differentiatie 99" (CD99) en "cluster van differentiatie 117" (CD117), geselecteerd als de meest veelbelovende doelwitten. Daarnaast wordt "disialoganglioside 2" (GD2) beschouwd als een veelbelovend doelwit vanwege de bekende hoge expressie in ES-biopsiemateriaal en de klinische beschikbaarheid van een FGS-tracer gericht tegen GD2. Vervolgens worden fluorescerende tracers gericht tegen CD99, CD117 en GD2 geconstrueerd en geëvalueerd op bindingsspecificiteit met behulp van flow cytometrie en immunofluorescentie microscopie. Deze experimenten bevestigen een hoge CD99-expressie, samen met lage tot matige expressie van CD117 en een lage expressie van GD2 in celculturen afkomstig van ES patiënten. Om het concept van tumor-specifieke FGS aan te tonen, worden de genoemde tracers aangebracht op vers gereseceerd tumor- en omliggend normaal weefsel van patiënten met ES. Wij concluderen dat tracers gericht tegen CD99 veelbelovend zijn voor FGS bij patiënten met ES, terwijl CD117- en GD2-tracers mogelijke alternatieven zijn.

In **Hoofdstuk 6** worden retrospectieve gegevens van 96 patiënten gepresenteerd die tussen 2015 en 2021 een reconstructie en fixatie met CF-platen hebben ondergaan, met een mediane follow-up van 35 maanden. In totaal kregen 22 (23%) patiënten complicaties. Mechanische complicaties omvatten: 1 (1%) aseptische loslating, 2 (2%) niet-geconsolideerde defecten en 7 (7%) structurele complicaties zoals plaat- of schroefbreuken. Niet-mechanische complicaties omvatten: 1 (1%) complicatie van wekedelen (dehiscentie van de operatiewond), 4 (4%) infecties, en 5 (5%) patiënten met lokale tumor recidieven. Bij pediatrische patiënten traden complicaties van botgroei op bij 2 (2%) patiënten. Vanwege het relatief lage complicatieprofiel concluderen wij dat CF-platen veilig kunnen worden gebruikt bij veeleisende reconstructies na resecties van bottumoren.

In **Hoofdstuk 7** wordt een systematisch literatuuronderzoek uitgevoerd om klinische en radiologische uitkomsten van patiënten behandeld met CF-platen te evalueren. Deze data, afkomstig uit 27 studies met in totaal 1297 patiënten, brengen geen verontrustend aantal complicaties aan het licht die verband houden met CF-plaatfixatie. Wij concluderen dat CF-platen een goed alternatief zijn voor metalen platen, maar gerandomiseerde onderzoeken met langdurige follow-up worden sterk aanbevolen om aanvullend bewijs te leveren voor het gebruik van CF-platen.

In **Hoofdstuk 8** analyseren wij 239 patiënten die tussen 2013 en 2020 met CF-pennen zijn behandeld vanwege (dreigende) pathologische fracturen, met een mediane follow-up van 17 maanden. Drieëndertig (14%) patiënten kregen complicaties. Er waren mechanische complicaties bij 12 (5%) patiënten, met onder andere structureel falen van het implantaat en het loslaten van schroeven. Niet-mechanisch falen omvatte: 8 (3%) infecties en 15 (6%) patiënten met lokale tumor recidieven. Uit onze analyse blijkt dat preoperatieve radiotherapie ter hoogte van de operatieplaats en femurchirurgie een verhoogd risico op complicaties geeft. De sterfte na 90 dagen en één jaar bedroeg respectievelijk 28% en 53%. De literatuur rapporteerde vergelijkbare complicatie- en sterftecijfers bij conventionele metalen implantaten, wat erop wijst dat CF-pennen als een veilig alternatief kunnen worden beschouwd.

In **Hoofdstuk 9** worden de artefacten op CT-beelden vergeleken tussen 11 patiënten die behandeld worden met CF-wervelkolom implantaten en 11 patiënten die behandeld worden met titanium-wervelkolom implantaten. Beide patiëntengroepen hebben tumor metastasen in de wervelkolom en ondergaan stereotactische ablatieve radiotherapie. Bij de CF-wervelkolom implantaten groep worden minder CT-artefacten waargenomen, wat de planning van radiotherapie kan vergemakkelijken. Desalniettemin zijn toekomstige studies van vergelijkende aard nodig om de toegevoegde klinische waarde van CF-implantaten te beoordelen, zoals nauwkeurige bestralingsplanning en verbeterde detectie van lokale tumor recidieven.

Appendix B

List of Publications

Rijs Z, de Groot PCJ, Zwitser EW, Visser CPJ. Is the Anterior Injection Approach Without Ultrasound Guidance Superior to the Posterior Approach for Adhesive Capsulitis of the Shoulder? A Sequential, Prospective Trial. Clin Orthop Relat Res. 2021 Nov 1;479(11):2483-2489. doi: 10.1097/CORR.0000000000001803. PMID: 33950868; PMCID: PMC8509907.

Rijs Z, Shifai AN, Bosma SE, Kuppen PJK, Vahrmeijer AL, Keereweer S, Bovée JVMG, van de Sande MAJ, Sier CFM, van Driel PBAA. Candidate Biomarkers for Specific Intraoperative Near-Infrared Imaging of Soft Tissue Sarcomas: A Systematic Review. Cancers (Basel). 2021 Feb 1;13(3):557. doi: 10.3390/cancers13030557. PMID: 33535618; PMCID: PMC7867119.

Rijs Z*, Jeremiasse B*, Shifai N, Gelderblom H, Sier CFM, Vahrmeijer AL, van Leeuwen FWB, van der Steeg AFW, van de Sande MAJ. Introducing Fluorescence-Guided Surgery for Pediatric Ewing, Osteo-, and Rhabdomyosarcomas: A Literature Review. Biomedicines. 2021 Oct 4;9(10):1388. doi: 10.3390/biomedicines9101388. PMID: 34680505; PMCID: PMC8533294.

Carbon-Fiber International Collaboration Initiative Research Group. Complications of patients with bone tumors treated with carbon-fiber plates: an international multicenter study. Sci Rep. 2022 Nov 8;12(1):18969. doi: 10.1038/s41598-022-23519-9. PMID: 36348055; PMCID: PMC9643370.

Rijs Z, Belt E, Kalisvaart GM, Sier CFM, Kuppen PJK, Cleven AHG, Vahrmeijer AL, van de Sande MAJ, van Driel PBAA. Immunohistochemical Evaluation of Candidate Biomarkers for Fluorescence-Guided Surgery of Myxofibrosarcoma Using an Objective Scoring Method. Biomedicines. 2023 Mar 22;11(3):982. doi: 10.3390/biomedicines11030982. PMID: 36979961; PMCID: PMC10046284.

Jeremiasse B*, **Rijs Z***, Angoelal KR, et al. Evaluation of Potential Targets for Fluorescence-Guided Surgery in Pediatric Ewing Sarcoma: A Preclinical Proof-of-Concept Study. Cancers (Basel). 2023;15(15):3896. Published 2023 Jul 31. doi:10.3390/cancers15153896.

Rijs Z, Weekhout A, Daniel S, et al. Carbon-fibre plates for traumatic and (impending) pathological fracture fixation: Where do we stand? A systematic review. J Orthop Traumatol. 2023;24(1):42. Published 2023 Aug 11. doi:10.1186/s10195-023-00724-4.

Lozano-Calderon SA, **Rijs Z**, Groot OQ, et al. Outcomes of Long Bones Treated With Carbon-Fiber Nails for Oncologic Indications: International Multi-institutional Study. J Am Acad Orthop Surg. 2024;32(3):e134-e145. doi:10.5435/JAAOS-D-22-01159.

Rijs Z, Saha P, Kawsar KA, et al. Evaluation of computed tomography artefacts of carbon-fiber and titanium implants in patients with spinal oligometastatic disease undergoing stereotactic ablative radiotherapy. Accepted for publication: Nature Scientific Reports, 2024.

* Both authors contributed equally

Appendix C

Curriculum Vitae

Zeger Rijs was born on 13 December 1993 in Amsterdam, the Netherlands. He grew up with his parents (Paul and Margreet), his older brother (Mees), and his frequently visiting half-sister (Eva). During his secondary school at the Anna van Rijn college, he was a competitive road cyclist, winning the road race in his hometown of Nieuwegein twice, placing third in the Junior Tour of Ireland 2012, and competing in the Dutch national championships. After graduating secondary school, he began medical studies at Leiden University and moved to Leiden. Although his focus shifted from cycling to studying, he joined the Dutch Granfondo Team, where he finished 2nd in the Granfondo Dubai in 2014 and participated in the Granfondo World Championships in Ljubljana (2014) and Ålborg (2015). His sporting activities provoked his interest in the musculoskeletal system, which grew during lectures given by orthopedic surgeons in his second year of medical school. After completing a six-month internship in Gynecology and Pediatrics in Surinam, he focused on orthopedic surgery by undertaking a senior internship in the Orthopedic Department at Haaglanden Medisch Centrum and a scientific research internship at Erasmus Medical Center, working on cartilage and bone regeneration.

After becoming a medical doctor, he began a PhD program on innovations in musculoskeletal tumor surgery under the supervision of prof. dr. M.A.J. van de Sande, dr. P.B.A.A. van Driel, and dr. C.F.M. Sier. He conducted several preclinical studies on fluorescence-guided surgery and designed an online registry to collect data of innovative carbon-fiber implants. Several studies were initiated in collaboration with internationally renowned orthopedic oncology centers. Over the following years, he published various scientific papers in internationally acclaimed peer-reviewed journals and presented his research at numerous international conferences. A noteworthy accomplishment was winning the award for best podium presentation at the International Society of Limb Salvage conference in Los Angeles in 2023. Zeger continued his career in the Orthopedic Department of the Groene Hart Ziekenhuis in Gouda as a resident-not-in-training and was admitted to the orthopedic surgery residency. In October 2024, he began working in the Surgery Department at Diakonessenhuis Utrecht. In january 2025, he started the one-and-a-half-year general surgery training, which is the first part of the six-year trajectory to become an orthopedic surgeon.

Appendix D

Acknowledgement (Dankwoord)

Prof. dr. M.A.J. van de Sande, beste Michiel, dankzij jouw vertrouwen, optimisme en waardevolle begeleiding heb ik dit promotietraject met veel plezier doorlopen en heb ik bereikt wat ik wilde bereiken. De operatieve, sociale en sportieve vaardigheden die jij hebt, maar ook de manier waarop je in het leven staat, zijn een inspiratie; ik ben dankbaar dat jij mij hebt begeleid.

Dr. P.B.A.A. van Driel, beste Pieter, jouw enthousiasme voor onderzoek, en je kwaliteiten om dit om te zetten naar ideeën voor onderzoek met als doel de (oncologische) orthopedische chirurgie te verbeteren zijn ongekend. Ondanks je drukke schema in Zwolle nam je altijd de tijd om mijn vragen te beantwoorden; bedankt voor de begeleiding en mooie samenwerking.

Dr. C.F.M. Sier, beste Kees, jij bent wat mij betreft het type onderzoeker die je normaal alleen tegenkomt in films. Als ras-Amsterdammer ben je direct in de communicatie en test je of anderen in staat zijn om kritisch na te denken; door jouw bijdrage hebben mijn studies een hoger niveau bereikt.

Collega-onderzoekers van de Orthopedie en Green-Light Leiden, assistenten en staf van de afdeling Orthopedie van het LUMC, met in het bijzonder Prof. dr. R.G.H.H. Nelissen. Ondanks mijn start tijdens het begin van de COVID-periode heb ik jullie leren kennen als een open en gezellige groep. De preklinische en klinische invalshoeken boden de juiste handvatten om mij te ontwikkelen als onderzoeker. De borrels, skivakantie, het padellen, en de vele congressen (waaronder de natte fietstrip naar Brussel met Robert en de gedenkwaardige fietstocht naar Kerkrade met Geert) maakte het een fenomenale tijd.

Vrienden van de C2, met in het bijzonder Geert, Timon, Anouk, Richard en Thies. Borrels met jullie lopen standaard uit de hand. Misschien maar goed dat een PhD in het LUMC 3 à 4 jaar duurt, en logisch dat niemand het afkrijgt binnen die tijd. Geert en Timon, met jullie als paranimfen weet ik zeker dat het een groot feest zal worden.

Nino en Jayne, beste vrienden van de middelbare school. Ondanks al onze streken en avonturen hebben we het ver geschopt. Benjamin is een geweldig cadeau in jullie leven, ik ben blij voor jullie als gezin.

Hamez, Kayou en Olivier, het is geweldig dat onze vriendschap sinds het begin van de studententijd is blijven bestaan. Het verbaast me niet dat we allemaal in opleiding zijn gekomen, drie van ons vier bij de Orthopedie. We gaan een mooie toekomst tegemoet, en onze vriendschap is voor het leven.

Fietsvrienden van de zachte kern, het fietsen is inmiddels bijzaak voor de meesten van ons, maar fanatiek zullen we altijd blijven. De humor van zes gasten in een bus, op weg naar adembenemend mooie gebieden, hoop ik nog vaak te mogen meemaken. Ingo, onze tochten richting Parijs, Tsjechië, Lissabon, en door de Balkan waren onvergetelijk.

Henk en Ria Wintermans, dankzij de mogelijkheid om in de weekenden bij jullie in Steensel te verblijven, kreeg ik de kans om deel te nemen aan wielerwedstrijden in België en leerde ik om door te zetten om mijn doelen te bereiken. Ria, je bent voor mij als een oma geworden, en ik hoop dat je nog vele mooie momenten mag beleven tijdens de reizen die je gaat maken. Bedankt voor jullie warmte, gastvrijheid en steun gedurende de tijd dat ik bij jullie mocht verblijven.

Lieve Paul, Margreet, Eva en Mees. Jullie onvoorwaardelijke liefde, is het belangrijkste wat er is. Jullie hebben mij altijd gestimuleerd om mijn dromen na te jagen. Ik wil jullie bedanken voor de steun en toeverlaat.

Tot slot, lieve Marit. Ik weet hoe leuk je het vindt dat je in het proefschrift staat. Ik ben ongelofelijk blij dat wij elkaar hebben ontmoet. Jouw humor, zorgzaamheid, en oprechtheid maken jou mijn grote liefde (en huisgenoot).